INTEGRATION OF ELECTRIC VEHICLES, RAPID AND ULTRA-RAPID CHARGERS INTO UK DISTRIBUTION NETWORKS

HASAN BERKEM SONDER

School of Engineering

Cardiff University

A THESIS SUBMITTED FOR THE DEGREE
OF DOCTOR OF PHILOSOPHY

March 2023

Table of Contents

List of Figures

List of Tables

List of Abbreviations

AC	Alternating Current
BEV	Battery Electric Vehicles
CCS	Combined Charging System
CHADEMO	Charge de Move — Move by Charge
DC	Direct Current
DNO	Distribution Network Operator
DoD	Depth of Discharge
DG	Distributed Generation
DQ	Direct Quadrature Axis
EPA	Environmental Protection Agency
ESO	Electricity System Operator
EV	Electric Vehicle
FC	Fuel Cell
FCH	Fuel Cell Hybrid
G2V	Grid-To-Vehicle
GHG	Greenhouse Gas
HEV	Hybrid Electric Vehicle
HV/MV	High Voltage/Medium Voltage
ICEV	Internal Combustion Engine Vehicle
IGBT	Insulated Gate Bipolar Transistor
MV/LV	Medium Voltage/Low Voltage
NEDC	New European Driving Cycle
OLTC	On-Load Tap Changer
OZEV	Office for Zero Emission Vehicles
PCC	Point of Common Coupling
PEV	Plug-in Hybrid Electric Vehicle
PI	Proportional Integrator
PLL	Phase Locked Loop
PQ	Active Power and Reactive Power Demand
PSCAD/EMTDC	Power System Computer Aided Design/Electromagnetic Transients Direct Current
PV	Photovoltaic
PWM	Pulse Width Modulation
SRF	Synchronous Reference Frame
SSEN	Southern and Scottish Electricity Network
SoC	State of Charge
SVC	Static VAr Compensator

UK	United Kingdom
UKGDS	United Kingdom Generic Distribution System
V2G	Vehicle-To-Grid
V2X	Vehicle-To-Anything
WLTP	Worldwide Harmonised Light Vehicle Test Procedure
WPD	Western Power Distribution

List of Symbols

A	Exponential zone amplitude for Shepherd model
A_c	Cross-sectional area of the conductor size
A_{CP}	Average charge power to reach 80% SoC
$\alpha\beta$	Alpha-beta frame variables
B	Shepherd battery exponential zone time constant
B_A	Actual busbar voltage
B_r	Rated power output of the battery energy storage unit
B_T	Target busbar voltage
B_{max}	Maximum susceptance
B_{min}	Minimum susceptance
C	Capacitance
C_{B1}, C_{B0}	Positive/negative, and zero-sequence susceptance (line)
C_d	Total charging demand at each minute
C_{damp}	Damping capacitance
C_{di}	Capacity discharged by any amount of current
C_E	Hourly energy cost
C_{filter}	Filter capacitance
C_{freq}	Carrier frequency
C_l	Cable length
CO_2	Carbon dioxide
C_p	Estimated cost of total power losses in the feeder
C_r	Releasable battery capacity
C_{R1}, C_{R0}	Positive/negative, and zero-sequence resistance (line)
C_t	Vehicle's estimated charging time to reach from 10% to 80% SoC
C_{te}	Vehicle's estimated charging time to reach target SoC of 80%
C_{X1}, C_{X0}	Positive/negative, and zero-sequence reactance (line)
C_γ	Total time of cable network operation
D_{1-6}	Freewheeling anti-parallel diodes
D_t	Total distance travelled by each EV model within SoC limits
E	No-load voltage for Shepherd model
E_c	Daily energy cost based on the power consumption
E_0	Constant voltage for Shepherd model
E_v	Energy consumption of each vehicle during charging sessions
f	Nominal system frequency
f_{co}	Cut-off frequency

f_{sw}	Switching frequency
$I^*{}_{dq}$	Two-phase dq frame reference currents
I_{av}	Average current in loss determination
I_{abc}	Three-phase abc frame grid currents
I_{bat}	Battery current
I_{bat_ref}	Reference battery current
I_c	Instantaneous magnitude of the RMS current
I_{dq}	Two-phase dq frame currents
I_i	Injected current at the ith busbar
I_{pp}	Peak-to-peak amplitude of the ripple current
I_{RMS}	RMS current in loss determination
I_s	Transformer secondary winding full-load current
it	Actual battery charge at each time step
K	Polarisation voltage for Shepherd model
k_i	PI controller integral gain parameter
k_p	PI controller tuneable parameter
L	Inductance
L_{damp}	Damping inductance
L_{grid}	Grid-side inductance
L_p	Loss of active power consumption
L_{rec}	Rectifier-side inductance
$M_n D$	Minimum distance travelled by each model prior to charging
$M_x D$	Maximum distance travelled by each model prior to charging
n	Harmonic order
$\omega, \omega t$	Angular frequency, angular position
P, P_{AC}	Active power in the AC system
P_{bat}	Reference battery power
P_{Gi}	Active power generated at the ith busbar
P_i	Active power injection at the ith busbar
P_L	Active power demand at the load busbar
P_m, P_{ref}	Measured and reference active power
ρ	Resistivity of the cable material at 20°C
R	Resistance
R_{damp}	Damping resistance
R_l	Operating resistance per required length of cable
$R_{l,new}$	New operating resistance per required length cable
R_r	Remaining range of vehicles prior to charging
R_{SoC}	Remaining SoC of vehicles prior to charging
R_v	Actual electric range of each EV model

Q, Q_{AC}	Reactive power in the AC system
Q_b	Rated capacity for Shepherd model
Q_{Gi}	Reactive power generated at the ith busbar
Q_i	Reactive power injection at the ith busbar
Q_L	Reactive power consumption at the load busbar
Q_m, Q_{ref}	Measured and reference reactive power
ϕ	Phase angle in PLL mechanism
ϕ'	Modified phase angle in PLL mechanism
θ_i	Voltage phase angle at the ith busbar
θ_j	Voltage angle at the jth busbar
S_{1-6}	IGBT switches for rectifier
S_{base}	Rated power for rectifier
S_{bk}, S_{bst}	Buck switch, boost switch
S_c	Short circuit level
S_d	Discharge rate of the battery energy storage unit
S_i	Scaled down discharge current for the MC3000 device
S_p	Power injected by the battery energy storage unit
S_s	Scaled down discharge current of the LG battery for tests
$SoC_{10\%}$	Minimum SoC constraint of the vehicle prior to charging
$SoC_{50\%}$	Maximum SoC constraint of the vehicle prior to charging
$SoC_{100\%}$	Maximum SoC/range on a fully charged battery
$SoC_{(0)}$	Initial SoC of the LG battery cell
SoC_d	Difference between the remaining and target SoC of vehicles
S_r	Rated energy capacity of the LG cell
S_{tx}	Rating of the substation transformer
SVC_m	Minimum required rating of the SVC device
$T_{abc-\alpha\beta}$	abc to αβ frame transformation
T_{abc-dq}	abc to dq frame transformation
$T_{\alpha\beta-dq}$	aβ to dq frame transformation
t_h	Daily number of usage hours
T_{R1}, T_{R0}	Positive/negative, and zero-sequence resistance (transformer)
T_{X1}, T_{X0}	Positive/negative, and zero-sequence reactance (transformer)
T_{RE}, T_{XE}	Earthing resistance and earthing reactance of transformers
$V^*{}_{abc}$	Three-phase abc frame reference voltages
$V^*{}_{dq}$	Two-phase dq frame reference voltages
V_{abc}	Three-phase abc frame voltages
V_{AC}	AC voltage
V_{ACm}, V_{ACref}	Measured and reference AC voltage
V_{amp}	Amplitude of the three-phase voltage signals

V_{av}	Average voltage in loss determination
V_{bat}	Battery voltage
V_{bat_ref}	Reference battery voltage
V_{DC}	DC link voltage
V_{DCm}, V_{DCref}	Measured and reference DC voltage
V_d	Difference between the actual and the target busbar voltage
V_i	Voltage magnitude at the ith busbar
V_j	Voltage magnitude at the jth busbar
V_{dq}	Two-phase dq frame voltages
$V_{L-L,rms}$	Line-to-line RMS voltage
V_{L-Ls}	Transformer secondary winding line-to-line RMS voltage
Y_i	Admittance at the ith busbar
Y_{ij}	Element of the admittance matrix
γ_{ij}	Line admittance angle between the ith busbar and jth busbar
V_{ref}	Reference voltage
ΔL_γ	Calculated daily total active power losses in the feeder
ΔP	Daily total active power consumption
$\Delta\omega'_g$	Damped transient response in the estimated frequency
ω'_g	Estimated frequency from the PLL mechanism
ωL	Decoupling terms
ω_n	Nominal frequency at the angular frequency
X	Reactance

List of Publications

<u>**JOURNAL PAPERS:**</u> First Author

The contribution parts of Chapter 6 and Chapter 7 <u>are ready for submission</u>:

1. **H. B. Sonder**, Y.-O. Udoakah, L. Cipcigan, "Real-time analysis and state of charge estimation of stationary battery energy storage systems connected to rapid charging hubs,"

2. **H. B. Sonder** and L. Cipcigan, "Estimation of demand and energy consumption of high-speed electric vehicle charging hubs in the UK,"

<u>**CONFERENCE PAPERS:**</u> First Author

The contribution part of Chapter 3 was <u>published</u> in:

3. **H. B. Sonder**, L. Cipcigan, and C. E. Ugalde-Loo, "Using electric vehicles and demand side response to unlock distribution network flexibility," *IEEE PES PowerTech Milano 2019*, Italy, 23–27 Jun. 2019.

The contribution parts of Chapter 4 and Chapter 5 were <u>published</u> in:

4. **H. B. Sonder**, L. Cipcigan, and C. E. Ugalde-Loo, "Voltage analysis on MV/LV distribution networks with the integration of DC fast chargers," *IEEE International Energy Conference (ENERGYCon 2020)*, Tunisia, 28 Sep.–1 Oct. 2020.

5. **H. B. Sonder,** L. Cipcigan, and C. E. Ugalde-Loo, "Integrating DC fast/rapid chargers in low voltage distribution networks," *Mediterranean Conference on Power Generation, Transmission, Distribution and Energy Conversion (MedPower 2020)*, 9–12 Nov. 2020.

The contribution parts of Chapter 6 were <u>published</u> in:

6. **H. B. Sonder**, L. Cipcigan, and C. E. Ugalde-Loo, "Demand estimation for electric vehicles at rapid charging hubs and peak load reduction using battery energy storage units," *CIRED Workshop on E-mobility and power distribution systems*, Porto, 2–3 Jun. 2022.

7. **H. B. Sonder**, E. Mudaheranwa, and L. Cipcigan, "Estimation of cable and transformer loading with electric vehicles and battery energy storage units," *IEEE International Energy Conference (ENERGYCon 2022)*, Latvia, 9–12 May. 2022.

BOOK CHAPTER

The contribution part of Chapter 2 was <u>published</u> in:

8. P. Nieuwenhuis, L. Cipcigan, **H. B. Sonder**, "The electric vehicle revolution. In: Letcher, T. ed. Future Energy 3rd Edition: Improved, Sustainable and Clean Options for Our Planet" *Elsevier*, pp. 227–241, 2020.

<u>JOURNAL PAPERS:</u> Co-author

9. E. Mudaheranwa, **H. B. Sonder**, L. Cipcigan, and C. E. Ugalde-Loo, "Estimation of Rwanda's power system inertia as input for long-term dynamic frequency response regulation planning," *Electric Power System Research*, vol. 207, vol. 207, Feb. 2022.

The following journal paper is under review:

10. E. Mudaheranwa, **H. B. Sonder**, and L. Cipcigan, "Feasibility study and impact mitigation with the integration of electric vehicles into Rwanda's power grid," *The Journal of the IAS*.

<u>CONFERENCE PAPERS:</u> Co-author

The following papers were <u>published</u> in:

11. E. Mudaheranwa, **H. B. Sonder**, and L. Cipcigan, "Feasibility study and impacts of EV penetration in Rwanda's MV distribution networks," *IEEE International Energy Conference (ENERGYCon 2020)*, Tunisia, 28 Sep.–1 Oct. 2020.

12. Y.-O. Udoakah, **H. B. Sonder**, and L. Cipcigan, "Low voltage distribution network simulation and analysis for electric vehicle and renewable energy integration." *12th Conference on IEEE Power & Energy Society Innovative Smart Grid Technologies (ISGT NA 2021)*, 16–18 Feb. 2021.

13. Y.-O. Udoakah, **H. B. Sonder**, and L. Cipcigan, "Nigerian distribution network feeder impact assessment with integration of electric vehicles," *IEEE International Energy Conference (ENERGYCon 2022)*, Latvia, 9–12 May. 2022.

14. Y.-O. Udoakah, **H. B. Sonder**, L. Cipcigan, and J. Liang, "Development of a viable black start restoration pathway and problem formulation sequence," *IEEE International Energy Conference (ENERGYCon 2022)*, Latvia, 9–12 May. 2022.

15. E. Mudaheranwa**, H. B. Sonder**, Y.-O. Udoakah, L. Cipcigan, and C. E. Ugalde-Loo, "Dynamic demand control for the stabilisation of the grid frequency," *2022 IEEE PES & IAS PowerAfrica Conference*, 22–26 Aug. 2022.

16. N. B. M. Shariff, **H. B. Sonder**, and L. Cipcigan, "Modelling charging profiles of electric vehicles on Malaysian distribution networks," *2022 IEEE International Conference on Power and Energy (PECon 2022)*, Malaysia, 5–6 Dec. 2022.

PROJECT/REPORT

The following report was prepared and submitted for the project that was commissioned by British Embassy in Beijing funded from UK Government Climate Diplomacy Fund:

17. L. Cipcigan, P. Wells, D. D. Snell, **H. B. Sonder**, K. Jakubiak, and L. Maybury, "Electric vehicle charging infrastructure in UK," *Electric Vehicle Centre of Excellence*, Cardiff University, Mar. 2021.

Acknowledgements

Abstract

This thesis examines the effects of increasing the uptake level of electric vehicles (EVs) in a generic medium-voltage distribution network. On a real low-voltage distribution network, the impact of integrating a dynamic battery charging model is also investigated. When and where EV charging loads are connected in distribution networks has a substantial effect on the severity of grid issues. It is necessary to ensure that the grids have sufficient hosting capacity and are accompanied by robust measures. Simulation results have demonstrated that increasing the number and rating of chargers increases power losses, voltage deviations, and distribution network equipment (cables and transformers) loading. At the transmission level, it has been shown that utilisation of transformer on-load tap changers, optimum placement of distributed generation units, and adequate sizing of static VAr compensator devices eliminate voltage violations. On the distribution level, coordinated smart charging systems, vehicle-to-grid chargers, and battery energy storage systems have proven effectiveness in reducing the peak loads.

A stochastic model is developed for estimating the energy consumption of EVs and quantifying the peak demand in a distribution network. Twenty stochastic scenarios are produces, and the worst-case scenario is selected for a detailed network analysis. According to the results of the worst-case scenario, simultaneously charging one Audi and two Tesla EVs between 17:00 and 18:00 would result in a fivefold increase in peak demand, causing the substation transformer to operate 30% above its maximum rated capacity. The results have shown that the substation transformer can accommodate a maximum demand of 432 kW without becoming overloaded in the worst-case scenario's peak period. By supplying the additional demand caused by EV charging, battery energy storage units are used to reduce transformer loading by up to 40%. In conclusion, increasing the rating of the substation transformer from 500 kVA to 660 kVA enabled the secure integration of EVs and high-power charging devices in the worst-case scenario.

Using lithium-ion batteries, discharge profiles for battery energy storage units are developed based on the stochastic charging profiles and the magnitude of the network's peak demand. These discharge profiles are then implemented into a battery charger and analyser unit to determine the relationship between the cell voltage and discharged capacity of the batteries. This relationship is used to estimate the usable capacity, state of charge, and depth of charge of lithium-ion batteries under different tests. The end-of-discharge voltage of the batteries (i.e., the voltage at which a battery's discharge stops) has never been reached during the tests. Due to their high energy density capability, lithium-ion batteries maintained over 85% of their capacities when they are used to accommodate the simultaneous charging demand of EVs during the peak periods.

CHAPTER 1

1. Introduction

1.1 Background

The largest source of human-caused Greenhouse Gas (GHG) emissions is the combustion of fossil fuels for electricity, heat, and transportation. The combustion of carbon dioxide (CO_2), methane, nitrous oxide, water vapour (which are all naturally occurring) and fluorinated gases are the primary gases responsible for the greenhouse effect [1]. In 2022, global carbon emissions from energy combustion and industrial processes increased by 0.9% to a new all-time high of 36.8 gigatonnes (measured in Gt CO_2 equivalents) [2, 3]. Figure 1.1 shows the global CO_2 emissions from energy combustion and industrial processes, and their annual change from 1990 to 2021.
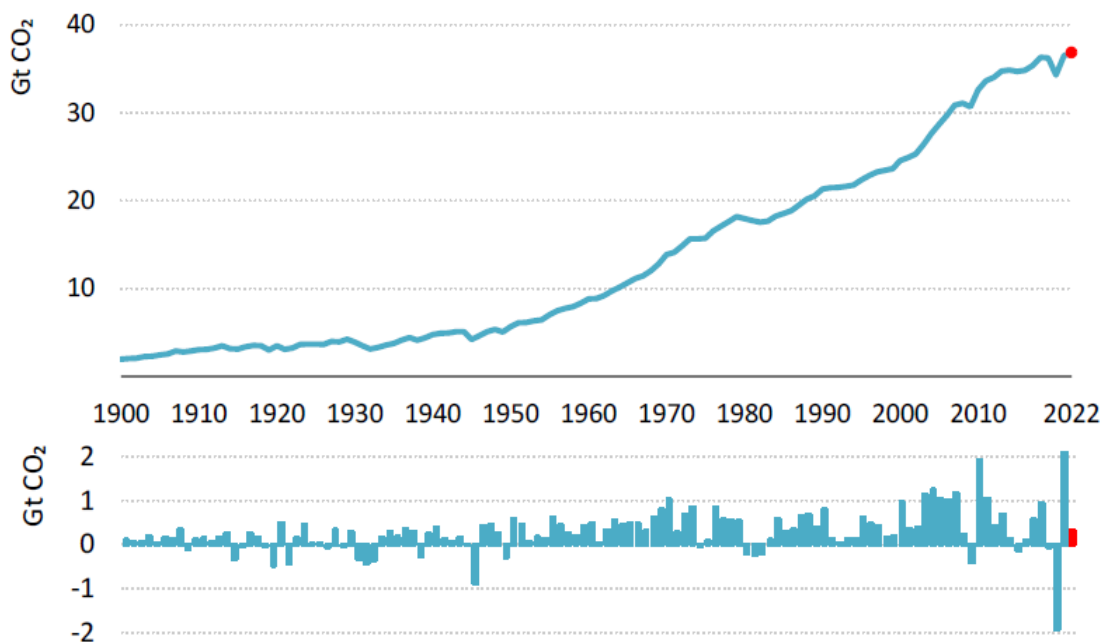
Figure 1.1: Global CO_2 emissions between 1990 and 2021 [4].

Almost three-quarters of emissions are attributed to energy use for transportation, industrial, and residential sectors, while the remainder is attributable to agricultural and other land use purposes. The *Paris Agreement*, which is a legally binding international agreement that unites all nations in the fight against climate change, was signed in 2016. The goal of this agreement has been to reduce global warming to far below 2°C, ideally 1.5°C, compared to pre-industrial levels. To achieve this long-term temperature target, countries and governments strive to reach global peaking of GHG emissions to create a climate-neutral future [5].

The act of reducing or eliminating a country's CO_2 emissions is critical for limiting global warming. However, there is no "one-size-fits-all" solution for completely decarbonising the electric supply. Numerous areas and sectors demand innovation, most notably the electrification of transportation and the decarbonisation of heat [2, 6]. For example, emissions from residential and industrial building activities are mainly attributable to space heating, industrial processing, water heating, lighting, and cooking. The utilisation of heat pumps is a very successful solution for providing energy-efficient heating and cooling solutions while reducing the emissions from buildings [7, 8].

Transportation emissions, on the other hand, account for nearly 25% of global GHG emissions and are mainly attributable to an increasing dependence on traditional internal combustion engine passenger vehicles on roads [9, 6]. Figure 1.2 shows that other modes of transportation also contribute to the increase in global CO_2 emissions.
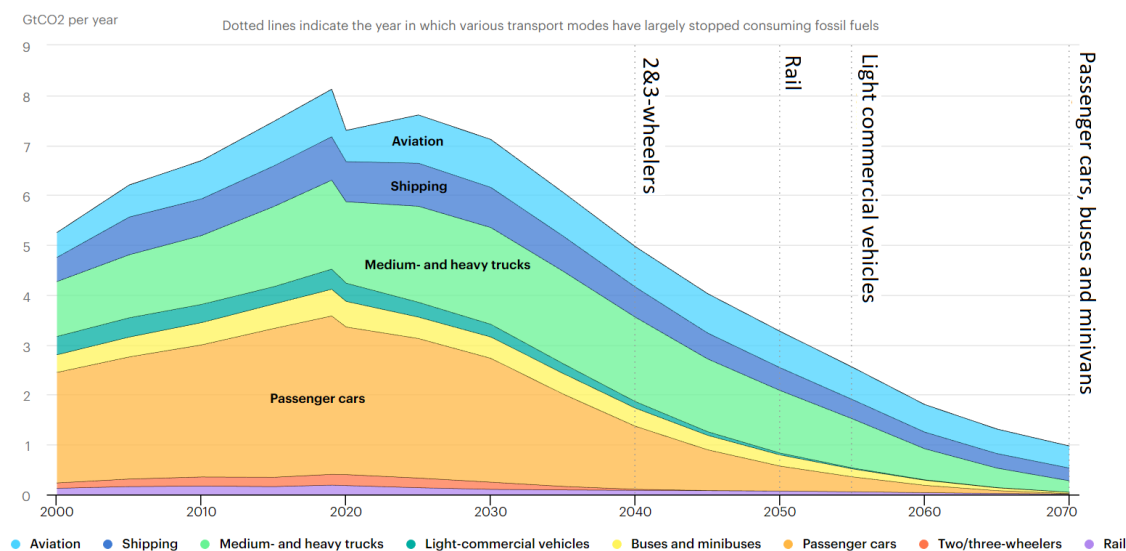
Figure 1.2: Global CO_2 emissions in transport by mode [10].

The transportation is the only energy-related sector where the emissions are still increasing relative to 2000 levels [9]. The sector has emitted around 100 million tonnes of carbon equivalent in 2020 [11, 12]. These are related to petroleum-fuelled passenger cars, buses, heavy goods vehicles, freight transport, lorries, off-road vehicles (such as lift trucks), and rail, air, and marine.

Ultra-low emission Electric Vehicles (EVs) have been highlighted as a technology on the route to a sustainable society, with the goal of replacing internal combustion engine vehicles (ICEV) on roads. The European Commission's 2030 targets include the reduction of carbon emissions from new vehicles, vans, and lorries by up to 37.5%, 31%, and 30%, respectively [11, 13, 14]. Furthermore, the 2050 regulations in the United Kingdom (UK) specify that GHG emissions should be cut by 100% compared to 1990 levels and that the sales of new petrol and diesel vehicles should cease by 2030 as part of the **Road to Zero** strategy outlined in the government's **Ten Point Plan** [15, 16].

Robust policy frameworks are also in place to support government plans to ban the sales of new petrol and diesel cars in 2030 and new hybrid cars in 2035. By 2035, the government of the UK wants for all new cars and vans to have zero tailpipe emissions. Several municipal governments, notably in the Greater London region, are developing clean air zones and ultra-low emission zones to improve air quality and to accelerate the adoption of EVs. The society is also encouraged to use public transport more often and, where possible, to prefer cycling and walking for shorter trips [14].

1.2   An Overview of Electric Vehicle Technology

Reduced reliance on ICEV and the transition to electric mobility will help to achieve net-zero targets on a global scale. Although some countries with smaller economies will take longer to achieve these targets, the transition to electric cars is expected to enable synergies with smart grids, increase the energy efficiency and security of nations, improve air quality, cut CO_2 emissions by up to 1.5 gigatons per year, and result in 1.5 million barrels of oil being saved per day [5, 17]. However, achieving zero emissions and transforming nations into net-zero emitters require extensive renewable energy deployment and innovative solutions across all sectors.

1.2.1 Electric Vehicle vs Internal Combustion Engine Vehicle

Over the course of its life, an EV emits 35% to 43% less emissions than an average ICEV [5, 18]. The *International Council on Clean Transportation* examined the lifetime GHG emissions of an average medium-sized gasoline ICEV and a battery electric vehicle (BEV) in Europe, the United States, China, and India in 2021 and forecasted the emissions for the year 2030. The comparisons are seen in Figure 1.3.
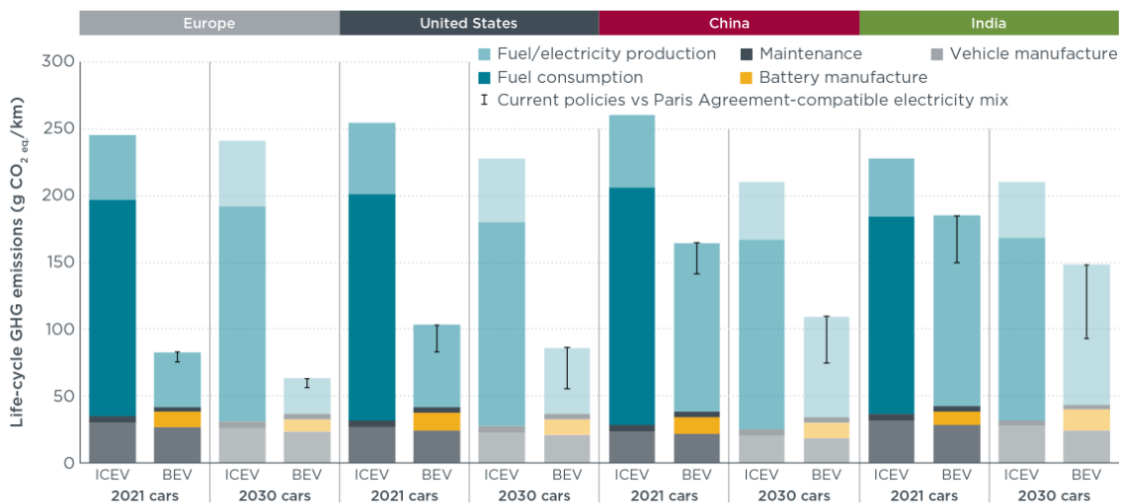
Figure 1.3: Lifecycle GHG emissions of average gasoline ICEV and BEV in Europe, the United States, China, and India [18].

Even among currently registered automobiles, BEVs have the lowest life cycle GHG emissions. As shown in Figure 1.3, the lifetime emissions of average medium sized BEVs registered today are already 66% to 69% lower than comparable ICEVs in Europe, 60% to 68% lower in the United States, 37% to 45% lower in China, and 19% to 34% lower in India. Moreover, as the electricity mix continues to decarbonise, the life-cycle emissions gap between BEVs and gasoline vehicles for the medium-sized cars expected to be registered in 2030 grows substantially [18].

Increasing the share of renewable in the energy mix and relying on lower-carbon alternatives will enable other nations to fulfil their carbon reduction targets [18–20]. While EVs emit no tailpipe emissions, however, they are powered by energy that is still mostly generated from fossil fuels in many parts of the globe. Energy is also used in the vehicle and battery production processes.

1.2.2 Advantages of Electric Vehicles

The significant sustainability advantages of EVs are obvious, including their capacity to help cut emissions and improve air quality. There are also financial advantages to electrification, including decreased fuel costs and incentive programmes that encourage clean energy use. EVs are envisioned as a critical component of our future smart, efficient, and flexible energy systems. EVs are quieter and cleaner than ICEVs, maximise industrial opportunities, promote the global shift towards clean growth, provide necessary grid services, and encourage the use of home storage [20].

In today's market, the typical upfront cost of an average ICEV is less than that of an EV, since the EV's cost structure is strongly determined by its on-board battery specifications [21]. However, EVs have lower running costs due to savings on fuelling costs [22, 23]. It is reported that the reduction in the price gap between an electric and an ICEV will accelerate the adoption rates of EVs in the future [14, 16, 24].

1.2.3 Types of Electric Vehicles

EVs are categorised in three different types, classed by the degree that electricity is used as their energy source. These types are classified as BEVs, Plug-in Electric Vehicles (PEVs), and Hybrid Electric Vehicles (HEVs) [24].

BEVs, often known as purely electric cars, emit no tailpipe emissions. They operate entirely on the power supplied by the on-board rechargeable battery packs. Tesla cars (e.g., Models 3, S, and X), BMW i3 series, Nissan LEAF, Volkswagen e-Golf, Kia Soul, Toyota Rav4, and Chevrolet Bolt series are some popular examples of BEV models on the market today [25, 26].

A PEV is a hybrid electric car with a big electric motor that can be powered by its on-board battery pack, or internally by the vehicle's internal combustion engine generator. The batteries of PEVs may be charged similarly to a BEV through a plug; however, the electric range is around 70 km in those vehicles. In addition, PEVs operate on battery power until the battery is fully depleted, at which point they switch to the combustion engine. BMW cars (e.g., Models 330e and i8), Kia Optima, Audi e-Tron (A3), Toyota Prius, Mercedes (e.g., Models C350e and S550e), and Porsche (e.g., Models Cayenne and Panamera S E-hybrid) are all popular PEV models on the market [25].

HEVs are a rare group of vehicles that combine an internal combustion engine system with an electric motor. The electric motor assists gasoline-powered engines, where the energy is generated completely by gasoline. Modern HEVs include regenerative braking systems (sometimes referred to as self-charging hybrids) and convert kinetic energy to electric energy to maximise vehicle efficiency. The hybrid electric car is the most prevalent type of HEV, but there are other forms of hybrid modes, including electric trucks (pickups and tractors), buses, aircrafts, and boats. Honda Civic and Toyota (e.g., Models Prius, Camry, and Corolla) are the most popular HEV brands on the market [25].

Other forms of vehicles that are less prevalent include Fuel-cell (FC) and Fuel-cell Hybrid (FCH). The former relies entirely on an electric motor for propulsion; however, the energy source is either hydrogen; which is extracted from gasoline, or hydrogen which is stored in the vehicle's on-board tank. The latter contains a battery or an ultracapacitor as an additional energy source to supplement the hydrogen that is produced by the fuel cell [27]. These vehicles are still in their infancy, and the exorbitant costs associated with fuel cells and the manufacture, transportation, and storage of hydrogen are the main barriers.

1.2.4 Battery Technology

The majority of EVs currently employ a similar battery technology. In a typical EV, hundreds of individual cells are packed and built into modules arranged in a series/parallel configuration to achieve the desired battery voltage and capacity. Lithium-ion batteries are the primary type of a rechargeable battery packs used in most EVs. Their qualities surpass those of other rechargeable batteries. Other types of batteries, such as lead-acid and nickel-cadmium (NiCd) batteries, contain higher concentrations of toxic heavy metals than lithium-ion batteries do. Lithium and carbon, the most common electrodes found in lithium-ion batteries, are lightweight on their own, resulting in much smaller and lighter batteries than lead-acid batteries.

Lithium-ion batteries have a higher energy density compared to their weight and last longer between charges than other rechargeable batteries, while retaining their high level of performance. The energy density of these batteries ranges between 260–270 Wh/kg, whereas lead-acid batteries range between 50–100 Wh/kg [28, 29]. Additionally, lithium-ion batteries have a low rate of self-discharge and do not require routine maintenance.

The advances in electronics, as well as in the manufacturing of lithium-ion batteries continue to lower the upfront cost of EVs. In 2010, the price of a lithium-ion battery pack was over $1,200 per kWh, whereas by 2021, that price has decreased by 89% to $132 per kWh. This is a 6% decrease from the 2020 price of $140/kWh [28, 30]. Falling battery costs have also prompted automakers to enhance the EV's battery capacity and range to alleviate range anxiety [30, 31], which is defined as the "*fear that a vehicle would not have enough range to reach its destination, leaving the driver stranded*." Increasing the battery capacity is one technique to alleviate range anxiety; however, this results in an increase in the vehicle's price and weight. Therefore, the suggested course of action is to generally enhance the charging infrastructure and increase the number of public chargers so that drivers can stop more often during longer journeys [31].

1.2.5 Battery Specifications of Electric Vehicles

In the coming years, EV purchasers will have a multitude of options and models to choose from. Each model is classed by its battery capacity and electric range. Table 1.1 shows the specifications of some popular BEV models on the market today.

Table 1.1: Specifications of some popular EV models from the 2017–2020 market

Vehicle Brand/Model	Battery Capacity (kWh)	Electric Range (km)
Audi e-Tron 55 quattro	95	436 (WLTP)
BMW i3	42	310 (WLTP)
Chevrolet Bolt	66	416.8 (EPA)
Hyundai Ioniq	28	200 (EPA)
Jaguar I-Pace	90	470 (WLTP)
Kia Soul	31.8	178.6 (EPA)
Nissan Leaf	40	243 (EPA)
Peugeot e-208	50	340 (WLTP)
Porsche Taycan 4S	79.2	466.7 (WLTP)
Renault Zoe R110	54.66	395 (WLTP)
Tesla Model 3 Long Range	79.5	518.2 (EPA)
Tesla Model S/X Long Range	100	600.3/527.9 (EPA)
Tesla Model Y Long Range	74	507 (EPA)
Volkswagen ID.3 Pro Perf	58	416 (WLTP)

Battery capacity and electric range are terms that are used interchangeably but have slightly distinct meanings. EVs with a larger battery capacity have the capability of travelling longer distances on a single charge, but often have greater upfront costs [7, 33, 34]. A manufacturer's stated electric range may often not be the same as the vehicle's real-world range on a fully charged battery. The actual electric range of each EV model is dependent on several variables, including average vehicle speed, consumer driving style and location (city or highway journey), traffic regulations, and weather conditions.

Automobile manufacturers use one of three testing standards to determine and quantify the range of EVs: The Environmental Protection Agency (EPA), the New European Driving Cycle (NEDC), and the Worldwide Harmonised Light Vehicle Test Procedure (WLTP). The EPA is typically the most realistic measure in simulating real-world driving conditions for American motorists and focuses on long-distance driving (e.g., highway), while NEDC is considered the least accurate. The NEDC and WLTP standards place a greater emphasis on urban and suburban travel, respectively [35, 36].

1.2.6 Charging Terminology for Electric Vehicles

Charging speed is one of the important considerations when it comes to EV models. Each model has a distinct charging speed, based on its type, model, and battery specifications. External variables, such as the ambient temperature, and the type and rating of a charging device also affect the charging speed. Unlike refuelling an ICEV, which takes just a few minutes, recharging an EV can take from 20 minutes to 15 hours, depending on the charging technique used [24, 25].

In the early 2010s, most cars could only be charged using slow-speed chargers rated at 3 kW. The terms "normal" and "fast" charging were used to refer to chargers that are rated at 7 kW and 10 kW, respectively. As the EV industry and battery technology have evolved and advanced over the years, the nomenclature for chargers has been updated. For example, slow chargers saw an increase of up to 7 kW, while fast chargers saw an increase of up to 22 kW. On the other hand, the term "normal" is nearly obsolete in the context of charging speed. The phrases rapid, ultra-rapid, and even extremely fast charging have been bandied around a lot in recent years [37].

A significant improvement in battery performance has been a key criterion in improving the range and the charging rates of EVs. While the range that EVs can travel on a fully charged battery is continuously improving, the recharging duration is long compared to the refuelling speeds of ICEVs. Rapid chargers are gaining popularity to obtain shorter recharging durations. However, these will provide technical hurdles for the grid, the battery system design, and the electrical architecture of the vehicle [7, 38].

In this thesis, the term "slow-speed" applies to single-phase Alternating Current (AC) chargers (rated at 3–7 kW), whereas "fast-speed" refers to chargers running in single-phase (rated at 7 kW) or three-phase (rated at 22 kW). Additionally, the phrases "rapid-speed" and "ultra-rapid-speed" refer to three-phase Direct Current (DC) chargers rated at 50 kW and 100–350 kW, respectively [36, 39]. The key characteristics of different charging methods and speeds are presented in Table 1.2.

Table 1.2: Characteristics of charging methods

Charger Speed	Charger Rating	Charge Duration
Slow — single-phase AC	3–7 kW	8–12 hours
Fast — single- or three-phase AC	7 kW or 22 kW	3.5–7 hours
Rapid — three-phase AC	43 kW	1 hour
Rapid — three-phase DC	50 kW	Less than 1 hour
Ultra-rapid — three-phase DC	Up to 350 kW	Less than 30 minutes

Today, most charging stations are AC-powered. The typical rating for AC chargers is available from 3–7 kW on a single-phase socket and 7–22 kW on a three-phase socket. Consumers generally use slow and fast chargers overnight or during the day, especially in areas like their homes or workplace parking lots.

While slow and fast charging are the foreseen primary options, rapid and ultra-rapid chargers are also gaining an increasing attention as the major secondary charging option. Rapid chargers have been mainly made available on highways with the benefits of reducing driver range anxiety, reducing service time at charging stations, and allowing drivers to charge their vehicles at conveniently accessible public outlets.

Rapid and ultra-rapid chargers mimic the operation of traditional gas refuellers in terms of recharging speed. These consume a greater quantity of energy from the grid over a shorter period. Rapid chargers are often more convenient for drivers who anticipate spending less time in certain areas (such as supermarkets and near highways and major A roads), or when the driver wants to charge immediately and is ready to pay a premium price for convenience (e.g., on a road trip or when you have a low battery level but are pushed for time) [34, 40, 41].

Overall, DC chargers are more costly to install and run than AC chargers since the power rating and the size of DC chargers are larger. Given the additional expense and strain on the grid, DC charging is generally not feasible daily. There is also another reason to avoid overloading on a rapid or ultra-rapid charger: it generates a lot of power, and handling it puts additional stress on the battery. Continuously using a DC charger is likely to reduce the lifespan of batteries [42].

1.3   Problem Statement

While electromobility has a promising future, its success and growth are inextricably linked to the hosting capacity of existing grids and the technology that enables widespread adoption of electric cars. Over time, the transition to electric mobility will alter the design and management of the entire power system to accommodate a significant increase in demand [10, 34, 37]. If many EVs are simultaneously connected to public charging stations during the network's peak load, the distribution network will experience increased congestion and loading issues. Increased EV charging will cause voltage fluctuations and voltage drops, increase power losses, and overburden distribution network equipment (such as cables and transformers) [43]. The severity of grid issues is significantly influenced by the time and location at which EV charging loads are charged and connected to distribution networks, respectively [34, 37].

The additional loads from widespread EVs may necessitate costly distribution system upgrades to maintain reliability; however, careful planning and innovative operations strategies can reduce or eliminate the need for such upgrades. In addition, EV charging infrastructure can support grid stability and improve distribution systems, particularly when coupled with distributed solar, storage, or equipped with smart charge management and grid-interactive support. This research proposes a variety of robust network reinforcement techniques, such as on-load tap changers (OLTCs), distributed generation (DG) units, static VAr compensator (SVC) devices, coordinated charging systems, vehicle-to-grid (V2G) chargers, and battery energy storage units, for mitigating the impact of increasing the number and rating of EV chargers on distribution networks and for expanding their hosting capacity.

1.3.1 Research Questions

The following research questions are answered in this thesis:

1. To what extent does the integration of EVs influence the operational characteristics of power networks at the transmission and distribution level? ii) What is the effect of increasing the uptake level of uncontrolled EV chargers?
2. (i) What technologies are feasible for connecting EVs without jeopardising the operational characteristics of distribution networks? (ii) How can the installation of transformer tap changers, DG units, SVC devices, coordinated charging systems, V2G chargers, and battery energy storage units enable the secure and reliable connection of EV charging loads in medium-voltage and low-voltage distribution networks?

3. (i) How can the hourly peak demand and energy consumption of rapid and ultra-rapid devices be estimated for different EV models? (ii) How often is the rated capacity of the substation transformer exceeded? (iii) In the worst-case scenario, what is the minimum size of a battery energy storage unit required for the network to operate safely? (iv) What is the minimum substation transformer size required to accommodate EV demand without becoming overloaded?

4. (i) How do the operating characteristics of lithium-ion batteries change under various discharge profiles? (ii) How can the battery State of Charge (SoC) and Depth of Discharge (DoD) be estimated experimentally under different discharge tests? iii) How much battery energy storage capacity remains when it is used to charge a group of EVs with different charging needs?

1.4 Thesis Objectives

Chapter 2 — Objectives: The current state-of-the-art in EV charging technology is reviewed to highlight the advantages and challenges introduced by the integration of EVs into grids. The main research gaps are also identified and discussed.

Chapter 3 — Objectives: The effects of increasing the number of uncontrolled rapid chargers are investigated on the steady-state operating characteristics of a generic High Voltage/Medium Voltage (HV/MV) distribution network. The IPSA+ Power simulation software and MATLAB are used to conduct load flow analysis under different scenarios.

1. A load flow analysis is performed (i) to calculate total active power losses and (ii) to examine steady-state voltage profiles with different EV uptake scenarios.

2. Tap settings have been calculated and installed on grid transformers.

3. Optimum locations of DG units and required sizing of SVC devices near critical network feeders are determined to eliminate voltage violations.

Chapter 4 — Objectives: Battery charger dynamics are developed and integrated into an AC grid to conduct dynamic load flow analysis in PSCAD/EMTDC (Power System Computer Aided Design/Electromagnetic Transients including DC) simulation software. The MC3000 battery charger unit is used to conduct tests with lithium-ion batteries.

1. The behaviour of a generic Shepherd battery model is demonstrated.

2. The charging and discharging characteristics of lithium-ion batteries are demonstrated under different settings.

Chapter 5 — Objectives: The interaction between slow, fast, rapid, and ultra-rapid charging technologies is investigated on the dynamic operating characteristics of a real low-voltage distribution network feeder.

1. Battery charger dynamics are integrated into a low-voltage distribution network feeder (i) to examine voltage fluctuations, (ii) to quantify cable overloading, (iii) to calculate power losses, and (iv) to calculate the cost associated with power losses.

2. The effects of i) upgrading the cable sizes, ii) using V2G chargers, and (iii) applying coordinated charging techniques are examined on the cable loading.

Chapter 6 — Objectives: A stochastic model is developed to estimate the charging demand and the energy consumption of different EV models with varying battery specifications. The maximum peak demand that is exerted on the substation transformer is also determined and the required sizing of the transformer is calculated to design a network for the worst-case scenario.

1. Different stochastic scenarios are produced, and the worst-case scenario is identified.

2. Stochastic charging profiles from the worst-case scenario are integrated into a real low-voltage distribution network feeder i) to quantify the hourly peak demand on the substation transformer.

3. The effects of V2G chargers and battery energy storage units are investigated on peak shaving.

4. The network is designed to operate safely under the worst-case scenario by installing a larger transformer based on the peak current and peak demand, and by accommodating the charging demand from battery energy storage units.

Chapter 7 — Objectives: Battery discharge profiles are developed and integrated into a physical battery charger and an analyser unit to investigate the capacity of stationary battery energy storage units that are used to meet the charging demand of different EV models with different charging requirements.

1. The relationship between the battery voltage and charging/discharging current, and battery voltage and discharge capacity are determined under different discharge profiles.

2. The SoC and DoD of the batteries are estimated under different scenarios.

1.5 Data Collection

Appropriate data collection methods (such as obtaining the modified network parameters and the responses from a vehicle charging survey) are significant for maintaining the integrity of research and reducing the likelihood of errors occurring. This section discusses in brief the process of collecting data on variables of interest.

The generic HV/MV British distribution network is modelled, simulated, and analysed in **Chapter 3**. This generic distribution network is modelled using the static PQ demand data of load busbars derived from [44].

EV batteries are emulated through computational methods to represent battery charging and discharging dynamics in **Chapter 4**. These are represented by the equivalent Shepherd models. The procedure for designing the Shepherd model and the parameter selection is available in the *Manitoba Hydro International Limited's Power Systems Technology Centre* [45, 46].

A real UK-based low-voltage distribution network feeder is modelled and simulated in **Chapter 5** utilising the line and demand profiles of British residential and commercial customers obtained from, *Western Power Distribution* (WPD), now National Grid Distribution [47]. Additionally, the updated line characteristics and cable installation parameters are obtained from WPD's ***Standard Technique: Relating to Low Voltage Underground Cable Ratings*** document [48] to analyse the effect of battery chargers on cables, and to calculate power losses and the cost associated with power losses.

The relevant data from [49] and [50] is obtained to calculate the percentile and daily distribution of fast- and rapid-speed charging events in the UK. The time distribution of charging events allows the method described in **Chapter 6** to generate stochastic charging profiles depending on the time of the day. Additionally, **Chapter 6** of this thesis integrates the survey results of 2,000 respondents from [51] to address and calculate the battery constraints and vehicle data, respectively.

Different lithium-ion battery packs are used for the experimental work. The MC3000 battery charger and analyser unit built by the SkyRC Technology [52] is used to analyse the charging and discharging characteristics of batteries under different settings.

1.6 Thesis Structure

The relationship between the main thesis chapters is demonstrated in Figure 1.4.
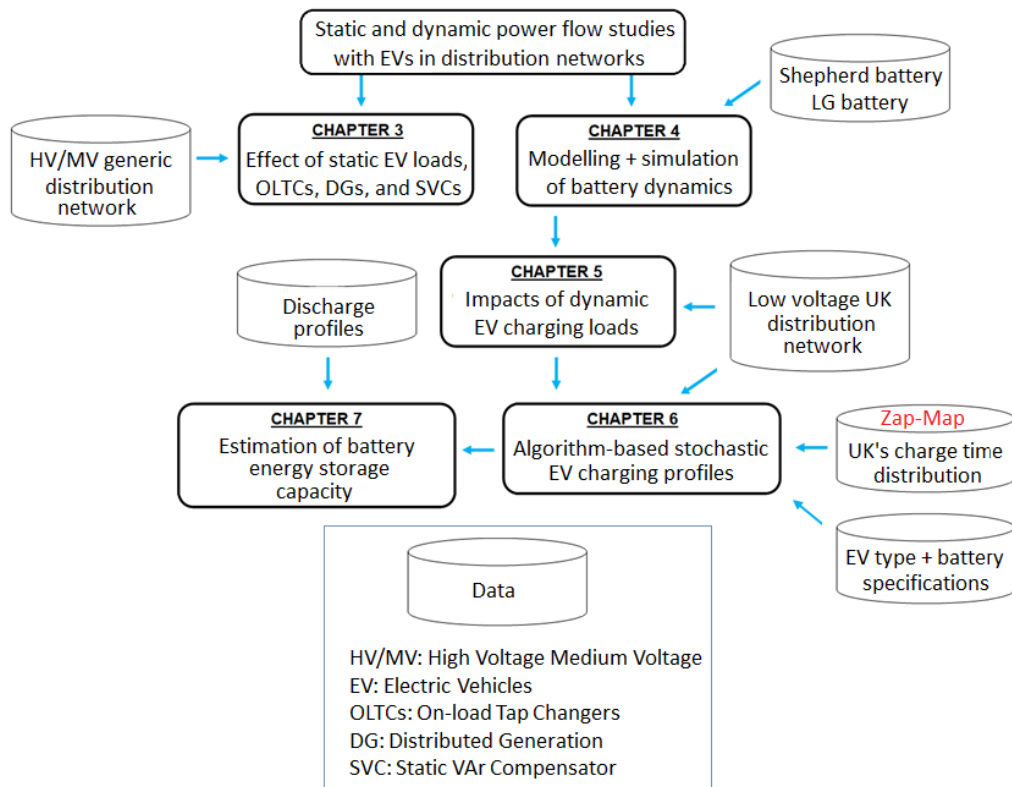
Figure 1.4: Relationship and flow between the main chapters.

Chapter 2: A comprehensive overview is given about (a) the global EV market growth and the current state of EV recharging technology, (b) the advantages associated with the grid-integration of EVs, and (c) the relevant field studies with respect to the modelling of EV charging loads, electrotechnical effects of EVs on distribution networks, and network reinforcement strategies, for addressing the main research gaps.

Chapter 3: A generic HV/MV distribution network is modelled to analyse the effects of increasing the uptake level of uncontrolled rapid chargers. It is demonstrated that the installation of tap changers on grid transformers and the optimal placement of DG units and SVC devices near critical points significantly reduces voltage deviations and active power losses.

Chapter 4: Battery charger dynamics are developed using generic Shepherd battery models. A physical battery charger is also used to conduct experimental work. This is a methodology chapter in which the battery dynamics are integrated into a low-voltage distribution network (for **Chapter 5** and **Chapter 6**), whereas in **Chapter 7** the physical charger equipment is utilised to conduct various tests with lithium-ion batteries.

Chapter 5: A real low-voltage distribution network feeder is modelled, and battery charger dynamics are integrated near different customers. A comprehensive network analysis is conducted to examine the effects of combining the operation of slow, fast, and rapid EV chargers.

Chapter 6: A algorithm is developed, and stochastic charging profiles are obtained for various EV models. The effect of stochastic scenarios is analysed on the low-voltage distribution network feeder. The effect of battery energy storage units is demonstrated on peak load reduction. The minimum required rating of the battery energy storage units and substation transformer is calculated to design a network to operate safely under the worst-case scenario.

Chapter 7: Stochastic charging profiles from **Chapter 6** are used to develop battery discharge profiles. These discharge profiles are then implemented into a physical battery charger and an analyser unit to investigate the operation characteristics of lithium-ion batteries.

Chapter 8: The work's main conclusions and results are summarised and presented. Suggestions for further study are made considering the main limitations and strengths in this research work.

CHAPTER 2

2. Literature Review

2.1 Introduction

Effective decarbonisation of the transport is entirely dependent on the development of a prominent global EV market, the establishment of a robust recharging infrastructure, and the deployment of regulatory frameworks [7]. Technical, sociological, economic, and political constraints must be overcome to achieve widespread adoption of EVs [20, 22]. Lack of charging stations and options (particularly in urban/metropolitan areas) [53], high charging infrastructure expenditures, high upfront vehicle prices, and long vehicle charge durations [21] are the main obstacles to EV adoption.

EV adoption in cities is influenced by situational and contextual factors. Situational factors, such as the city's location, cannot be changed. Vehicle ownership, on the other hand, varies based on the city's population, its socioeconomic context, the city's structure (politically and geographically) and the quality, accessibility, and frequency of other modes of transport [7, 21]. In 2020, ten million electric cars were on the roads of the globe. Sales of electric cars accounted for nearly 4.6% of total sales worldwide. The availability of electric car models expanded and new projects for vital battery technologies were initiated. The policies, which mostly consisted of purchase subsidies and/or car purchase and registration tax refunds, were intended to narrow the price gap between electric and internal combustion vehicles. However, to reach a trajectory compatible with the Sustainable Development Scenario and achieve full compliance with the *Paris Agreement* by 2030, 230 million EVs would need to be on the road [7, 21, 22].

2.1.1 Chapter Structure

- **Section 2.2** reviews the key enablers and barriers for electric mobility. Additionally, it reviews the relevant governance, global EV market growth, and the current state of EV recharging technology.
- **Section 2.3** reviews the advantages associated with the grid-integration of EVs. Recent projects and developments within Great Britain are also reviewed.
- **Section 2.4** reviews the relevant field studies and discusses the main challenges with the modelling and integration of EV charging loads in distribution networks. Research gaps are also identified and then related to the contribution of thesis.
- **Section 2.5** summarises and discusses the key findings of the chapter.

2.2   State-of-the-art of Electric Vehicle Technology

The electrification of the transport sector requires multiple enablers to make the transition a success [54]. The interaction between enablers is shown in Figure 2.1.
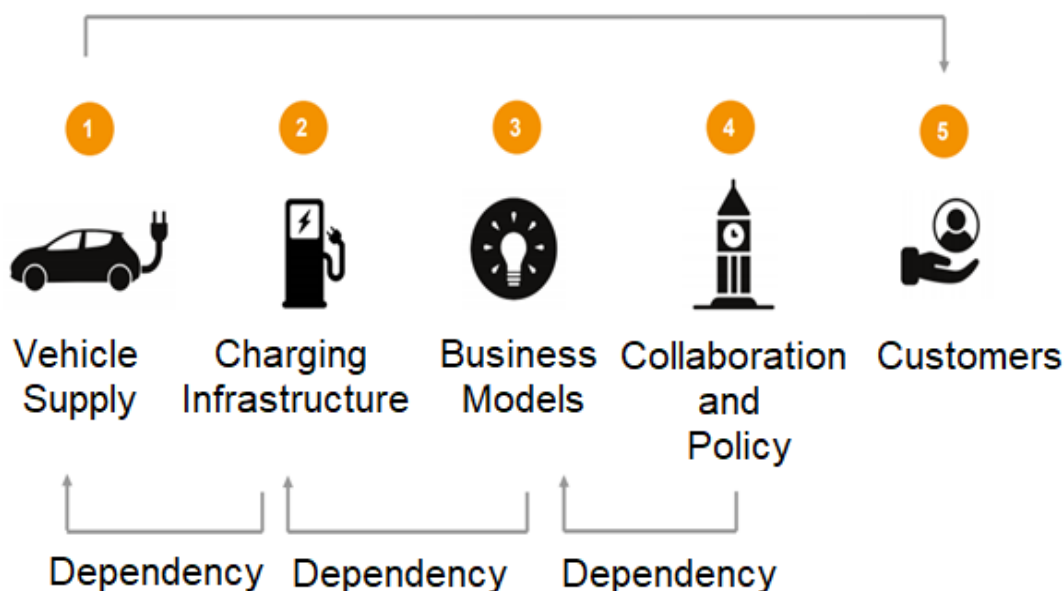
Figure 2.1: Key enablers for future of mobility.

The first enabling factor is an adequate **vehicle supply**. A competitive EV market with a diverse range of vehicle models is critical for expediting the transition. The EV supply chain is slightly distinct from the supply chain for conventional ICEVs. What distinguishes EVs is that they are mechanically simpler with fewer components, but their technology makes mass production more difficult.

Public charging infrastructure is an important area that requires further attention. Assuring an extensive recharging infrastructure is encouraging drivers to switch to electric. Additionally, expanded public recharging infrastructure alleviates drivers' concerns about range anxiety. A lack of charging infrastructure and lengthy charging durations contribute to range anxiety. Range anxiety can be alleviated in part by increasing the battery capacity. However, since this results in an increase in the vehicle's price and weight, the recommended course of action is to improve the charging infrastructure and reduce charging times.

The third enabler is **novel business models** and **finance mechanisms**. Costs associated with public charging infrastructure are prohibitively high, while charge station utilisation rates remain low. Therefore, novel business strategies and financial support are necessary to demonstrate the technology's potential [54].

The fourth enabler is **cooperation across sectors** with an effective government policy. The EV transition brings together a diverse range of industries, from automotive to energy, transportation, and public sector. Thus, cooperation across diverse sectors, as well as the appropriate amount of 'carrot and stick' from the government, are required to encourage ICEV drivers to purchase and switch to electric cars [54].

Finally, **customers**, who are at the centre of this transition, are a significant enabler. It is vital to raise consumer knowledge and demonstrate why switching to electric will benefit the environment and the individuals in society.

The high initial cost of EVs was a significant barrier in the beginning of 2010s. However, expenses are rapidly declining over the past few years, and the total cost of EV ownership (which includes operating costs) is already considerably near to, if not cheaper, than that of ICEV. As the market develops and volumes rise, economies of scale in all segments of the automotive industry and supply chain will result in further cost reductions over the next decade. However, the reduced battery prices will have the greatest influence on EV affordability.

Battery costs account for up to 40% of the initial cost of an average BEV. However, battery prices have decreased by 85% on average since 2010 and are likely to continue to decline in the upcoming years. Further cost reductions on this magnitude will alter the economics of EV ownership, resulting in an exponential EV sales growth within the next decade [55]. The technology is advancing, and the chemistry of batteries is developing on the market. Automakers and major fleet operators are taking long-term decarbonisation objectives seriously and speeding their electrification investments, while policymakers continue to drive the market towards lower emissions.

2.2.1 Government Perspective

Packages of policy incentives are provided in many countries to increase the attractiveness of EVs. As policy measures intervene with the generalised cost of EV-use, they can be considered as attributes of EVs that can be influenced by governments. Policy measures can be purchase-based and use-based incentives. An example of a purchase-based policy incentive is a subsidy for purchasing an EV or a tax refund for registering an EV. Examples of usage-based policies include the use of bus lanes and exemptions from congestion charging [20, 22].

Incentives are crucial for closing the significant cost gap between electric and gasoline vehicles [13, 21]. Purchase-based policy incentives decrease the fixed cost of EV-use, while usage-based incentives decrease the marginal cost of EV-use [20, 22].

In the UK, government interventions include funding industrial development to deliver the real reductions in emissions needed by establishing exemplar cities or regions that are pioneers in promoting EVs (e.g., Go Ultra Low Cities: Dundee, London, Milton Keynes, Nottingham, Oxford, York, the West of England, and the Northeast), encouraging market growth through incentives, establishing legal and regulatory frameworks for charging infrastructures, and deploying policies at the local level [20, 22, 56].

In October 2019, the UK government unveiled its decarbonisation strategy, while the *Department for Transport* defined six strategic goals and issued ***Decarbonising Transport: Setting the Challenge*** in March 2020 to provide the groundwork for the strategy's implementation [56]. These strategic goals are the (i) the decarbonisation of road vehicles, (ii) decarbonisation of how people get their goods and services, (iii) acceleration of model shift to public transport, (iv) tackling air quality and reducing carbon in a global economy, (v) introduction of place-based solutions (particularly at the community level), and (vi) consideration of the UK as a hub for green transport technology and innovation.

2.2.2 Global Electric Car Market Growth

In 2020, after a decade of strong expansion, the worldwide electric car stock hit the 10 million units, a 43% increase over 2019. Electric car registrations increased by 41% in 2020, despite the pandemic-related worldwide downturn in car sales in which global car sales dropped by 16% [57]. Sales of EVs doubled in 2021 from the previous year to a new record of 6.6 million. Back in 2012, just 120,000 electric cars were sold worldwide. In 2021, more than that figure have been sold each week.

In 2021, about 10% of global car sales were electric, four times the market share in 2019. This boosted the total number of electric cars on the world's roads to around 16.5 million, or three times the amount in 2018. In the first quarter of 2022, two million electric cars were sold worldwide, a 75% increase from the same period in comparison to 2021 [58–60]. Canada, China, Japan, the United States, and some major European nations have dominated the overall market over the past decade. The growth of global electric car stock in the last decade is shown in Figure 2.2.
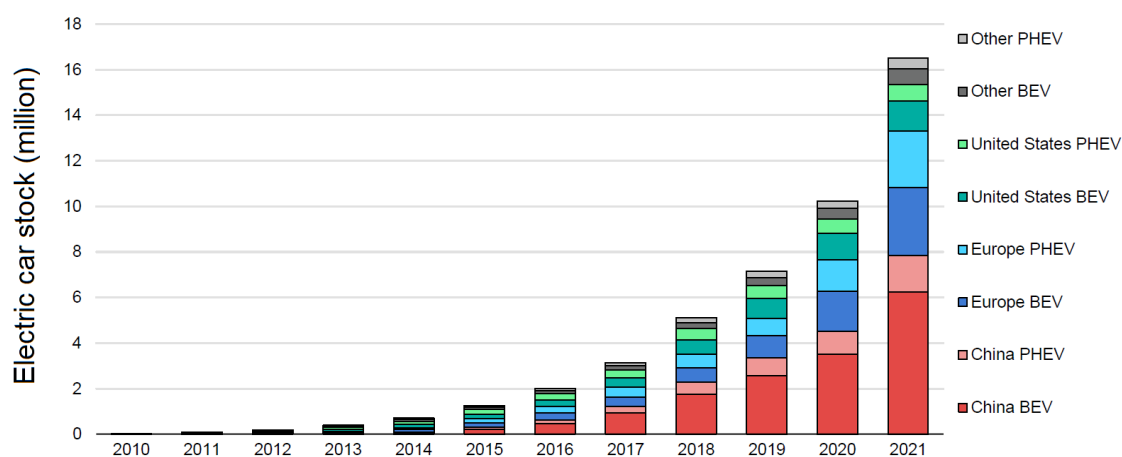
Figure 2.2: Global electric car stock: 2010–2021 [60].

The global electric car stock chart refers to passenger light-duty BEVs and PEVs only. The 'other ' legend includes Australia, Brazil, Canada, Chile, India, Japan, Korea, Malaysia, Mexico, New Zealand, South Africa, and Thailand, whereas Europe includes the EU27, Norway, Iceland, Switzerland, and the UK. Sales were highest in the People's Republic of China ("China" hereafter), where they tripled compared to 2020 to 3.3 million after several years of relative inactivity. China became the first country to phase in new energy vehicle regulations, exempt customers from taxes, acquire emission credits produced by EV sales, and considerably reduce imports from other countries [59, 60].

China and Europe accounted for more than 85% of worldwide sales of electric cars in 2021, followed by the United States (10%) where the sales have doubled from 2020 to reach 630,000 units. Sales in Europe increased by two-thirds year-on-year to 2.3 million. The Netherlands (82% of all electric car registrations), Norway (73%), the UK (62%), and France (60%) had the highest share of BEVs in Europe [58–60].

It is expected that there will be 11 million EVs by 2030 and 36 million EVs 2040 on the road in the UK, according to National Grid's *Future Energy Scenarios* [61, 62]. On the other hand, Japan's *Green Growth Strategy* established a rule that all new automobiles sold after 2030 must be electric to fulfil the country's 2050 net-zero targets. This approach needs the government to boost its investments by 30–50% beyond the 2020 level.

One factor for limited adoption in certain areas is the disparity in price between electric and gasoline vehicles. Additionally, in particular regions and countries, a shortage of home and workplace chargers is a contributing reason for a lower EV adoption [16, 58, 60]. Nevertheless, further improvements and lower battery costs suggest that BEV sales will expand at a higher pace in the next few years [16, 59].

2.2.3 Recharging Technology

Recharging is a significant component of a healthy EV ecosystem and requires significant developments and robust charging infrastructure to help achieve widespread market growth. Charging infrastructure is commonly referred to as a 'chicken and egg' problem, since both EVs and their charging technologies need the presence of the other. The creation of a charging infrastructure requires sustained EV adoption to reassure customers that there will be sufficient demand for the investment and expenditure [63]. A robust charging network and a variety of charging options, on the other hand, will not only be a technical need but also a crucial facilitator for customer acceptance [64].

With respect to facilitating customer acceptance, *NewMotion* conducted a survey to gain insight into improving the charging experiences for EV drivers. The most significant changes for a better charging experience included faster charging options (48%), improved availability of charge points (46%), and a single payment card to be used for all public charging stations (41%), as seen in Figure 2.3.
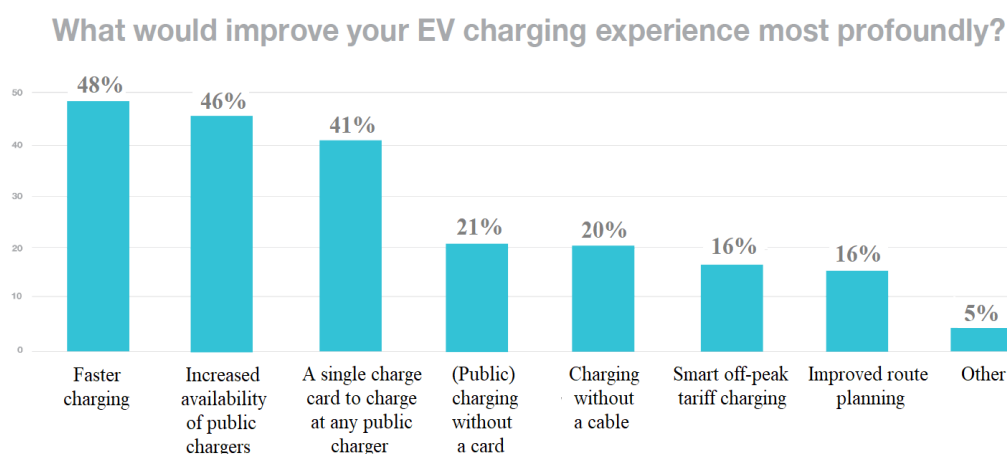
Figure 2.3: EV driver survey on improving charging experience [64].

Faster charging options are a significant improvement in the Netherlands, whereas in Germany, the UK, and France, the availability of charging stations is more important among drivers. The transition to a single card payment for a smoother charging experience at public outlets is also a key enabler among many drivers [64].

2.2.4 Charging Standards

Battery chargers come in different forms of connectors. These include Combined Charging System (CCS), the Japanese CHAdeMO (CHArge de Move — move by charge), the Chinese version operating under the GB/T, the Tesla Supercharger, and the ChaoJi standard (based on the combination of GB/T and CHAdeMO) [34, 65]. Over the past decade, the CHAdeMO and Tesla have gained widespread popularity [66].

Each connector is specifically engineered to operate at different ratings and levels. The specifications and the characteristics of each connector and charging standard are presented in Table 2.1.

Table 2.1: Characteristics of charging standards [65]

Standard	CHAdeMO	CCS Type 1	CCS Type 2	GB/T	Tesla	ChaoJi
Compliant Standards	IEEE/2030.1.1 IEC/62916-3	SAE J1772 IEC/62916-3	IEC/62916-3	IEC/62916-3	No related items	CHAdeMO and GB/T
Connector Inlet						
Max. Voltage (V)	1000	600	900	750	500*	1500
Max. Current (A)	400	400	400	250	631*	600
Power (kW)	400	200	350	185	250*	900
V2G Function	Yes	No	No	No	Unknown	Yes
Start Year	2009	2014	2013	2013	2012	2020
*: The specifications of Tesla Supercharger are estimated based on its market labels.						
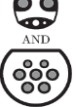
CCS has Type 1 (single-phase plug offers up to 7.4 kW) for the North American market and Type 2 (three-phase plug offers up to 43 kW) for the European and Australian markets. CCS is compatible with Audi, BMW, Opel, Phoenix, Porsche, and Volkswagen models, whereas CHAdeMO is compatible with Japanese models (such as the Nissan Leaf and Mitsubishi). The GB/T standard is exclusively available in China and India, whereas Tesla has its own charging standard, notably, the Supercharger.

2.2.5 Private vs Public Chargers

The primary choices are private or home charging, public charging infrastructure in dense regions, and long-distance public charging infrastructure on motorways [13, 20, 56]. There were around 7.3 million chargers worldwide in 2019, with 88.3% of them representing slow-speed private chargers, while 8.1% representing slow-speed public chargers and 3.6% representing fast-speed public chargers [67], as seen in Figure 2.4.
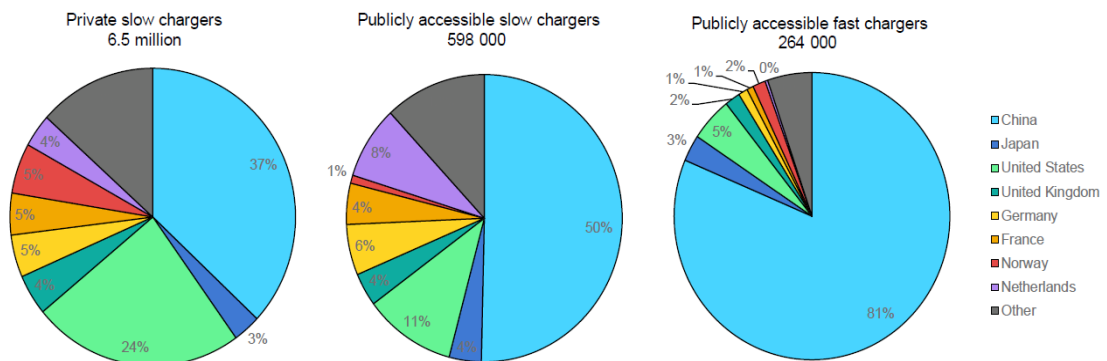
Figure 2.4: Private and public charger distribution by country: 2019 [67].

China accounted for 37% and 60% of privately and publicly accessible chargers, respectively. China's high percentage of ownership is a result of the country's quick deployment and rollout of chargers in dense metropolitan cities. China's achievement in promoting charger usage has also resulted in a sharp increase in the global number of publicly accessible chargers from 862,000 in 2019 to 1,300,000 in 2020 [54, 58–60].

As for the UK, the *European Alternative Fuels Observatory* (which is the European Commission's key reference portal for alternative fuels, infrastructure, and vehicles in Europe has shown that the number of charging points per 100 kilometres of road has increased from 42 in 2011 to 570 in 2019. Furthermore, *Highways England* (formerly the Highways Agency) has committed £15 million to ensuring that charge points are available on 95% of the Strategic Road Network (which includes motorways and some major A-roads) [54]. In November 2019, the *Department for Transport* produced a 'league table' of EV charging availability in local authorities around the UK, emphasising [68, 69]:

- At the end of 2019, there were more EV charging stations (around 9,000) than gas stations (around 8,400).

- There are over 100 local authorities with less than ten public charging devices per 100,000 of population.

- Installation of rapid charging stations is accelerating in cities and on highways. Over 95% of all highway service locations have at least one rapid charger.

- By 2030, the number of public rapid chargers required is estimated to grow from 4,000 in the last quarter of 2020 to 30,000.

2.2.6 Charger Archetypes

In the context of EV charging, 'where-to-charge' and 'how-to-charge' are significant. Each charging location is optimal for individuals with varying charging requirements. For example, publicly available AC chargers in urban areas are beneficial for those who are unable to charge at work or at home, while public DC chargers on highways are beneficial for those making long journey trips on or near motorway junctions.

The UK government has allocated £500 million to a public-private charging infrastructure investment fund to improve the charging infrastructure for new households and adopt a more centralised strategy to expand charger locations [68]. The proportion of EV public charger types in the Southern and Scottish Electricity Network (SSEN) connection zones of the UK is shown in Figure 2.5.
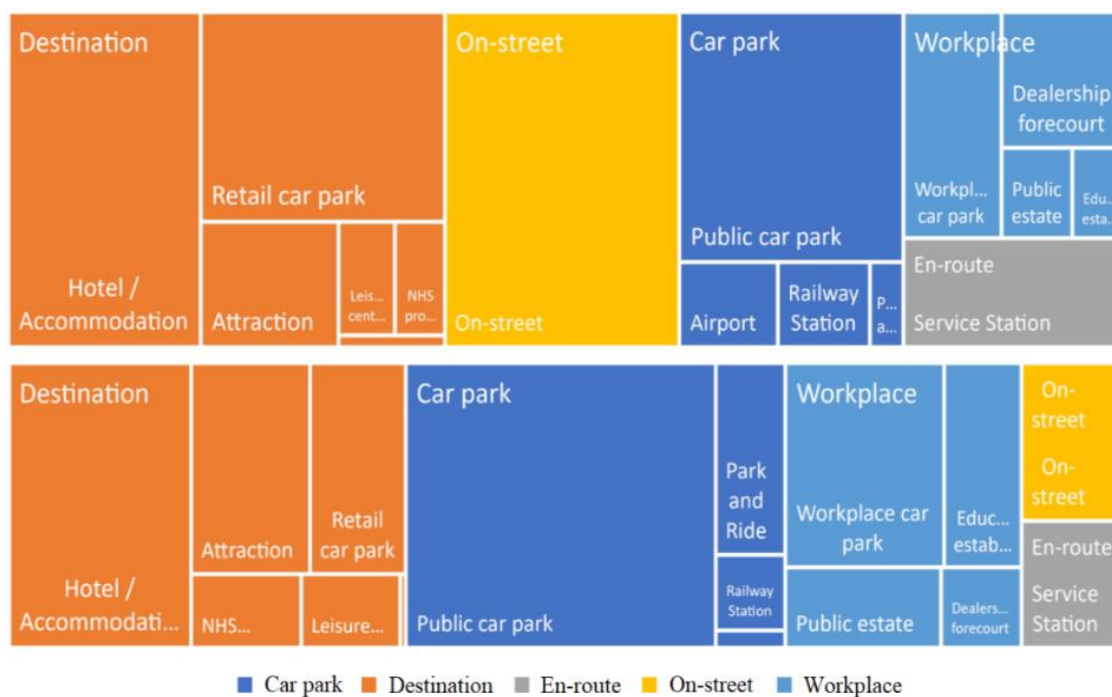
Figure 2.5: Proportion of charger locations in the Southern (top) and Scottish (below) zones [68].

The area size reflects the percentage of EV chargers in each category within SSEN connection zones. Scotland has a larger share of charges in public car parks, public workplaces, and other public venues. Different government initiatives in each licence region could partially explain these disparities. ChargePlace Scotland, a nationwide network of EV chargers built by the Scottish government with grant money from local authorities and other organisations, operates around 73% of EV chargers in Scotland. This more centralised approach to charging infrastructure has increased the amount of EV chargers in centralised public parking areas such as car parks, park and rides, public estates, and educational facilities [68].

In the Southern licence region, the bulk of charging infrastructure is privately operated. Approximately 50% of the chargers in this region are managed by Pod Point, POLAR, and Ubitricity. This has resulted in a more dispersed EV charging infrastructure, including on-street, shop parking lots, hotels, and other tourist destinations [68].

2.2.6.1 Home Charging

Private home chargers account for over 90% of all chargers installed globally. Drivers find charging at home quite handy since it needs no new infrastructure and EVs can be charged using the existing standard electrical outlets. Home charging is much cheaper than using public infrastructure, particularly during periods when the night-time energy costs are lower. Under the **Electric Vehicle Homecharge Scheme**, the *Office for Zero Emission Vehicles* (*OZEV*) is granting homeowners incentives with funding for 75% of the costs of installing charge point in a UK domestic property [70].

Consumers who own EVs can either have a wall box put on the outside wall of their houses or utilise the vehicle's included portable slow-speed charging cable. The latter variant utilises a conventional three-pin connector and is powered by a household source. The cost of installing a home charger is determined by the charger's smart features. For example, a 7-kW wall box unit costs around £300 to install, whilst a simple 3-kW charger costs approximately £100 to install. Certain automobile manufacturers even provide a complimentary wall box fitting with the purchase of their vehicles [70, 71].

2.2.6.2 On-street Charging

Around 24% of people in England have no access to off-street parking [72], and hence on-street chargers are beneficial for these who have no access to off-street parking. The *Energy Savings Trust* administers the **On-street Residential Chargepoint Scheme**, funded by *OZEV*. This funding is available to local authorities to encourage individuals by increasing the availability of on-street charge points in residential streets.

On-street charging is emerging in the form of using the existing street infrastructure and converting lamp posts into charge points. This contributes to the reduction of power consumption of lamp posts. Ubitricity is one of the first service to emerge, who is responsible for integrating this type of charging equipment into the existing street furniture and providing its customers the option of purchasing a smart cable for charging through lamp posts around London. Spring of 2020 saw the installation of approximately 200 lamp post chargers operated by **EB Charging** in Brighton, thanks to *OZEV* funding. Some places have dedicated parking, while others are shared. These chargers are accessed through a smartphone app that manages accounts and payments [73].

Connected Kerb, a British company, is creating new kerbside chargers with the intention of assisting individuals lacking off-street parking by providing new charging infrastructure alternatives. The charging post utilises the home's electrical source. There is a parking space designated as "EV permit holder" to guarantee that parking is accessible for the owner, along with appropriate notice on the owner's garden wall [73].

2.2.6.3 Workplace, Fleet Charging and Destination Charging

Chargers are often provided at workplaces for the usage of workers who travel to work. Workplace chargers are similar to home chargers in terms of recharging speeds but often use a Type 2 connector with a three-phase connectivity [74]. The *OZEV* originally provided a voucher-based **Workplace Charging Scheme** to assist qualified enterprises and organisations with up to 75% of the upfront expenditures (up to £350 per socket) and installation costs of a workplace charger [75].

Commercial fleets may charge their vehicles wherever there are public charging stations or at charging depots. Electrification and charging of fleets seem to be a significant business opportunity. Employees, workplace, car-sharing, logistics and service (delivery trucks), municipalities (large commercial vehicles), and public transit (buses and taxis) are all examples of fleet vehicles [76]. This charging method is classified as charge at work, charge at depots, and charge on-route. Car-sharing fleets now need an average of one rapid charger for every ten electric cars, while urban electric buses require one ultra-rapid charger for the start and finish of their routes [76].

Destination charging is provided using closed networks of chargers. Tesla's charging network exemplifies a closed network of chargers with a broad network of destination chargers [77]. This method of charging is often designed in locations where the vehicle intends to stop for a limited period (e.g., at a shopping mall or at a restaurant). Although many destination chargers are free to use, it may sometimes be necessary to reserve and book a charging space in advance.

2.2.6.4 On-route and Hub-based Charging

On-route charging is associated with public places where the motorist spends even less time charging the vehicle (e.g., while buying a coffee at a service station). This type of charging can provide higher energy to the vehicle per charging session. Recently, there has also been a considerable interest in charging through hubs. This kind of charging infrastructure comprises the establishment of a single location with a range of charging services to accommodate motorists' varying needs. The list of hub-based charging projects in the UK is shown in Table 2.2.

Table 2.2: Developments for hub-based forecourt charging projects in the UK

Company	Location	Number of Charging Devices
GRIDSERVE	Essex	6 AC chargers (22 kW)
		24 DC chargers (90–350 kW)
Go Ultra Low West (GULW)	Bristol & Bath Science Park	1 AC charger (7–22 kW)
		5 DC chargers (50-kW)
Energy Superhub – Led by Pivot Power and Oxford City Council	Oxford	16 AC chargers (7–22 kW)
InstaVolt	Banbury	8 DC chargers (125 kW)
BP Pulse	Around the UK	24 DC chargers (300 kW)
HyperHub (EvoEnergy)	York	4 DC chargers (50 kW)
		4 DC chargers (150 kW)
Shell	Fulham	9 DC chargers (175 kW)
Osprey	Around the UK	12 DC chargers (150–175 kW)

Ecotricity and GRIDSERVE Sustainable Energy Limited are pioneering this industry to generate demand for significant expansion of EV charging infrastructure in the UK [78, 79]. In December 2020, the UK's first and most advanced charging station forecourt, which provides simultaneous charging for 36 cars (6 AC chargers, 24 DC chargers, and 6 Tesla chargers) and has a food court and shop space on-site, has opened to the public.

While many EV drivers charge at home or at work, public rapid charger networks in the form of hub offer vital charging assistance and the ability to expand travel distances. Most hub-based charging networks provide a range of charging choices, including slow, fast, and rapid chargers. These hub-based facilities reassure the public that the UK will have the charging infrastructure necessary for widespread EV adoption.

2.3   Grid Benefits Provided by Electric Vehicles

National Grid estimates that without smart charging and V2G technology, EVs may increase today's demand by 30% and add up to 24 GW to peak demand by 2050 [80]. The EV batteries are crucial in the transition to decentralised systems, alleviating certain grid constraints and improving network capacity. EVs can also participate in grid-to-vehicle (G2V) and V2G services based on the direction of power transmission between the grid and the vehicle. G2V effectively charges EVs by directing electricity from the grid to the vehicle (unidirectional power flow), whereas V2G enables stored energy to be released to the grid through an EV battery (bidirectional power flow). Additionally, electricity may flow between a building and an EV, in which case the EV can power the building if it is not in use [43, 81].

2.3.1 Vehicle-to-Grid

V2G has garnered considerable interest and is seen as an intriguing 'win-win' solution for both the environment and the user. The technology enables EV owners to generate new revenue streams and results in energy bill savings by storing and discharging energy back to the grid or their own properties when it is most needed (particularly during peak demand and when the energy prices are high) [82]. The potential net returns from a V2G charger vary between $90 and $4,000 each year, depending on the power capacity and electrical connections of grids [83].

While V2G has several advantages, there are also certain obstacles. With more frequent charging and discharging, V2G can shorten the lifespan of a battery, even if only a small fraction of its capacity is utilised daily. Energy is also lost during the V2G, as current efficiencies range between 50% to 70%. The specialised hardware for V2G makes V2G expensive [81, 83, 84].

Through their own experimental V2G programmes, Octopus Energy, EDF Energy, OVO Energy, and Electric Nation are contributing to the development of a better grid in the Great Britain [82]. Electric Nation has installed the first of 100 V2G chargers in January 2020 as part of a trial with multiple energy suppliers to investigate the effects of V2G charging on low-voltage electricity networks, assist Distribution Network Operators (DNOs) in gaining a better understanding on the technical and economic aspects of V2G chargers, and in providing recommendations for a commercial and policy framework to foster collaboration in the energy market [85]. Table 2.3 contains a detailed list of V2G trials conducted by different lead partners over the past few years in the Great Britain.

Table 2.3: A list of projects and lead organisations for V2G trials in the Great Britain

Project Title	Lead Partner	Description	Services Offered
PowerLoop	Octopus Energy	It is a domestic V2G demonstration project that contains 135 chargers and is used for home energy management.	Arbitrage Distribution services Time shifting Emergency backup
V2GO	EDF Energy	Through real-world V2G field experiments from 100 EV charging sites, the project focused on V2G for EV fleets.	Arbitrage Frequency response Time shifting
Sciurus	OVO Energy	One of the biggest residential V2G initiatives, which installed over 300 bidirectional V2G household chargers at no cost.	Arbitrage
e4Future	Nissan Motor	A large-scale V2G demonstration also focuses on fleet vehicles, using up to 1,000 BEVs.	Arbitrage Distribution services Frequency response Time shifting
Bus2Grid	SSE Services	A multi-megawatt large-scale demonstration of the V2G technology with the goal of charging 28 electric buses at London depots.	Arbitrage Frequency response Time shifting
EV-elocity	Cenex	A techno-economic business model for the V2G will be assessed in business parks and airports.	Arbitrage Time shifting
E-Flex	Cisco International	Using active EV fleets to demonstrate the V2G technology's value chain and economic advantages to commercial fleet owners and regulators.	Distribution services Frequency response Time shifting

The Department of Business, Energy, and Industrial Strategy and the OZEV funded the V2G programmes, which was implemented by Innovate UK (non-departmental public entity operating at arm's length from the Government) as part of UK Research and Innovation. These initiatives were also partially sponsored by the Network Innovation Allowance, which is part of *OFGEM's* (*Office of Gas and Electricity Markets*) regulatory strategy to ensuring that adequate income is generated through incentives, innovation, and outputs to operate the networks effectively [82, 85, 86].

In addition, the *Vehicle-to-Grid Britain Project* offers a better understanding of the fundamental factors influencing the V2G's roll-out. This project aims to determine the long-term viability of V2G opportunities in British power markets, to quantify the size of potential opportunities under various scenarios, to highlight key market drivers, and to provide insight to stakeholders [86].

2.3.2 Storage Entities with Vehicle-to-Grid Capability

The capacity of EVs to store energy generates new value propositions for V2G services. The V2G is an effective solution for ensuring grid stability when a renewable energy, such as a battery energy storage, is included. The V2G also improves the grid's self-balancing capability, which is critical when renewables are integrated into the grid [37]. For example, by using a V2X technology (vehicle to anything) or vehicle-to-building, renewable energy sources are utilised to lower the system's peak demand. Mobile energy storage and supply flexibility enabled by V2G reduce the requirement for generation and transmission expenditures while increasing energy security and network efficiency.

Electric fleets can also participate in V2G services to achieve economies of scale, provide active power support and frequency control to power grids, store excess renewable energy generation, participate in demand side response, and implement load levelling and peak load shaving [20, 81, 87]. The concept of load levelling and peak shaving through V2G is shown in Figure 2.6.
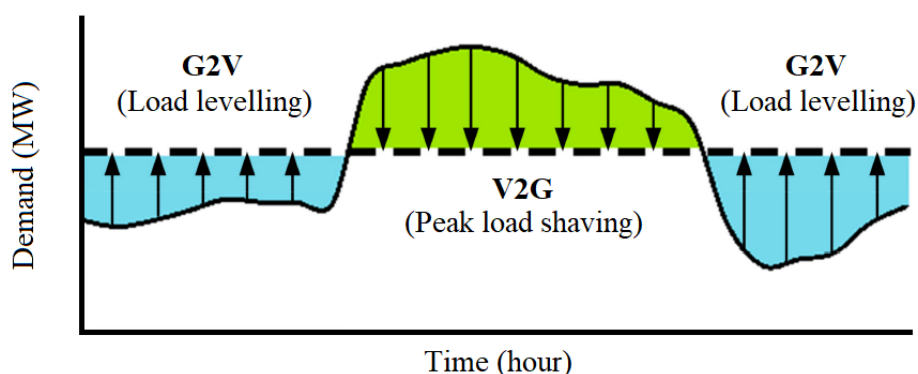
Figure 2.6: Load levelling and peak load shaving with EVs [88].

Utilities need to balance their generation capacity with the consumption of customers. Customer demand and consumption patterns are not constant as they vary from peak load to minimum baseload throughout the day, as shown in Figure 2.6. Load levelling decreases large fluctuations in customer demand that occurs because of the variations in the electrical demand. This approach stores additional power during periods of light loading (off-peak hours), particularly after midnight. It also involves delivering the stored power during periods of high loading. On the other hand, peak shaving minimises spikes in demand and smoothens peak loads out during periods of high demand. With an on-site battery energy storage unit, one can charge his batteries when electricity rates are cheap (i.e., during off-peak hours or with your free solar energy), and then discharge those batteries to avoid paying peak prices during the most expensive times [83, 89].

2.3.3 Solar Power

Innovative battery solutions are solar energy's strongest allies. Solar energy has paved the road for a future of affordable clean energy during the last decade. Now, with a little more innovation and widespread deployment, batteries, whether in EVs or as stationary storage systems, will enable the growth of solar photovoltaic (PV) to enter a new, even faster phase. Solar combined with a battery energy storage system is one of the most effective methods to reduce and shave peak loads during periods when electricity costs are high. Solar combined with storage also has the capability to optimise the building's energy consumption, and to charge and discharge EVs at ideal times to minimise and smooth out peak loads, and lower the cost of demand charges [89, 90]. The GRIDSERVE's hub-based forecourt adheres to a 'sun-to-wheel' principle, with a part of the energy used produced locally through solar canopies built above charger cabinets. Additionally, there is a 6-MWh battery storage system on-site that assists in balancing the local energy grid and shifting energy usage to useful and cheaper periods [79, 91].

Several research studies have already shown that customers strongly favour solar energy [92]. For example, it is demonstrated that those interested in purchasing an EV are also interested in solar energy (and vice versa), and are therefore likely to acquire both, but not necessarily at the same time [93]. Recently, companies such as Tesla and Sonnen noticed the growing consumer desire for integrated EV and renewable energy offerings and began providing packages that include an EV and solar PV charging applications [94–96]. Another research discovered that offering an EV with solar-powered charging to homeowners increases their desire to purchase an EV [97]. This is a particularly important conclusion, since it implies that these types of packages can simultaneously accelerate the adoption of EVs and solar energy, both of which are mentioned by the United Nations' *Emissions Gap Report* [92].

However, individuals who are renters, or who are unable to install their own solar panels (such as due to the high upfront cost or a lack of sunlight on their property), currently have no option for charging their EVs at home using personal solar PV units. Therefore, a sizable portion of the market is generally excluded from the advantages of a product package consisting of a solar system and an EV [92].

2.3.4 Smart Charging

Smart charging refers to a system in which the car and charging unit communicate through a two-way communication protocol while exchanging information and data. This two-way communication enables the adaptation of a smart charging cycle according to the driver's and the grid's needs. Through two-way communication, drivers can monitor and regulate their charging and discharging cycles, while also optimising the energy use of their households, without overloading the grid [12, 37].

The ***Automated and Electric Vehicles Act 2018*** empowers the government to require that all charge stations supplied or built in the UK have smart functionality through primary and secondary legislation [98]. Smart meters will also help EVs move into the mainstream. Around 35% of homes in the EU have smart meters installed as of 2018. Smart meter penetration is expected to reach 77% and 92% in 2024 and 2030, respectively. Other nations, like Denmark, Estonia, Italy, Malta, Spain, and Sweden, currently have smart meter adoption rates of more than 80% [99].

Different forms of smart charging methods have been and continue to be tested with customers, with the aim of determining their possible system impacts. For example, tariff schemes with defined peak and off-peak periods can effectively shift vehicle charging away from times when the demand is at its highest [12]. The concept of smart charging of EVs is demonstrated in Figure 2.7 and Figure 2.8.
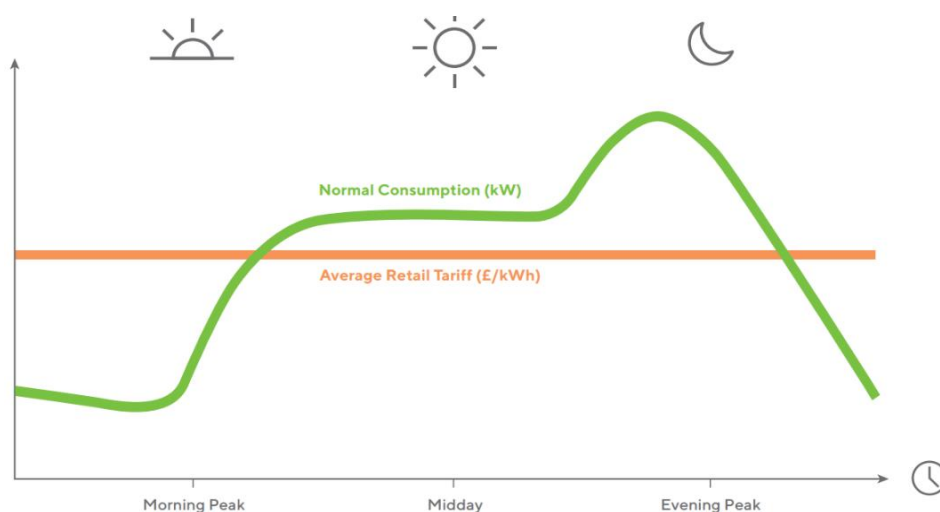
Figure 2.7: Impact of dumb charging on daily energy consumption [12].
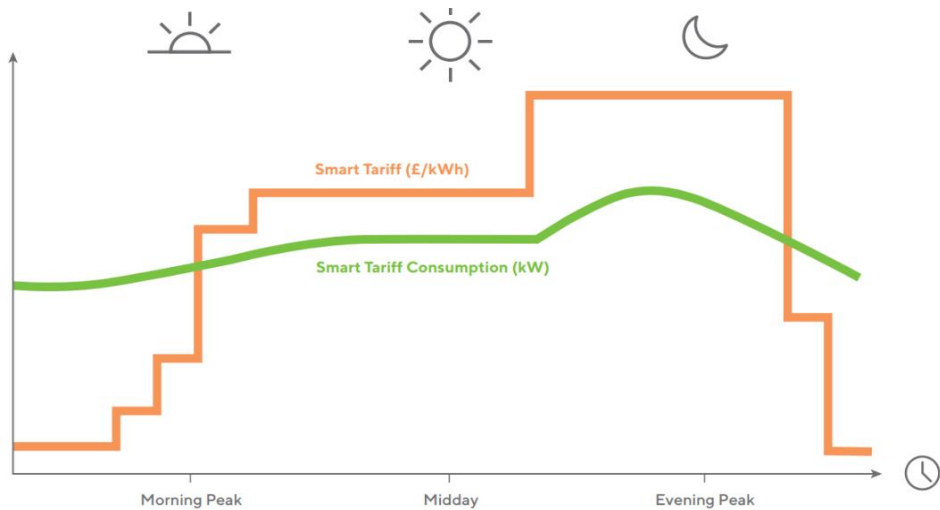
Figure 2.8: Energy consumption with smart tariff and charging [12].

It is seen that charging EVs without using smart methods (i.e., dumb charging) increases evening peak demand. With smart charging and intelligent pricing signals, EV charging may help eliminate excessive demand variations while saving EV owners money by moving charging load to off-peak hours [100]. If the charging infrastructure is not designed and operated as an integrated part of the evolving smart grid, significant costs will be incurred, which will eventually be met by consumers. These costs can be considerably lowered if EV charging is seen as a flexible resource that adapts to the requirements of the electrical grid. Smart charging has the potential to result in cost savings for DNOs, and even offers valuable flexibility resources for households [100].

2.3.5 Ancillary Services

Grid reliability, supply and demand balance, and power transmission to buyers can be maintained by ancillary services that are necessary in a power system. When a V2G system is bidirectional, it can provide higher-quality ancillary services, improved voltage regulation and frequency control, load management, and efficient spinning reserves. The National Grid Electricity System Operator (ESO) has increased the range of technologies able to participate in its ancillary services market. The new platform for ancillary services optimises power access by enabling demand side management [101, 102]. EVs, for example, have the potential to significantly increase localised demand flexibility by enabling consumers to reduce or shift their electricity consumption during peak periods (for example, demand side response services incentivise businesses to shift their electricity consumption in response to a signal ensuring the safe operation of the electricity systems) to help the ESO and local DNOs [101, 103, 104].

At larger penetration levels and for the supply of near-real-time balancing and ancillary services, more complex smart charging techniques, such as direct control mechanisms (active power control and reactive power control, will be required. For example, the *Vehicle-to-Grid Britain Project* evaluated the long-term feasibility of V2G potential in British power markets, specifically their capacity to contribute to a flexible energy system. It was discovered that import savings and arbitrage possibilities would increase, but their sustainability will rely on the effect of battery degradation [83]. In conclusion, there is a continuous change in the requirements and commercial arrangements for ancillary services at the ESO and DNO levels, and competing technologies are becoming more diverse, so the business models of EVs must be flexible and adaptable to navigate this complex market [86, 101–104].

2.4 Related Work

While the expansion of EVs and accompanying charging stations benefit the environment and concomitant economic growth, EVs also introduce negative effects based on how they are connected to the power grid and how they are charged [37]. EV integration is generally classified by two charging schemes: uncontrolled and controlled charging. Before considering alternative methods or techniques to reduce the negative impacts in the grid, it is necessary to understand them.

Uncontrolled (also termed as uncoordinated) charging (i.e., no restraints on the charging of the vehicle, with all residents allowed to charge any time throughout the day) causes increased peak demand, since charging often happens when residents get home from work, resulting in most of the energy demand from charging occurring during the peak period. An increased number of EV charging activities during the network's peak load, for example, will alter the planning and management of all grid-connected operations, introduce voltage fluctuations, increase power losses, overload distribution network equipment (such as cables and transformers), and introduce power quality issues (such as current and voltage harmonics) [43]. According to a study, uncontrolled EV charging has the potential of increasing the daily peak demand from 3% (3.2 GW) up to 60% (37 GW) in the Great Britain [105].

Controllable charging, also known as managed charging (restraints are applied while charging the vehicle by offsetting the charging time of any resident to off-peak hours), is thus seen to be the preferable method, in which EVs are charged at the time specified by DNOs [43, 81]. Through managed charging options, utilities have the capability to remotely regulate vehicle charging to better match the needs of the grid.

When it comes to the effects of EVs on the grid, the current literature focuses primarily on decentralised or high-voltage transmission grids' electrotechnical effects [106]. Only a few studies have attempted to incorporate both, but these have not established a convincing link between different voltage levels. On the other hand, many studies have been conducted in recent years to investigate charging strategies that may mitigate the negative effects of EV charging on the distribution grid and the capacity of available electricity generation to meet the increased load. In addition, the uncertainty factors of charging behaviour of EVs are regarded as a crucial input for modelling EV loads; however, these are often overlooked in the literature [107]. The plug-in time (charging-start time), charging duration, and location of EV charging have a significant impact on the severity of grid issues [34, 37]. To analyse the effects of EVs, a dependable model capable of simulating the travel patterns of a large fleet of EVs and their charging demand at various locations are required [108].

This section is subdivided into four parts comparing, contrasting, and synthesising the available literature relevant to the (i) modelling of EV charging loads (**Section 2.4.1**), ii) electrotechnical effects of EV charging loads incorporating different network voltage levels (**Section 2.4.2**), iii) network reinforcement strategies to mitigate impacts on the grid (**Section 2.4.3**), and iv) main research gaps that are addressed (**Section 2.4.4**).

2.4.1 Modelling of Electric Vehicle Charging Loads

System operators must ensure supply stability and security by tailoring the grid structure and operation to the network's individual features and components. System operators are also interested in accurately estimating the charging demand to anticipate the consequences and requirements of infrastructure upgrades with large uptake levels of EVs [109]. However, the charging demand of uncontrolled EVs is difficult to estimate due to small number of registered actual cases and uncertainties associated with individual driving behaviour and non-linear charging profiles of various EV models [110].

In the literature, most authors have modelled EV charging loads based on travel data and consideration of generic vehicle specifications [111], while ignoring a few crucial factors [112]. Some studies assumed that EVs have a constant adoption rate [113], travel a constant daily distance [114], are charged at the same time [115] and same rate [116], and have the same energy consumption [117, 118]. However, since the nature of EV charging is more stochastic, other dynamic factors should also be considered by exploring the non-linearity of charging parameters for developing more accurate estimation models [119].

Deterministic and stochastic models are generally developed to represent the charging pattern of EVs and their corresponding load patterns in distribution networks [112]. In deterministic models, distribution network constraints are used to estimate the threshold level of EV penetrations at which thermal ratings would be exceeded. For quantitative analysis in probabilistic studies, stochastic models are utilised to simulate the randomness and heterogeneity of EVs [120]. Deterministic models are mainly used for evaluating the long-term effects of EV charging [121] and are not applicable for evaluating the short-term effects [119].

2.4.1.1 Deterministic Approach

Early studies that modelled the charging requirements of EVs mainly relied on the utilisation of a deterministic approach. In this approach, it is assumed that charging begins at a fixed time after the completion of the final trip of the day or whenever the vehicle is parked at home [122]. Variation in estimated charging demand is then solely attributable to varying vehicle use, which is generally taken by sampling raw vehicle data [113] or providing a relative likelihood that the value of the random variable (i.e., energy use and arrival times of the vehicles) would be close to that sample [123].

Deterministic models generally involve simplistic scenarios and assumptions. For example, it is assumed that EVs would make three 40 km trips per day and only be charged after these trips [124]. However, the total distance covered by each EV is in fact different. In another study, it is assumed that EVs are always charged at 18:30 at home [125]. The selection of this time is to represent the daily charging activity of residences at home. However, this assumption is mainly attributable to private chargers that are installed at home and ignores the utilisation and distribution rates for public charging stations. The impact of V2G charger on lowering the peak demand is analysed, with all EVs available for V2G charging at 18:00 [126]. Similarly, this is a very simplistic assumption because EVs typically participate in V2G schemes when their batteries are fully charged, which is unlikely in this instance given that this time of day is generally considered as the plug-in time for majority of EVs with depleted batteries.

For the estimation of potential structural and economic effects of EVs, such as on charging infrastructure, power supply, and power prices, diverse EV charging models are required, which indicate at what point in time how many EVs are being charged at what locations and how much energy is required to charge them. Due to the computational effort required to model detailed driving and charging patterns, energy-system models commonly aggregate EV-specific loads [127]. The aggregated EV load profiles under uncontrolled and controlled charging scenarios are estimated through deterministic modelling to study the impact on the energy system [128].

Some research has also been carried out with uncertain factors associated with solar PV output and charging power of EVs by relying on load flow analysis. Load flow can analyse the operating characteristics of a power system under various uncertainties. The randomness of power generated by PV and the randomness of charging profiles of EVs are modelled by deterministic load flow models [129]. It is demonstrated that the annual yield of the PV panels (kWh per capita) is higher than the charging load of the EVs [130]. Another study found that the PV production in the day can accommodate the EV charging load in the evening [120]. The load flow analysis is carried out to provide cumulative density functions of branch power flows, nodal voltages, and line losses for many EVs [131]. However, assumptions show that the plug-in time for EVs is always predefined in these studies.

2.4.1.2 Stochastic Approach

Stochastic models have steadily attracted more interest as they tend to yield higher accuracy than deterministic models [108, 132]. Stochastic models are better suited for estimating the load profiles that utilities and system operators may use to modify their infrastructure to support a high penetration of EVs and their charging methods [111, 112]. These models need to be developed by considering variables associated with individual EVs, including their plug-in time, charging locations, SoC levels prior to charging, and battery capacity [133]. In addition, the computation of other more complex variables, including non-linear charging profiles [134, 135], charging duration [136], cumulative power demand, energy consumption of vehicles during charging [135], travel patterns [137], and the number of EVs being charged concurrently, must be considered in these models. Due to uncertainties and/or a lack of data, it is difficult to consider all these variables at once, so the majority of the existing literature makes assumptions about certain charging parameters.

Estimating the energy consumption of EVs is a complex task due to the inherent difficulty in predicting when an EV will start charging and how long it will stay connected to the grid [113]. It is suggested that the energy consumption of vehicles conforms to a predefined probabilistic distribution, rather than the characteristics or behaviours of the drivers [138]. However, this variable is also affected by the initial battery SoC of the vehicles [139]. The authors of [140, 141] estimated the energy consumption of vehicles by assuming a constant charge power over a defined time. Similarly, the daily charging power of vehicles is calculated based on the ratio of their energy consumption to charging over time [142]. These authors did not consider the non-linear characteristics of battery charging and assumed that charge power and energy consumption stay constant until the vehicles reach their final/target SoC levels. However, this is a very

simplistic assumption because the relationship between charge power and battery SoC is not linear. In **Chapter 6** of this thesis, the non-linearity in the charge power with respect to an increasing battery SoC is implemented to accurately determine the energy consumption of different EV models with varying battery specifications.

In the literature, many stochastic models are developed to investigate the effect of EV charging on residential areas. These models typically use home-related parameters, such as time of departure of EVs from home, arrival time of EVs at home, and daily travel distance of EVs, while ignoring variations at different locations and making simplistic assumptions [108]. A preliminary analysis of the effect of EVs on residential power grid is analysed [143], whereas a technique for determining the charging time of EVs in residential regions is proposed in another study [144]. The estimation of charging demand of private urban EVs in the residential area is also studied, based on the factors including parking and charging characteristics of EVs [145]. The charging load model for EVs in residential areas is developed [146], and the issue of peak-load superposition is investigated by analysing the simultaneous charging rate [147]. The authors extracted the hourly aggregated load demand of a fleet of PEVs [148] and quantified the power delivered to them through a domestic transformer [149]. In most of these studies, however, the vehicles are of the same generic type with same battery specifications. It is also assumed that the arrival time of EVs to start charging at home is uniformly distributed and hence the overall load always peaks between 17:00 and 18:00 for distribution networks [139]. Using different probability density functions, the impact of domestic uncontrolled EV charging on the voltage and line thermal [150], and transformer overloading is investigated [151].

In [152], stochastic EV parameters are used to model the travel pattern of EVs under the assumption that EVs are only charged at home. The modelling method of EV charging load in residential areas is simulated using the distribution characteristics of SoC levels and the arrival times to the charger [153]. The distribution of SoC levels may have a significant role in determining the power requirement, since EVs with higher average initial SoC levels prior to charging may need less charging power [154]. Using the Gaussian distribution to simulate arrival times, charging times, and departure times for an EV fleet, an illustration of the stochastic charging scenario is also presented [155]. However, the Gaussian distribution does not reflect the actual law with the stochasticity nature of EV charging [145]. Modelling the total charging demand for an EV charging station and a nearby residential neighbourhood is also suggested [156]. However, the future of EVs is unknown, particularly in terms of battery capacity and deployment of more rapid chargers, which might cause grid issues necessitating careful coordination of charging plans for many cars [157].

It is summarised that the variation in charging location enables a bigger picture for analysing the hosting capacity of distribution networks [158, 159]. In relation to this, several research works are carried out to estimate the charging demand of EVs at other, non-residential places (i.e., public charging points). The arrival time of EVs is one of the most important variables in predicting the charging demand at public charging stations, and it does not typically occur after 17:00 like in the case of residential charging. It is estimated that rapid charger utilisation rates will fluctuate throughout the day, with 45% of events taking place between 15:00 and 19:00, when most of the vehicles' batteries are depleted [53]. To simulate the arrival rate of the vehicles in charging stations, the current literature employs a variety of methods [160]. Monte Carlo Simulation technique is used to generate stochastic EV charging load profiles at various places during the day, often at work and at home [150, 151]. An EV use model is proposed to mimic the time-spatial distribution of vehicles and their SoC levels for impact study on the grid [161]. Similarly, a time-spatial EV charging-power demand estimation model used a Poisson distribution while considering the vehicle arrival rate and time at fast-charging stations near highways [162]. The authors of [163] and [164] employed a predefined arrival rate established by the arrival time distribution of ICEVs at gas stations to predict the arrival time of EVs at public charging stations. In another study, the traffic flow from the highway where the charging hubs are installed is utilised to determine the arrival time of EVs by varying their SoC levels and battery capacities [165]. It is also suggested that the arrival time distribution of the charging events should be estimated based on the geographical characteristics of the area [166, 167].

A methodology combining random simulation cases and statistical analysis is developed through probabilistic load flow analysis to improve the accuracy due to lack of real data [156, 168]. It is demonstrated that probabilistic load flow analysis based on point estimate technique is a very effective and accurate method when it comes to dealing with the effect of uncertainty in load demand due to EVs in the distribution network [169]. In addition, field measurements from a charging station are used to model the SoC distribution and the number of EVs in each time interval [170]. The authors of [171] expanded upon this to model the EV charging loads in different charging scenarios, which are formed considering the stochastic distribution of SoC levels. However, the distribution of SoC levels prior to charging is significantly influenced by the EV's battery type and capacity. Another study found that older EV models with smaller battery capacities are typically charged when the SoC is between 25% and 75% of the battery capacity [172]. In their stochastic models, several studies analysed the utilisation of commercial and private EVs with different battery specifications [172–175]. Their findings indicate that SoC levels will vary, thereby influencing the outcomes of stochastic models.

Overall, the majority of these studies have low accuracy due to the use of simplistic assumptions, the absence of real data from newer EV models and the charging time distribution, and the consideration of generic EV models [160, 165]. In addition, most of these studies base their EV charging models on residential activities and the dependence of slow speed chargers. Residential profiles are ideal for predicting the charging demand of EVs parked at a private charging location (e.g., home or workplace) during a specified time [53], but they cannot be used to characterise the demand of EVs that are charged at public rapid and ultra-rapid charging stations. In many instances, the unpredictable nature, high power consumption, and short duration of EV rapid charging make it a grid capacity problem rather than an energy problem [160]. Therefore, understanding the load profile of recent EV models on rapid chargers is also essential. Lastly, the effects of EV deployment are generally estimated based on assumptions regarding the randomness characteristics of the older EV models, while ignoring the heterogeneity characteristics of the newer EVs on the market [120].

2.4.2 Electrotechnical Effects on Different Network Levels

The three stages of the electricity supply are generation, transmission, and distribution. The power generation includes the production of electricity and the distribution of it to customers. Using high voltage transmission lines, the transmission system transmits electricity to grid supply points. Through the national grid's lines, electricity is transmitted from 400-kV, 275-kV, and 132-kV power plants to customers [176]. Figure 2.9 shows the schematic diagram of the UK electricity distribution.
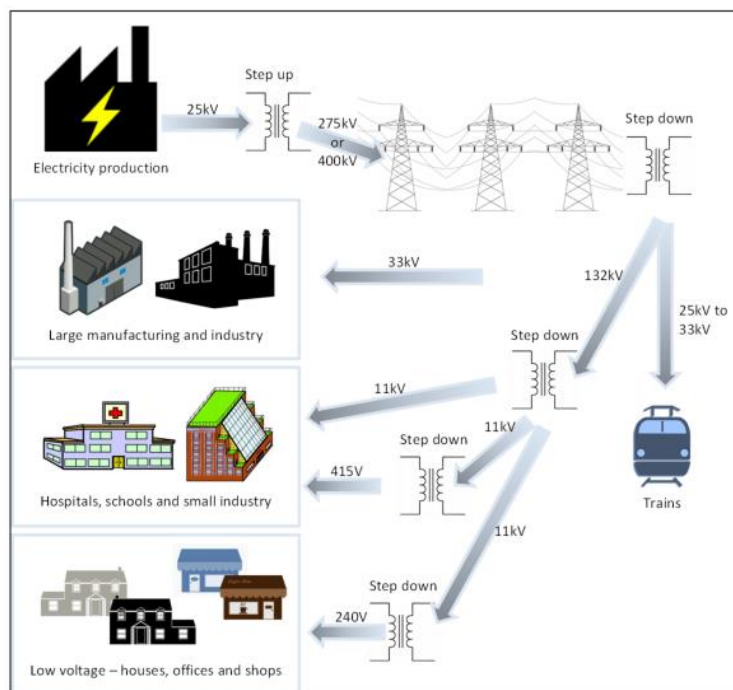
Figure 2.9: Schematic diagram of the UK electricity distribution system [177].

Most field studies examine the impact of EVs on the low-voltage level of distribution grids, particularly through electrotechnical analyses. While some use more artificial grid and mobility data, others already rely on empirical evidence and real data, assuming different EV charging patterns [106].

2.4.2.1 Impact on Transmission Networks

It may be necessary to install additional generation capacity, such as fossil fuel power plants since the transmission system's maximum power output may be insufficient to satisfy the increased peak demand. In addition, the charging demand for EVs may alter the demand profile, which may lead to even bigger changes when a renewable energy system is installed. The impact of the additional load on the transmission and distribution systems depends on its location and time. If the load is concentrated in a specific place, some transmission lines may be required to carry currents more than their rated capacities, hence increasing the resistive losses in the high-voltage network [176]. Therefore, the charging requirements and the impacts of EVs must be quantified not only in the distribution systems, but also in the transmission systems [107, 178].

Generally, the impact of EVs on the transmission side is less severe [106]. A preliminary investigation of the German transmission grid is studied [179]. However, only the potential increase in the load is considered. In another study, it is demonstrated that there are only minimal effects on the German transmission grid up to 2030 and 22 million PEV (50% of market share) due to the introduction of nodal pricing method (in which the national network is divided into different nodes) [180]. The transmission grid's highest voltage level appears to be effectively sized for market shares of up to 50% [106]. This is particularly accurate when controlled charging is considered [176, 181]. Changes in peak demand [182] and energy consumption [183] have been estimated at the transmission level. However, transmission line loading was not investigated (since this would require estimating the position and size of the load). The simulation of PEV charging in the Korean power grid is undertaken by using a stochastic technique for transmission system design. Statistical information on ICEV travels is utilised to develop an individual PEV charging profile. It is determined that EV charging may contribute significantly to the transmission system's peak demand [178].

Current research in charging station planning mainly focuses on urban networks [184]. Since rapid and ultra-rapid chargers will be near highways and rural areas, rural networks must also be addressed, which would automatically increase and alter the network topology from < 69 kV distribution systems to sub-transmission (69–138 kV) and transmission (> 138 kV) systems [40].

2.4.2.2 Impact on Distribution Networks

The impact on the distribution network is often seen as more severe. Each distribution network is connected to the higher-voltage system via a transformer rated for a maximum demand; if this demand is exceeded, the transformer must be upgraded [176]. Additionally, resistive losses will grow, resulting in a higher network voltage drop. For appliance safety, busbar voltages must be within 10% of the unitary voltage [185], therefore if the voltage drop increases too much, network operator action is required.

Numerous case studies at the low-voltage side of the distribution networks have mainly quantified the effect of EV charging on voltage fluctuations [186], voltage imbalance [187], power losses [188], cable loading, and transformer loading [189], using a single network case study. Voltage study entails quantifying voltage dips and fluctuations before and after EV chargers are integrated into distribution feeders, whereas power loss analysis includes the determination of active power losses in cables and networks because of the increasing demand for EV charging. Cable loading evaluation entails doing current analysis on the cables to ascertain the degree of overloading. Transformer loading assessment, on the other hand, focuses on analysing the peak loading on the transformer and analysing the ageing and degradation effect.

The variance in network topology, vehicle use, and demand must be accounted for before generalising these results to the entire distribution system [176]. The effect of EV charging on network voltages is investigated using a 22-kV network under four different scenarios: Scenario I with peak substation load and weekday charging, Scenario II with peak substation load and weekend charging, Scenario III with low substation load and weekday charging, and Scenario IV with low substation load and week-end charging. It is demonstrated that the voltage fluctuations are worsened in Situation I in the network due to higher peak demand in weekdays [190]. An installation of a capacitor bank is proposed near the charging station to improve the voltages in a medium-voltage distribution network [191]. It is shown that chargers rated at 60 kW does not violate the flicker limits. However, the utilisation of 150-kW, 240-kW, and 350-kW chargers causes flicker limits to be surpassed in a medium-voltage network [192].

Many studies have examined the effects of domestic charging on the low-voltage networks. The impact of EV charging on a European low-voltage distribution network is studied [193]. It is concluded that the network is robust enough to support a 1–2% EV penetration rate. It is found that increasing the penetration rate of EVs worsens the voltage profiles in a 13-node [194] and 14-node distribution networks [195]. A benchmark low voltage microgrid network that consists of residential, industrial, and commercial feeders is used to examine the impact of varying the uptake level of EVs [196]. It is found

that only the commercial feeder experiences voltage violations with an EV uptake level of 30% and 50% between 18:00 and 19:30. Another work showed that voltage violations occur due to uncontrolled charging between 17:00 and 22:00 [197]. Similarly, the maximum voltage deviation with uncontrolled and controlled charging regimes is 13.50% and 0.98%, respectively [198]. Total active power and reactive power losses are 40% and 37.5% less, respectively, when controlled charging schemes are used instead of uncontrolled charging schemes [199]. It is shown that the total peak demand increases by 44.1% and power losses increase by 42% when 80 units of 30-kW chargers are connected to a distribution network feeder between 18:00 and 19:00 [200].

Power cables represent a large proportion of installed assets for network operators [201]. The impact of uncontrolled chargers (rated at 3.7 kW, 6.9 kW, 11.1 kW) and controlled chargers on the cable loading of a Swedish residential network is investigated [202]. The loading on two residential cables is investigated: L27 and L23 that serve up to 166 and 218 customers, respectively. With 3.7-kW chargers, 99.52% and 99.23% of L27 and L23 handle the load at the highest uptake level, whereas with 11.1-kW chargers, this reduces to 57.89% and 73.85%, respectively. It is also shown that cables exceed their maximum design limits (i.e., cable ampacity is surpassed) when more than 35% of the 155 households are equipped with a domestic charger between 17:00 and 22:00 [197]. The loading on the network cables increases by 31% when 80 units of inductive chargers (rated at 30 kW) are connected to a distribution network feeder between 18:00 and 19:00 [200].

Since transformers in their current form will remain in use in power systems for many decades to come due to their widespread application, the effects of typical smart grid operations, such as EV charging, must be accurately evaluated in terms of transformer health and performance [203]. Different charging scenarios are conducted to assess the impact of PEV charging on transformer insulation life [204]. It is shown that the transformer's baseload increases by 70% 200 customers use rapid chargers between 21:00 and 22:00 [205]. In another study, it is demonstrated that the transformer loading surpasses 73% of its maximum capacity when domestic chargers are used from 18:00 to 19:30 [196]. The effect of using V2G chargers and combining them with smart and coordinated charging solutions prevents transformer loading [206] and reduces the stress on transformers [203]. Incorporating a solar PV and a battery energy storage system is also effective to reduce the stress [207]. Despite the advantages of providing coordinated and smart solutions, however, one must also consider the reliance on a potentially failing communication infrastructure [208] and the computational difficulty associated with a large EV deployment [209].

2.4.3 Network Reinforcement Strategies

The grid is unlikely to accommodate EV charging loads without experiencing any changes in its operating characteristics. This phenomenon is generally attributed to two main causes. Primarily, the grid's hosting capacity may be insufficient, resulting in grid-side issues when the system reaches its hosting capacity limits [158, 159]. Secondly, demand fluctuates throughout the day, and issues emerge when charging loads coincide with the network's peak loading hour [34, 37]. As a result, DNOs must avoid both undersupply and oversupply to maintain a balance of supply and demand.

Numerous technologies and strategies have been developed and suggested to relieve and smooth peak demand, as well as to lower demand costs associated with EV charging during peak loading hours. The main strategies include conventional and classical network reinforcement methods and demand reduction techniques. In case of network reinforcement, however, expenditures on both the grid owner's and customer's sides are necessary. From the customer's position, the use of smart chargers and smart meters has become common. From the grid owners' standpoint, cable and transformer resizing may be necessary when extra loads are added to the network [210].

2.4.3.1 Distributed Generation Placement

The voltage deviations and power losses in the distribution level of the network should be effectively mitigated because of their dominance when compared to the transmission systems [211]. Continuation power flow and optimisation methods concerning the placement of DGs in power systems are the most common techniques used to improve voltage stability, reduce power losses, improve system efficiency and reliability, and reduce expenses related to transmission in distribution networks [212, 213]. Extensive research on DG allocation problem is conducted in literature. Continuation power flow method is used by combining continuous and static power flow to analyse voltage stability and identify weakest busbars in the network [212, 214, 215]. The placement of DGs at congested busbars and the placement of EVs at robust busbars are determined using a voltage stability index technique in an IEEE 33-busbar test network [216]. It is demonstrated that DGs improve the minimum steady-state voltage by 12.2% and reduce the active power losses by 56.25%. Satish and Vinod [217], Sanjay et. al. [218], Truong et. al. [219], Saha and Mukherjee [220], Selim et. al. [221], and Quadri et al. [222] have presented various DG allocation techniques that are useful for determining the candidate location for DG placement to improve voltage profiles and reduce system losses to a reasonable degree.

2.4.3.2 Installation of Transformer Tap Changers

In the classical network reinforcement method, EV chargers are considered as conventional uncontrollable loads. Therefore, investments are made on classical network assets, including cables (e.g., increase in size) and transformers (e.g., installation of larger transformers or equipping them with tap changers), to manage peak loads. However, network reinforcement in densely populated areas is quite challenging since the costs associated with transformer and cable oversizing are significantly high [223]. DNOs, are therefore, using the traditional tap installation methods at the HV/MV and MV/LV substation transformers [224]. A network optimisation model for the placement of MV/LV transformers equipped with OLTCs is proposed in [225]. Another study subsequently presented a coordinated planning technique for demonstrating the benefits of OLTC transformer investments at microgrid/utility border sites [226]. The common issues with OLTC placement are also addressed in [227]. Cheng et. al. [228] attempted to improve the voltage profile in distribution system by controlling the on-load tap-changing transformer in coordination with the charging station in the presence of solar PVs. However, only one of these studies considered the integration of charging stations near these transformers.

2.4.3.3 Peak Demand Reduction

The peak demand reduction strategy minimises the charging demand. Using a smart charging control system or incentive-based energy tariffs to shift demand peaks to off-peak hours is a viable option for avoiding costly reinforcement work. However, there is still a considerable distance to travel before smart charging solutions are widely adopted [201]. The use of battery energy storage units is widely adopted for reducing the demand. An overview on the different types of battery energy storage technologies with the integration of EV charging stations in smart grids is given in [229]. Another study used a test feeder and designed a charging station equipped with diesel generator, solar energy, and storage system, to provide peak-load shaving, to optimise the capacity and to minimise the cost of charging station in [230]. The optimal sizing of stationary battery energy storage systems to reduce the peak load of charging stations equipped with rapid chargers is proposed in [231–233]. The modelling of a hybrid energy storage system (a combination of superconducting magnetic energy storage and battery energy storage units) to reduce the peak demand and to support the charging demand from rapid chargers is also proposed in [234]. The peak load reduction in distribution network is proposed by controlled charger algorithm of EVs, solar PV units, and battery energy storage systems [235, 236]. Since battery degradation is still an issue with storage units, the use flywheel hybridisation to improve battery life is also suggested [237, 238].

2.4.4 Research Gaps

Firstly, although low-voltage distribution networks are extensively analysed in the literature, the impact of EVs on HV/MV distribution networks is frequently overlooked [106]. The modification of transformer taps settings and the evaluation of the required reactive power compensation services near EV chargers to improve steady-state voltage profiles and to minimise power losses at the medium-voltage distribution side are also not the subject of a comprehensive research. **Chapter 3** addresses this gap as follows:

- A generic HV/MV distribution network in the UK is modelled and then analysed using load flow studies at varying uptake levels of rapid EV charger adoption. The effect of using transformer taps, and the optimal placement and sizing of DG units and SVC devices are also investigated in depth.

Secondly, many studies only model EVs as uncontrollable static charging loads in distribution networks. This type of modelling imposes no restrictions on EV charging and assumes that all residents charge at any time during the day, especially when they return home from work. For a more comprehensive network analysis, it is necessary to develop and implement a dynamic model for battery chargers with smart charging capability in distribution networks. **Chapter 4** and **Chapter 5** address these gaps as follows:

- A dynamic battery charging model is developed in **Chapter 4** and integrated in a low-voltage distribution network in **Chapter 5**. The effect of combining slow-speed, fast-speed, and rapid-speed battery charging dynamics is analysed.

- The combined effects of controllable and uncontrollable charging methods on the operational characteristics of a low-voltage distribution network are investigated. This strategy also allows for the investigation of the effect of V2G and coordinated smart charging techniques under different scenarios to mitigate the impact of peak demand on the distribution network equipment.

Thirdly, the stochasticity of charging occurrences is often overlooked in the literature [239, 240]. When selecting where to locate the chargers that need much lower power levels, stochasticity is sometimes disregarded, since these charging events have little influence on the grid. Many studies, therefore, opt to create candidate sites for high-power chargers by means of using service stations [240], estimated traffic demand and patterns [208], or static data [209]. Charging stations equipped with multiple rapid and ultra-rapid devices may require up to tens of MW from simultaneous charging events. Thus, in the case of installing these stations, which might result in multi-MW spikes in grid demand, the stochastic behaviour of charging events must be fully examined to assess the grid's hosting capacity [40, 208].

The research gap among stochasticity of charging events is the absence of heterogeneity in the modelling of EV charging demand [120]. **Chapter 6** of this thesis addresses the following to bridge the research gap:

- Sale statistics for different EV models are considered to derive information about the EV market share in the stochastic model.

- Different EV models with real data are considered and their timely distribution to a multi-charger hub is simulated based on a real data obtained from Zap Map and local authorities in the UK.

- Non-linear SoC dependent charging curves for different EV models are used to i) estimate the charging duration of vehicles (i.e., how long do they stay connected to the grid), and ii) calculate the energy consumption of vehicles (i.e., how much energy does each vehicle request from the grid to achieve an 80% battery SoC).

- Stochastic charging profiles are integrated into a real distribution network feeder to quantify the hourly peak demand and to estimate the transformer's peak load.

- The impact of battery energy storage units is analysed on the network's and transformer's peak loads. The frequency with which the charging demand will exceed the system's capacity is also determined.

Lastly, current research focuses mostly on the computational modelling and integration of EV chargers and their batteries. However, the combination of computational modelling with the experimental work is usually overlooked in the literature. **Chapter 7** of this thesis addresses this gap as follows:

- Different battery energy storage discharge profiles are developed based on the stochastic charging profiles derived from **Chapter 6**. These discharge profiles are then integrated into a physical battery charger and an analyser unit through the utilisation of lithium-ion battery packs to obtain the relationship between i) battery voltage and discharge current, and ii) battery voltage and remaining battery capacity. These relationships are used to estimate the SoC and DoD of lithium-ion batteries to experimentally assess their viability for supporting vehicle charging and reducing energy consumption that must be met by the local distribution grid.

- The estimation of SoC and DoD of batteries under various discharge profiles is used to quantify the amount of usable energy after storage units have been used to provide demand response services for the grid.

2.5 Summary

As EVs continue to gain popularity, it is critical to build a robust public charging infrastructure. Public chargers are less often used than private chargers installed at the driver's home, or workplace. Within the next decade, rapid and ultra-rapid chargers will obtain a greater market share. However, these chargers account for a significant portion of overall energy usage, since quick charging entails transferring enormous quantities of electricity from the grid to the battery in a matter of minutes. For example, charging 100 EVs simultaneously on 100-kW chargers adds 10 MW of load to the grid's base demand.

The grid may not be capable of accommodating high charging demand without experiencing changes in its operational characteristics. Many studies in the field have highlighted numerous grid-side issues associated with the integration of battery chargers and concluded that the severity of grid issues is largely affected by the time and place at which EV charging loads are charged and connected into distribution networks, respectively [241]. However, most of the existing research focuses on the integration of residential (3–7 kW) and workplace (7–22 kW) chargers. The number of studies considering rapid and ultra-rapid chargers is limited. This is mainly due to small number of commercial vehicles capable of exploiting the rates of rapid and ultra-rapid chargers. In addition, limited amount of research addresses the problem of estimating EV demand at multi-charger hubs with EV heterogeneity considered [120]. Many studies assume that EVs are a generic type with fixed battery capacity and the EV demand is proportional to residential demand because many drivers plug in their vehicles upon arrival at home (and this demand usually coincides with basic residential activities between 17:00 and 20:00). These assumptions produce a single-peak EV demand profile in the evening, and this strategy has the flow of omitting stochasticity with the variation in EV models and utilisation of public charging stations. To bridge this gap, this thesis develops a stochastic model for estimating the demand of a public charging station by using non-linear SoC dependent charging curves for different EV models.

It should be made clear that estimating EV demand for rapid chargers is more challenging than estimating EV demand for residential households. This is primarily due to data confidentiality for public charging stations. Due to similar plug-in periods and durations, residential charging profiles are often identical. As for the rapid charging, however, every motorist has a daily pattern or route that he or she follows. Consequently, rapid charger utilisation rates fluctuate throughout the day due to stochasticity [35]. How often one charges his/her car on a rapid charger also depends on factors such as the type of car and distance travelled [242]. **Chapter 6** of this thesis is devoted to solving and addressing this gap in the research.

CHAPTER 3

3. Effect of Increasing the Uptake Level of Electric Vehicles on HV/MV Distribution Network

3.1 Introduction

While EVs provide several benefits for the grids, they also provide several challenges for DNOs. As a result of the increased energy demand, DNOs will need to upgrade and/or reinforce the distribution infrastructure, such as by installing larger transformers and upgrading cables.

The research indicates that traditional network reinforcement strategies are often used to assist the connection and operation of EV charging loads. An extensive literature review has shown that there is no published research about (i) adjusting the OLTC settings of transformers and (ii) determining the required sizing of SVC devices, near the rapid chargers and charging stations in HV/MV distribution networks. This chapter's main objective is to analyse how increasing the number (uptake) of uncontrolled rapid chargers affects the steady-state voltages and active power losses under different voltage control measures in a medium-voltage distribution network. Through a load flow study, IPSA+ Power simulation software and MATLAB are used to assess the impact of rapid charging stations on a generic HV/MV distribution network.

3.1.1 Chapter Structure

Section 3.2 presents the model and data of the generic HV/MV distribution network under examination. The methodology for calculating and installing tap changers for transformers is presented. Ten different scenarios concerning the increased number of rapid chargers and charging stations are also presented.

Section 3.3 conducts a load flow analysis (i) to identify critical and weak busbars that are susceptible to voltage violations and, as a result, require network reinforcement, (ii) to calculate active power losses and (iii) to examine steady-state voltages, under different EV uptake scenarios in the network.

Section 3.4 discusses the optimum placement DG units and the optimum sizing of SVCs devices.

Section 3.5 discusses the main findings and concludes the chapter.

3.2 Distribution Network Model

The distribution network is a collection of power system network models that are representative of British distribution networks. The distribution model in this chapter represents a mixed-use suburban area. The generation point is fed by two 500-MVA grid transformers connected at the 275/132-kV substation. The network is mostly radial and has connections to 33 kV, 11 kV, and 6.6 kV substations. The network's data is acquired from [41] and its schematic diagram is represented in Figure 3.1.
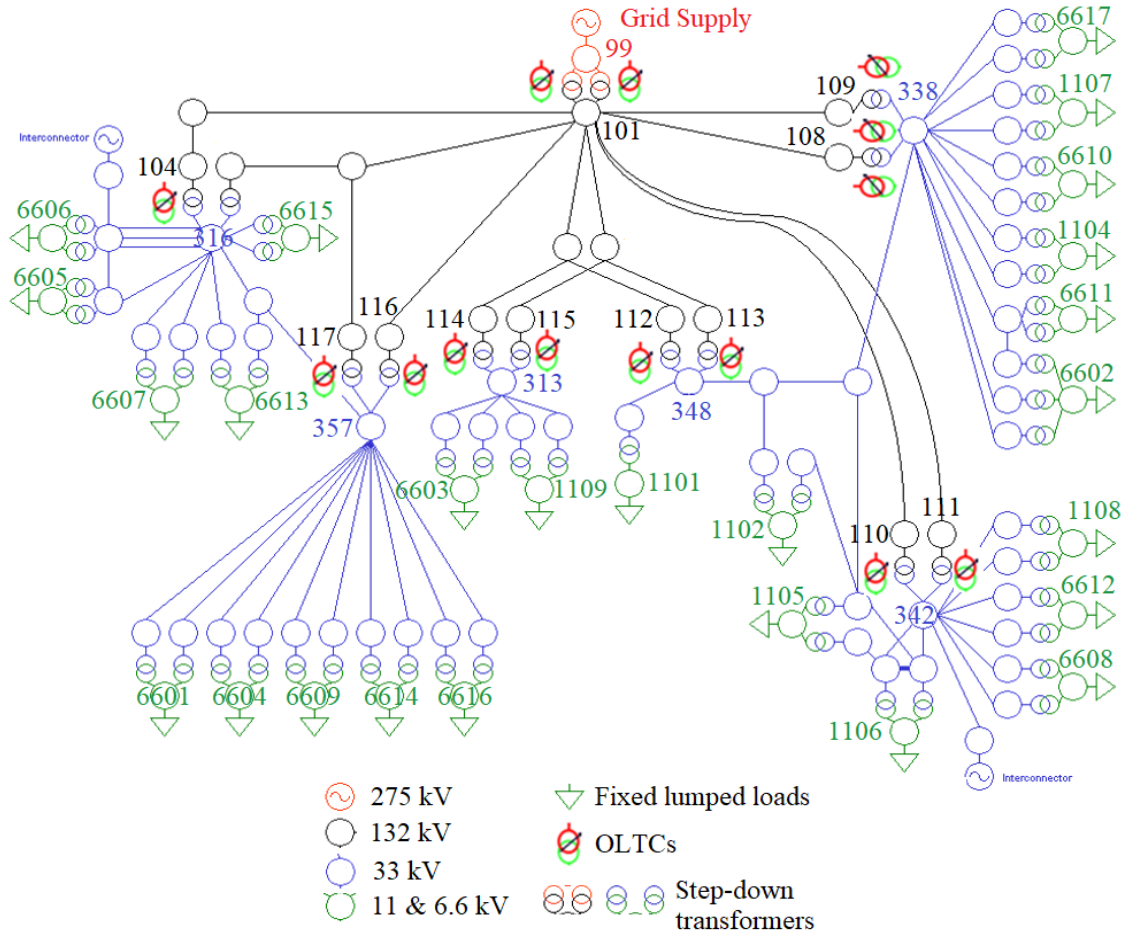
Figure 3.1: Simplified schematic diagram of the generic HV/MV distribution network.

The network is made up of 102 busbars, 25 of which represent aggregated load busbars modelled as static loads. The schematic diagram depicts substation busbars as red (275 kV generating point), black (132 kV), blue (33 kV), and green (11 kV and 6.6 kV) circles. The supply point is designated by busbar '99' (slack busbar) at the top of the schematic diagram, while customers are represented by green triangles at the far end of each load busbar. Three generators power the network (two of which serve as interconnectors that supply and/or absorb energy from other neighbouring networks). Network assumptions and detailed data selection are given in the following subsections.

3.2.1 Baseload Demand

The network is comprised of 25 load busbars, connected at the 11-kV and 6.6-kV load busbars. Each busbar is modelled as a constant and lumped PQ load that represents an aggregated demand and consumption of an area. Table 3.1 presents the data for active power demand and reactive power consumption of 25 load busbars.

Table 3.1: Baseload demand of the load busbars in the network

Load Busbar	P (MW)	Q (MVAr)	Voltage (kV)	Busbar Type
1101	15.55	10.10	11	Commercial or Industrial
1102	15.65	3.98	11	Commercial or Industrial
1104	7.84	9.30	11	Residential
1105	15.02	3.28	11	Commercial or Industrial
1106	10.37	2.07	11	Commercial or Industrial
1107	12.67	3.25	11	Commercial or Industrial
1108	5.24	0.96	11	Residential
1109	17.82	9.77	11	Commercial or Industrial
6601	15.41	4.98	6.6	Commercial or Industrial
6602	17.4	6.72	6.6	Commercial or Industrial
6603	17.94	4.77	6.6	Commercial or Industrial
6604	17.71	5.89	6.6	Commercial or Industrial
6605	15.45	4.32	6.6	Commercial or Industrial
6606	21.46	5.39	6.6	Commercial or Industrial
6607	23.52	7.23	6.6	Commercial or Industrial
6608	15.55	8.64	6.6	Commercial or Industrial
6609	2.51	0.54	6.6	Residential
6610	17.5	7.19	6.6	Commercial or Industrial
6611	7.63	2.89	6.6	Residential
6612	23.02	8.55	6.6	Commercial or Industrial
6613	15.08	4.82	6.6	Commercial or Industrial
6614	15.85	5.74	6.6	Commercial or Industrial
6615	6.69	4.32	6.6	Residential
6616	15.23	6.33	6.6	Commercial or Industrial
6617	16.42	0.34	6.6	Commercial or Industrial

Due to lack of data, the type of load busbars is not known but represents the aggregated demand profile for a typical British distribution network model. In the GB, however, a single 132-kV substation transformer typically serves 9,216 customers, while two of the same transformers serve 18,432 customers [243, 244]. In addition, a typical residential feeder generally has a total demand of between 5–10 MW [245].

The network, based on these arguments, comprises of five load busbars (e.g., 1104, 1108, 6609, 6611, and 6615) that are considered as residential feeders since the total active power demand connected to these points is less than 10 MW. The remainder of load busbars is considered as commercial and/or industrial feeders in the network. In this thesis, rapid chargers and charging stations are connected near the commercial and industrial feeders. Detailed data regarding the network lines, branches and transformers is presented in the appendices (see **Appendix A.1**). It should be clarified that transformer tap settings and tap positions are not available in the dataset and hence next subsection is concerned with the calculation and determination of the ideal tap settings for grid transformers in the distribution network.

3.2.2 Transformer Tap Settings

Since transformers are not equipped with individual taps, the network comes with voltage violations out of the box, even before the installation of EV charging devices in the network. In practice, transformers are generally equipped with taps that allow the turns ratio to be adjusted to compensate for supply variance. These taps allow the output voltage to approach the rated output voltage when the input voltage is outside the rated input voltage range.

Changing the input voltage or the number of turns on the transformer windings is the simplest way to modify the output voltage of a transformer. Taps are typically provided on the high voltage winding because this winding has a greater number of turns, allowing for more precise voltage regulation. Transformer taps operate on the principle of changing the number of turns in one winding and hence changing the turns ratio of the transformer [246]. Tap changers exist in two primary types for transformers: no-load tap changers and on-load tap changers. The latter, which typically have 33 taps (one at the centre "rated" tap and sixteen positive and sixteen negative taps to increase and decrease the turn ratio, respectively) allow for a 10% voltage variation (each step providing 0.625% variation) from the nominal transformer rating. Equation (3.1) is used to determine the positions of the transformer taps.

$$Tap\ Position\ (\%) = \left[1 - \frac{B_A}{B_T}\right] \times 100\% \qquad (3.1)$$

Where:

B_A is the actual busbar voltage (kV),

B_T is the target busbar voltage (kV).

The difference between the actual and the target busbar voltage is defined as V_d. This parameter is used to determine the optimum tap position for transformers. Using (3.1), the calculated tap positions and selected tap settings for grid transformers in the network are shown in Table 3.3.

Table 3.2: Calculated tap positions and selected tap settings for grid transformers

Transformer	Controlled Busbar	V_d	Tap Position (%)	Tap Setting (%)
99/101	All	0.947	5.3	−7.5
99/101	All	0.947	5.3	−7.5
104/316	6605, 6606, 6607, 6613, 6615	0.982	1.8	−2.5
116/357	6601, 6604, 6609, 6614, 6616	0.975	2.5	−2.5
117/357	6601, 6604, 6609, 6614, 6616	0.975	2.5	−2.5
114/313	1109, 6603	0.968	3.2	−5
115/313	1109, 6603	0.968	3.2	−5
112/348	1101	0.955	4.5	−5
113/348	1101, 1102	0.955	4.5	−5
108/338	1104, 1107, 6602, 6610, 6611, 6617	0.975	2.5	−2.5
109/338	1104, 1107, 6602, 6610, 6611, 6617	0.975	2.5	−2.5
109/338	1104, 1107, 6602, 6610, 6611, 6617	0.975	2.5	−2.5
110/342	1102, 1105, 1106	0.982	1	−2.5
111/342	1108, 6608, 6612	0.982	1	−2.5

The calculations show that all transformers have negative tap settings. This is because the voltage on the target busbar is lower than the threshold limit and hence the turns ratio on the primary winding of the transformer are regulated to adjust and bring the voltage on the secondary winding side to operate within an acceptable level. The main grid transformers (99/101) have bigger tap settings than other transformers since these transformers provide the highest voltage support to the network and have the largest percentage difference between the actual and the target busbar voltages.

Generally, common tap configurations include +2.5%, +5%, and −2.5%, −5% of the rated tap; however, some transformers also have additional taps. For example, a tap setting of −2.5% is chosen for 110/342 and 111/342 transformers for a calculated tap position of 1% since this is the nearest possible selection according to the variation in the step increment in the simulation software. Again, a tap setting of 2.5% is selected for a calculated tap position of 2.5% for 116/357, 117/357, 108/338, and 109/338 transformers, since this is the closest and most ideal available setting from the general tap configurations in the simulation software. The effect of equipping grid transformers with ideal tap settings on the steady-state nodal voltages during the baseload in the network is shown in Figure 3.2.
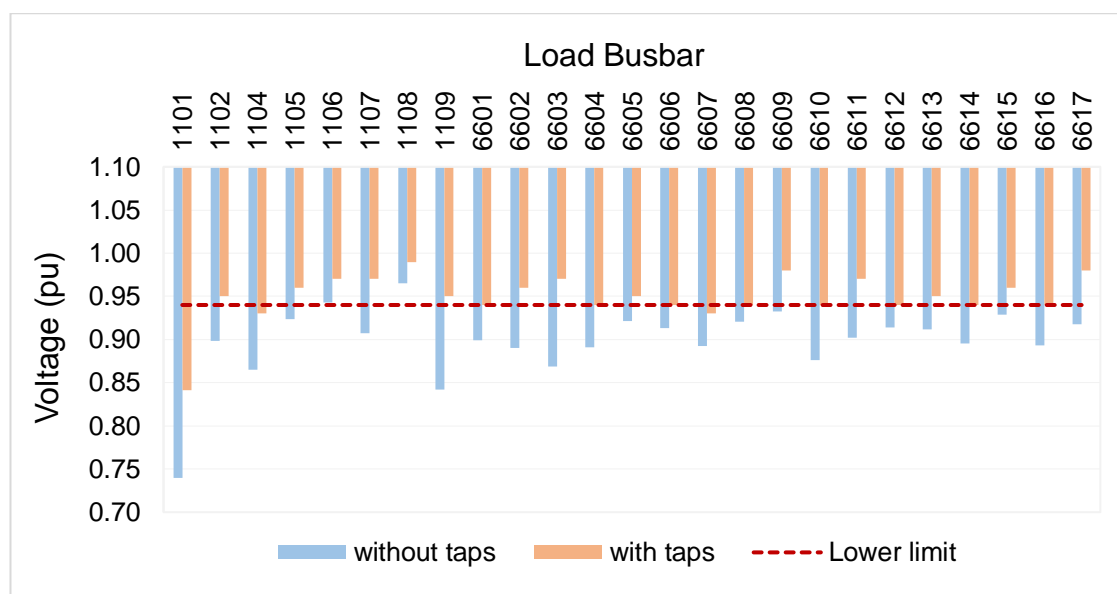
Figure 3.2: Steady-state busbar voltages with and without transformer taps.

DNOs in the UK are required to serve customers at 11-kV and 6.6-kV within ±6% of the nominal voltage (1.0 p.u.) to ensure network security and stability [247, 248]. The maximum and minimum values should be maintained within the ranges of 1.06 p.u. and 0.94 p.u., respectively. The results by the blue coloured bars indicate that 23 of 25 load busbars are exceeding their permissible lower voltage limits, when the network is modelled using the provided data and transformers are assumed to have no taps. Only two load busbars, namely, 1106 and 1108, operate within permissible voltage limits without taps in place. The orange-coloured bars indicate that the majority of load busbars operate within permissible voltage limits as a result of fitting transformers with optimal tap settings. However, it is observed that three load busbars, namely, 1101, 1104, and 6607 continue to exhibit voltage violations and operate beyond the minimum voltage limit of −6%. The voltage at these busbars is 0.84 p.u., 0.93 p.u., and 0.93 p.u., respectively.

The main reason why load busbars 1104 and 6607 exhibit voltage violations is primarily due to low power factor, caused by a higher load current and hence higher line losses near the feeders. On the other hand, load busbar 1101 is identified as the most critical and weakest feeder in the network, which is mainly due to the utilisation of a single substation transformer serving the commercial zone (see **Figure 3.1**) and high reactive power consumption (see **Table 3.1**).

3.2.3 Scenarios for Electric Vehicle Charging Stations

This chapter studies the effect of increasing the number of EV charging stations in the network. Different uptake scenarios are considered and charging stations are only connected near the non-residential feeders in the network. Table 3.3 presents different uptake scenarios for the connection of chargers.

Table 3.3: Description for EV uptake scenarios

Scenario	Number of Stations	Total Charging Demand (MW)	Load Busbars
S1	2	2.7	1101, 1102
S2	4	5.4	S1, 1105, 1106
S3	6	8.1	S2, 1107, 1109
S4	8	10.8	S3, 6601, 6602
S5	10	13.5	S4, 6603, 6604
S6	12	16.2	S5, 6605, 6606
S7	14	18.9	S6, 6607, 6608
S8	16	21.6	S7, 6610, 6612
S9	18	24.3	S8, 6613, 6614
S10	20	27	S9, 6616, 6617

There are 20 non-residential load busbars in the network and ten scenarios are considered for the connection of EVs. It is assumed that each non-residential load busbar has one charging station and each scenario introduces two additional charging stations in the network. This is to keep the rate of increase in the EV penetration equal for each scenario. Charging stations are modelled and connected near the existing load busbars as a constant lumped PQ load to represent simultaneous charging of vehicles in the network. The increase in the scenario number increases the total number of EVs connected in the network. Scenario S1 has only two charging stations connected to load busbars 1101 and 1102, whereas Scenario S2 has four charging stations connected to load busbars 1101, 1102, 1105, and 1106. The connection points for charging stations are determined based on the order of load busbars in the network.

It is assumed that Tesla superchargers are connected in each charging station due to their popularity and data availability. As of December 2022, Tesla operates 40,432 Superchargers in 4,470 stations globally, averaging more than nine chargers per station [249]. Therefore, this chapter assumes that each charging station has nine Supercharger (rated at 150 kW) operating simultaneously. This charging rate and charging type are selected since it is the dominant charging technology in many Tesla's charging locations [250]. Multiplying the number of charging stations (2) by the number of Superchargers (9) and the rating of each Supercharger (150 kW) yields the 'Total Charging Demand' for each scenario in the third column of Table 3.3.

3.3 Load Flow Analysis

Load flow analysis is conducted to investigate the effect of each scenario on the network. **Section 3.3.1** analyses active power losses, whereas **Section 3.3.2** examines the steady-state voltage profiles.

3.3.1 Power Losses

In electric networks, transmission across large distances results in power losses. The number, type, and size of consumers, as well as the network topology, all influence the severity and amount of power losses. Losses are an inherent element of power distribution, and a greater knowledge of network losses enables operators to make informed choices about how to run, maintain, renew, and upgrade the network most efficiently [251]. The loss of power consumption is calculated by (3.2) [252]:

$$L_p = \frac{P_L{}^2 + Q_L{}^2}{V_{av}{}^2} \times \frac{I_{RMS}}{I_{av}} \times R \tag{3.2}$$

Where:

L_p is the loss of active power consumption (kW),

V_{av} is the average voltage in loss determination (V),

I_{RMS} is the RMS current in loss determination (A),

I_{av} is the average current in loss determination (A).

Along with calculating the amount and severity of losses, it is also critical to determine their location in the network. Power losses are determined by calculating the difference between power arriving from the transmitting end busbar and power departing from the receiving end busbar. Figure 3.3 is presented to demonstrate how branch losses add up to make the total active power losses in different areas of the network.
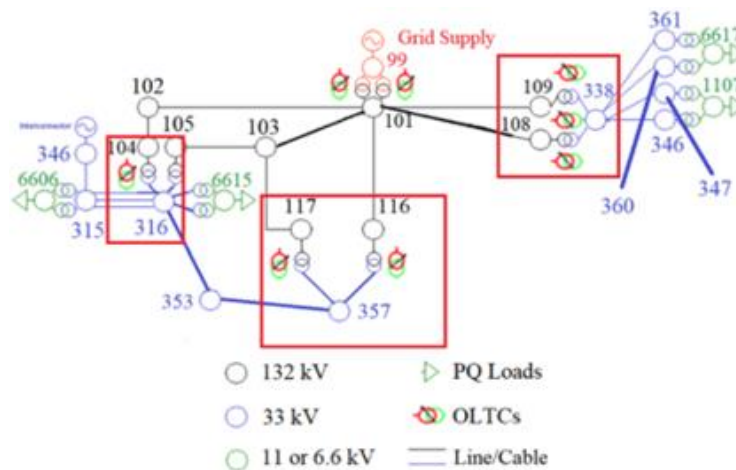
Figure 3.3: Section of the distribution network.

Transformers fitted with tap changers are also highlighted in the schematic diagram. These transformers link the busbars 104/316 on the left, 109/338 and 108/338 on the right, and 117/357 and 116/357 in the schematic diagram's centre. Active power losses in the areas marked by the red boxes are calculated and shown in Table 3.4.

Table 3.4: Active power losses in the marked areas of the network

Sending Busbar	Receiving Busbar	Sending Busbar Power (MW)	Receiving Busbar Power (MW)	Losses (MW)
104	316	45.95	45.83	0.12
108	338	30.69	30.59	0.10
109	338	30.48	30.38	0.10
109	338	29.94	29.84	0.10
116	357	33.09	32.96	0.13
117	357	30.16	30.05	0.11

With reference to the network schematic diagram in Figure 3.3, the largest active power losses (0.13 MW) occur between substation busbars 116 and 357. Losses between busbars 108/338 and 109/338, on the other hand, are equal since they are supplied and feed the same substation point in the network. Power losses are slightly less between busbars 108/338 and 109/338 on the right-hand side of the diagram than between busbars 104/316, 117/357, and 116/357, since this region is served by three transformers equipped with tap changers.

A load flow analysis is performed in IPSA+ Power simulation software to compute and calculate the network's total active power losses under different scenarios. The results of the load flow analysis are shown in Table 3.5.

Table 3.5: Total active power losses under different scenarios

Scenario	Active Power Losses (MW)
Baseline	6.82
S1	7.22
S2	7.38
S3	7.51
S4	7.66
S5	7.84
S6	8.01
S7	8.19
S8	8.33
S9	8.52
S10	8.67

The baseline demand and power losses in the network are 364.5 MW and 6.82 MW, respectively. It is evident from Table 3.5 that increasing the number of charging stations increases the overall losses in the network. For example, the addition of two charging stations in Scenario S1 increases these losses from 6.82 MW to 7.22 MW. When the maximum number of charging stations is reached, the power losses reach 8.67 MW.

Active power losses account for a small portion of the network's total power demand. These losses in Scenario S10 account for 2.4% of the total network demand. This value is less than the average amount of losses specified by the DNOs [253].

3.3.2 Voltage Profiles

Steady-state voltages drop because of the increased current flow via cables, which occurs as a result of increasing active power demand and reactive power consumer consumption. A load flow analysis is performed in IPSA+ Power simulation software to compute and calculate the load busbar's steady-state nodal voltages under different scenarios. The results of the load flow analysis are seen in Figure 3.4 and Figure 3.5.
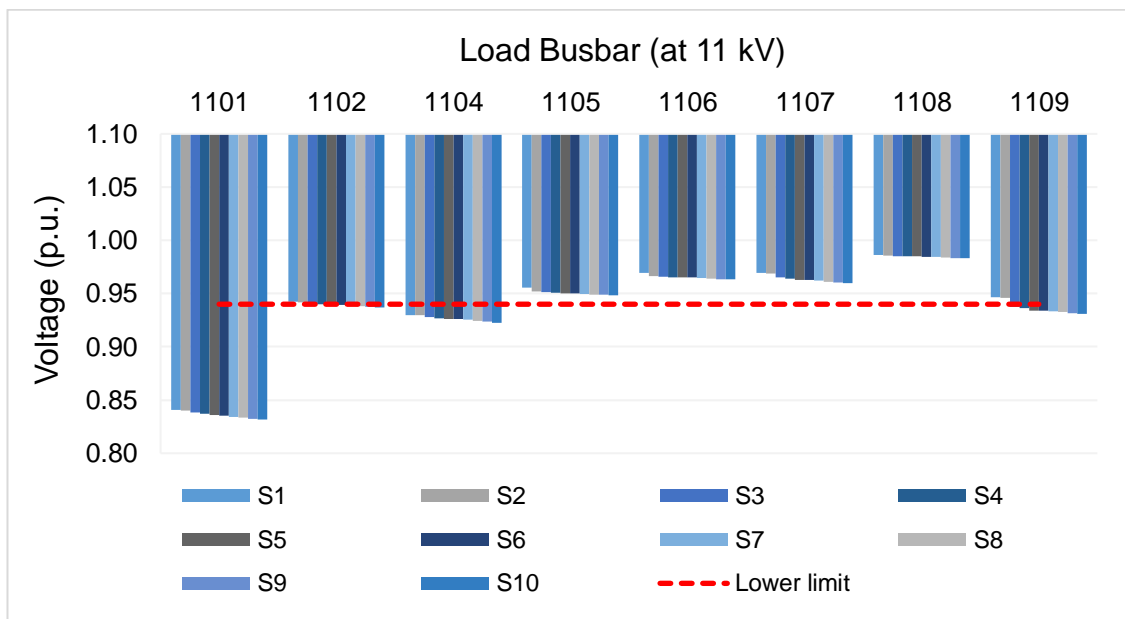
Figure 3.4: Voltage profiles at the 11-kV busbars under different scenarios.
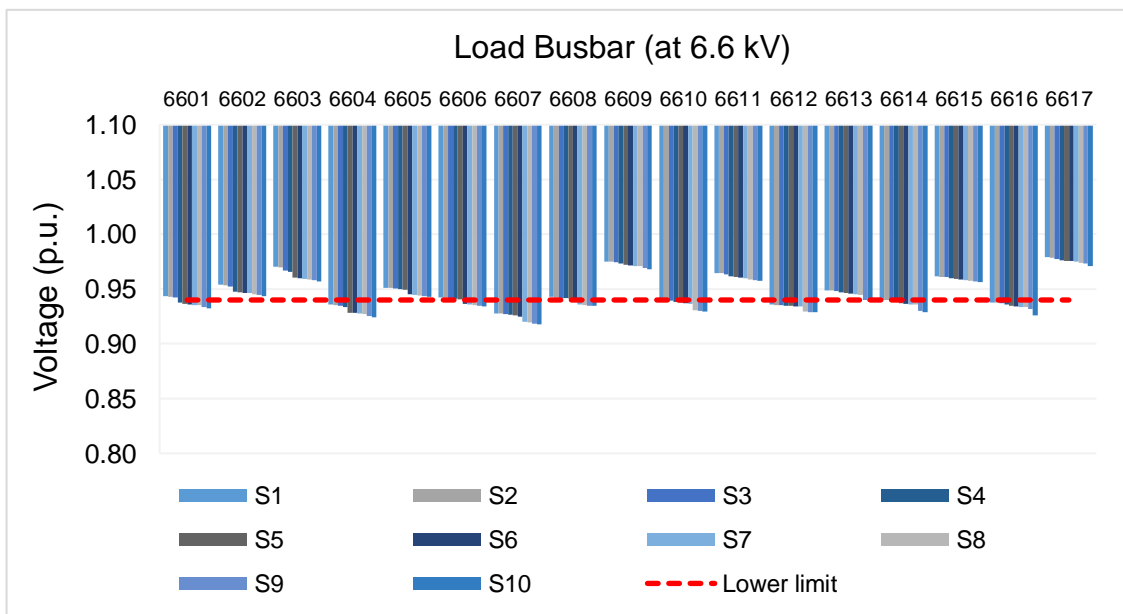
Figure 3.5: Voltage profiles at the 6.6-kV busbars under different scenarios.

It is observed that the steady-state voltage difference between each scenario is very small for each individual load busbar. This is because the aggregated charging demand is relatively lower than the overall base network demand. Comparing Scenario S1 to Scenario S10, for example, the nominal voltage of load busbars decreases nearly around 1% on average. Some load busbars are impacted less, indicated by the fact that the rate of voltage drop is negligible as the number of charging stations increases in the network. Other load busbars, on the contrary, experience greater voltage drops due to high reactive power consumption (particularly 1101, 1109, 6604, and 6607). Nonetheless, it is evident from the results that increasing the number of charging stations at the load busbars increases the network's voltage drop and introduces voltage violations.

In addition, 12 of these load busbars (such as 1105, 1106, 1107, 1108, 6602, 6603, 6605, 6609, 6611, 6613, 6615, and 6617) do not experience voltage violations under any scenario. According to **Table 3.1**, four of these load busbars (e.g., 1108, 6609, 6611, and 6615) are regarded as residential areas devoid of a charging station and with a significantly lower PQ demand compared to other load busbars. On the other hand, certain load busbars (such as 1109, 6612, and 6616) only begin to exhibit voltage deviations at the higher uptake levels, particularly after the installation of eight charging stations at Scenario S4.

To ensure network security and stability, DNOs in the UK are required to serve customers at these load busbars within ±6% of the nominal voltage during disturbances. Load flow analysis demonstrates conclusively that tap changers are insufficient to maintain steady-state voltages between 1.06 and 0.94 p.u. as many load busbars operate at less than 0.94 p.u., especially as the number of charging stations increases in the network. Therefore, this thesis proposes optimal placement of DG units and optimal sizing of SVC devices near the network's critical and weak feeders in the next section.

3.4   Impact of Voltage Control Measures on the Network

As demonstrated with load flow analysis, the utilisation of tap changers is not sufficient to bring voltages to operate within acceptable limits with the increasing number of EVs and their charging stations. The optimum placement of DG units and minimum sizing of SVC devices near the rapid charging stations are proposed to improve voltages and reduce power losses in the distribution network. The optimal location and sizing of DG and SVC units are the key variables for voltage stability and power loss minimisation. In this section, the optimal location of DGs is determined based on the continuation power flow method to improve the voltage stability.

3.4.1 Optimum Placement of Distributed Generation Units

Continuation power flow method is selected due to its high precision, simple implementation with static load profiles (which is the case in this modelling study), and requirement of few iterations. This method is based on a predictor-corrector scheme. This scheme finds an estimate for the next load flow solution from a specified pattern of increase in the load. In the estimation of the load flow solution stage, the tangent vector, which is a vector that is tangent to a curve at a given point, is calculated [212, 213]. A typical sequence for calculation of the tangent vector is shown in Figure 3.6.
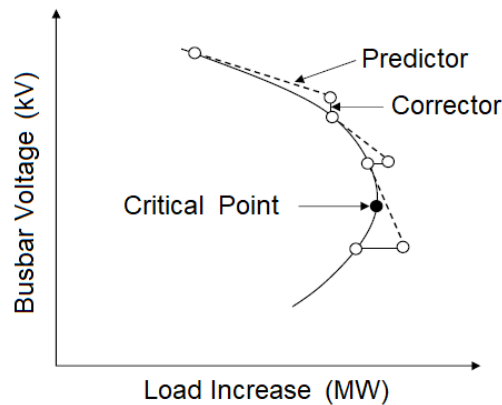
Figure 3.6: Predictor-corrector scheme.

The black line indicates the voltage on the given busbar for an increase in the load. This tangent vector provides information regarding the critical or weak busbar in the system, which is the busbar with a high ratio of differential voltage change to differential load change [214]. The method applies a set of continuing power flow solutions (through Newton-Raphson) based on the change in the specific load to identify the weakest busbar in the system [215]. The change in load can be considered as an increase in the network's active and reactive power demand (i.e., due to EV chargers) [212].

The difference in mathematical formulation compared to the typical non-linear power flow equations in this method is the addition of a variable to identify the change in the load. The mathematical formulation of this method is given with reference to Figure 3.7.
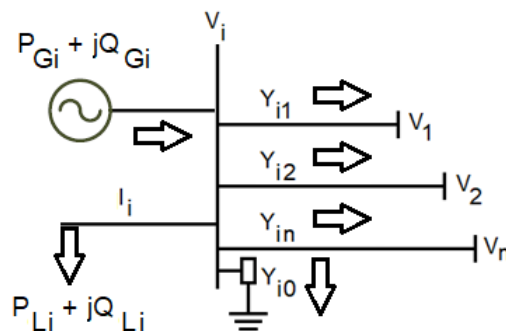
Figure 3.7: Power flow to and from the ith busbar.

The injected current (I_i) for the ith busbar in Figure 3.7 is determined as follows:

$$I_i = \frac{(P_{Gi} - jQ_{Gi}) - (P_{Li} - jQ_{Li})}{V_i *} \tag{3.3}$$

Where:

P_{Gi} is the active power generated at the ith busbar (MW),

Q_{Gi} is the reactive power generated at the ith busbar (MVAr),

P_{Li} is the active power demand at the ith busbar (MW),

Q_{Gi} is the reactive power demand at the ith busbar (MVAr),

V_i is the voltage magnitude at the ith busbar (kV).

The injected current can also be expressed in the form of admittance [214]:

$$I_i = V_i Y_{i0} + Y_{i1}(V_i - V_1) + Y_{i2}(V_i - V_2) + Y_{in}(V_i - V_n) \tag{3.4}$$

Where:

Y_i is the admittance at the ith busbar (the reciprocal of the impedance).

Since the active power and voltage magnitude of each voltage-controlled generator busbar are known, (3.4) can be rewritten in compact form as [214]:

$$I_i = \sum_{j=1}^{n} Y_{ij} V_j \tag{3.5}$$

Where:

Y_{ij} is the element of the admittance matrix (S),

V_j is the voltage magnitude at the jth busbar (kV).

To find successive load flow solution using continuation power flow based on Newton-Raphson, the general form of power flow equation is formulated by calculating the real and imaginary parts of the complex power at the ith busbar [212, 215]:

$$P_i = \sum_{j=1}^{n} |V_i| |V_j| |Y_{ij}| \cos(\theta_i - \theta_j - y_{ij}) \tag{3.6}$$

$$Q_i = \sum_{j=1}^{n} |V_i| |V_j| |Y_{ij}| \sin(\theta_i - \theta_j - y_{ij}) \tag{3.7}$$

Where:

P_i is the active power injection at the ith busbar (MW),

Q_i are the reactive power injection at the ith busbar (MVAr),

θ_i is the voltage phase angle at the ith busbar (MW),

θ_j is the voltage angle at the jth busbar (MVAr),

γ_{ij} is the line admittance angle between the ith busbar and jth busbar (°).

With the continuation power flow method, the reformulated power flow equations are determined to represent the change in active power demand and reactive power demand with respect to the change in the voltage magnitude and with respect to the change in the voltage angle [212, 213, 215].

Using MATLAB and IPSA+ Power simulation software, this method is applied by formulating the non-linear power flow equations. DG units are connected near the most congested substation feeders where voltage drops are greatest. This method not only improves the voltage at the critical load busbar, but it also provides local voltage control for the load busbars closest to the critical load busbar. The type of DG units is not specified in the IPSA+ Power library each generic DG unit can be considered as a PV and/or battery storage as they are two of the most common and fastest growing distributed energy resources in the market. These energy sources can typically be sized and installed on-site to meet specific demand requirements. In this chapter, each DG unit is installed with a capacity of 5 MW, since this represents the lower limit of the most cumulative installed PV capacity range in the UK [254]. With DG units installed near the optimally chosen substations, the network's total active power losses are calculated under different scenarios and presented in Table 3.6.

Table 3.6: Total active power losses under different scenarios with DG units

Scenario	Active Power Losses (MW)	Losses Reduction due to DGs (%)
Baseline	6.24	8.5
S1	6.53	9.6
S2	6.66	9.8
S3	6.71	10.7
S4	6.78	11.5
S5	6.87	12.4
S6	6.98	12.9
S7	7.09	13.4
S8	7.17	13.9
S9	7.26	14.8
S10	7.32	15.6

Simulation results indicate that the utilisation of DG units significantly reduces active power losses compared to a scenario when the network is modelled without any DG units in place (as seen in **Table 3.5**). In the baseline scenario, power losses decrease from 6.82 MW (when DGs are not present) to 6.24 MW (when DGs are present). Even though network losses increase as the number of charging stations increases, they only account for 1.8% and 2% of the total network demand in the first and last scenarios, respectively.

The steady-state nodal voltages with the optimum placement of DG units under different scenarios are also investigated in the network. Simulation results are presented in Figure 3.8 and Figure 3.9 for 11-kV and 6.6-kV load busbars, respectively.
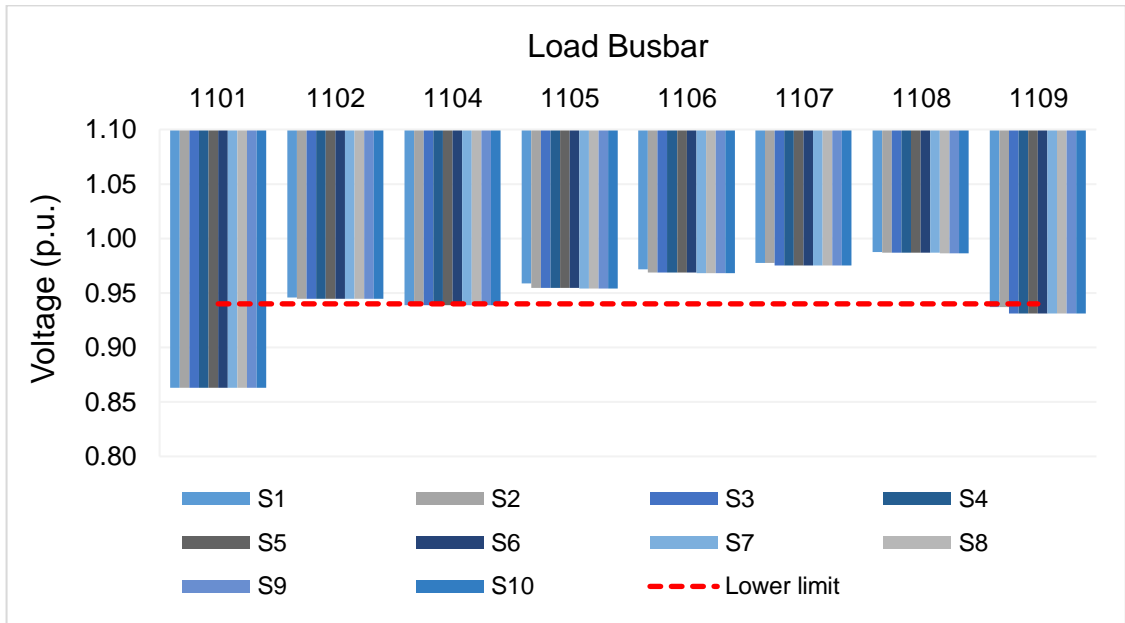
Figure 3.8: Voltage profiles at the 11-kV busbars under different scenarios with DG units.
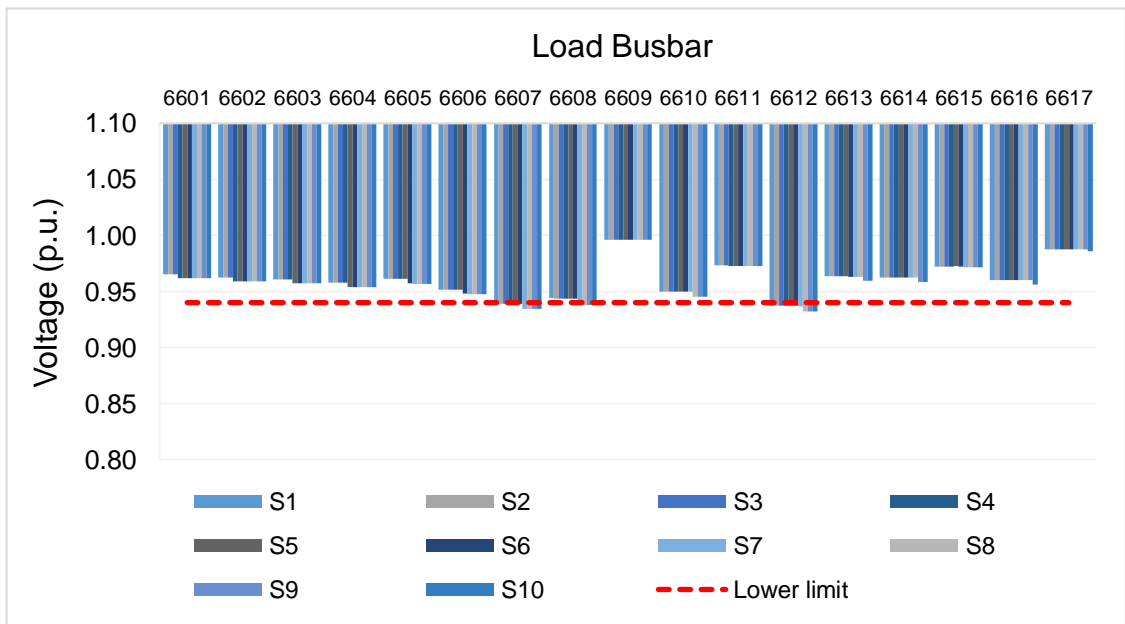
Figure 3.9: Voltage profiles at the 6.6-kV busbars under different scenarios with DG units.

Due to the greater ratio of network demand to charging demand, the steady-state voltage difference between each scenario is negligible for every individual load busbar. Previously, 12 busbars were operating within acceptable limits, while 13 busbars had voltage violations in the absence of DGs during the worst-case scenario (see **Figure 3.4** and **Figure 3.5**). With the optimum placement of DG units, however, four load busbars (1101, 1109, 6607, and 6612) are still exhibiting voltage violations.

In all scenarios, load busbar 1101 has the lowest operating steady-state voltage in the network, with a voltage magnitude of 0.86 p.u. on average. Load busbar 1109, on the other hand, does not exhibit violations until six charging stations are connected to the network (Scenario S3 onwards). This point has a 0.93 p.u. steady-state voltage magnitude. Furthermore, load busbars 6607 and 6612 experience violations when Scenarios S7 and S8, respectively, are implemented in the network. It is seen that the optimum placement of DG is not completely sufficient, and this is mainly due to inadequate sizing of DG units and high consumption of reactive power in the network. For this reason, this thesis also addresses the optimum sizing of SVC devices to provide the required reactive power compensation services to improve the steady-state voltages of those four load busbars.

3.4.2 Optimum Sizing of Static VAr Compensator Devices

SVC devices are used for regulating power factor and providing reactive power compensation services near the violated load busbars in the network [255]. The SVC device used in this thesis represents a generic thyristor-controlled capacitor configuration based on the maximum and minimum voltage threshold levels. The operating principle of this device is given in Figure 3.10.
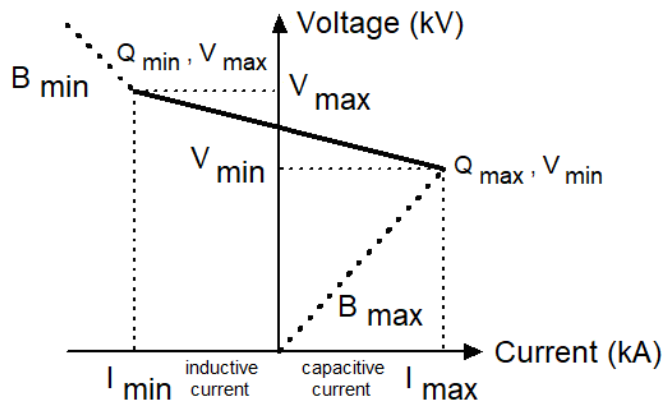
Figure 3.10: Operating principle of the SVC device.

When the upper limit of SVC inductance is reached, the upper voltage limit (Q_{max}) is reached. Similarly, the lower voltage limit (Q_{min}) is reached when the maximum SVC capacitance limit is attained. The inductive and the capacitive current are calculated by:

$$I_{max} = jB_{max}V_{min} \qquad (3.8)$$

$$I_{min} = jB_{min}V_{max} \qquad (3.9)$$

Where:

B_{max} is the maximum susceptance (the inverse of the reactance),

B_{min} is the minimum susceptance (the inverse of the reactance).

At minimum voltage, which occurs when the number of charging stations on a network increases, the SVC must inject reactive power, which is equivalent to a capacitive load, into the network. In load flow analysis, SVC characteristics are defined by two pairs of points, (Q_{min}, V_{max}) and (Q_{max}, V_{min}), as represented in the diagram in Figure 3.10. IPSA models the SVC by injecting reactive power into the busbar, the size of which is proportional to the busbar voltage and change in the load.

The variable reactive power output of the SVC compensates for the voltage and load variations caused by the cycling active power for optimal voltage stabilisation [256]. Therefore, the size of the SVC device is determined for each scenario due to variations in the PQ demand because of increase in the number of charging stations. The minimum required rating of the SVC devices to keep the voltages at the point of connection within the design limits is determined by (3.10) [255]:

$$SVC_m = Q_L + \frac{P_L^{\,2}}{2S_c} + \frac{R}{X}P_L \qquad (3.10)$$

Where:

SVC_m is the minimum required rating of the SVC device (MVAr),

Q_L is the reactive power consumption at the load busbar (MVAr),

P_L is active power demand at the load busbar (MW),

S_c is the short circuit level (250 MVA),

R/X is the resistance to reactance ratio of the system.

The SVC device's minimum required rating is determined by the PQ data at the connection point. The short circuit level of 250 MVA has been selected for the modelling of 11 kV substations [257]. For distribution branches operating at 11 kV, the 'R/X' ratio of 0.67 is chosen based on the reference provided in [255]. Using (3.10), the minimum required sizing of the SVC devices is calculated for the worst-case scenario, as depicted in Table 3.7.

Table 3.7: Sizing of SVC devices under different scenarios

Connection Load Busbar	Demand (MW)	Consumption (MVAr)	Sizing of SVC Device (MVAr)
1101	16.9	11	22.9
1109	19.2	10.5	24.1
6607	24.9	7.6	25.5
6612	24.4	9.1	26.6

Since there are only four load busbars experiencing voltage violations in the network, four SVC devices are installed. The calculations indicate that the SVC device's rating increases in proportion to the PQ demand. To prepare the network for the worst-case scenario, the size of each SVC is determined based on the peak demand at each individual load busbar (i.e., at the highest EV uptake level).

With DG units and SVC devices are present in the network, a load flow analysis is initially performed to calculate the network's total active power losses under different scenarios. The results of the load flow analysis are shown in Table 3.8.

Table 3.8: Total active and reactive power losses under different scenarios with SVC devices

Scenario	Active Power Losses (MW)
Baseline	5.53
S1	5.67
S2	5.78
S3	5.83
S4	5.9
S5	5.98
S6	6.09
S7	6.17
S8	6.24
S9	6.31
S10	6.37

It is seen that the introduction of reactive power compensation services by four SVC devices increases the maximum network throughput and the potential of active power flow. This, as a result, reduces power losses significantly. As compared to previous cases with DG units in place, power losses even account for a smaller portion of the network's total power demand. For example, active power losses in Scenario S10 only account for 1.7% of the total network demand.

Furthermore, the steady-state nodal voltages with SVC devices in place under different scenarios are also investigated and their results are shown in Figure 3.11 and Figure 3.12.
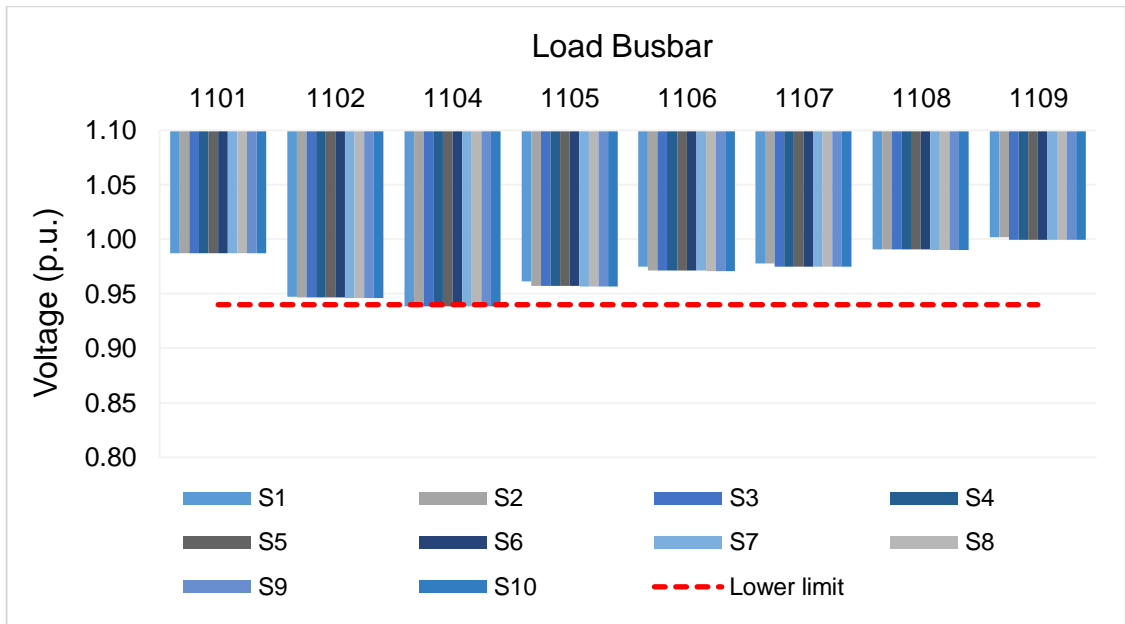
Figure 3.11: Voltage profiles at the 11-kV busbars under different scenarios with SVC devices.
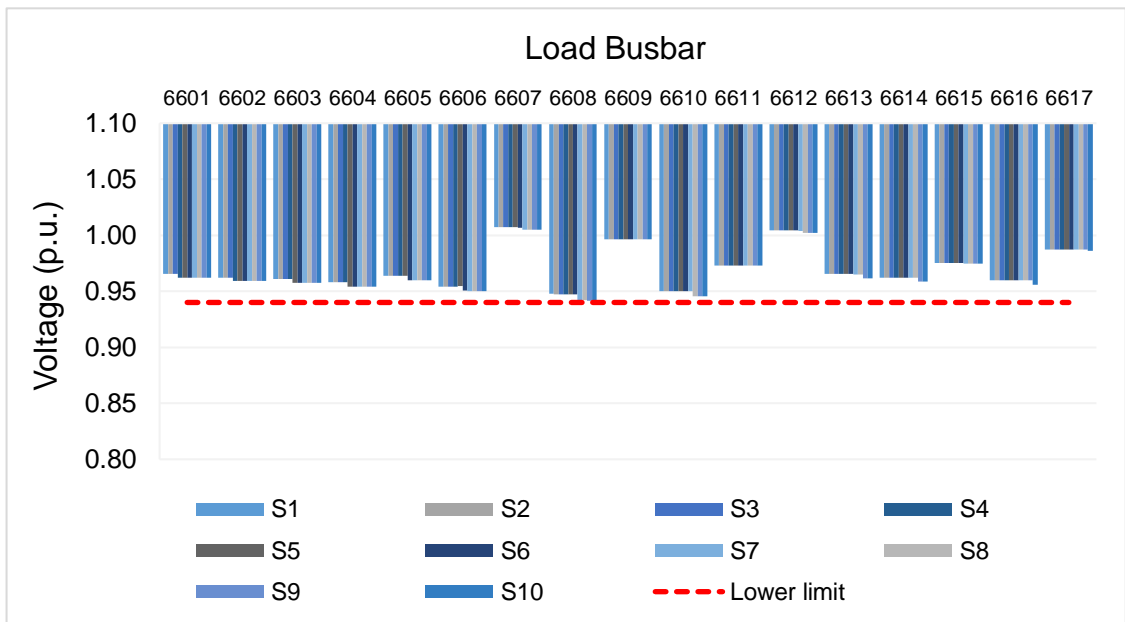
Figure 3.12: Voltage profiles at the 6.6-kV busbars under different scenarios with SVC devices.

The inclusion of SVC devices reduces the voltage drops and maintains acceptable voltage limits at each load busbar in the network. Overall, the largest voltage improvement with the SVC devices is seen at the points where SVCs are connected to. SVC devices have little to no effect on the steady-state voltages of busbars positioned further away from the point where reactive power compensation services are provided. For example, the use of SVC devices during the worst-case scenario increases the steady-state voltages at the violated load busbars (1101, 1109, 6607, and 6612) from 0.86 p.u., 0.93 p.u., 0.93 p.u., and 0.93 p.u. to 0.99 p.u., 1.0 p.u., 1.01 p.u., and 1.0 p.u., respectively. It is also clear that the utilisation of SVC devices stabilises the operating voltages at each load busbar.

3.4 Summary

The steady-state operating characteristics of a generic HV/MV British distribution network are examined using different EV uptake scenarios in IPSA+ Power simulation software. Active power losses and voltage profiles are calculated under different EV charging scenarios and voltage control measures. The importance of installing tap chargers on transformers and placing DG units and SVC devices near optimum network points is evaluated in this chapter.

Simulation results have shown that adjusting the tap settings and installing tap changers on 14 transformers at and near the main generation point improves the voltage profiles of 22/25 busbars during the baseload scenario. However, it is important to analyse the network after the implementation of sensitivity analysis and consideration of different scenarios by increasing the number of charging stations and EV units incrementally. This would give more confidence of that a wide range of possible realistic scenarios are considered.

It is demonstrated that commercial and industrial feeders with higher demand and consumption are more susceptible to voltage violations as the number of charging stations increases in the network. Alternatively, load busbars located closer to the point of generation and transformer with taps in place, as well as to the substation feeders equipped with DG units and SVC devices, are less affected. Simulation results demonstrated unequivocally that DG units should be placed at optimal locations to reduce power losses and eliminate voltage violations in the network. The optimal sizing of voltage control measures is also crucial, especially if the number of charging stations grows as anticipated. In the worst-case scenario, the utilisation of four DG units near critical substations and four SVC devices near critical load busbars reduced power losses by up to 15.6% and 26.5%, respectively.

It has been shown that steady-state busbar voltages are managed to operate within permissible DNO limits with the inclusion of SVC devices. However, increasing the rating of the SVC devices also results in an increase in the system's cost. Although the cost of SVCs varies based on the device rating and specifications, the cost of an 0.2-MVAr SVC device suitable for an 11-kV substation connection typically varies between $1,000–20,000 in the Chinese market [258].

CHAPTER 4

4. Computational Modelling and Simulation, and Experimental Testing of Batteries and Chargers

4.1 Introduction

The dynamic behaviour of power systems has changed dramatically in recent years because of growing use of power electronic interfaced technologies. These technologies alter the system's behaviour and provide new issues for DNOs. The impact of connecting EV chargers as constant lumped PQ loads to test networks has been widely examined in the literature and reviewed in **Chapter 2**. However, this approach to EV charging modelling generally restricts the network analysis to steady-state examination. This chapter therefore presents the modelling of battery dynamics in more detail.

This is merely an introductory/methodology chapter demonstrating how the charging of batteries is accomplished. In the first section, the key parameters of the generic Shepherd battery model are simulated. Random parameters are used to demonstrate that charging occurs as intended. In **Chapter 5** and **Chapter 6**, the developed charger circuitry and Shepherd model are integrated into a real low-voltage distribution feeder for detailed network analysis.

In the second section of this chapter, physical slow-speed battery charger is used to show how charging and discharging occurs for lithium-ion batteries. In **Chapter 7**, the physical charger equipment is used to conduct different battery discharge tests.

4.1.1 Chapter Structure

Section 4.2 reviews the mathematical modelling and operational principles of the battery dynamics.

Section 4.3 demonstrates the characteristics of the battery dynamics through different simulation cases. The difference between G2V and V2G is also shown.

Section 4.4 introduces the physical lithium-ion batteries and the slow-speed battery charger unit used to conduct different tests. Preliminary tests are conducted to demonstrate how charging and discharging occur.

Section 4.5 summarises the main findings of the chapter.

4.2 Alternating Current vs Direct Current Charging

EV charging is classified into two broad types, depending on the electricity and chargers used: AC and DC chargers. The batteries of EVs are often charged by the grid (in the form of AC power). However, since the EV's batteries are only capable of storing DC power, power electronic devices are required to convert energy throughout the charging process. Figure 4.1 shows the main difference between AC and DC chargers.
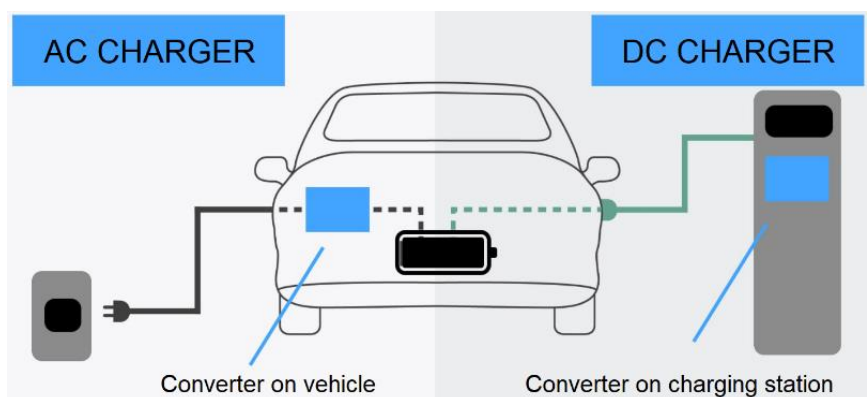
Figure 4.1: AC vs DC charging for electric cars.

AC charging requires an AC-to-DC converter since the outlet, for example, AC mains (AC-type plug), gives AC power, and the car battery requires DC electricity. The car is equipped with its own on-board converter, which performs the conversion within the vehicle itself. DC charging, on the other hand, utilises an off-board converter, also known as public EV supply equipment, to generate DC power for the vehicle. This DC power and electricity are then sent to the battery, where an additional DC-to-DC conversion is performed to acquire the appropriate voltage and current rating for charging to take place [34, 259].

DC chargers are quicker than AC charges since the DC power is provided directly to the vehicle's battery. To supply more power to charge the battery, a larger converter is generally required. A DC charge point installation requires significant grid power. Consequently, its production, installation, and operation costs are quite high, resulting in higher charging rates. However, the absence of AC-to-DC conversion in DC charging reduces the complexity and increases the efficiency of DC chargers [34, 259].

4.2.1 Connection Topology of Battery Chargers

Electricity supply is commonly broken down into three stages: generation, transmission, and distribution. Battery chargers for EVs are generally connected to the distribution side through power converters. The simplified connection architecture of a typical battery charger in a residential distribution feeder is shown in Figure 4.2.
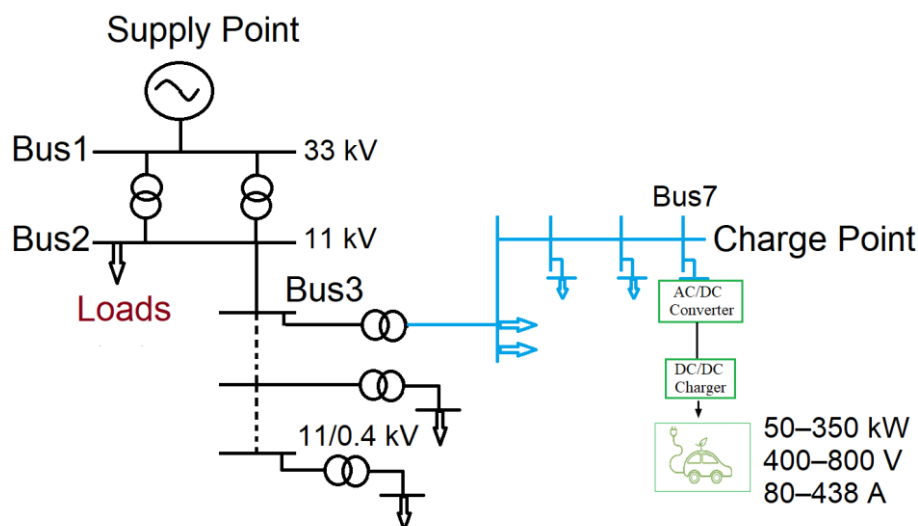
Figure 4.2: Connection topology of a battery charger in a typical distribution network.

The simplified network schematic is comprised of a 33-kV supply point. Transformers reduce the voltage to 11 kV for the nearest substation denoted by Bus1 in the schematic diagram. Several outgoing feeders are supplied by the 11/0.4 kV transformers near the 11-kV substation point. The blue zone depicts the low-voltage side of a segmented distribution network that is made up of several residential load busbars.

A battery charger is attached to Bus7 in the schematic design. This point is selected for demonstration reasons. An AC-to-DC converter, also termed as rectifier, is the first power electronic interfaced technology used in the battery charger topology. At the connection busbar, the rectifier converts from the AC to a sufficient DC voltage and current [217, 260]. The next step involves the connection of a DC-to-DC charger, which is made up of a DC-to-DC converter and a battery circuit.

4.2.2 Rectifier Topology

The rectifier is the charger system's initial power electronic unit at the AC side. A simplified two-level voltage source converter topology to rectify AC into DC is used. The schematic diagram of a two-level voltage source converter is shown in Figure 4.3.
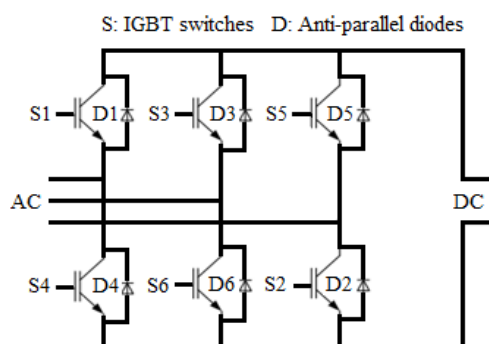
Figure 4.3: A schematic diagram of a two-level rectifier topology.

Two-level voltage source converter topologies are commonly used in grid-connected battery charging applications. The topology is divided into three phases, each of which contains an upper and a lower arm. Each arm is constructed using an Insulated Gate Bipolar Transistor (IGBT) switch and an anti-parallel diode, as shown by the 'S' and 'D' symbols, respectively. Each IGBT switch can be modelled to provide a sufficient rated voltage and current for achieving the charging process of the battery. Switching on IGBTs from the same arm and phase simultaneously would result in a short circuit in the rectifier's DC link. Thus, switches from different phases and arms should be regulated simultaneously (e.g., S1 and S6) [261].

4.2.3 Rectifier Synchronisation

Without effective synchronisation, the rectifier cannot achieve the required DC voltage and current. Synchronisation enables the transfer of energy from the grid to the rectifier end [262, 263]. The synchronisation process occurs at the point where the charger is connected to. This point is termed as the *Point of Common Coupling* (PCC), at which point power is transferred between the grid and the battery. The sequence of the synchronisation process between the grid and the battery is shown in Figure 4.4.
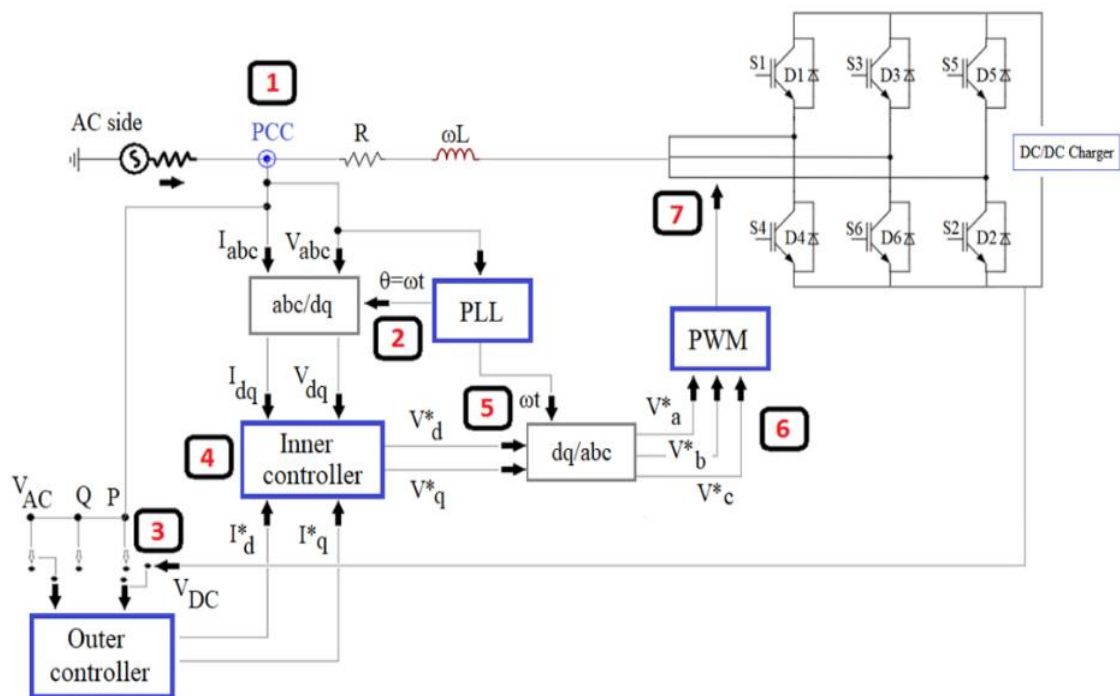
Figure 4.4: Synchronisation sequence of the grid and the rectifier.

1) The measurements of the three-phase grid current (I_{abc}), three-phase grid voltage (V_{abc}), AC voltage (V_{AC}), active power (P) and reactive power (Q) are extracted from the PCC from the AC side.

2) Using a Phase-Locked Loop (PLL) mechanism, three-phase grid current and three-phase grid voltage variables are fed into the *abc* to *dq* (direct quadrature) transformation block and synchronised with the grid frequency. The PLL operates on the fundamental principle of a feedback system with a proportional-integral (PI) regulator monitoring the phase angle (ϕ) from the PCC [264, 265]. Zero crossing, stationary reference frame, and synchronous reference frame (SRF) are the three primary PLL methods used for phase-angle tracking. SRF-PLL is used in this study due to its popularity and simpler implementation [265]. The detailed modelling of the PLL mechanism is given in the appendices (see **Appendix B.2**).

3) The outer controller block receives four input signals: V_{AC}, P, Q and DC link voltage (V_{DC}). This block then generates reference current variables in '*dq*' frame: $I *_d$ for 'd' frame and $I *_q$ for 'q' frame [260]. It uses a feedback system with a PI regulator to calculate the error signal between one of the four input signals and its measured value from the PCC. The calculated error signal is then input into the inner controller block. The detailed loop designs for the outer and inner controllers are given in the appendices (see **Appendix B.3** and **Appendix B.4**).

4) The inner controller block receives the output signals of the outer controller block and then produces reference voltage variables in '*dq*' frame: $V *_d$ for 'd' frame and $V *_q$ for 'q' frame. These variables are then input into the *dq* to *abc* transformation block and synchronised to the grid frequency through the PLL [265].

5) The *dq* to *abc* transformation block generates three-phase reference voltage variables in '*abc*' frame: $V *_a$ for phase 'a', $V *_b$ for phase 'b', and $V *_c$ for phase 'c' [261, 262, 266].

6) The Pulse-width Modulation (PWM) approach is then initialised using the three-phase reference voltage variables to trigger IGBT switches and force operate the rectifier. The rectifier then allows current to pass to the DC side.

7) PWM is a standard approach that provides a constant input AC voltage to the rectifier and generates a regulated output DC voltage. Switching signals are generated by comparing the instantaneous magnitude of a high-frequency carrier waveform to sinusoidal input reference voltage signals [267, 268]. The fundamental principle of PWM is shown in Figure 4.5.
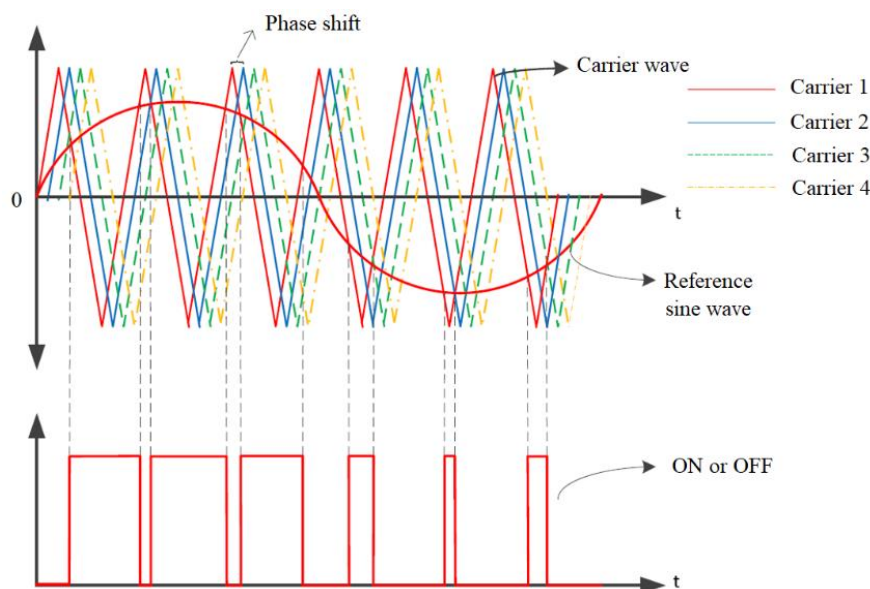
Figure 4.5: Phase-shifted multicarrier PWM technique.

The graph uses a generic PWM technique to display the phase shift of the carrier waveforms with respect to the generic reference sine wave plotted against time in the horizontal axis. Each carrier signal runs at the same frequency and has a peak-to-peak value of identical magnitude. These carrier signals are separated by a phase shift. The reference sine wave is generated and compared to each of these high-frequency carrier signals for each time step represented by the horizontal axis. Based on the comparison, the switching pattern for the IGBTs is determined, as shown by the bottom graph in Figure 4.5. The switching pattern indicates that the IGBT is active when a binary value of 1 is present but is inactive when a binary value of 0 is present [268, 269].

4.2.4 DC-to-DC Charger Topology

On the DC side, the charger circuit is composed of a DC-to-DC converter and a battery equivalent model. Both components are connected in series to efficiently generate and manage the power delivered to the battery pack [270].

4.2.4.1 DC-to-DC Converter

Different DC-to-DC converter topologies, including the buck and boost converters, are commonly used in battery applications. The former is used to charge the battery, whilst the latter is used to discharge it. To accomplish both charging and discharging of the battery, a combination of the two, namely, buck–boost topologies are generally used. This research addresses both the charging and discharging characteristics of the batteries, using the buck–boost topology. The schematic diagram of the buck–boost topology is shown in Figure 4.6.
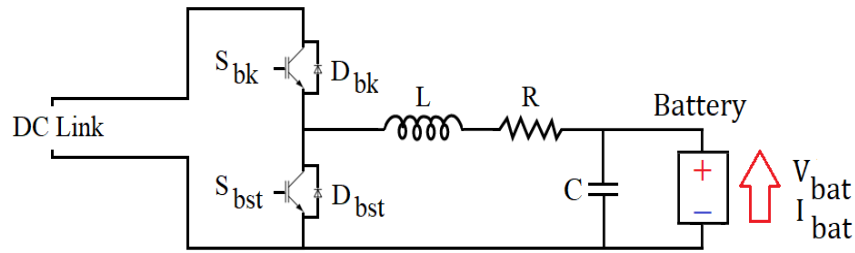
Figure 4.6: Simplified schematic diagram for buck–boost converter.

These converter topologies are constructed using two IGBT switches: S_{bk} and S_{bst}, two anti-parallel diodes: D_{bk} and D_{bst}, an inductor (L), a resistor (R), and a capacitor (C) to charge and discharge the battery. The direction in which the current flows dictates whether the capacitor or the battery attached to the output terminal is charged or discharged.

For example, the current flows from the grid to the battery in charging mode by activating the buck switch (S_{bk}) and deactivating the boost switch (S_{bst}). Additionally, by activating the boost switch while discharging the battery, the current direction is reversed as it flows from the battery to the grid end [270–272].

The simplified controller loops for buck and boost switching are shown in the appendices (see **Appendix B.5**). The detailed modelling and selection of data for power electronics and switching are also shown in the appendices (see **Appendix B.7**).

4.2.4.2 Shepherd Battery Equivalent Model

In this study, a rechargeable ideal open-circuit voltage-controlled source representing a generic Shepherd battery model available in PSCAD/EMTDC simulation software's library, is used. The specifications of the generic Shepherd battery model are acquired from [46]. Figure 4.7 shows the simplified battery equivalent circuit of the model.
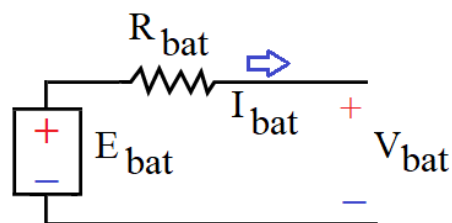
Figure 4.7: Ideal equivalent battery circuit for Shepherd model.

The simplified battery model is comprised of an ideal regulated voltage source connected in series with a battery resistor (R_{bat}). The determination of the regulated voltage source at each time step is given by [46]:

$$E = E_0 - K\frac{Q_b}{Q_b - it} + A^{(-Bit)} \qquad (4.1)$$

Where:

E is the no-load voltage for Shepherd model (V),

E_0 is the constant voltage for Shepherd model (V),

K is the polarisation voltage for Shepherd model (V),

Q_b is the rated capacity for Shepherd model (kWh or Ah),

it is the actual battery charge at each time step (%),

A is the exponential zone amplitude for Shepherd model (V),

B is the exponential zone time constant for Shepherd model (1/Ah).

This expression demonstrates the battery's non-linear nature. It is assumed that the battery voltage stays proportional to the current flowing through it while charging and discharging, whilst the battery resistance remains constant [46]. The battery voltage under no-load circumstances can be changed by substituting the 'it' terms in (4.1) with the actual battery SoC, as expressed by (4.2):

$$E = E_0 - K\frac{1}{SoC} + Ae^{-BQ_b(1-SoC)} \qquad (4.2)$$

The expression does not take temperature into account and assumes that the battery behaviour is identical in each simulated instance. The appendices include other modelling aspects and parameters for the Shepherd battery model (see **Appendix B.1**)

4.3 Simulation of Shepherd Battery Model

This section uses the PSCAD/EMTDC simulation software to show how the generic Shepherd battery model charges and discharges under different settings. It should be noted that the simulation results are only intended to illustrate how the Shepherd battery model's parameters change under different conditions.

4.3.1 Slow vs Fast Charging

Two EV battery charging speeds are emulated to compare slow and fast charging. It is assumed that the first battery has a rated capacity of 40 kWh, and it is charged on a single-phase charger (rated at 7 kW), while the second battery has a rated capacity of 42.2 kWh, and it is charged using a three-phase charged (rated at 22 kW). Figure 4.8 shows the charging of both batteries under different charging power, whereas Figure 4.9 shows the discharging of both batteries under different charging power.
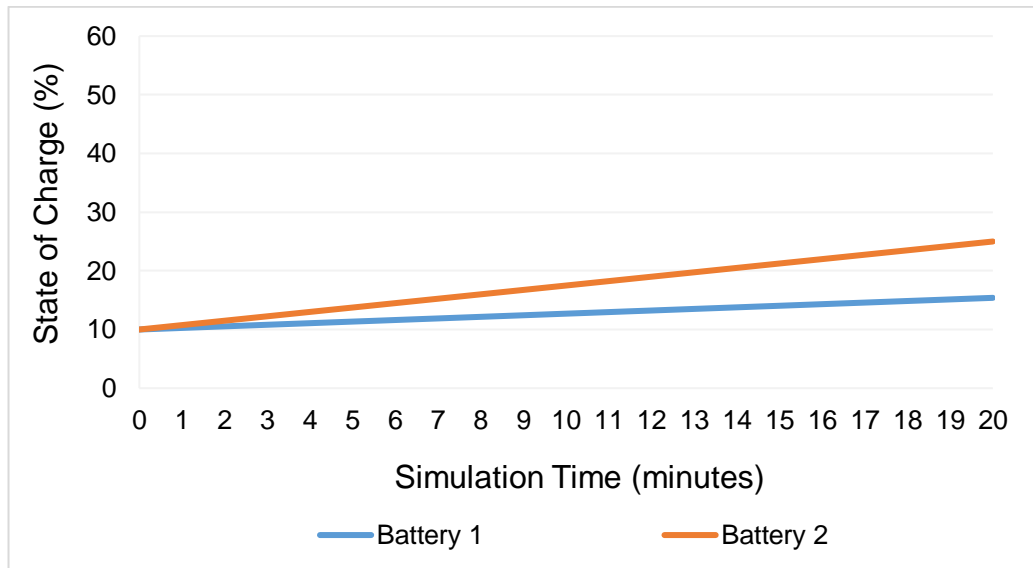
Figure 4.8: Charging profiles of batteries under different charging power.

The graph depicts the battery SoC (in %) in the vertical axis, as a function of simulation time (in minutes) in the horizontal axis. It is assumed that both batteries begin charging at 10% SoC and receive a constant charge power for 20 minutes. The SoC of the first battery increases from 10% to 15.4%, while the second battery reaches 25% after 20 minutes. A 22-kW device's increased charging power charges the second battery nearly three times faster than the first battery due to nearly tripled current value.
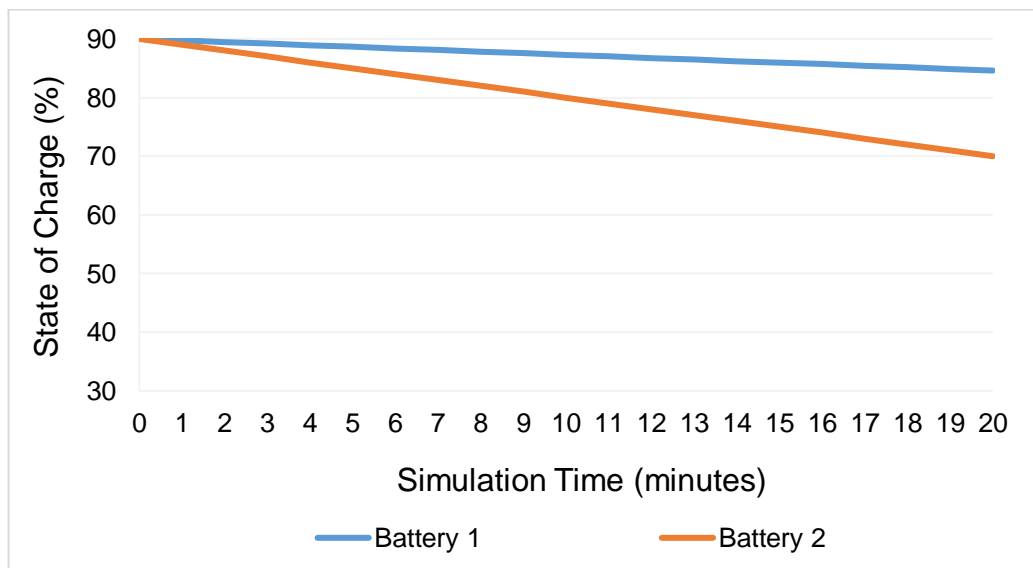
Figure 4.9: Discharging profiles of batteries under different charging power.

The graph depicts the battery SoC (in %) in the vertical axis, as a function of simulation time (in minutes) in the horizontal axis. It is assumed that both batteries begin discharging at 90% SoC. After 20 minutes, the SoC of the first battery reduces to 84.6%, whereas it decreases to 70% for the second one. The rate of charging and discharging is faster on the second battery since it draws three times more power and hence current than the first battery.

4.3.2 Rapid Charging

A typical battery of a popular Tesla Model S is emulated and simulated with its specifications to demonstrate how rapid charging works. A Model S has a rated battery capacity of 90 to 100 kWh and a nominal voltage of around 400 V [27, 33]. Two rapid charging devices are used to compare the charging speeds of the emulated batteries: the 75-kW and the 150-kW. The charging profile of the batteries under both charging devices is shown in Figure 4.10.
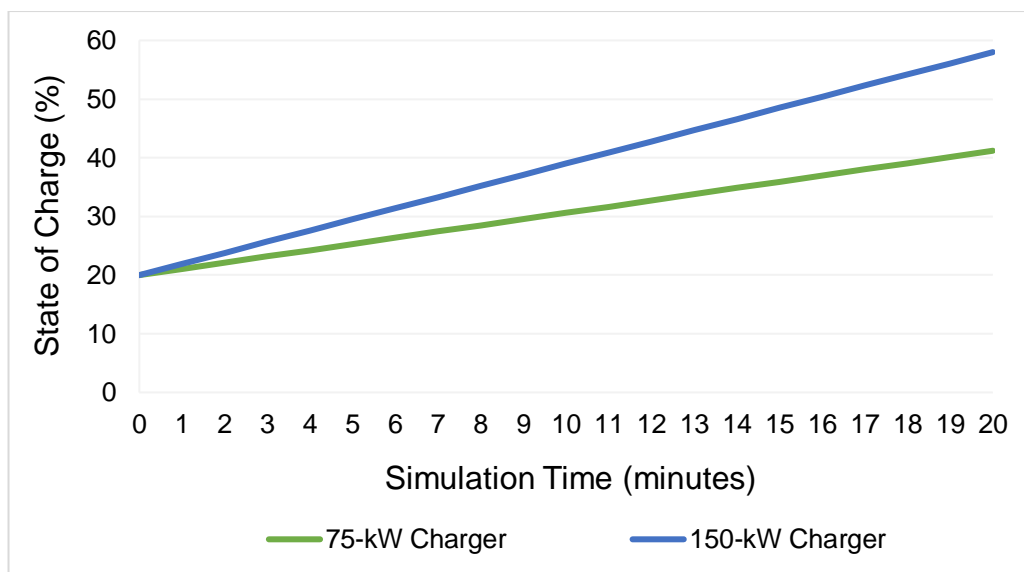
Figure 4.10: Charging profiles of batteries using 75-kW and 150-kW devices.

It is assumed that both batteries start charging from a SoC of 20%. The 150-kW device charges the second battery (represented by the blue line) at double the current of that of 75-kW device, resulting in a faster charging speed overall. After 20 minutes on the 75-kW charging device, the first battery (represented by the green line) achieves 41.2% SoC, while on the 150-kW device, it achieves 58% SoC.

4.3.3 Variable Charging Power

In a typical charging station, the driver picks the physical charging unit, but the amount of power provided is entirely dependent on what the car asks for up to the charger's maximum rate [242]. In this part, the effect of varying the charge power on a generic battery model is shown in Figure 4.11 and Figure 4.12.
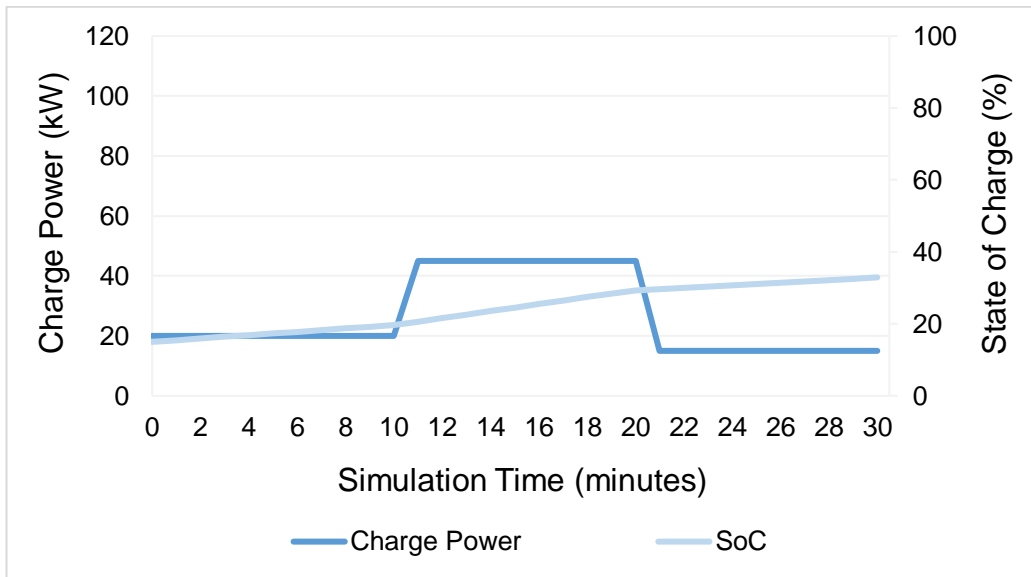
Figure 4.11: Controlled charging profile of a generic EV battery.

The graph demonstrates the charging speed in the vertical axis (in kW), as a function of the battery SoC (%) in the secondary vertical axis.
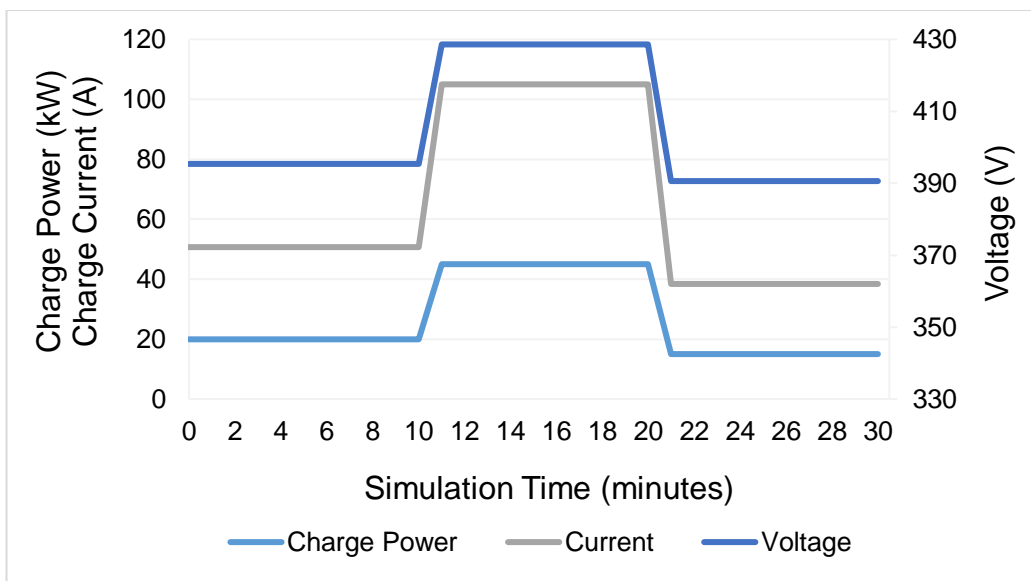
Figure 4.12: Generic EV battery parameters during controlled charging.

The graph in Figure 4.12 depicts the charge power (in kW) and charge current (in A) in the vertical axis, as a function of the battery voltage (in V) in the secondary vertical axis.

In the presented scenarios, the charging power supplied to the generic battery is randomly regulated at different time steps. At the start of charging, the battery has a SoC of 15% and is charged at a fixed rate of 20 kW. After ten minutes, the charging power is increased to 45 kW. Following the change in charge power, the charging current (current delivered to the battery) increases from nearly 50 A to 105 A (as seen in Figure 4.12), while the charging voltage (battery terminal voltage) rises from nearly 400 V to 428.6 V.

It is indicated that the current and voltage are directly proportional to each other during charging and raising the charging power increases the vehicle's charging speed (i.e., steeper SoC curve).

The charging power is reduced and maintained at 15 kW throughout the last part of the simulation (between 20–30 minutes), which also reduces the charging current, battery voltage, and the rate of charging. It should be emphasised that charging power is regulated arbitrarily for demonstration purposes to test the battery dynamics.

4.3.4 Grid Power at the Point of Common Coupling

The final part of this section demonstrates how battery chargers influences and alters power flows in the network. The AC grid is simulated as a simple distribution network with different loads, including residential and EV loads, connected to it. Simulation cases are performed and the effect of G2V and V2G charging is shown in Figure 4.13.
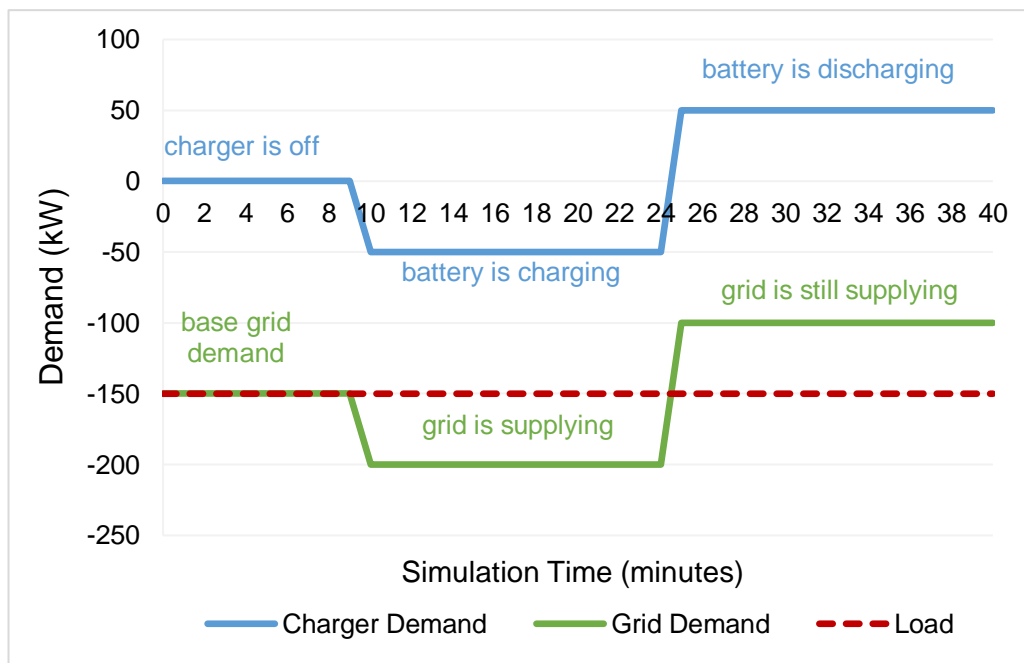
Figure 4.13: Modified power flow with battery charging and discharging.

The graph depicts the demand (in kW) (i) of the EV charger (blue line), (ii) grid (green line), and (iii) load (red line) in the vertical axis, as a function of simulation time (in minutes) in the horizontal axis. The direction of electricity flow is simply shown by the positive or negative magnitudes. For example, between 0–10 minutes, the battery charger is switched off, and the load absorbs a fixed demand of 150 kW — represented by the negative magnitude. Grid demand matches baseload demand throughout this time. However, when the 50-kW charger is switched on and the battery is being charged at a constant rate between 10–24 minutes, the grid starts supplying 200 kW — also represented by the negative magnitude.

At the last stage of the simulation, the battery charger's operation is reversed, and the energy stored in the battery is discharged and injected back into the grid through V2G technology. This is shown by the positive demand magnitude for the battery between 25–40 minutes. At this point, the grid is still supplying energy, but its demand is reduced from 200 kW to 100 kW due to the V2G charger injecting power to the grid.

4.4 Experimental Testing of Batteries and Chargers

This section is only intended to present the physical charger equipment and demonstrate how the charging is achieved. Experiments are conducted (i) to analyse the charging and discharging characteristics of physical lithium-ion batteries under different settings. The experimental kit is also used in **Chapter 7**.

4.4.1 Battery Models and Battery Charger Units

Lithium-ion PANASONIC NCR18650PF battery packs are used for the experiments. The model of the PANASONIC battery packs is shown in Figure 4.14. The MC3000 Universal battery charger and an analyser unit (developed by SkyRC Technology), as shown in Figure 4.15, is used to charge and discharge the battery.

Figure 4.14: PANASONIC NCR18650PF lithium-ion battery cells [273].

Figure 4.15: MC3000 Universal battery charger and an analyser unit [52].

It should be noted that the small-scale and slow-speed SkyRC MC3000 battery charger has only four slots (meaning only four battery cells can be charged, discharged, and monitored simultaneously). Due to budgetary constraints, a larger (in size and rating) battery charger and analyser unit could not be purchased and utilised for more comprehensive testing. The maximum charge rate for the MC3000 is 2 A constant current for charging and 1 A for discharging [52]. Charging and discharging batteries at higher rates would need battery cooling to prevent battery explosion. This charger is also monitored and controlled through a computer software, namely, MC3000 Monitor client version 1.05, to analyse the charging and discharging characteristics of physical battery cells in real time.

4.4.1.1 Relevancy of Experimental Work and Selection of Battery Cells

The majority of EVs employ hundreds of individual cells that are packed and built into modules arranged in a series/parallel configuration to achieve the desired battery voltage and capacity. For example, the most common Tesla models (Model S and Model X) consist of around 7,104 units of 18650 cylindrical cells [274]. The Model S consists of 74 cells, 6 groups in series for a module, and 16 modules in series ($74\ cells \times 6\ groups \times 16\ modules = 7,104\ cells$). Recently, Tesla engineers have modified the battery pack so that each module can have up to 516 cells ($86\ cells \times 6\ groups \times 16\ modules = 8,256$). This has also increased the rated capacity of Model S battery packs from 85 to 100 kWh [275].

In an EV, hundreds of cells are assembled to form a battery pack, and each cell must be individually monitored to ensure that the battery pack operates in a safe and efficient manner. This requires a dedicated control method known as the battery management system. The primary function of this system is to ensure that the battery pack operates safely. Since a battery pack in a typical EV is composed of cells with an individual voltage rating, the battery management system ensures that the cells within the pack are not discharged beyond the threshold limit [276]. This is why the experimental work is conducted to analyse the relationship between an individual cell's battery voltage and discharge capacity to ensure that discharge end voltage for cells is not reached under different scenarios and discharge profiles. It should be specified that the physical charger unit can charge/discharge up to four battery cells simultaneously. However, the discharge current decreases as the number of occupied slots increases (hence the increased charge/discharge time). During the experiments, a single slot (i.e., a single cell) is utilised to take advantage of the maximum discharging current capability of the charger unit and to simplify battery monitoring.

In addition, it is important to mention that the simulation cases for battery charging focus on the control of charging power through current limiters, so that the effect of increasing the rating of battery charger can be studied on the network. On the other hand, the experimental work for charging focuses on the control of charging and discharging current, so that the effect of increasing and decreasing the current can be seen on the cell voltage, which is then used to determine the discharged capacity and hence estimate the battery SoC and DoD under different scenarios in **Chapter 7**.

4.4.2 Charging and Discharging at Constant Current

The PANASONIC batteries used for this experiment are assumed to have a maximum charging current and a maximum charging voltage of 1 A and 4.2 V, respectively. For the first experiment, the PANASONIC cell is charged under different current settings: a constant current of 1 A and a constant current of 0.5 A. The starting battery voltage is assumed to be 4.1 V, which indicates that the battery pack is not fully charged. The charging speed of the cell is shown in Figure 4.16.
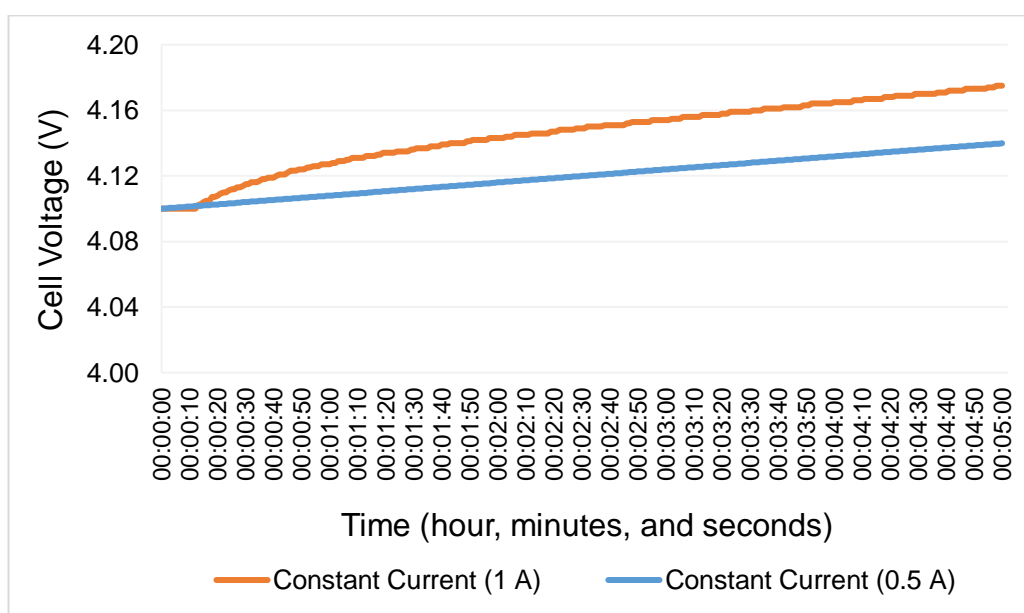
Figure 4.16: Charging of the PANASONIC cell at 1 A and 0.5 A.

The vertical axis of the graph indicates the battery cell voltage (in V), while the horizontal axis is based on a 24-hour time format (in hour, minutes, and seconds) since the battery charger and an analyser unit uses this format while producing battery charging/discharging profiles. It should be noted that the length of the experiment is limited to five minutes for demonstration reasons. At a larger charging current, the cell voltage rises more rapidly.

For the second experiment, the PANASONIC cell is discharged from a nominal cell voltage of 4.1 V with a constant current of 0.8 A and with a constant current of 0.5 A. It should be emphasised that these discharge current values are chosen randomly to demonstrate the diversity in the discharging profiles of lithium-ion batteries under different and various settings. Figure 4.17 compares the discharge profiles for the PANASONIC cell under two discharge current settings.
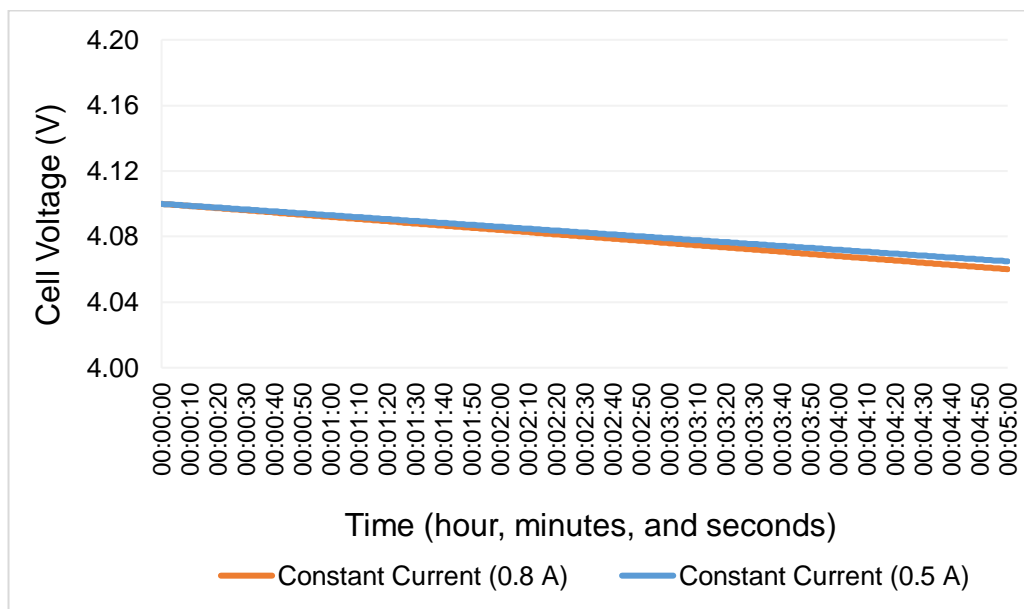
Figure 4.17: Discharging of the PANASONIC cell at 0.8 A and 0.5 A.

The vertical axis represents the voltage of the PANASONIC cell (in V), whereas the horizontal axis represents the time elapsed (in hour, minutes, and seconds). With a discharging current of 0.8 A and 0.5 A, the voltage of the PANASONIC cell reaches from 4.1 V to 4.06 V and from 4.1 V to 4.065 V, respectively. The rate of discharge is just marginally quicker (as seen by the orange line) when the discharging current is larger.

4.4.3 Charging and Discharging at Variable Current

At random intervals, the charging and discharging currents supplied to the PANASONIC battery cell are varied for this chapter's concluding experimental tests. These tests are more practical for determining how the change in current affects the lithium-ion cells' charging rate. In the concluding chapter of this thesis, the impact of varying the rate of discharge of lithium-ion battery cells is examined in greater detail.

The effect of varying the charging current and discharging current for the PANASONIC cell is presented in Figure 4.18 and Figure 4.19, respectively.
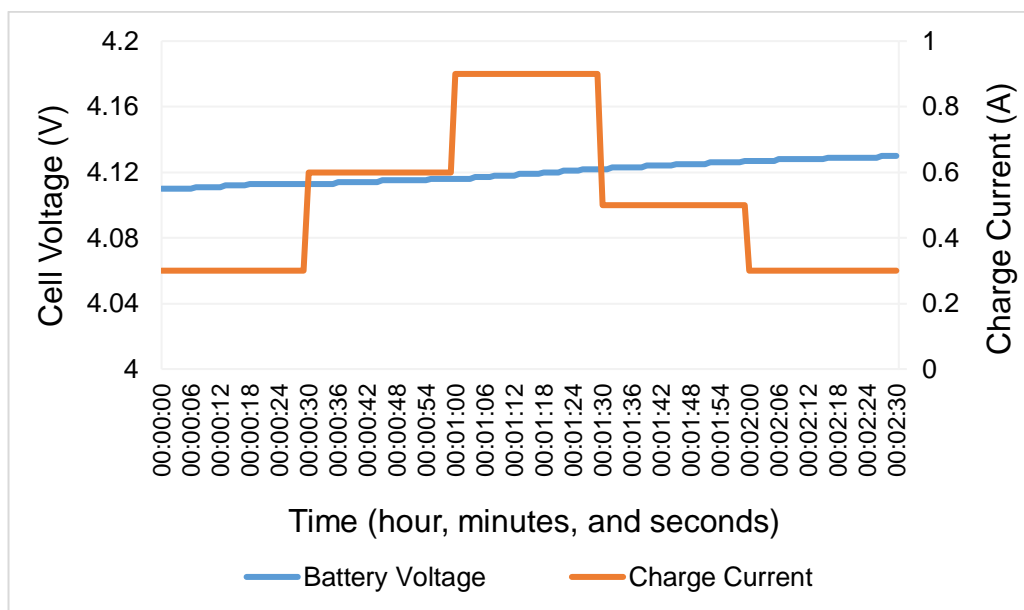
Figure 4.18: Charging the PANASONIC cell at a variable current profile.

The graph shows the PANASONIC cell voltage (in V) in the primary vertical, as a function of the charging current (in A) in the secondary vertical axis. The horizontal axis represents the duration (in hour, minutes, and seconds) of the experiment (150 seconds). The battery is first charged at a rate of 0.3 A. After 30 seconds, the current at which the battery cell is charged is doubled. The maximum charging current of 0.9 A is applied between 60 and 90 seconds. The charging current is then initially reduced to 0.5 A and then to 0.3 A between 90 and 120 seconds, and 120 and 150 seconds, respectively. The battery's cell voltage reaches from 4.11 V to 4.13 V once the experiment is completed.
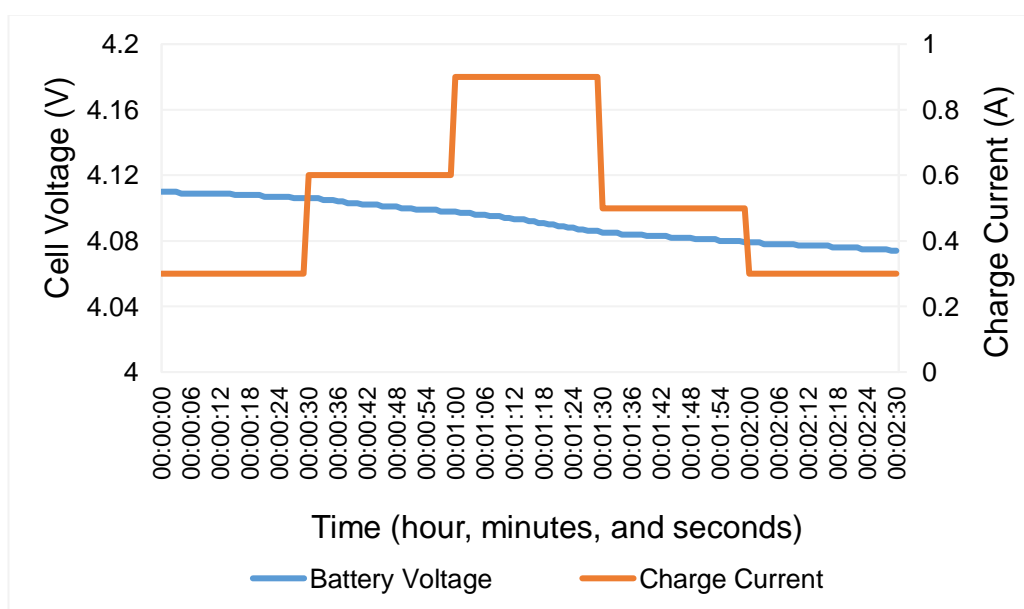
Figure 4.19: Discharging the PANASONIC battery cell at a variable current profile.

Identical charging current values are applied to the PANASONIC battery cell while discharging. The battery is first discharged at a current of 0.3 A. After 30 seconds, the discharge current is raised to 0.6 A, and then increased to 0.9 A between 60 and 90 seconds. The rate of change in cell voltage rises between 30 to 60 seconds due to the maximum discharge current of 0.9 A. In the last phase of the test, the current is initially lowered to 0.5 A and then to 0.3 A. The battery's cell voltage reaches 4.074 V after 150 seconds.

4.5 Summary

The technology and components required to integrate battery chargers and Shepherd battery models into the distribution level of power networks are reviewed and presented in this chapter, respectively. Simulation studies demonstrated the impact of controlling the battery's charging power. As the charging power can range from 3 kW to 250 kW, simulation studies will provide greater flexibility for this research work in **Chapter 5** and **Chapter 6**.

On the other hand, a physical slow-speed battery charger and an analyser unit is used to present the charging and discharging characteristics of lithium-ion batteries through different tests. Experimentation revealed the impact of regulating the charging current injected into the battery. Although the physical charger used in this research has limitations regarding its rating and inability to charge/discharge an entire battery pack, it will aid in the integration of different discharge profiles based on the stochastic charging profiles that will be developed by the algorithm described in **Chapter 6**. The incorporation of discharge profiles will enable the estimation of the SoC, DoD, and discharged capacity of lithium-ion batteries.

In conclusion, most of this chapter is considered as a methodological component of the thesis for the following three chapters to perform dynamic analysis using battery chargers and battery packs. The conducted battery tests also increase the validity of developed battery dynamics and allow the author and other researchers to attempt to discover something new about the battery packs, as well as to explain 'why' something occurs and 'how' something can be improved in the context of charging the EV batteries. Finally, it should be noted that the results presented in this chapter only serve to illustrate the practical application of both charging techniques through simulation and experimental methods.

CHAPTER 5

5. Impact of Integrating Different Battery Chargers on a Low-Voltage Distribution Network

5.1 Introduction

The effect of integrating uncontrolled EV chargers on distribution networks has been extensively analysed in the literature, and in **Chapter 3** of this thesis using a medium-voltage network. However, very little research investigates the implications of integrating different charging technologies and non-linear dynamic EV chargers into low-voltage distribution networks simultaneously. The PSCAD/EMTDC simulation software is used to effectively model and incorporate dynamic characteristics of battery chargers into a real low-voltage UK distribution network feeder in this chapter. The integration of different charging technologies adds diversity and accuracy to the dynamic analysis of the networks. For example, drivers who travel short distances may find that home charging is a convenient option, while those who travel longer distances may choose to utilise public chargers while at work or at destination. Therefore, this chapter is important as it compares the effects of different charging modes at different network locations.

The main goals of this chapter are (i) to analyse the interaction between different charging scenarios on a real low-voltage distribution network feeder that serves both residential and commercial customers and (ii) to investigate the effect of increasing cable dimension, V2G chargers, and coordinated charging techniques.

5.1.1 Chapter Structure

Section 5.2 presents the low-voltage distribution network feeder, load profiles of the residential and commercial customers, and the charging scenarios.

Section 5.3 conducts a dynamic analysis (i) to examine the daily voltage variations and voltage drops, (ii) to analyse cable current and cable overloading, and (iii) to calculate power losses and the cost of power losses in the feeder.

Section 5.4 examines three cable overloading mitigation strategies, including (i) the oversizing of cables, (ii) the implementation of V2G chargers, and (iii) the utilisation of controlled charging techniques, during periods of increased network demand.

Section 5.5 discusses and summarises the main findings of the chapter.

5.2 Low-Voltage Distribution Network Modelling

The network under examination is a representation of a British urban residential distribution feeder covered by National Grid Distribution. This feeder is chosen due to i) the representation of a real distribution network, ii) the availability of variable load profiles over a 24-hour period, and iii) the diversity of customer types. The network enables a better understanding of the impacts of different battery chargers during various time intervals, and the variation in customer types enables the better analysis of different network points. The network comprises of a 500-MVA three-phase 33-kV voltage source at the generation point, connecting two 15-MVA transformers to the 11-kV substation, where eight outgoing feeders exist. The schematic diagram of the distribution network is shown in Figure 5.1.
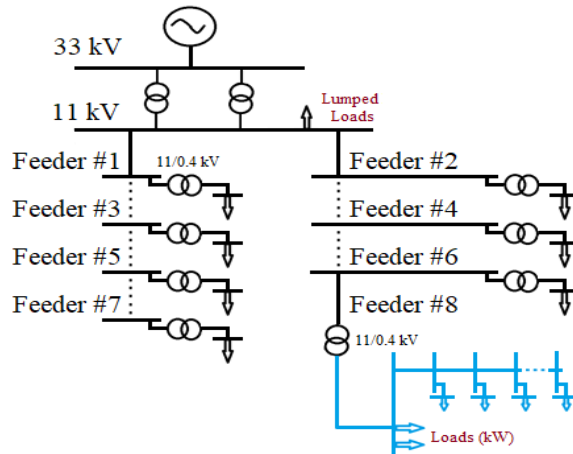
Figure 5.1: Simplified representation of the distribution network.

Eight outgoing feeders are represented from Feeder #1 through Feeder #8 in the schematic diagram. Each feeder supplies a 500-kVA 11/0.433 kV transformer and includes the cumulative load of customers. Feeders #1 to #7 are modelled as aggregated PQ loads, while Feeder #8 is modelled in detail using real customer data over a period of 24-hours. The simplified nodal representation of Feeder #8 is represented in Figure 5.2. Detailed network data is also presented in Table 5.1 and Table 5.2.
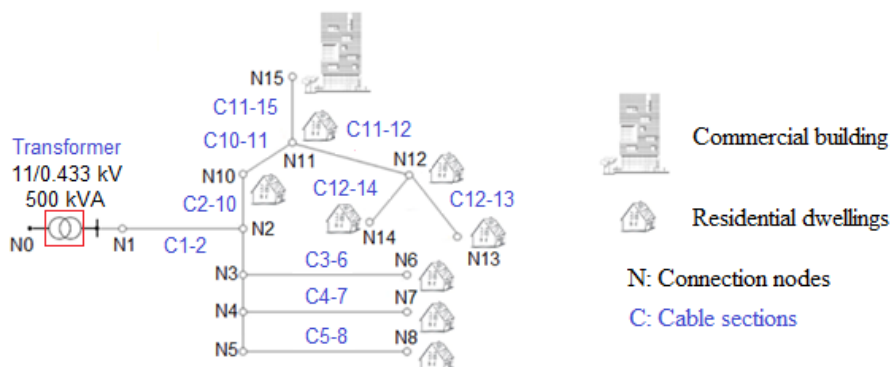
Figure 5.2: Simplified nodal representation of Feeder #8.

Table 5.1: Number and type of customers at each connection node in the feeder

Between Nodes	Connection Node	Number of Buildings	Building Type
N3–N6	N6	6	Residential
N4–N7	N7	7	Residential
N5–N8	N8	8	Residential
N2–N10	N10	6	Residential
N10–N11	N11	6	Residential
N11–N12	N12	12	Residential
N12–N13	N13	8	Residential
N12–N14	N14	10	Residential
N11–N15	N15	1	Commercial

Table 5.2: Specifications and operating resistances of cables in the feeder

Cable Section	Type	Length (m)	Ampacity (A)	Operating Resistance per 1000 m (Ω)	Operating Resistance per Length (Ω)
C1-2	Copper	10	514	0.0928	0.000928
C3-6	Copper	30	197	0.4637	0.013911
C4-7	Copper	35	197	0.4637	0.0162295
C5-8	Copper	50	197	0.4637	0.023185
C2-10	Copper	65	514	0.0928	0.006032
C10-11	Wavecon	40	251	0.32	0.0128
C11-12	Wavecon	70	251	0.32	0.0224
C12-13	Wavecon	30	251	0.32	0.0096
C12-14	Wavecon	40	251	0.32	0.0128
C11-15	Copper	20	156	0.7027	0.014054

The low-voltage feeder serves 64 customers of which 63 are residential dwellings and one is a commercial building. In the feeder, the building connection points are denoted by the symbol 'N'. The feeder is composed of several connection nodes labelled from Node N1 to Node N15. The substation entry point is denoted by the 500-kVA transformer connected between Node N0 and Node N1. It should be noted that Node N9 does not exist, and has been omitted from the schematic diagram. Residential dwellings and commercial building are connected at the far end of each line for simplicity. For example, between Nodes N3–N6, there are six residential dwellings, all of which are connected at Node N6. The only commercial building, on the other hand, is connected at Node N15. Although the feeder has a single commercial building, its peak consumption is equivalent to that of ten residential households. Node N12 has the largest number of dwellings (12), while Node N6, Node N10, and Node N11 have the fewest number of dwellings (6) in the feeder.

In the investigated part of the low-voltage distribution network feeder, only two cable types (depicted by the symbol 'C' in Figure 5.2) are used: copper subterranean conductors and Wavecon/Waveform cable with a solid aluminium conductor. The ampacity of the cables, which is defined as the maximum current each cable is allowed to carry, is used to determine the degree of overloading in **Section 5.3**. Due to the low operational reactance of cables, they are solely represented as simply resistive phase impedance in the modelling study.

5.2.1 Customer Baseload Profiles

The daily load profiles of 64 customers are obtained according to the number of households and buildings at each connection node. This is achieved by using and obtaining the typical load profiles and characteristics of an urban British residential and commercial building available as a dataset in [47, 277]. It should be noted that since there is insignificant diversity in the load profile of each building, the same load profiles are considered for each residential dwelling in the modelling study. The load profiles of a single residential and a commercial building in the feeder are illustrated in Figure 5.3.
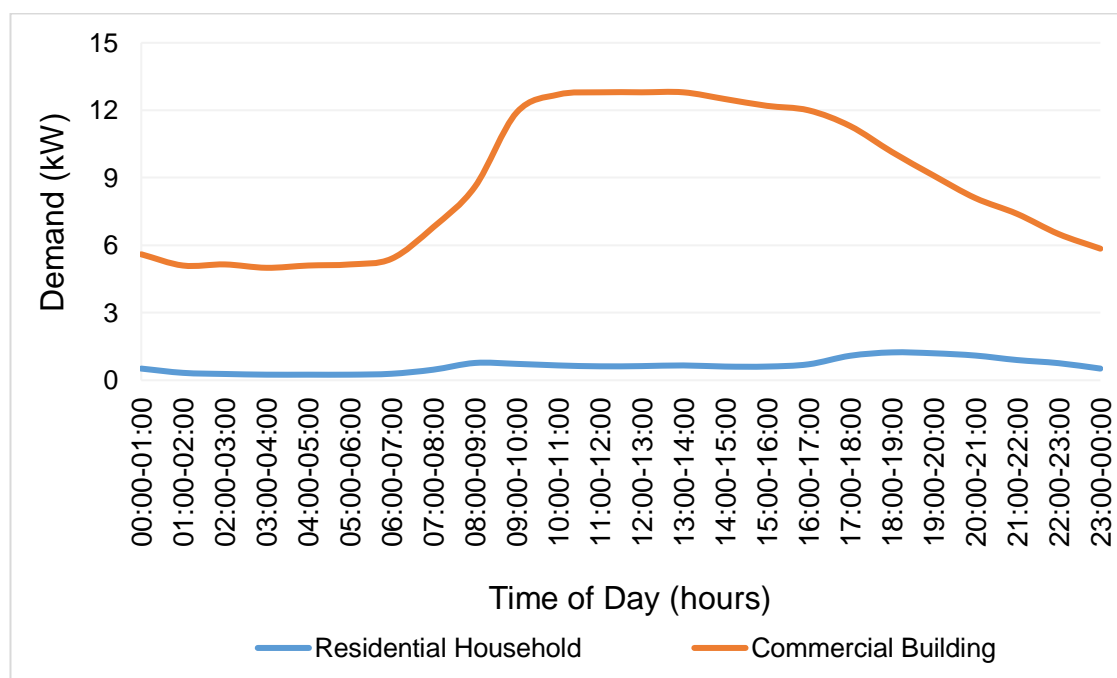
Figure 5.3: Daily load profiles for a typical British residential and a commercial building.

The graph depicts typical daily load patterns in a 'top-of-the-hour' format. It is assumed that the demand remains constant for the entire hour for simplicity. According to the load profiles, the lowest demand interval for both residential and commercial buildings is between 03:00 and 05:00. The commercial building's total demand is 5 kW, while a residential household's total demand is around 0.25 kW during the off-peak hours.

On the other hand, peak demand of 12.8 kW often occurs between 11:00 and 14:00 at the commercial building. Between 18:00 and 20:00, when homeowners return from work and depend on home activities such as cooking, bathing, heating, cooling, and lighting, the peak demand of 1.24 kW is exhibited at the residential dwelling.

Daily load profiles for the investigated feeder are also obtained based on the number of buildings at each connection node. For example, the peak demand of a single residential dwelling between 17:00 and 18:00 is multiplied with ten to obtain the aggregated demand for customers between Nodes N12–N14 (see **Table 5.1**). The same method is used for the remaining connection nodes and the daily load profiles at each connection node in the feeder are obtained, as seen in Figure 5.4.
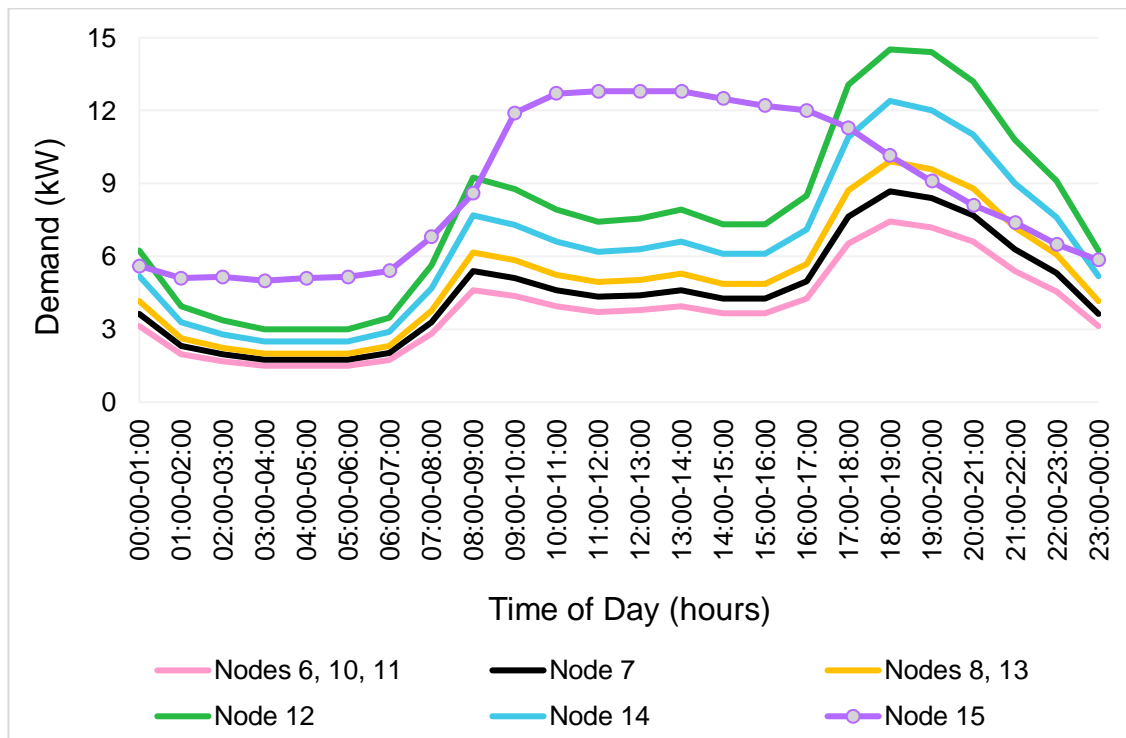
Figure 5.4: Daily baseload profiles at each connection node.

The graph depicts the variance in customers' daily load profiles using six distinct curves, classified according to the number of buildings at each node. The daily load profile for the commercial building — represented by the purple curve is identical to that of the one seen in Figure 5.3 since the network only has one commercial building. However, the demand of residential dwellings is scaled up due to the larger number of residential customers. Node N6, Node N10, and Node N11 each contains six households of the same type in the network, which are all represented by the pink load curve. Similarly, the yellow curve represents the daily demand profile for Node N8 and Node N13 with eight residential dwellings of the same type. The overall minimum base feeder demand is 20.8 kW between 03:00 and 04:00 (also denoted as off-peak), whereas the maximum base demand is 87.9 kW between 18:00 and 19:00 (also denoted as on-peak).

Demand change is minimal every three hours in the network, and therefore, daily load profiles are scaled down into eight intervals to reduce simulation time. For every three hours on the network, the average demand at each connection node is calculated. For example, the average demand between 00:00 and 03:00 is calculated as the first interval and is denoted by the period 0–3h. Table 5.3 shows the calculated average baseload demand for every three hours in the distribution network feeder.

Table 5.3: Averaged demand for every three hours at each connection node

Hour (h)	0–3h	3–6h	6–9h	9–12h	12–15h	15–18h	18–21h	21–00h
Node 6	2.3	1.5	3.1	6.1	4.0	4.8	7.1	4.4
Node 7	2.6	1.8	2.9	4.7	4.4	5.6	8.3	5.1
Node 8	3.0	2	4.1	5.4	5.1	6.4	9.4	5.8
Node 10	2.3	1.5	3.1	6.1	4.0	4.8	7.1	4.4
Node 11	2.3	1.5	3.1	6.1	4.0	4.8	7.1	4.4
Node 12	4.5	3	6.1	8.0	7.6	9.6	14.0	8.7
Node 13	3.0	2	4.1	5.4	5.1	6.4	9.4	5.8
Node 14	3.8	2.5	5.1	6.7	6.3	8.0	11.8	7.3
Node 15	5.3	5.1	6.9	12.5	12.7	11.8	9.1	6.6
Demand (kW)	29.1	20.9	38.5	61	53.2	62.2	83.3	52.5

Between 3–6h, the minimum base demand is 20.9 kW, while the maximum base demand is 83.3 kW between 18–21h in the network. These figures are like the one shown on an hourly basis in Figure 5.4: 20.8 kW (minimum) and 87.9 kW (maximum).

5.2.2 Integration of Electric Vehicle Charging Load Profiles

Dynamic battery chargers from **Chapter 4** are incorporated into the distribution feeder. Various charging scenarios are considered for customers (classified by their charging rates) and implemented in different areas of the feeder, as shown in Table 5.4.

Table 5.4: Choice of charger modes during different hours of the day

Time of Day	Charger Mode	Charger Rating (kW)	Connection Node
00:00–03:00	One slow-speed	3–4.5	N6
03:00–06:00	One slow-speed	3–4.5	N6
06:00–09:00	One fast-speed	22	N8
09:00–12:00	One fast-speed	22	N14
12:00–15:00	One fast-speed	22	N12
	One rapid-speed	45	N15
15:00–18:00	One rapid-speed	45	N15
18:00–21:00	One ultra-rapid speed	150	N15
21:00–00:00	One slow-speed	3–4.5	N6

It should be mentioned that all chargers operate at their maximum theoretical power capacity for the duration of the 3-hour interval. This allows the network to be examined during the worst-case scenario. It is also assumed that each chosen connection node has only one charger due to node limitations with the PSCAD licence. The PSCAD version utilised in these studies is the educational one with limited number of nodes.

The integration of different charger modes provides a better representation for examining how the dynamic operational characteristics of low-voltage distribution networks are affected with respect to the time and location of a charging activity. Slow-speed chargers are often used by residential customers who charge their cars for extended periods of time overnight. To imply this, customers at Node N6 are provided with a slow-speed charger (rated at 3–4.5 kW) that operates between 21:00 and 06:00. Additionally, a fast-speed charger (rated at 22 kW) is installed and operated at Node N8 between 06:00 and 09:00, at Node N14 between 09:00 and 12:00, and at Node N12 between 12:00 and 15:00. Different hours and locations are selected to expand the availability of chargers and to add diversity in the charging profiles. Rapid chargers (rated at 45 kW) are connected near the commercial building through a 0.4/0.69 kV transformer. Between 12:00 and 15:00, the first rapid charger is connected, while the second is connected between 15:00 and 18:00. These hours are used to represent lunch and after-work hours, allowing drivers to charge at their destination locations, just before returning home for the evening. Additionally, between 18:00 and 21:00, an ultra-rapid charger (rated at 150 kW) is installed and operated near the commercial building. This period is selected for the drivers to recharge their vehicles for the following day.

The calculated average baseload demand for every three hours in the distribution network feeder (see **Table 5.3**) increases due to the addition of these charger modes. The increase in the baseload demand is shown in Table 5.5.

Table 5.5: Averaged demand for every three hours with EV charging load profiles

Hour (h)	0–3h	3–6h	6–9h	9–12h	12–15h	15–18h	18–21h	21–00h
Node 6	6.8	6	3.1	6.1	4.0	4.8	7.1	8.9
Node 7	2.6	1.8	2.9	4.7	4.4	5.6	8.3	5.1
Node 8	3.0	2	26.1	5.4	5.1	6.4	9.4	5.8
Node 10	2.3	1.5	3.1	6.1	4.0	4.8	7.1	4.4
Node 11	2.3	1.5	3.1	6.1	4.0	4.8	7.1	4.4
Node 12	4.5	3	6.1	8.0	29.6	9.6	14.0	8.7
Node 13	3.0	2	4.1	5.4	5.1	6.4	9.4	5.8
Node 14	3.8	2.5	5.1	28.7	6.3	8.0	11.8	7.3
Node 15	5.3	5.1	6.9	12.5	57. 7	56.8	159.1	6.6
Demand (kW)	33.6	25.4	60.5	83	62.5	107.2	233.3	57

The data in Table 5.5 is obtained by adding the maximum theoretical power output of each connection node's charging demand with the baseload demand from Table 5.3. It should be clarified that since not all connection nodes have an EV charger, some node demand at certain intervals stays the same in both Table 5.3 and Table 5.5. In Table 5.5, the instances in which the averaged demand due to EV charging profiles increases are denoted by the blue font. For example, between 15:00 and 18:00 (i.e., 15–18h), the demand at Node 15 increases from 11.8 kW in Table 5.3 to 56.8 kW in Table 5.5, as this node has one 45-kW charger operating at its maximum theoretical power output. The largest demand change occurs between 18–21h, when the total base demand rises from 83.3 kW to 233.3 kW with the addition of 150-kW charger.

5.3   Impact of Charging Activities on the Feeder

Section 5.3.1 examines the daily voltage variations, **Section 5.3.2** analyses cable loading. **Section 5.3.3** calculates power losses and the cost associated with losses.

5.3.1 Voltage Variations

Daily voltage variations are analysed at each connection node during the baseload and after the addition of EV charging load profiles in the network. Simulation results concerning nodal voltages are presented in Figure 5.5 and Figure 5.6.
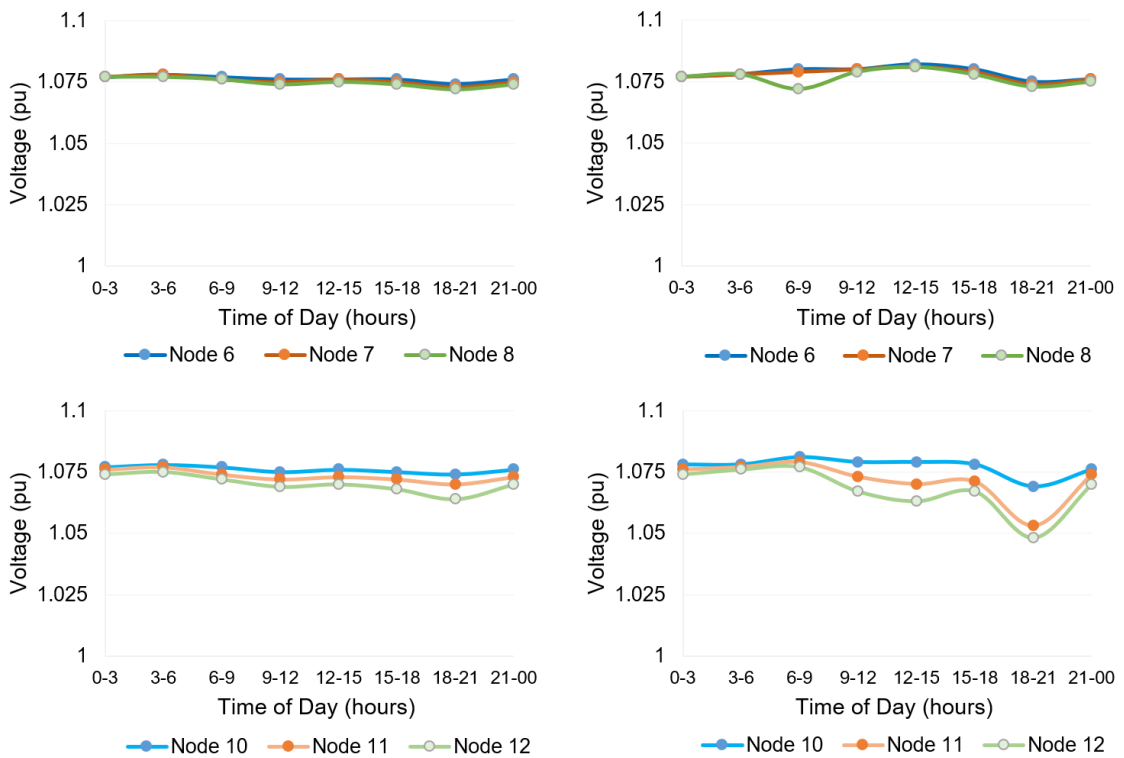
Figure 5.5: Voltage profiles at Nodes N6 to N12 without (left) and with (right) EV chargers.

Nodal voltages at Node N6 to Node N12 without EV chargers fluctuate slightly during the day. Between 18–21h, residential dwellings at Node N12 have a minimum voltage of 1.064 p.u. Following the charging activities, customers at Node N8, Node N10, Node N11, and Node 12 experience voltage drops, as seen on the right side of Figure 5.5. Customers at Node N7, on the other hand, do not experience any significant voltage changes since there is no EV charger connected at this point in the feeder.

When the 150-kW charger is in operation between 18–21h, the minimum voltage at the nearest nodes, e.g., at Node N11 and Node N12, is around 1.05 p.u. However, nodes that are situated further away from rapid and ultra-rapid chargers (particularly Node N6, Node N7, and Node N8) experience smaller voltage drops throughout the day. Additionally, nodes with slow and fast chargers connected to them experience lower voltage fluctuations.
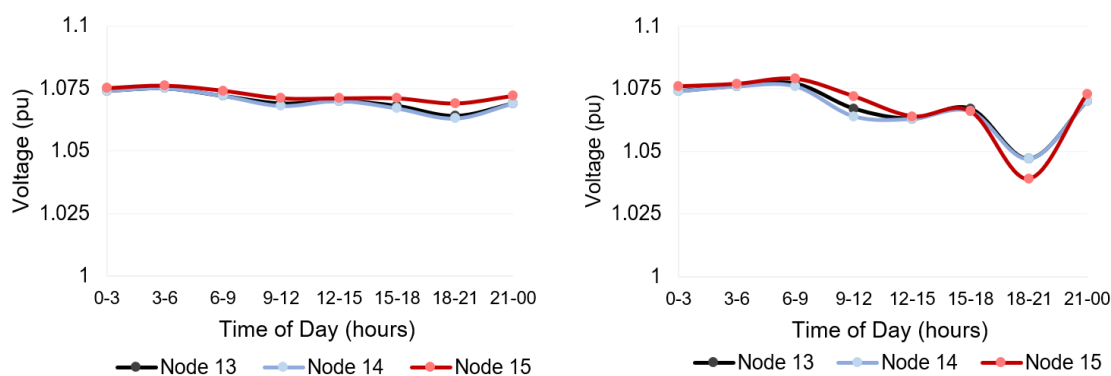
Figure 5.6: Voltage profiles at Nodes N13 to N15 without (left) and with (right) EV chargers.

Between 18–21h, Node N15 exhibits the largest voltage drop in the network, owing to the addition of the 150-kW charger. The nodal voltage during these peak hours drops by 2.8%; from 1.07 p.u. to 1.04 p.u. It should be clarified that the DNOs in the UK are required to serve customers at the low-voltage feeders within +10% and −6% of the nominal voltage to ensure secure and regulatory operating limits. Simulation results demonstrated in this section show that the investigated feeder does not experience any voltage violations, and all the nodal voltages at the customer points are maintained within the regulatory threshold limits while the EV chargers are present in the network.

Voltage imbalance, which is defined as the difference in voltage between the phases of a three-phase system, is also investigated in this part. It is often produced by an unequal distribution of single-phase load over three phases. Voltage imbalance between the phases of a three-phase system is analysed during the baseload and with a single-phase battery charger (rated at 3 kW) near one of the residential dwellings in the network. Simulation results concerning voltage imbalance are represented in Figure 5.7 and Figure 5.8.
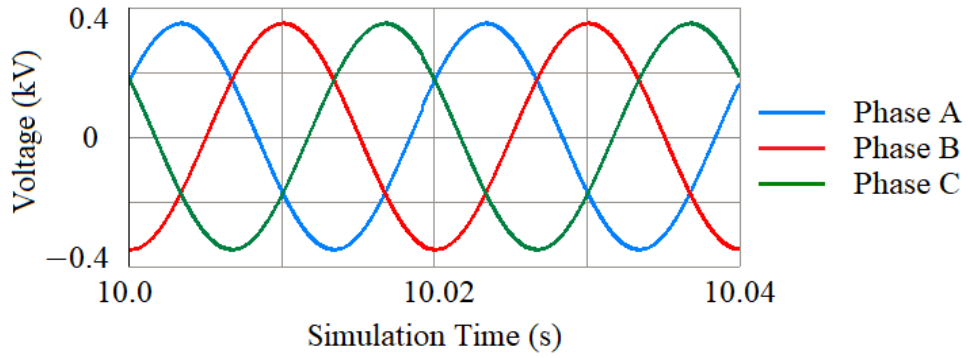
Figure 5.7:Phase voltages during the baseload.

Simulation results demonstrate the sinusoidal phase to ground voltage response of all three phases along a cable segment during the baseload. Each phase is balanced and the voltage across each phase is approximately 0.23 kV (given by dividing the line-to-line voltage of 0.433 kV by the square root of three).
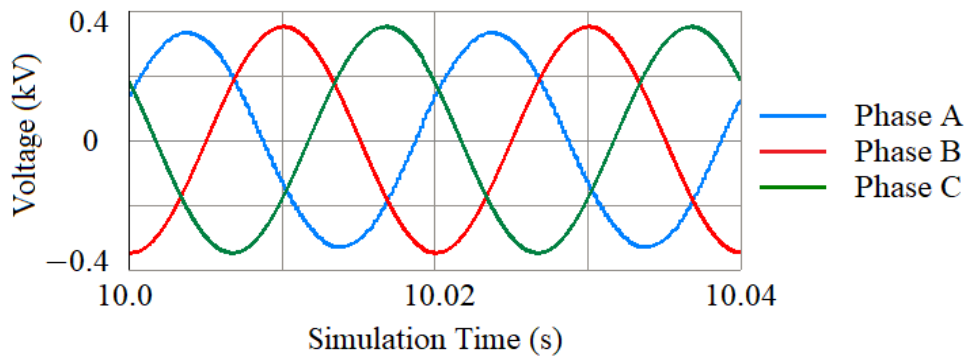
Figure 5.8: Phase voltages with a single-phase battery charger.

The single-phase battery charger is connected on Phase A for demonstration purposes, and the findings indicate a minor imbalance among three phases. Phase B and Phase C maintain the same voltage responses and have identical peak to peak values. Phase A, on the other hand, experiences a minor imbalance due to the residential charger. The integration of this charger on Phase A also causes minor voltage drops along the line, as shown in Figure 5.9.
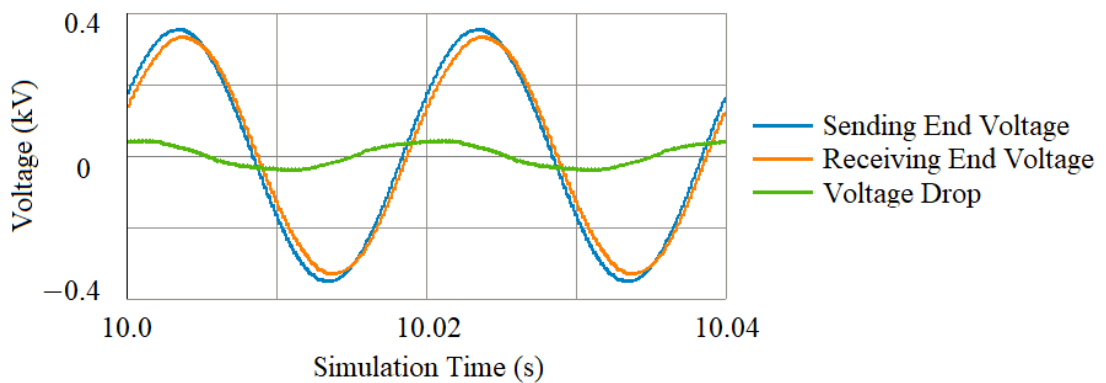
Figure 5.9: Voltage drop along the cable where a single-phase battery charger is connected to.

The voltage drop is determined by measuring the instantaneous voltage at the cable's sending and receiving ends. With reference to the simplified nodal representation of the low-voltage feeder (see **Figure 5.2**), the sending end is designated as Node N3, while the receiving end is designated as Node N6. Given that the charger is connected at the end of this line and given that there are three single-phases, Phase A to Phase C, the bulk portion of the current through cable C3-6 flows into Phase A due to charger, resulting in a small voltage drop down the cable — illustrated by the green line in Figure 5.9. The magnitude of this drop is related to the increase in electrical potential caused by the current flowing down the cable and is mostly determined by the charger's size. It is anticipated that a charger with a higher rating would result in a larger voltage drop.

5.3.2 Cable Loading

Current flow in the feeder is examined to determine the hosting capacity of supply cables when EV charging loads are present. The hosting capacity of cables is determined by quantifying the amount of instantaneous RMS current and then comparing this to the ampacity/rating of the cables (presented in Table 5.2). The magnitudes of cable currents are obtained during the baseload and after the addition of EV charging load profiles Simulation results concerning cable currents are shown in Figure 5.10, Figure 5.11, and Figure 5.12.
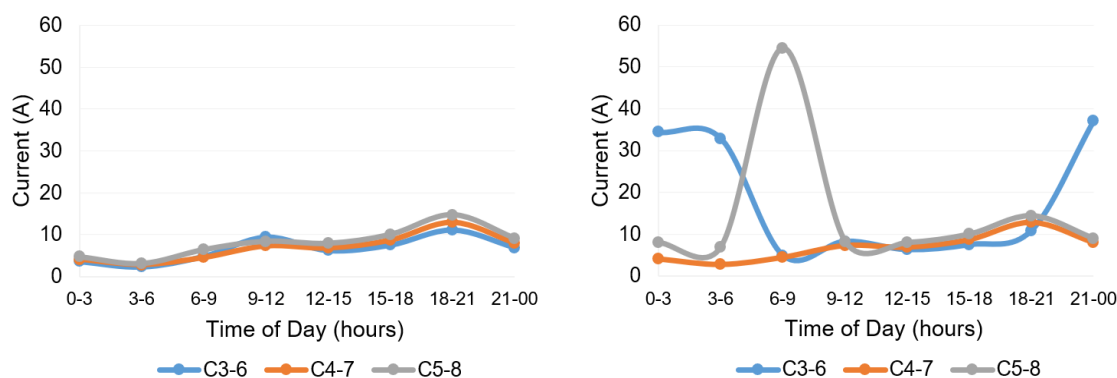
Figure 5.10: Current in C3-6, C4-7, and C5-8 without (left) and with (right) EV chargers.

Cables C3-6, C4-7, and C5-8 all carry a comparable amount of current when the network has no EV chargers. These cables are responsible for delivering power to the residential dwellings connected at Node N6, Node N7, and Node N8, respectively. When a slow-speed charger is connected at Node N6 between 21:00 and 06:00 and a fast-speed charger is connected at Node N8 between 06:00 and 09:00, the current begins to increase slightly in these cables. However, the EV chargers do not cause any overloading in these cables. On the other hand, the current in cable C4-7 is almost identical during the baseload and after the addition of EV charging load profiles, since there is no EV charger connected near the customers at Node N7 (see **Table 5.4**).
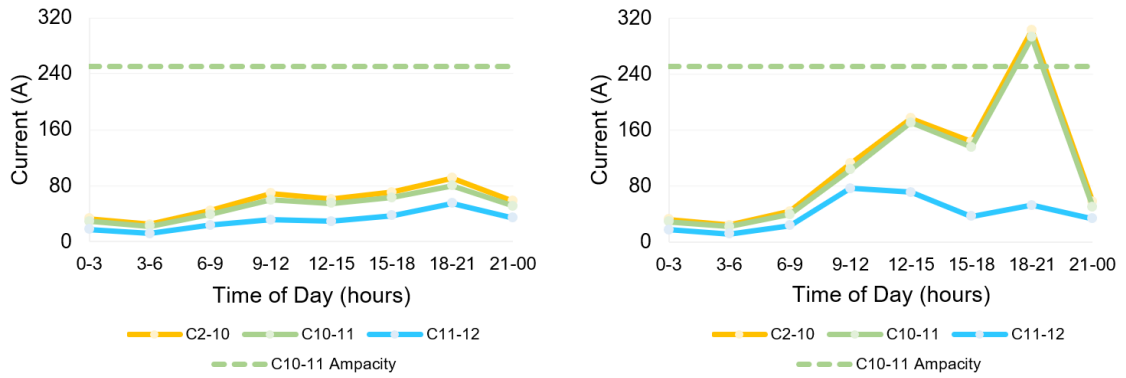
Figure 5.11: Current in C2-10, C10-11, and C11-12 without (left) and with (right) EV chargers.

Larger current flow is observed through cables C2-10, C10-11, and C11-12 in the feeder, due to increased demand of residential dwellings near Node N10, Node N11, and Node N12. Between 18:00 and 21:00, cables C2-10 and C10-11 carry a peak current of 91 A and 80 A, respectively, during the baseload. However, the peak current rises to 303 A for cable C2-10 and to 293 A for cable C10-11 since the 150-kW charger operates at its maximum theoretical power output. The ampacity of cable C10-11 (which is 251 A as seen in **Table 5.2**), is exceeded by 16.7% between 18:00 and 21:00, whereas all other cables manage to operate within normal design limits. This cable is responsible for delivering power to residential dwellings at Node N11.
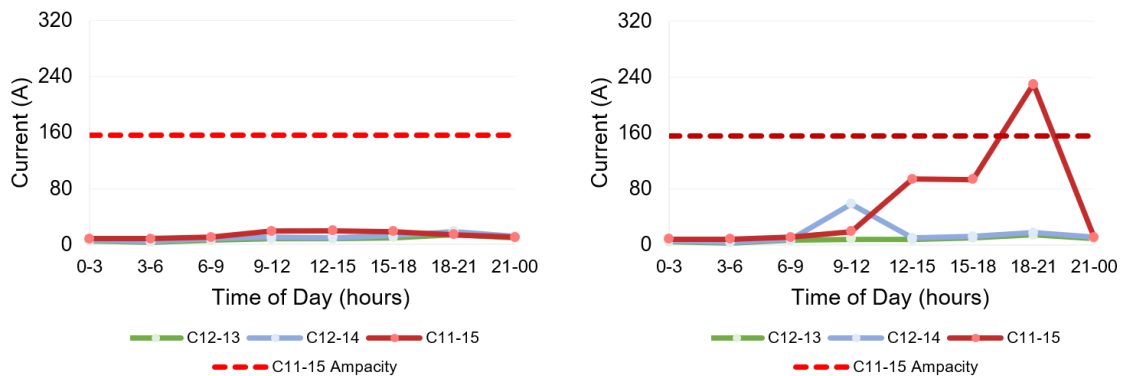
Figure 5.12: Current in C12-13, C12-14, and C11-15 without (left) and with (right) EV chargers.

The current magnitudes in cables C12-13, C12-14, and C11-15 are similar during the baseload. These cables provide power to the buildings at Node N13, Node N14, and Node N15, respectively. Between 09:00 and 12:00, when the 22-kW charger is in use, the current in C12-14 increases from 10.3 A during the baseload to 58.6 A. The largest current increase occurs at the point of commercial building, which causes cable C11-15 to surpass its ampacity of 156 A by 47.4% between 18:00 and 21:00.

Simulation results indicate that the cables providing power to customers near Node N11 and Node N15 are experiencing overloading when the 150-kW charger operates at its maximum power capacity between 18:00 and 21:00 in the distribution feeder. These cables are next to one another near the commercial building and are heavily congested.

Different techniques for reducing the cable overloading are proposed and examined in **Section 5.4** of this chapter.

5.3.3 Active Power Losses

Increased current flow leads to an increased cable temperature, increased network demand, and therefore increased power losses. Using (5.1), active power losses are calculated during the baseload and after the addition of EV charging load profiles in the feeder.

$$Active\ Power\ Losses\ (kW) = \frac{3 \times I_c^{\ 2} \times R_l}{1000} \tag{5.1}$$

Where:

R_l is the operating resistance per required length of cable (Ω),

I_c is the instantaneous RMS current in the cables (A).

Table 5.6 shows the calculated active power losses based on the current magnitudes during the baseload. Table 5.7 shows the calculated active power losses after the addition of EV charging load profiles.

Table 5.6: Active power losses in the cables during the baseload

Cable	0–3h (kW)	3–6h (kW)	6–9h (kW)	9–12h (kW)	12–15h (kW)	15–18h (kW)	18–21h (kW)	21–00h (kW)	Total Losses (kW)
C1-2	0.01	0.003	0.01	0.02	0.02	0.03	0.05	0.02	0.163
C3-6	0.001	0.0002	0.001	0.004	0.002	0.002	0.01	0.002	0.0222
C4-7	0.001	0.0004	0.001	0.003	0.002	0.004	0.01	0.003	0.0244
C5-8	0.002	0.001	0.003	0.005	0.004	0.01	0.02	0.01	0.055
C2-10	0.013	0.011	0.04	0.09	0.07	0.09	0.15	0.06	0.524
C10-11	0.032	0.02	0.06	0.14	0.12	0.15	0.24	0.1	0.862
C11-12	0.021	0.01	0.04	0.07	0.06	0.09	0.2	0.08	0.571
C12-13	0.001	0.0003	0.001	0.002	0.002	0.003	0.01	0.002	0.0213
C12-14	0.001	0.001	0.002	0.004	0.004	0.006	0.01	0.005	0.033
C11-15	0.003	0.003	0.005	0.02	0.02	0.014	0.01	0.004	0.079
Losses (kW)	0.085	0.05	0.163	0.358	0.304	0.4	0.71	0.286	2.35

The cables experience the smallest power losses between 03:00 and 06:00, when the base network demand is at its lowest. Cables C2-10, C10-11, and C11-12, on the other hand, experience the largest losses, between 18:00 and 21:00 due to increased residential demand in the feeder. Total active power losses in the investigated feeder without any EV chargers add up to 2.35 kW during the baseload.

Table 5.7: Active power losses in the cables with EV chargers

Cable	0–3h (kW)	3–6h (kW)	6–9h (kW)	9–12h (kW)	12–15h (kW)	15–18h (kW)	18–21h (kW)	21–00h (kW)	Total Losses (kW)
C1-2	0.01	0.009	0.03	0.05	0.11	0.08	0.32	0.03	0.639
C3-6	0.05	0.05	0.001	0.003	0.002	0.002	0.01	0.06	0.178
C4-7	0.001	0.0004	0.001	0.003	0.002	0.004	0.01	0.003	0.0244
C5-8	0.002	0.001	0.21	0.005	0.004	0.01	0.01	0.006	0.248
C2-10	0.02	0.01	0.04	0.23	0.57	0.37	1.66	0.06	2.96
C10-11	0.033	0.02	0.06	0.41	1.13	0.71	3.30	0.1	5.763
C11-12	0.021	0.01	0.04	0.4	0.35	0.09	0.19	0.08	1.181
C12-13	0.001	0.0003	0.002	0.002	0.002	0.003	0.006	0.002	0.0183
C12-14	0.001	0.001	0.003	0.13	0.004	0.01	0.012	0.005	0.166
C11-15	0.003	0.003	0.005	0.016	0.37	0.37	2.23	0.004	3.001
Losses (kW)	0.142	0.105	0.391	1.249	2.544	1.649	7.748	0.35	14.18

Active power losses in cables C4-7 and C12-13, which provide energy to dwellings at Node N7 and N13, are nearly identical for each interval without and with EV chargers in operation. Due to the absence of chargers at these nodes, their aggregated demand stays the same for both scenarios (with and without chargers). However, these losses slightly increase when their neighbouring nodes have charging activities in the network.

Cables C2-10, C10-11, and C11-15 have the largest active power losses with EV chargers connected to the network, especially when the 150-kW charger is in operation. The losses in those cables during the peak interval are calculated as 1.66 kW, 3.30 kW, and 2.23 kW, respectively. Total daily power losses rise from 2.35 kW to 14.18 kW when the EV chargers are in operation.

5.3.3.1 Cost Calculation of Active Power Losses

Using the baseload demand and power losses in different cable sections, the energy cost and the cost of the losses are calculated by (5.2) and (5.3), respectively [278]:

$$E_c = \Delta P \times t_h \times C_E \tag{5.2}$$

Where:

E_C is the daily energy cost based on the power consumption (£/day),

ΔP is the daily total active power consumption (kW),

t_h is the daily number of usage hours (hours),

C_E is the hourly energy cost (28p/kWh [279]) (£/kWh).

$$C_p = \Delta L_\gamma \times C_E \times C_\gamma \tag{5.3}$$

Where:

C_p is the estimated cost of total power losses in the feeder (£/kWh),

ΔL_γ is the calculated daily total active power losses in the feeder (kW/day),

C_γ is the total time of cable network operation (days).

It is assumed that the feeder and the EV demand, as well as the hourly energy cost remain unchanged throughout the calculating period. It is also assumed that the amount of active power losses remains unchanged for every three-hour interval in the network. For example, the total feeder losses between 0–3h is 0.085 kW. However, during the calculation of the E_C, this is used as 0.255 kW (scaled-up by three) since the above expression takes into consideration the fixed price in each hour.

Using the calculated power losses in Table 5.6 and Table 5.7, the cost of energy consumption and the cost of losses are calculated during the baseload and after the addition of EV charging load profiles, as shown in Table 5.8 and Table 5.9, respectively.

Table 5.8: Calculated energy consumption in the feeder

Baseload Daily Feeder Demand	Daily Feeder Demand (with EVs)	Baseload Daily Feeder Consumption	Daily Feeder Consumption (with EVs)
1202.1 kW	1987.5 kW	28,850 kWh/day	47,470 kWh/day

The baseload daily energy consumption in the feeder is 28,850 kWh in the absence of EV chargers and 47,470 kWh in the presence of EV chargers.

Table 5.9: Calculated daily cost of energy consumption and power losses in the feeder

Baseload Daily Energy Consumption Cost	Daily Energy Consumption Cost (with EVs)	Baseload Cost Calculation for Power Losses	Cost Calculation for Power Losses (with EVs)
£8,070.7	£13,291.6	£47.4	£285.9

The daily energy consumption cost increases from £8,071 to £13,292 when the charging scenarios are implemented into the network. Based on the calculated active power losses in Table 5.6 and Table 5.7, the daily cost associated with power losses is also calculated to be approximately £47.4 in the absence of EV chargers. This is well aligned with the value given in [251], where it is stated that with losses of around 5% or 8% in distribution, the total cost of losses is projected to be roughly £50. Additionally, the daily cost of losses is determined to be approximately £285.9 with charging activities.

5.4 Cable Overloading Mitigation Techniques

The cable infrastructure near the commercial charging point is not intended to support an ultra-rapid charger, especially during the periods of high demand. The 150-kW charger exhibits overloading conditions for two cable sections (see **Section 5.3.2**). Three following cable loading mitigation techniques are proposed in this section:

- **Section 5.4.1** increases the size of two overloaded cable conductors and recalculates their operational resistances.
- **Section 5.4.2** proposes the introduction of two small-scale V2G chargers near the congested network cable sections.
- **Section 5.4.3** examines the effect of using a coordinated charging strategy during the periods of high demand.

5.4.1 Increased Cable Size

The conductor size of two overloaded cables: C10-11 and C11-15, is increased based on the load current. WPD's *Standard Technique: Relating to Low Voltage Underground Cable Ratings* datasheet [48] is utilised to determine the new cable size.

The sizes of cables C10-11 and C11-15 are upgraded to the nearest available standard size as per the datasheet. Cable C10-11's size is increased from 95 mm^2 to 120 mm^2, while the size of C11-15 is increased from 25.8064 mm^2 to 95 mm^2. The ampacity of these cables is also updated to 284 A and 263 A, respectively [48]. The new operating resistance ($R_{l,new}$) per required length of these cables is given by (5.4):

$$R_{l,new} = \frac{\rho \times C_l}{A_c}$$

(5.4)

Where:

ρ is the resistivity of the cable material at 20°C (Ωm),

A_c is the cross-sectional area of the conductor size (m^2).

According to [280], the resistivity of the cable material is 2.8 x 10^{-8} for aluminium-based conductors (C10-11) and 1.7 x 10^{-8} for copper-based conductors (C11-15). The revised operating resistance values for the cables are shown in Table 5.10.

Table 5.10: Operating resistances of cables with upgraded sizes

Cable	Type	Length (m)	$R_{l,old}$ (Ω)	$R_{l,new}$ (Ω)	Updated Ampacity (A)
C10-11	Wavecon	40	0.0128	0.0093	284
C11-15	Copper	20	0.014054	0.0036	263

After increasing the conductor sizes of cables C10-11 and C11-15, the magnitudes of cable currents are analysed after the addition of EV charging load profiles. Simulation results are represented in Figure 5.13. It should be clarified that all other cables are simulated using their original sizes as they are not exposed to any overloading condition and operate within acceptable design limits.
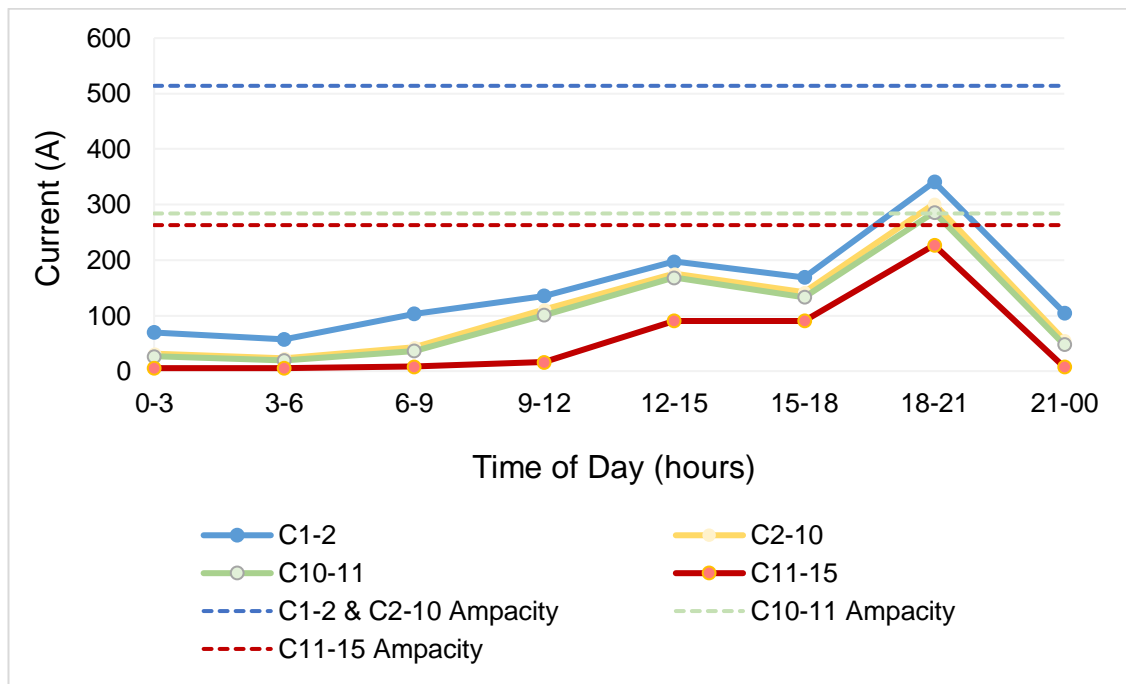
Figure 5.13: Current measurements in C1-2, C2-10, C10-11, and C11-15 with new cable sizes.

Increasing the conductor size for C10-11 and C11-15 slightly reduces the magnitude of RMS current in the cables. The peak current in C10-11 reduces from 293 A to 286 A, whereas the peak current in C11-15 reduces from 230 A to 227 A. Cable C11-15 is no longer overloaded since it carries a current that is less than its new ampacity rating at a conductor size of 95 mm^2. However, cable C10-11 still exceeds its ampacity by 0.7% during the peak network demand.

5.4.2 Integration of Vehicle-to-Grid Chargers

The first V2G charger is connected near the residential dwellings at Node N10, whereas the second V2G charger is connected near the dwellings at Node N11. V2G chargers are rated at 7.5 kW, to represent a typical device rating for a residential bidirectional charger as reported in [281]. The connection points for the V2G chargers are chosen based on their proximity to the commercial building and commercial cable in the feeder. The location of V2G chargers is shown in Figure 5.14.
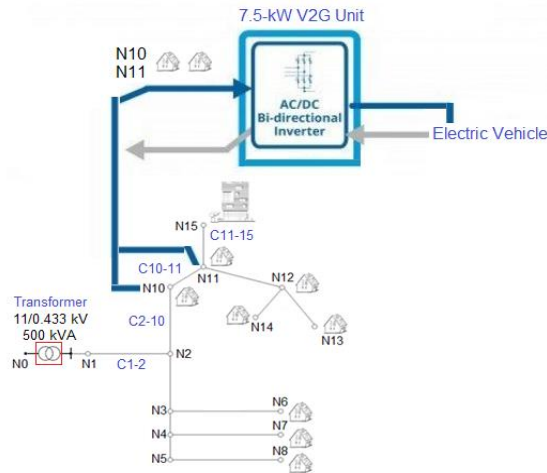
Figure 5.14: V2G locations near the residential buildings at Node N10 and Node N11.

The effect of V2G chargers on the cables' RMS current during the periods of overloading is presented as a tabulated data in Table 5.11.

Table 5.11: Effect of V2G chargers on cable current between 18:00 and 21:00

Cable	RMS Current Before V2G (A)	RMS Current After V2G (A)	Ampacity (A)
C1-2	341.2	326	514
C2-10	303.3	289	514
C10-11	293	276	251
C11-15	230	237	156

The results only indicate the cables' RMS currents near the overloaded sections between 18:00 and 21:00, when the 150-kW charger is in operation. The other cables do not experience any overloading conditions, and hence has not been analysed. With the two V2G chargers in place and operation, the current flowing through the substation cable C1-2 reduces from 341.2 A to 326 A. Similarly, the current in cable C2-10 decreases from 303.5 A to 289 A, whereas it decreases from 293 A to 276 A in cable C10-11. The effect of V2G on reducing the RMS current in three cable sections is obvious. However, the utilisation of two V2G chargers increases the RMS current from 230 A to 237 A in cable C11-15.

The results demonstrate that since the rating of V2G chargers is identical to the size of local loads at residential dwellings, V2G chargers result in a small reduction in current across the customers supplied by C2-10 (near Node N10) and C10-11 (near Node N11). However, since the V2G charger's rating is relatively small compared to the size of ultra-rapid charger, reversed power flow results in an increase in current at Node N15. The V2G technology is not feasible to eliminate the overloading of the commercial cable.

5.4.3 Coordinated Charging

Two approaches are proposed to reduce loading on the network and cables. The first approach reduces the capacity of the ultra-rapid charger during the peak hours by extending its operation from a three-hour interval to a six-hour interval. This means that the maximum theoretical output of the charger is halved in each interval; however, the total charger capacity is still the same. This approach uses the original cable sizes, and its effect is shown in Figure 5.15.
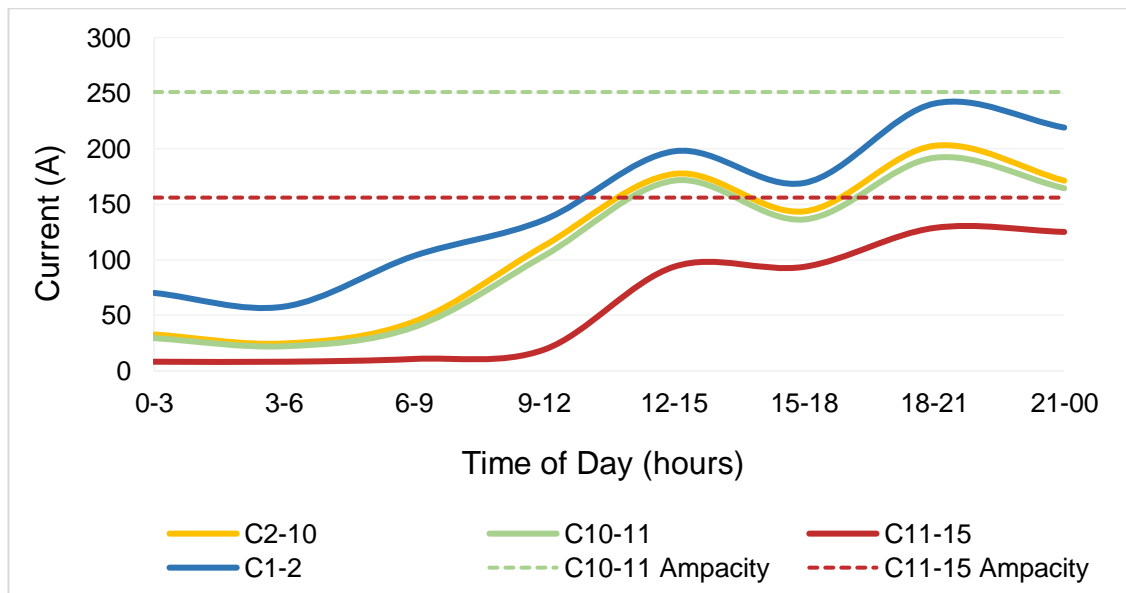
Figure 5.15: Cable currents during coordinated charging.

The graph only depicts the RMS current in cables near the congested areas, notably, in C1-2, and C2-10, C10-11, and C11-15. In comparison to previous mitigation approaches in Section 5.4.1 and Section 5.4.2, this approach causes the current in the cables to increase between 21:00 and 00:00. The increase in current, however, is within the range of permitted cable ratings. The two overburdened cables, notably, C10-11 and C11-15, are no longer in critical condition with this charging approach.

The second approach also uses the original cable dimensions but reduces the rating of the charger from 150 kW to 100 kW, whilst keeping the charger's operation hours to be between 18:00 and 21:00. The effect of this approach is shown in Figure 5.16.
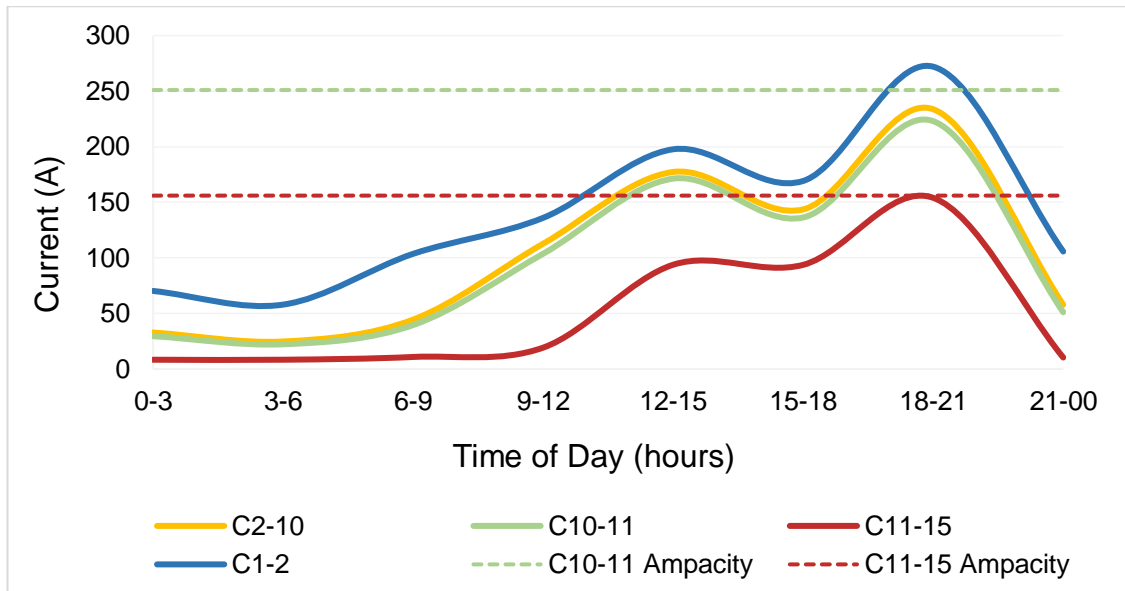
Figure 5.16: Cable currents with reduced charger theoretical power.

The graph in Figure 5.16 also indicates the cables' RMS current near the congested cable sections. In this approach, the peak current in C10-11 reduces to 223 A, which is approximately 11.2% below its ampacity rating. Cable C11-15, on the other hand, carries current that is equivalent to the ampacity of the conductor. This means that the cable has no more headroom but manages to operate within acceptable design limits. This is also shown by the dashed and normal red lines. The threshold limits for other cables are omitted in Figure 5.15 and Figure 5.16 since they are not overloaded in any way when the chargers are in operation.

5.4.3.1 Coordinated vs. Uncoordinated Charging

Overall, the two proposed methods demonstrate that cable loading and power losses, as well as network peak demand, can be substantially reduced. As demonstrated by the first method, the loading on the main cable (C11-15) close to the charging station can be reduced by as much as 45.7% during the peak period if the capacity of the 150-kW charger is halved and controlled to operate for six hours (i.e., shifted to operate during off-peak hours for three hours). This method would reduce peak demand and power losses at the charging station by up to 47% and 70%, respectively. In contrast, the second method has shown that the loading on Cable C11-15 can be reduced by up to 32%, while the peak demand and power losses at the charging point can be reduced by up to 31% and 54%, respectively. Although it is difficult to make a direct comparison to the literature since each network topology is unique and each study employs different coordinated charging technologies based on the type and rating of the charging device, these figures regarding peak reduction, losses, and loading are consistent with studies that compared the two charging methods [105, 197, 199, 200].

5.5 Summary

A low-voltage British distribution network feeder is modelled and simulated using PSCAD/EMTDC simulation software with dynamic residential and commercial consumer profiles in this chapter. Mixed charging scenarios and activities are implemented near different customers to examine the feeder's dynamic operating characteristics during different time periods of the day, including off-peak and on-peak hours.

According to the simulation findings concerning voltage analysis, distribution customers will always experience voltage fluctuations, regardless of the chargers' rating, type, and location in the network. However, it is reasonable to conclude that the larger the charger rating is, the higher the voltage drops are (particularly during periods of high demand), and the higher the cable loading and power losses are. The simulation findings also indicated that the voltage dips are largest at and near the commercial building due to the addition of the ultra-rapid charging device.

Commercial high-powered chargers present a significant load compared to typical household and commercial appliances. Therefore, two neighbouring underground cables near the commercial point were overloaded and the network was unable to handle an ultra-rapid charger between 18:00 and 21:00. Three different proposed approaches for reducing cable loading in the network have been investigated:

- The first approach examined the impact of increasing conductor size on the overloaded cables. Increasing the conductor size increases the maximum current capability of cables, but this comes at the expense of high costs for DNOs. This approach resulted in current reduction of 2.4% and 1.3% in cables C10-11 and C11-15, respectively. However, the ampacity of C10-11 was still exceeded by 0.7%.

- The second approach evaluated the integration of two small-scale V2G chargers near the residential customers during the peak hour. The V2G chargers resulted in current reduction in certain cables but increased the current at the commercial point. It can be summarised that V2G chargers alter power flows and increase current near the commercial point. This strategy also proved to be ineffective at minimising cable overloading since the ultra-rapid device's size was incomparable to the size of local loads and residential V2G chargers.

- The final approach examined the regulation and coordination of the charger's operational hours and capacity. The optimum results have been achieved in this method, and the cables were operating within acceptable limits.

CHAPTER 6

6. Estimation of Demand and Energy Consumption of Electric Vehicles at Rapid Chargers

6.1 Introduction

There is increasing interest in charging stations located in the form of hubs or forecourts. These hubs are generally built as standalone charging stations or directly connected on the existing premises of a gas station. The UK's first hub-based charging forecourt (which is opened by GRIDSERVE) offers a mixed of charging devices (rated from 22 kW to 350 kW) to meet the needs of a diverse range of motorists. While the number of hub-based projects is likely to expand rapidly to enable drivers to charge at conveniently accessible public sites, this growth is likely to introduce pulsating loads for the grid. To the best knowledge of the author, there is no work devoted to the demand estimation of hub-based charging stations with a variety of BEV models in the literature.

Using the stochastic model, chapter goals are (i) to estimate the charging demand, charging duration, and energy consumption of different EV models, (ii) to estimate the network demand and peak transformer loading on the low-voltage distribution network from **Chapter 5**, (iii) to investigate the effect of V2G and battery energy storage units on peak load shaving, (iv) to determine the hosting capacity of the substation transformer, and (v) to calculate the minimum required sizing of the battery energy storage unit and substation transformer to design a network for the worst-case scenario.

6.1.1 Chapter Structure

Section 6.2 presents the distribution of charging events from UK's public chargers.

Section 6.3 explains the stochastic model's development stage in detail.

Section 6.4 presents different cases from the stochastic model.

Section 6.5 develops a simulation model by incorporating stochastic charging profiles into a low-voltage distribution network i) to estimate the peak demand on the substation transformer, ii) to analyse the impact of V2G and battery energy storage units on peak load shaving, iii) to determine the hosting capacity of the substation transformer, and (v) to calculate the required sizing of the substation transformer and storage units.

Section 6.6 presents the findings and conclusions of the chapter.

6.2 Public Charging Device Statistics in the UK

Since 2015, the number of rapid chargers in the UK has been steadily increasing. The growth rate in the number of public rapid charging devices is shown in Figure 6.1.
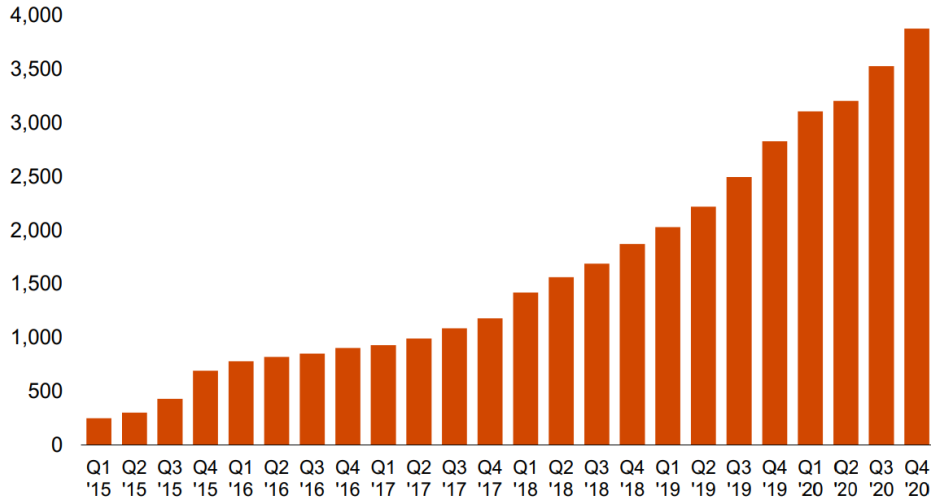
Figure 6.1: Growth in UK rapid charging devices since 2015 [205].

Rapid charging station installation is growing in the UK, particularly in cities and along key trunk roads and highways. In January 2021, there were over 20,000 public charging stations, of which 4,000 were representing rapid charging devices. The number of public stations is estimated to surpass 30,000 by 2030 [68, 69]. The geographical distribution of rapid charging devices in the UK is shown in Figure 6.2.
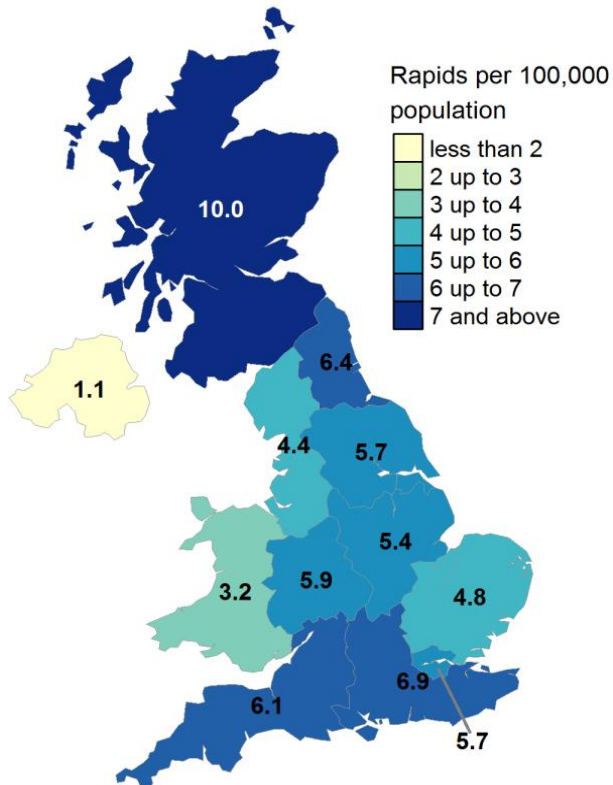
Figure 6.2: Rapid charging devices per 100,000 of population by UK region [282].

Scotland, as shown by the regional distribution chart in the North of the island, has the greatest density of rapid charging devices per 100,000 of population, while Northern Ireland and Wales have the lowest density. Regional disparities in distribution are mainly the result of bidding for government financing for charging devices. Certain local governments have applied for government funding for chargers, while others have not. Charge point operators and owners may opt to replace or decommission devices permanently or temporarily, or some devices may be inaccessible owing to chargers' maintenance and breakdowns in particular regions. For example, some devices have been turned off, and access to certain sites has been restricted during the COVID-19 pandemic [282].

6.2.1 Frequency of Charging Events

The *Department for Transport's* report on *Electrical Chargepoint Analysis of Local Authority Rapids* in [49, 282] provides data on 27 local authorities in the UK that received funding for the installation of public chargers between 2017 and 2018. Between these dates, a total of 108,746 charging events have been recorded in the UK. The statistics from these events are shown in Table 6.1.

Table 6.1: Charge point statistics by local authorities between 2017 and 2018

Weekday	Number of Events	Average Charge Duration (mins)	Average Energy Consumption (kWh)	Average Charge Power (kW)
Monday	15,191	37	10.9	17.7
Tuesday	15,502	39	10.8	17.1
Wednesday	15,544	38	11.0	17.4
Thursday	15,817	38	10.8	17.1
Friday	16,922	42	11.0	15.7
Saturday	15,716	36	11.2	18.7
Sunday	14,054	37	11.6	18.8
All events	108,746	38	11.0	17.5

The data shows that the vehicles are plugged in and charged for an average of 38 minutes, while consuming 11 kWh on average throughout the charging sessions. These variables, however, vary according to the specifications of the vehicle battery and the type of chargers, which were not available due to data confidentiality. The average charge power of 17.5 kW from the charging events shows that the vehicles are charged using fast-speed charging technologies. As discussed in **Chapter 1** and **Chapter 2** of this thesis, recent developments in the battery technology are pushing EVs to receive up to 350 kW on ultra-rapid devices.

However, the number of EV models capable of charging at rapid and ultra-rapid devices is small on the today's market due to limitations with the current battery technology. Therefore, the number of studies assessing the practicality of these high-power chargers is limited in the literature. To bridge the main gaps in the literature, an algorithm based on vehicle-specific data and chargers operating between 40–350 kW is developed to produce stochastic charging profiles and to estimate EV charging demand based on the rising number of rapid charging devices for the upcoming years.

6.3 Development of the Algorithm

Specific vehicle information (such as its brand, model, and battery specifications) and external data concerning the charger's type and rating are confidential in Table 6.1. An algorithm is thus developed to create stochastic charging profiles from popular BEV models that are capable of charging on rapid and ultra-rapid devices. The algorithm consists of five main parts:

1. The daily time frequency and distribution of charging events for the UK are obtained and presented in **Section 6.3.1**. Additionally, the percentile distribution of real-world charging events is calculated and input into the algorithm.

2. **Section 6.3.2** discusses the various types, specifications and charging characteristics of the EV models under consideration. Popular EV models capable of charging at rapid devices are used for realistic demand estimation scenario.

3. The calculation of the vehicles' data prior to charging is given in **Section 6.3.3**. Additionally, vehicle and battery constraints are determined and calculated.

4. **Section 6.3.4** determines the estimation of vehicles' recharging duration and energy consumption throughout the charging sessions.

5. The algorithm's flowchart and operation process are detailed in **Section 6.3.5**.

Each part is ultimately combined to develop an algorithm for creating stochastic charging profiles. It should be noted that some assumptions — where relevant data cannot be obtained are considered to facilitate the algorithm's development.

6.3.1 Frequency and Distribution of Charging Events

The timely distribution of vehicles at public charging stations is a key data because the charging may influence the grid's operating characteristics if it occurs during the network's peak hours. The data from [49, 50, 282] is used to obtain the timely distribution of charging events in the UK. This is presented in Figure 6.3.
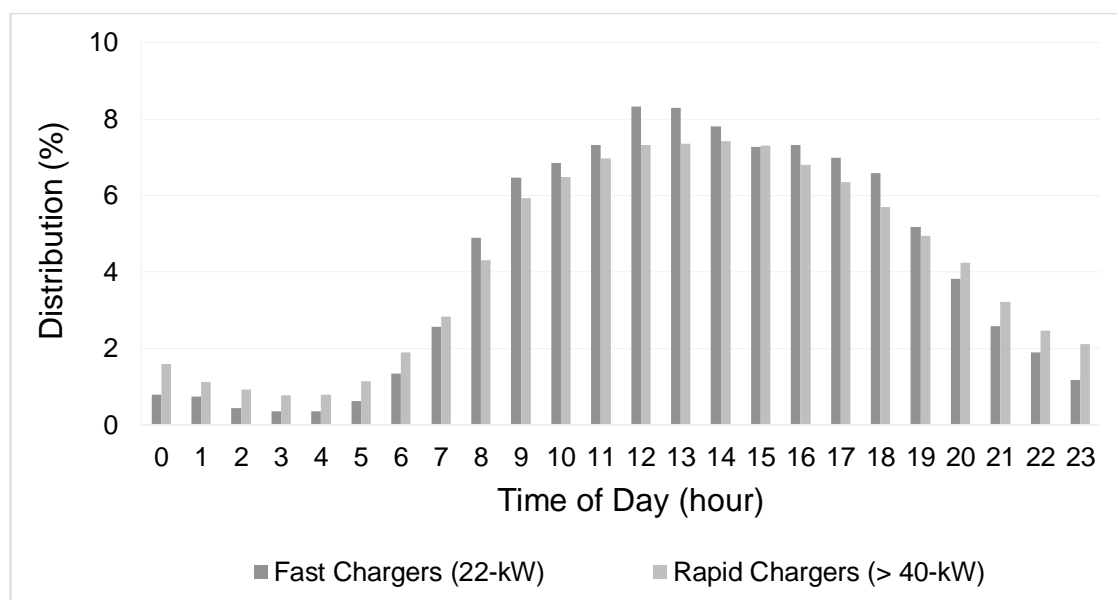
Figure 6.3: Frequency and timely distribution of public charging events in the UK.

The graph displays frequencies in a 'top-of-the-hour' format. The frequency of charging occurrences — shown by the dark grey bars represents the frequency of charging events from fast-speed chargers between 2017 and 2018 [49]. From December 2020 [50], the bright grey bars indicate the frequency of rapid chargers. While both sources are from separate time periods, the time distribution of charging events is identical. The percentile distribution of charging events in the UK is scaled down into eight intervals to simplify the algorithm development, as seen in Table 6.2.

Table 6.2: Percentile distribution of charging events during different time intervals

Hour (h)	Distribution (%) [49]	Distribution (%) [50]	Mean Distribution (%)	Number of Vehicles
00:00–03:00	1.97	3.64	2.81	1
03:00–06:00	1.33	2.71	2.02	1
06:00–09:00	8.8	9.02	8.91	3
09:00–12:00	20.64	19.39	20.02	7
12:00–15:00	24.43	22.11	23.27	8
15:00–18:00	21.6	20.46	21.03	7
18:00–21:00	15.6	14.88	15.24	5
21:00–00:00	5.66	7.79	6.73	2

Table 6.2 shows the percentile distribution of fast and rapid chargers, as well as the mean distribution from both charger speeds. In the UK, the overall percentile distribution of charging events between 12:00–15:00 is nearly 23% and between 15:00–18:00 is nearly 21%. The third charging peak occurs between 09:00–12:00 (20% of the total events), whereas only a small number of individuals (7%) charge between 00:00–06:00.

Table 6.2 also shows the number of individual vehicles charging during different time intervals in the network, which is determined based on the total number of vehicles (34) in the network. The total number of vehicles is determined based on the national statistics and travel surveys. According to a 2021 data conducted by *National Travel Survey*, most of the population in Great Britain lives in households with one car (45%), two cars (33%) or none (22%) [283]. In this study, the greatest proportion of the general population is considered, and the maximum number of cars per household is limited to one. This is equivalent to 28 vehicles from 63 residential dwellings in the network feeder under consideration. In addition, the *Office for National Statistics* conducted a survey in late 2021 and found that nearly half of the adult drivers are planning to switch to an electric car within the next decade [284]. This thesis used the *National Travel Survey* results to assume that the car ownership for households refers to electric only.

The topology of the network used in this chapter is also considered to determine the total number of vehicles. The national data for the proportion of households with access to one, two, or no cars is available; however, the proportion of commercial buildings and consumers with access to a number of cars is not defined in the surveys. Therefore, the real data concerning the residential household to commercial building demand ratio is used (see **Figure 5.3**) to determine the average number of consumers and the proportion of EV ownership from the commercial building. It is found that the average demand from the commercial building is nearly equivalent to the demand of 14 residential households [47]. Using the greatest proportion of the general population, this is equivalent to six additional vehicles due to the commercial building, making the total number of vehicles 34 in the network. It should also be mentioned that the allocation of EVs for the households is not relevant, since all EVs are charged at the same place, near the commercial building in the network. As discussed in **Chapter 5**, this point is selected as it is feasible to accommodate high-power charging devices (see **Figure 5.2**).

On the other hand, the number of vehicles for each interval is determined based on the percentile distribution scaled down to the total number of vehicles considered in the modelling study. For example, the average charge time (termed as mean distribution) start is 8.91% between 06:00 and 09:00. Taking 8.91% of the total number of vehicles and rounding to the nearest integer results in three vehicles being charged at the hub. Among other calculations, the busiest hour is between 12:00 and 15:00 at the hub. The arrival times of the vehicles at the charging point are not determined at random, but rather based on the mean distribution of charging events derived from real data obtained from 108,746 charging events [49] and [50] as seen in Figure 6.3 and Table 6.2. However, the stochasticity is considered to produce different charging intervals during the specified time window for each vehicle in each run of the algorithm.

Each vehicle visits the station for charging just once in the day. Once a vehicle has been charged, it is removed from the cluster of vehicles represented by the 'splice()' function, which modifies the array's content while deleting the previously chosen vehicle in the algorithm [285]. The algorithm is used to compute the number of vehicles for each interval based on the mean distribution of charging occurrences. Intervals with a higher mean distribution (e.g., between 12:00–15:00) imply a greater possibility of vehicles charging concurrently at the station compared to an interval with a lower mean distribution (e.g., between 00:00–03:00). The algorithm's method for deciding the allocation of charge time for each vehicle is explained as follows:

- Using the randomiser function, the algorithm selects a vehicle of any model, and then allocates a random charging time interval.

- For simplicity, the vehicles could only be charged at the start of each hour. For example, if the algorithm allocates a vehicle to charge between 12:00 and 15:00, it only starts charging at 12:00, 13:00, or 14:00.

- The selected vehicle is then removed from the cluster and the previous steps are repeated until all the remaining vehicles have been assigned a charging slot.

6.3.2 Selection and Characteristics of Vehicles

Five popular BEV models with large market shares capable of rapid and ultra-rapid charging are chosen. Different models are examined to provide diversity in the algorithm and to account for drivers' different charging needs and requirements. The types and specifications of the selected BEVs are found from [26, 286], and seen in Table 6.3.

Table 6.3: Specifications of the chosen BEV models

Brand/Model	Battery Capacity (kWh)	Range (km)	Number of Units
BMW i3 (2019)	42	310	4
Audi e-Tron 55 quattro (2020)	95	436	5
Kia e-Niro 4 (2020)	64	453.8	6
Jaguar I-Pace (2019)	90	470	8
Tesla Model 3 Performance (2021)	79.5	507	11

BMW i3 (2019), Audi e-Tron (2020), Kia e-Niro 4 (2020), Jaguar I-Pace (2019), and Tesla Model 3 Performance (2021) are among the selected vehicles. Each model has a unique battery capacity and range, with the 42-kWh BMW model having the lowest range, while the 79.5-kWh Tesla Model having the greatest range. The range estimations from [36, 287] are utilised based on a mixed driving style (i.e., city and highway) during the mild weather conditions.

The total number of EV units in Table 6.3 is 34, which is the total number of assigned vehicles in the charging station on a given day. This number is determined based on the diversity of the BEV models and the likelihood of drivers switching to electric. Statistics from 2019 and 2020 show that BMW i3, Audi e-Tron, Kia Niro, Jaguar I-Pace, and Tesla Model 3 account for nearly 50% of the total registrations of fully electric cars in the UK [26, 286].

The number of each specific model is also determined based on the vehicle shares scaled down to the network feeder considered in the modelling study. For example, Tesla Model 3 accounted for around 30% of total shares in 2020 [26], which is approximately equivalent to eleven units from a total of 34 assigned vehicles. The number of units for BMW, Audi, Kia, and Jaguar models, on the other hand, is determined as four, five, six, and eight, respectively.

Each model has a different charge profile based on the type and rating of the charging device. While the driver often selects the physical device in a public charging station, the quantity of power supplied to the vehicle is completely dependent on the amount of power requested by the vehicle battery up to the charger's maximum rate [242]. For example, a Kia e-Niro 4 on a 175-kW CCS device cannot draw more than 50 kW [33, 242]. This criterion, however, varies for each model on the market.

The charging characteristics of each model on various rapid and ultra-rapid devices are presented in Table 6.4.

Table 6.4: Charging characteristics of the selected EV models

Brand/Model	Device Rating	Maximum Charge Power (kW)
BMW i3	50-kW CCS	49
Audi e-Tron 55 quattro	175-kW CCS	155
Kia e-Niro 4	50-kW CCS	50
Jaguar I-Pace	175-kW CCS	104
Tesla Model 3 Performance	175-kW	148
Tesla Model 3 Performance	350-kW CCS	194

Three popular rapid charger connectors are used for the vehicles: the 50-kW CCS, the 175-kW CCS, and the 350-kW CCS. BMW and Kia models are solely charged on the 50-kW CCS, while Audi and Jaguar are solely charged on the 175-kW CCS device. Tesla models are charged both on the 175-kW CCS and 350-kW CCS devices. It is seen from Table 6.4 that the rating (kW) of the device is not necessarily supplied to the battery due to limitations. The charging characteristic of each model on the market is different and limited by the on-board battery. Figure 6.4 compares and shows the charging characteristics (i.e., relationship between power and battery SoC) of each model.
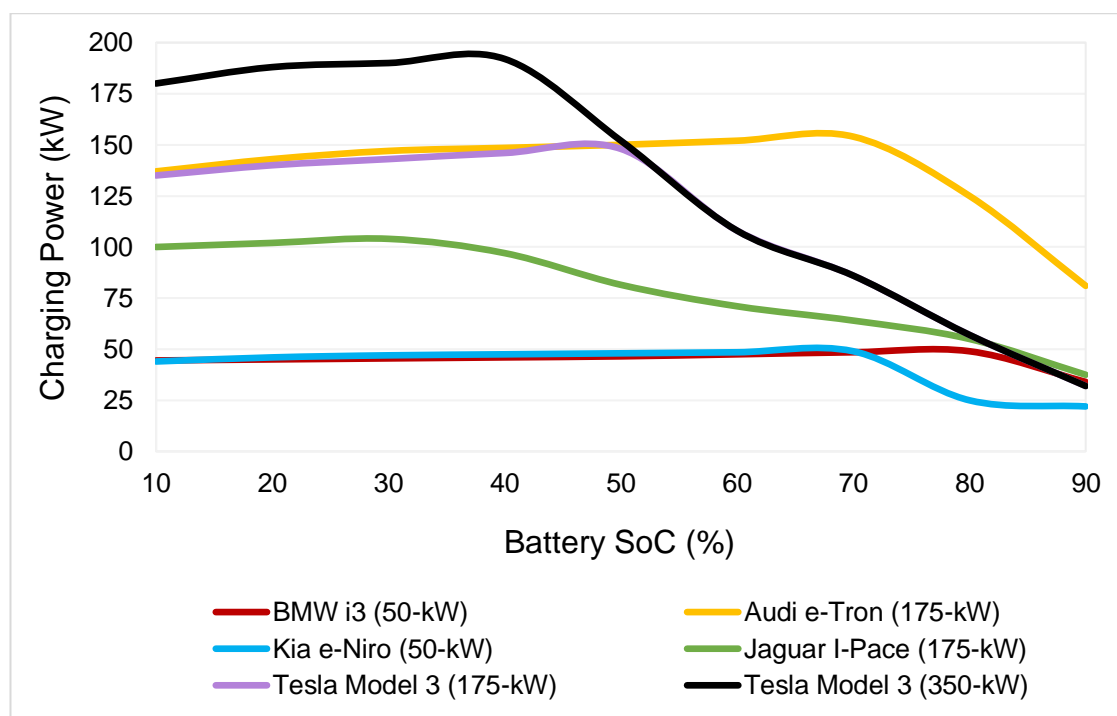
Figure 6.4: Relationship between charging power and battery SoC for each vehicle model [242].

The graph depicts the charge power in the vertical axis (in kW) as a function of the battery charge level, SoC (in %) in the horizontal axis. Each vehicle has its own characteristics, and the starting power of each model is completely dependent on the vehicle's remaining battery SoC. Audi and Jaguar vehicles, for example, are charged on 175-kW devices, but may draw up to 155 kW and 104 kW as their theoretical maximum power, respectively. On the other hand, BMW and Kia models may draw up to 49 kW and 50 kW during a charging session on a 50-kW device, respectively. Lastly, Tesla models can draw up to 148 kW and 194 kW, respectively, from the 175-kW (V2) and 350-kW (V3) CCS devices [36, 242, 287].

As seen from the charging curves, the vehicles cannot be charged at a constant rate due to battery constraints. For example, BMW and Kia vehicles are charged at a steady pace until the battery reaches about 70% capacity. Beyond this point, the charging speed progressively decreases for Kia models, whereas BMW models achieve to manage the charging rate until the battery is about 80% full. A Jaguar car consumes about 100 kW until its battery is roughly 35% charged, at which point the speed progressively decreases. An Audi model charges at or around 150 kW until the battery reaches 70% capacity. Tesla models are somewhat different, and their charging speeds substantially decrease when the battery is about 50% and 40% full on a 175-kW and 350-kW device, respectively.

The main factors that influence charging speeds are [288]:

- Battery capacity: the larger the vehicle's battery is, the longer is the charge time.

- Battery SoC: charging a fully depleted battery takes longer than topping up the battery from 50% SoC.

- Vehicle's maximum charging rate: a vehicle's battery can only charge at the maximum rate that the vehicle is capable of drawing.

- Environmental variables: the ambient temperature may also influence battery operating temperatures. When the vehicle's battery gets cold, the charge pace decreases. The optimal temperature for batteries is typically between 20°C and 30°C, but some batteries charge more quickly at or around 40°C [242].

In general, charging power and speed for most cars on the market drop considerably when the SoC reaches 80% at rapid devices. With respect to this, a customer study survey revealed that 94% of respondents at rapid charging devices power their vehicles until the battery SoC reaches 80% [51]. Typically, a motorist will charge up to 80% and then may decide to top up to 100% overnight using a residential charger [242, 288].

6.3.3 Vehicle Constraints Prior to Charging

Prior to charging, an EV's remaining range and SoC are equal to a petrol vehicle's remaining mileage. The remaining range and SoC of an EV are determined by the distance travelled after a full charge. The developed algorithm's methods for calculating the vehicles' remaining range and SoC are described as follows:

- For each model, a range limit is selected based on the vehicles' SoC restrictions. It is assumed that vehicles have a minimum of 10% and a maximum of 50% SoC prior to charging.

- The lower SoC limit is set based on the vehicles' lowest battery SoC in Figure 6.4, whereas the upper limit is set based on the poll in [51], in which over 75% of the respondents said that their EV's average SoC level is ≤ 51% prior to charging.

- Additionally, according to the charging data from 108,746 events, EVs consume between 9.2–20.5 kWh during charging sessions [49]. For city driving, a popular EV model (e.g., a 30-kWh Nissan Leaf SL) with a range of 172.2 km consumes 17.2 kWh per 100 km [36]. This means that the average Nissan driver will charge when the vehicle's remaining range is between 54–119 km. If the driver maintains an average constant speed, the vehicle's SoC prior to charging will be between 31–69%. This gives an average remaining SoC of 50% for the drivers.

Using the SoC constraints, the *Maximum Distance* (M_xD) and the *Minimum Distance* (M_nD) travelled by each model prior to charging are calculated with (6.1) and (6.2), respectively.

$$M_xD \ (km) = R_v - \frac{R_v \times SoC_{10\%}}{SoC_{100\%}} \qquad (6.1)$$

$$M_nD \ (km) = \ R_v - \frac{R_v \times SoC_{50\%}}{SoC_{100\%}} \qquad (6.2)$$

Where:

R_v is the actual electric range of each EV model (km),

$SoC_{10\%}$ is the minimum SoC constraint of the vehicle prior to charging (%),

$SoC_{100\%}$ is equivalent to maximum SoC/range on a fully charged battery (%),

$SoC_{50\%}$ is the maximum SoC constraint of the vehicle prior to charging (%).

The M_xD of each vehicle is equivalent to the maximum distance it can drive on a fully charged battery until the battery SoC shows 10%, whereas the M_nD refers to the minimum distance that each vehicle can drive after a full charge until the battery SoC is 50%. These equations assume that each vehicle starts its journey with a maximum battery SoC. The calculated range limits for each model are demonstrated in Table 6.5.

Table 6.5: Maximum and minimum range limits of the chosen EV models

Brand/Model	Actual Electric Range (km)	Maximum and Minimum Range Limits within SoC Constraints (km)
BMW i3	310	155 < *Distance Travelled* > 279
Audi e-Tron 55 quattro	436	218 < *Distance Travelled* > 392.4
Kia e-Niro	453.8	226.9 < *Distance Travelled* > 408.4
Jaguar I-Pace	470	235 < *Distance Travelled* > 423
Tesla Model 3 Performance	507	253.5 < *Distance Travelled* > 456.3

Each model has its own set of maximum and minimum range limits, due to the vehicles' varying battery specifications. According to the calculations, a BMW vehicle with a 310-km range would have a remaining SoC of 50% and 10%, respectively, if it travels 279 km and 155 km on a full charge. Other estimates indicate that Audi models travel between 218–392.4 km, Kia models between 226.9–408.4 km, Jaguar models between 235–423 km, and Tesla between models 253.5–456.3 km prior to arriving and charging at the station.

The algorithm generates a random number — also termed as *Distance Travelled* (D_t) between these limits, using the 'roll()', 'math.floor()', and 'math.random()' functions. These functions roll an integer between the maximum and minimum range limits and produce a floating number [289, 290]. The *Remaining Range* (R_r) of vehicles are then calculated based on the randomly generated distance travelled values with (6.3).

$$R_r \; (km) = R_v - D_t \tag{6.3}$$

The R_r of a vehicle is calculated by subtracting the actual vehicle range from the total distance travelled on a fully charged battery. Following the remaining range calculation, the *Remaining SoC* (R_{SoC}) of the vehicles is also calculated, according to (6.4).

$$R_{SoC} \; (\%) = \frac{R_r}{R_v} \times SoC_{100\%} \tag{6.4}$$

As it can be seen, the vehicle's remaining battery capacity is entirely dependent on the predetermination and computation of SoC constraints, and randomisation of the *Distance Travelled* before reaching a charging hub.

6.3.4 Charging Duration and Energy Consumption of Vehicles

The length of recharging (i.e., time it takes for an EV to reach its target SoC) is the final step in determining the vehicle data to create stochastic charging profiles. This is a metric that is dependent on the battery size, the remaining battery capacity, the vehicle's and charging device's maximum charging rates, the target SoC and the average power used during a charging session. For example, some drivers charge their vehicles from near-empty to full battery state, whereas others charge from 10% to 80%, or simply top up to a desired SoC from 50–60%. It is difficult to provide an exact charging time for EVs since charging speeds vary due to a variety of factors. Even vehicles of the same model and SoC levels prior to charging can be recharged under different durations on the same charging device. Charge time estimates for various BEV models on different devices are available in [30, 36, 242, 287, 288]. This chapter makes use of the recharge estimates from [30, 242], because these provide the estimated durations for reaching up to 80% battery SoC from 10% battery SoC. These estimates, as also shown in Table 6.6, are chosen since the minimum and maximum SoC values at the start and finish of charging are set to 10% and 80%, respectively.

Table 6.6: Generic recharge time estimates of the chosen EV models

Brand/Model	Battery Capacity (kWh)	Average Charge Power (kW)	10% to 80% Charge Time (mins)
BMW i3	42	47 (on a 50-kW CCS)	36
Audi e-Tron 55 quattro	95	146 (on a 175-kW CCS)	26
Kia e-Niro	64	45 (on a 50-kW CCS)	63
Jaguar I-Pace	90	85 (on a 175-kW CCS)	44
Tesla Model 3 Performance (V2)	79.5	124 (175-kW CCS)	27
Tesla Model 3 Performance (V3)	79.5	148 (350-kW CCS)	23

The average charge power represents the power drawn to charge the battery from 10% to 80% of its capacity. BMW and Kia vehicles on a 50-kW CCS device draw an average of 47 kW and 45 kW, respectively, to reach to 80% SoC from 10% SoC. Jaguar and Audi vehicles take an average of 85 kW and 146 kW from a 175-kW device, respectively. Tesla vehicles receive 124 kW and 148 kW from 175-kW and 350-kW CCS devices, respectively [36, 242].

Overall, the time required to reach 80% of battery capacity increases as the ratio of battery capacity to average charge power increases. For example, the average power supplied to a BMW and a Kia vehicle on a 50-kW device is almost the same, yet the Kia charges at a much slower pace due to its 1.5 times larger on-board battery capacity. Audi and Tesla vehicles on a 175-kW CCS charging device draw an average of 146 kW and 124 kW, respectively; nevertheless, the Tesla model charges at a quicker pace owing to its smaller on-board battery size. According to real-world charging results, the Model 3 charges 42% faster than an Audi model on a 350-kW CCS device [291].

Equation (6.5) is introduced for estimating the vehicles' recharging durations based on their calculated R_{SoC} levels.

$$C_{te} \ (mins) \ = \frac{C_t \times SoC_d}{SoC_{70\%}}$$

(6.5)

Where:

C_{te} is the vehicles' estimated charging time to reach target SoC of 80% (mins),

C_t is the vehicles' estimated charging time to reach from 10–80% SoC (mins),

SoC_d is the difference between the remaining and target SoC of vehicles (%),

$SoC_{70\%}$ is the max. SoC difference between the minimum and target SoC (%).

Since the vehicles generally charge up to 80% in a rapid charging device [242], it is assumed that the vehicles' target SoC is 80% in (6.5). If an Audi vehicle with a 30% remaining battery capacity arrives to charge at the hub, for example, its estimated recharge time on a 175-kW CCS device will be 19 minutes, according to (6.6).

$$C_{te}\ (mins) = \frac{26\ mins\ \times (80\% - 30\%)}{SoC_{70\%}} \approx 19\ \text{mins} \tag{6.6}$$

Lastly, the energy consumption of each vehicle may also be determined, using (6.7).

$$E_v\ (kWh) = \frac{A_{CP} \times C_{te}}{60\ minutes} \tag{6.7}$$

Where:

E_v is the energy consumption of each vehicle during charging sessions (kWh),

A_{CP} is the average charge power to reach from R_{SoC} to 80% SoC (kW).

6.3.5 Methodology and Flowchart of the Algorithm

The algorithm developed in this chapter produces stochastic scenarios based on the constraints and limits of the vehicle models before returning the calculated parameters of them. In addition to estimating EV demand, the algorithm generates stochastic EV charging profiles based on the randomly distributed travel distances of various EV models. This 'randomly' generated travel distances are determined within the predefined battery SoC constraints from the survey results [51]. In addition, the considerations for generating charging time are not completely random; rather, they are stochastically generated within a specified time window using actual data from Zap Map and 108,746 charging events from local authorities in the UK.

The DENO, which is a simple, secure, and modern runtime that is based on the V8 JavaScript engine, is chosen to develop the algorithm. DENO supports TypeScript out of the box, which is a popular superset of JavaScript created by Microsoft. TypeScript brings a huge advantage while developing the algorithm by providing type and error checking, which results in less error-prone code and better performance during execution. It is also used to add optional static typing to the language, and to correct any type-related errors quickly (avoiding compile-time errors caused by syntax violations). For example, if a number is substituted for a string that must include the object's name, the programme immediately indicates that it was expecting a string instead.

The algorithm begins by identifying 34 cars, five distinct vehicle models, and battery specifications of the vehicles as inputs. Initially, the structure of the inputs and objects is established in the algorithm. These include the number of cars, their brand and model, the frequency, and interval at which charge time begins, the battery parameters (capacity and range of vehicles), and the vehicles' calculated recharge durations. These are created as functions that accept objects containing the name (which must be a string — for example, the name for the EV brand) and data (which must be a number — for example, the number of each EV model or the data about a vehicle's battery capacity). The next phase includes randomly determining the remaining range of vehicles within the computed SoC constraints. Rolling a number within the minimum and maximum range limitations is accomplished using the 'roll()', 'math.floor()', and 'math.random()' functions. The vehicles' remaining range and remaining SoC are determined using the randomly generated distance travelled data. The remaining battery metrics are then used to estimate the recharging duration of the vehicles. The simplified flowchart of the algorithm is illustrated in Figure 6.5.
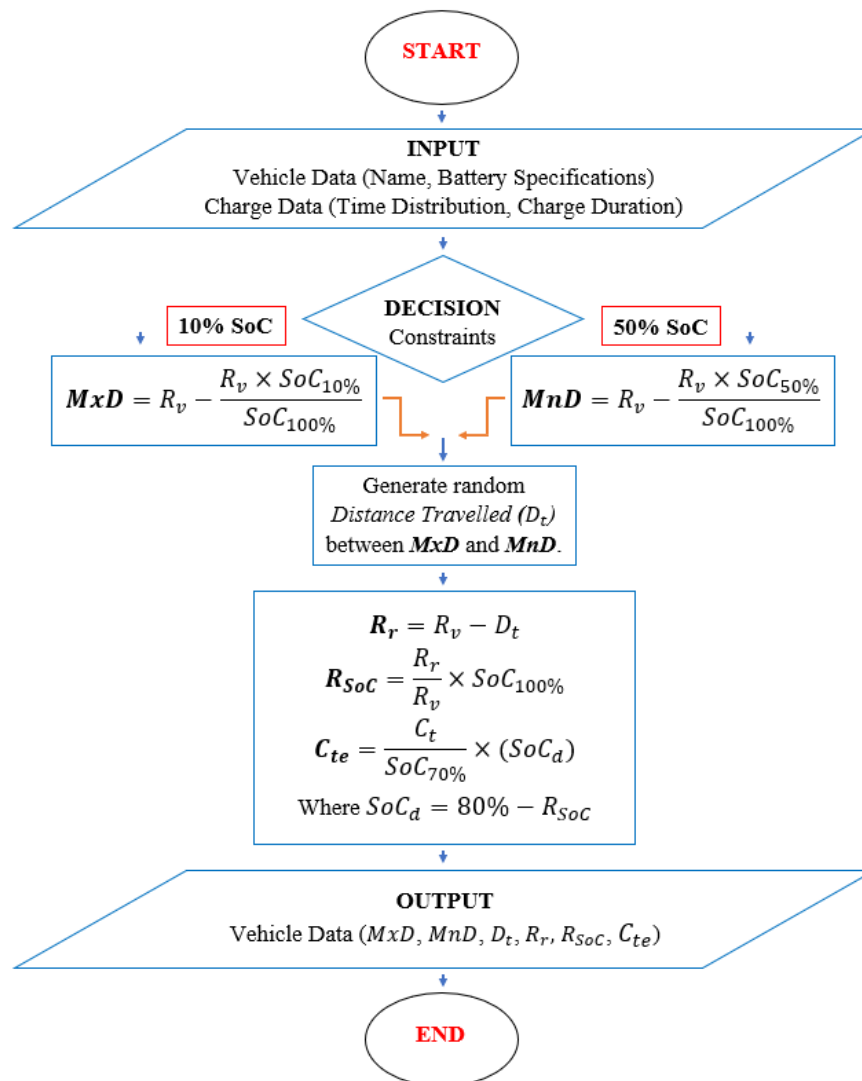
Figure 6.5: Simplified flowchart of the algorithm.

The appendices provide the codes and the layout of the algorithm script in more detail (see **Appendix D.2**).

6.4 Algorithm Results

The frequency of daily charging events during various time intervals from Figure 6.3 and Table 6.2 is used in conjunction with the predefined SoC limits to generate the distribution of charging events for 34 vehicles in each algorithm run. The algorithm is run 20 times to let the stochasticity play out and draw a more general conclusion for the results. This section shows the detailed stochastic results obtained from the algorithm.

6.4.1 Stochastic Distribution of Charging Events and Vehicles

In order to simplify the presentation of the results, two distinct runs are obtained from the algorithm, with each run showing the distribution of 10 aggregated cases on a single graph. Figure 6.6 and Figure 6.7 show the timely distribution of charging events and stochastically determined battery SoC for each vehicle model.
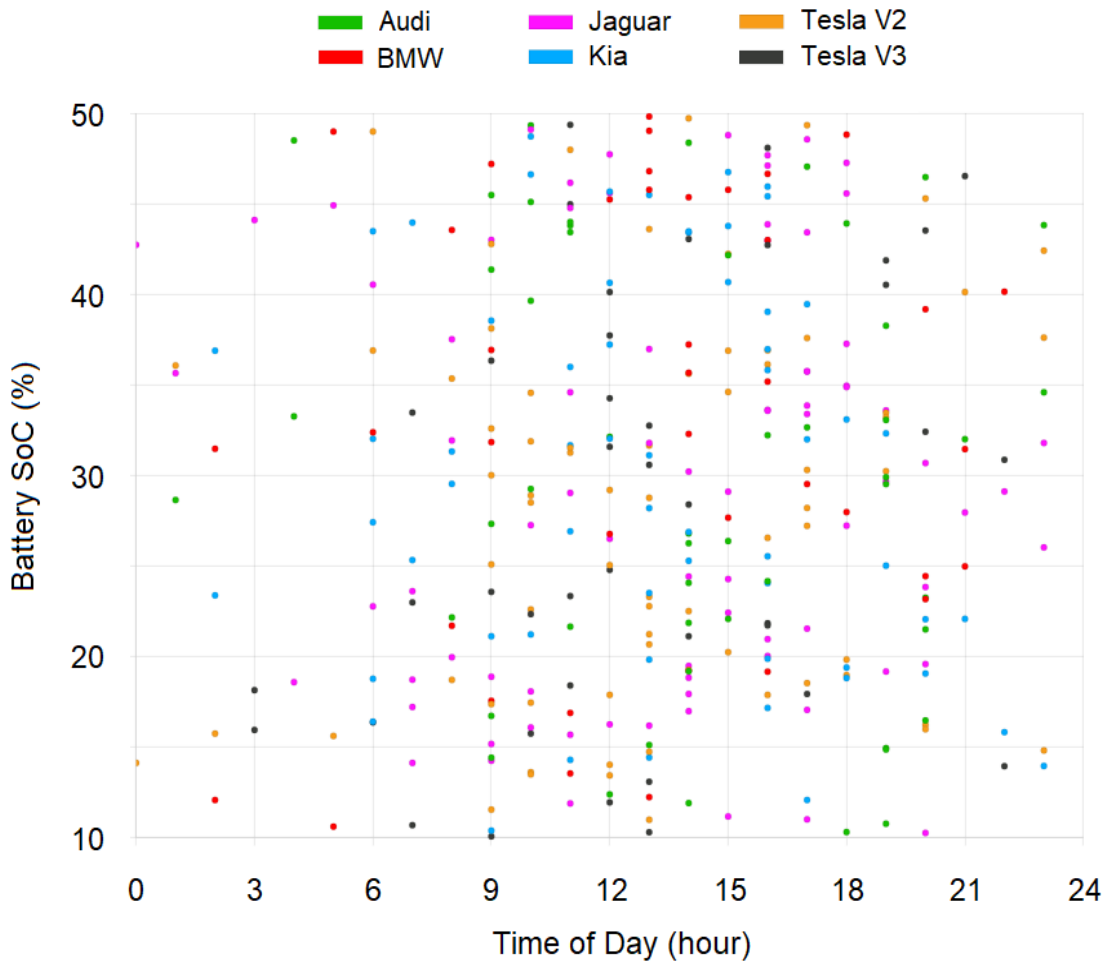
Figure 6.6: Stochastic distribution of charging time and battery SoC for vehicles (Case 1 to 10).
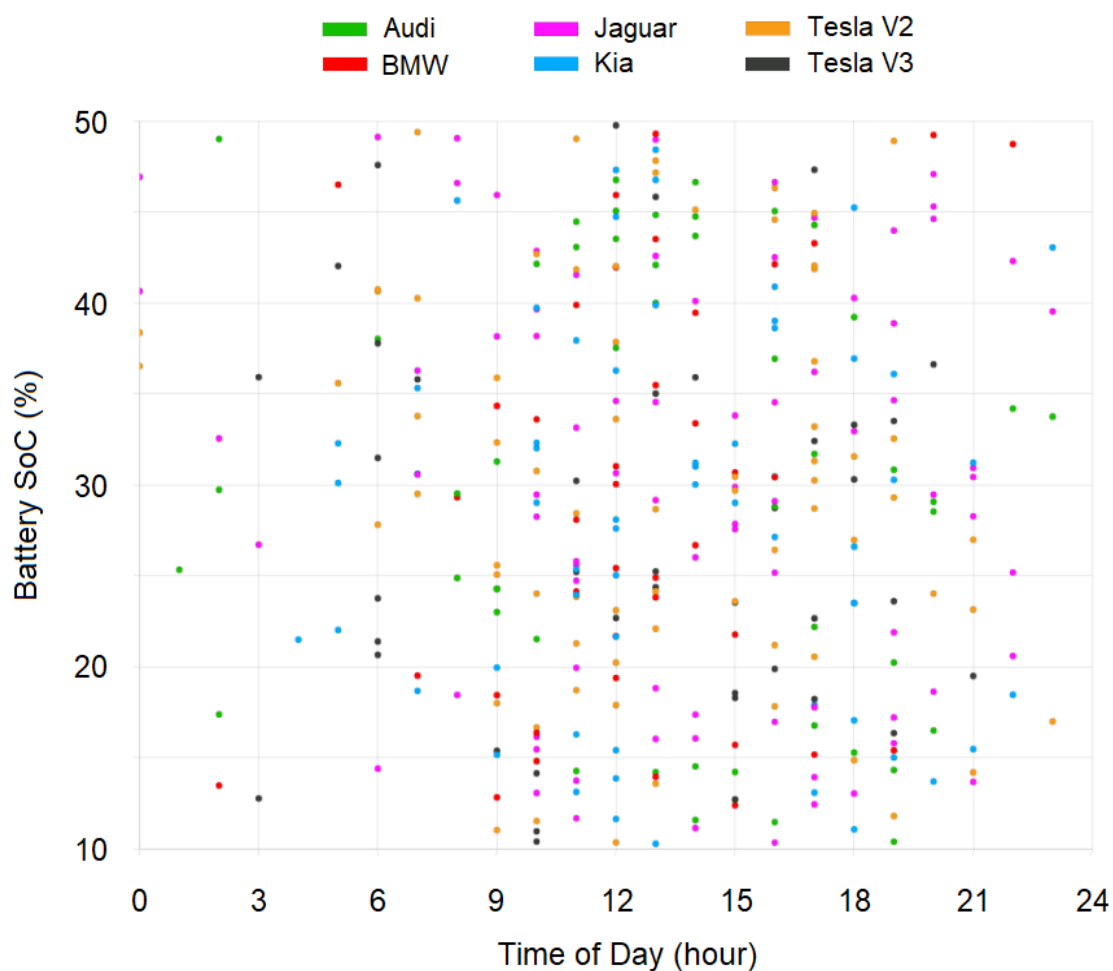
Figure 6.7: Stochastic distribution of charging time and battery SoC for vehicles (Case 11 to 20).

The primary vertical axis of both graphs depicts the stochastic battery SoC (in %) as a function of the stochastic charging time in the horizontal axis (in hours). Most charging events are observed to occur between 09:00 and 18:00. Also observed is the stochastic spread of the battery SoC for each vehicle model. Each graph displays the stochastic data for 340 vehicles, and a total of 680 vehicles are utilised to estimate the energy demand and consumption from 20 cases. The subsequent subsections examine the calculated and estimated energy demand of the vehicles in greater detail.

6.4.2 Stochastic Distribution of Energy Consumption

Each case is individually analysed using the calculated energy consumption of 34 vehicles. This also permits the comparison of each case's vehicle energy consumption distribution and the identification of the case with the highest demand and energy consumption from the stochastic charging activities (i.e., worst-case scenario for the grid). The appendices provide a tabular representation of the energy consumption for a total of 680 vehicles derived from the algorithm from all cases (see **Appendix D.3**). On the following page, the stochastic energy consumption from 20 cases is presented.
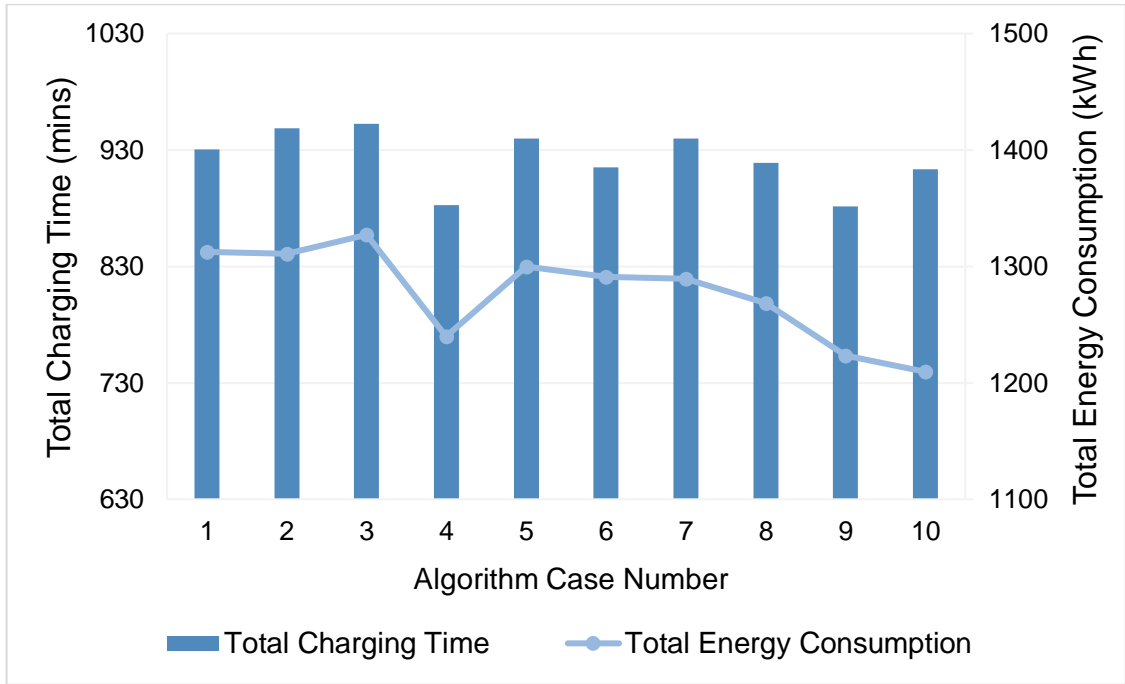
Figure 6.8: Stochastic distribution of total charge time and energy consumption (Case 1 to 10).
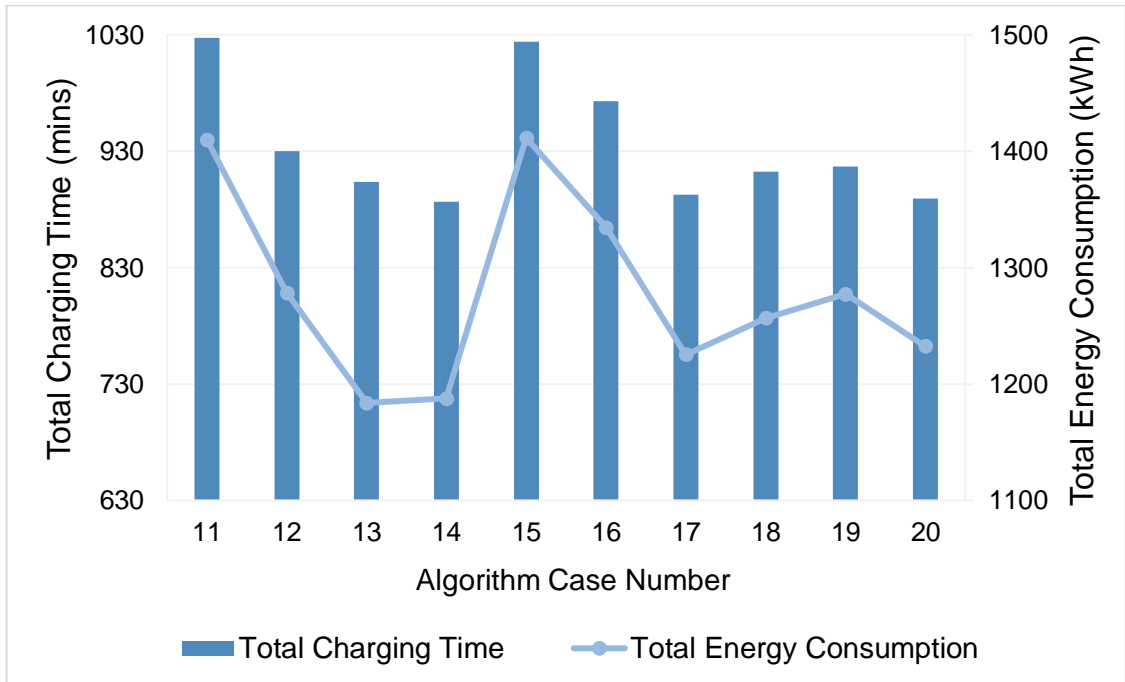
Figure 6.9: Stochastic distribution of total charge time and energy consumption (Case 11 to 20).

Figure 6.8 and Figure 6.9 depict, in the primary vertical axis, the total (combined) charging time for each corresponding case, i.e., the duration all 34 vehicles remained connected to achieve 80% battery SoC throughout the entire day (in minutes), as a function of the total energy consumption (in kWh) of 34 vehicles in the secondary vertical axis. Figure 6.8 shows the stochastic distribution of total charging time and energy consumption from Case 1 to Case 10, whereas Figure 6.9 shows the stochastic distribution of total charging time and energy consumption from Case 11 to Case 20.

The relationship between charging time and energy consumption appears to be directly proportional. However, it should be noted that, the battery SoC of the vehicles prior to charging significantly affect the duration of charging and the magnitude of energy consumption (see **Section 6.3.4**). This indicates that cases containing a larger number of vehicles with lower battery SoCs will necessitate longer charging times and require the grid to provide more energy than cases where the vehicles start charging at higher SoC levels. This is due to the limitations of the batteries in each model, as the charging power for most models decreases as the battery SoC increases (see **Figure 6.4**).

Due to the stochastic nature of the vehicles and charging events, the results demonstrate that each case produces a unique scenario for the grid. The total vehicle charging time ranges from 881 minutes (calculated in Case 9) to 952.3 minutes (calculated in Case 3), whereas the total energy consumption ranges from 1183.7 kWh (calculated in Case 13) to 1411.3 kWh (calculated in Case 15). It should be clarified that although there is a direct relationship between the charging time and the energy consumption of vehicles, this does not imply that the vehicles requiring the longest time to reach 80% battery SoC consume the most amount of energy. This is a result of the varied characteristics and types of the vehicle models considered in this study. Case 11 has the longest charging time for vehicles to complete charging (1,027.5 minutes); however, Case 15 uses the most electricity from the grid (1411.3 kWh). Case 13 vehicles use the least amount of energy to reach their target battery SoC levels (1183,7 kWh); however, Case 9 vehicles complete charging in the least amount of time (881.4 minutes).

When analysing the severity of grid issues, the time of charging, the location of charging, and the amount of electricity consumed by the vehicles are the most important factors to consider [241]. For this reason, this study examines the impact of stochastic charging activities by analysing the two scenarios in which vehicles remain connected to the grid the longest (Case 11) and consume the most electricity from the grid (Case 15).

6.4.3 Worst-Case Scenarios

In this section, the detailed calculation of vehicle data for scenarios where the grid is subjected to worst conditions is presented. Table 6.7 initially shows the stochastic distribution of 68 vehicles from two worst cases. To facilitate the presentation of the results, each vehicle model is assigned a number. For example, four BMW vehicles are represented as B1 to B4, five Audi vehicles are designated as A1 to A5, six Kia models are designated as K1 through K6, and eight Jaguar models are designated as J1 to J8. For Tesla vehicles, it is assumed that seven of them are charged using 150-kW devices (i.e., T1 to T7), while the other four are charged on 350-kW devices (i.e., T8 to T11).

Table 6.7: Stochastic timely distribution of vehicles in Case 11 and Case 15

Charge Time (hour) (Case 11)	Vehicle Number (Case 11)	Charge Time (hour) (Case 15)	Vehicle Number (Case 15)
00:00	No Vehicle	00:00	No Vehicle
01:00	No Vehicle	01:00	No Vehicle
02:00	A2	02:00	J7
03:00	No Vehicle	03:00	T8
04:00	No Vehicle	04:00	No Vehicle
05:00	K5	05:00	No Vehicle
06:00	J3, T1	06:00	No Vehicle
07:00	No Vehicle	07:00	K4, T5
08:00	A5	08:00	J5
09:00	B4, J7, K4	09:00	T10
10:00	T5	10:00	A5, J2
11:00	B2, J8, K3	11:00	B1, J4, J6, T2
12:00	A1, B3, K6	12:00	A1, B3, B4, K2, T7
13:00	B1, J2, T2, T6	13:00	A4, K1
14:00	A3	14:00	B2
15:00	J1, T3, T7	15:00	K5
16:00	J4	16:00	J3, T3, T6
17:00	J5, T9, T10	17:00	A3, T4, T9
18:00	K1, T11	18:00	K6, T1
19:00	A4, J6, T4	19:00	T11, A2, J8
20:00	No Vehicle	20:00	No Vehicle
21:00	T8	21:00	J1, K3
22:00	K4	22:00	No Vehicle
23:00	No Vehicle	23:00	No Vehicle

Charge start time entries are shown in a 'top-of-the-hour' style in Table 6.7. With reference to the mean percentile distribution of charging events in Table 6.2, intervals with a high probability of charging occurrence have four or five vehicles charging concurrently, whilst intervals with a low probability of charging occurrence either do not have any vehicles charging or have just one to two vehicles charging. It should be noted that although the algorithm schedules certain EVs to begin charging at the same time, this does not mean that they complete charging at the same time due to differences in their battery specifications and variations in their charging profiles. The duration of recharging also depends on the average power requested by each vehicle to reach 80% battery capacity. More relevant data throughout the charging of the vehicles in Case 11 and Case 15 is also presented in Table 6.8 and Table 6.9, respectively. These are key data while quantifying the peak demand on the substation transformer in **Section 6.5**.

Table 6.8: Calculated charging data of the vehicles in Case 11

Vehicle Model and Number	Remaining SoC (%)	Estimated Recharge Time (mins)	Average Charge Power (kW)	Estimated Energy Consumption (kWh)
B1	35.5	22.9	47.3	18.1
B2	28.1	26.7	47	20.9
B3	30	25.7	47.1	20.2
B4	18.4	31.7	46.7	24.7
A1	37.5	15.8	148.4	39.1
A2	29.7	18.7	148.3	46.2
A3	11.6	25.4	146.8	62.1
A4	10.4	25.9	146.6	63.3
A5	29	18.8	148.2	46.4
K1	23.5	50.9	45.5	38.6
K2	15.2	58.4	45.6	44.4
K3	13.1	60.2	45.5	45.7
K4	18.5	55.4	45.6	42.1
K5	30.1	44.9	45.8	34.3
K6	21.7	52.5	45.6	39.9
J1	33.8	29	76.8	37.1
J2	34.5	28.6	76.3	36.4
J3	14.4	41.2	84.6	58.1
J4	29.1	32	79.4	42.3
J5	13.9	41.5	85	58.8
J6	17.2	39.5	83.8	55.2
J7	38.2	26.3	74.6	32.7
J8	11.7	43	85.1	61
T1	27.8	20.1	119.4	40
T2	47.8	12.4	103.4	21.4
T3	30.4	19.1	118.5	37.7
T4	11.8	26.3	124.1	54.4
T5	24	21.6	121	43.6
T6	24.1	21.5	121	43.4
T7	23.6	21.8	121	44
T8	19.5	19.9	142.1	47.1
T9	32.4	15.64	130.3	34
T10	22.7	18.8	139.7	43.8
T11	33.3	15.4	129	33.1

Table 6.9: Calculated charging data of the vehicles in Case 15

Vehicle Model and Number	Remaining SoC (%)	Estimated Recharge Time (mins)	Average Charge Power (kW)	Estimated Energy Consumption (kWh)
B1	24.1	28.7	46.9	22.4
B2	33.4	24	47.7	19.1
B3	31	25.2	47.1	19.8
B4	25.4	28.1	46.9	22
A1	46.8	12.4	148.4	30.4
A2	20.2	22.2	147.7	54.6
A3	22.2	21.5	147.9	53
A4	40	14.9	148.4	36.9
A5	42.1	14.1	148.4	34.9
K1	10.3	63.8	45.4	48.3
K2	25	49.5	45.5	37.5
K3	15.5	58.1	45.6	44.2
K4	18.7	55.2	45.6	42
K5	29	45.9	45.4	34.7
K6	23.5	50.9	45.5	38.6
J1	30.9	30.9	78.4	40.4
J2	16.1	40.1	84.1	56.2
J3	25.5	34.5	80.7	46.4
J4	25.8	34.1	80.7	45.9
J5	18.4	38.7	83.5	53.9
J6	20	37.8	82.9	52.2
J7	32.5	29.8	77.4	38.4
J8	21.9	36.5	82.3	50.1
T1	31.6	18.7	117.5	36.6
T2	18.7	23.6	122.6	48.2
T3	46.3	13	109.3	23.7
T4	31.3	18.8	118	37
T5	33.8	17.8	116.3	34.5
T6	17.8	24	122.9	49.2
T7	10.3	26.9	124.5	55.8
T8	12.8	22.1	146.6	54
T9	18.2	20.3	143.5	48.6
T10	15.4	21.2	145.4	51.4
T11	16.3	20.9	144.8	50.4

It should be clarified that the average charge power in Table 6.8 and Table 6.9 is different from the base average charge power values in Table 6.6, since this is a parameter that is dependent on the remaining battery SoC of the vehicles prior to charging. A comparison is made across various models on the same CCS devices with similar remaining battery SoC levels prior to charging from Case 15:

- A2, with a remaining SoC level of 20.2% and an estimated recharging duration of 22.2 minutes, draws around 148 kW on average to reach 80% battery capacity on a 175-kW CCS device, while it consumes 54.6 kWh from the grid to reach to its target SoC.

- J6, on a 175-kW CCS device with a 20% remaining battery SoC capacity consumes around 52.2 kWh from the grid and charges in 38 minutes. The average drawn power for this vehicle to reach from 20% battery SoC to 80% battery SoC is around 83 kW.

- T2, on a 175-kW CCS device with a 18.7% remaining battery SoC capacity consumes around 48 kWh from the grid and charges just in 24 minutes. The average drawn power for this vehicle to reach from 18.7% battery SoC to 80% battery SoC is around 123 kW.

The comparison of three competing long-range models reveals that although all vehicles begin charging at the identical SoC levels, the Tesla model consumes less energy because its battery is more efficient for long range driving.

6.4.4 Comparison of General Vehicle Data

In the last subsection, a general comparison is made among 680 vehicles and between each model by calculating the average charging time and energy consumption for all cases combined. This comparison is shown in Table 6.10.

Table 6.10: Combined and averaged recharging duration and energy consumption of 680 vehicles

Vehicle Model	Average Recharging Time (mins)	Average Energy Consumption (kWh)
BMW	25.2	19.8
Audi	18.6	45.8
Kia	45.8	34.6
Jaguar	31.7	41.8
Tesla (V2)	19.7	39
Tesla (V3)	17.2	38.7

Calculations based on 20 cases indicate that while Kia models consume less energy than Audi, Jaguar, and Tesla models, it takes them longer to reach 80% battery SoC. BMW models consume the least energy to reach 80% battery SoC, but their average charging times are longer than Audi and Tesla models. The increased range and relatively quick recharging times of Tesla vehicles distinguish them not only from other models in this study, but also from other vehicles on the market. This demonstrates why Tesla models currently dominate market share.

6.5 Impact of Stochastic Charging Profiles on a Distribution Network Feeder

In this section, the stochastic charging profiles from the worst-case scenario are integrated near the distribution network feeder's only commercial building (Node N15) to quantify the daily peak demand and loading. The commercial building is chosen to make a realistic scenario, since these types of points generally have access to three-phase grid connection and have the capability of hosting rapid and ultra-rapid chargers. The topology and the characteristics of the feeder customers are demonstrated in Figure 6.10. The same network was also used in **Chapter 5**.

Connection Node	Consumer Type
N6	Residential
N7	Residential
N8	Residential
N10	Residential
N11	Residential
N12	Residential
N13	Residential
N14	Residential
N15	Commercial
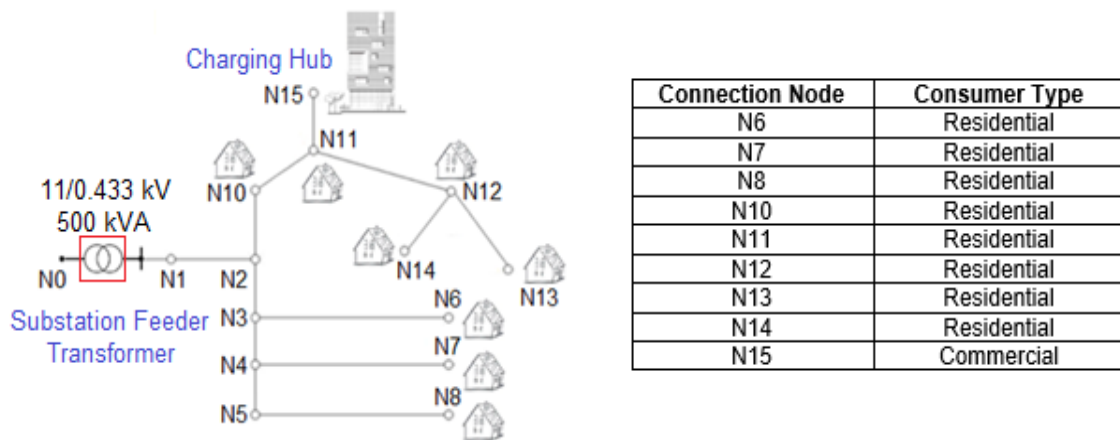
Figure 6.10: Distribution network feeder under examination.

Section 6.5.1 examines the effect of stochastic charging profiles on the peak demand at the charging point (Node N15) and at the substation transformer (between Node N0 and Node N1). **Section 6.5.2** analyses how individual EV charging affects the demand profiles on a minute-by-minute basis. **Section 6.5.3** examines the impact of installing V2G chargers and battery energy storage units near the charging point in the network. **Section 6.5.4** investigates transformer loading without and with the inclusion of a battery energy storage unit near the charging hub.

6.5.1 Hourly Peak Demand in the Network

The peak demand before the integration of stochastic charging profiles (baseload) and the peak demand after the integration of stochastic charging profiles are compared at the network's charging station and at the substation transformer throughout the entire day with the stochastic charging of 68 vehicles from Case 11 and Case 15. Simulation results are demonstrated in Figure 6.11.
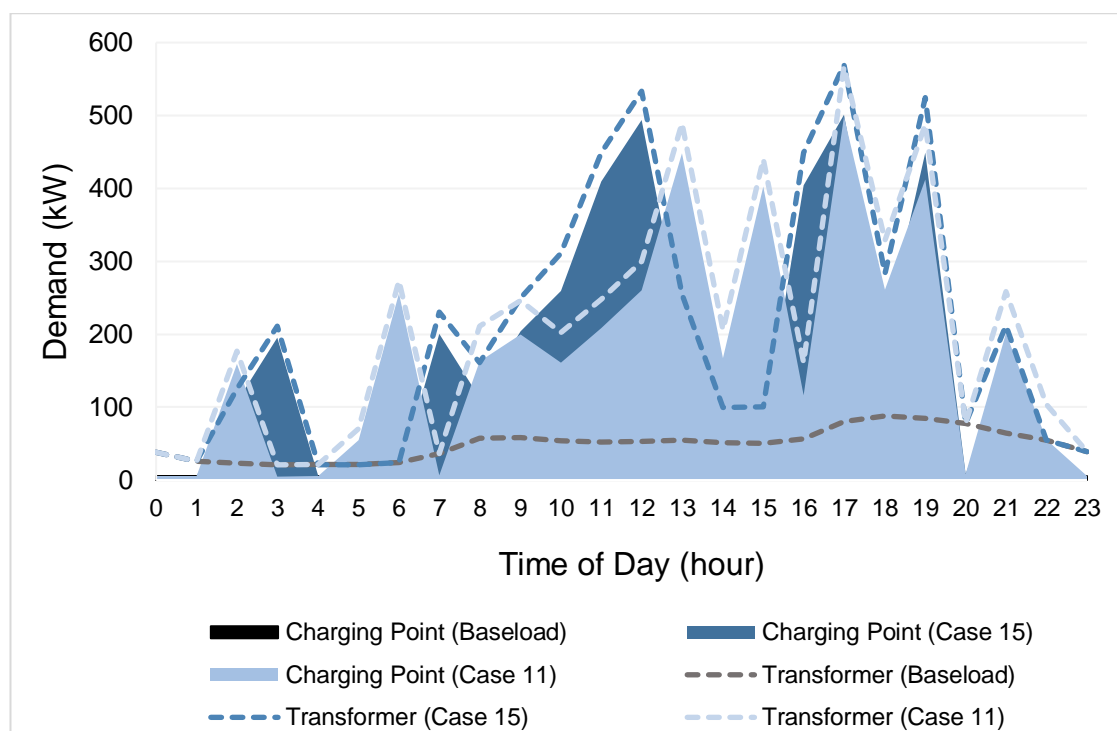
Figure 6.11: Hourly peak demand during baseload and with stochastic charging profiles.

The graph shows the hourly peak demand (in kW) at the charging point and at the substation transformer during baseload and with the addition of stochastic charging profiles from Case 11 and Case 15. The baseload demand at the charging point is a typical load profile of a commercial building; however, it is not visible as it is a very small value compared to the demand with charging activities (see **Figure 5.3**). The baseload demand at the transformer is the aggregated demand of the feeder's 64 customers.

According to [46, 47], the overall percentile distribution of charge time between 12:00 and 21:00 in the UK is approximately 62%, and Figure 6.11 illustrates the significant rise in peak demand when the stochastic charging events take place between these hours. Both Case 11 and Case 15 scenarios generate similar network load profiles. Due to differences in vehicle models, midday and late afternoon witness the greatest variation. Observations indicate that the peak demand in the late afternoon (between 16:00 and 17:00) is higher than the peak demand at other times of the day, mainly due to the increased residential and electricity demand as customers return home from work. Since afternoon peaks are more dominant due to the likelihood of charging events, this chapter focuses more on these peak periods to provide a more detailed investigation of how the system will operate at scale (i.e., nationwide). For Case 11, the afternoon peak demand starts at 17:00 when J5, T9, and T10 begin charging simultaneously. On the other hand, the afternoon peak starts at 17:00 when A3, T4, and T9 begin charging simultaneously for Case 15 (see **Table 6.7**). As shown in Figure 6.11, the peak demand at the charging point and substation transformer nearly approaches 500 kW and 570 kW, respectively.

It should be clarified that the differences in peak magnitudes are due to the different SoC levels of the vehicles. Nonetheless, it is evident from the results that Audi, Tesla, and Jaguar vehicles significantly contribute to the peak demand. On the other hand, the peak demand at the charging point does not remain constant for the entire hour since the aggregated charge power drawn by vehicles changes with an increase in the battery SoC (see **Figure 6.4**). In the following subsections, minute-by-minute fluctuations in peak demand are analysed in detail from the afternoon peak periods. Even though the peak demand profiles of Case 11 and Case 15 are identical at the start of 17:00, the remainder of this chapter focuses solely on the load profiles of Case 15, as this scenario requires the grid to provide more energy for the EVs to complete charging (see **Figure 6.9**).

6.5.2 Effect of Battery SoC on the Peak Demand

As discussed, the aggregated charge power drawn by each vehicle changes with respect to an increase in the battery SoC. The network demand is a dynamic variable that is substantially influenced by the behavioural changes of customers and drivers. Figure 6.12 and Figure 6.13 show how the afternoon peak demand varies on a minute-by-minute basis with concurrent charging of various vehicles.
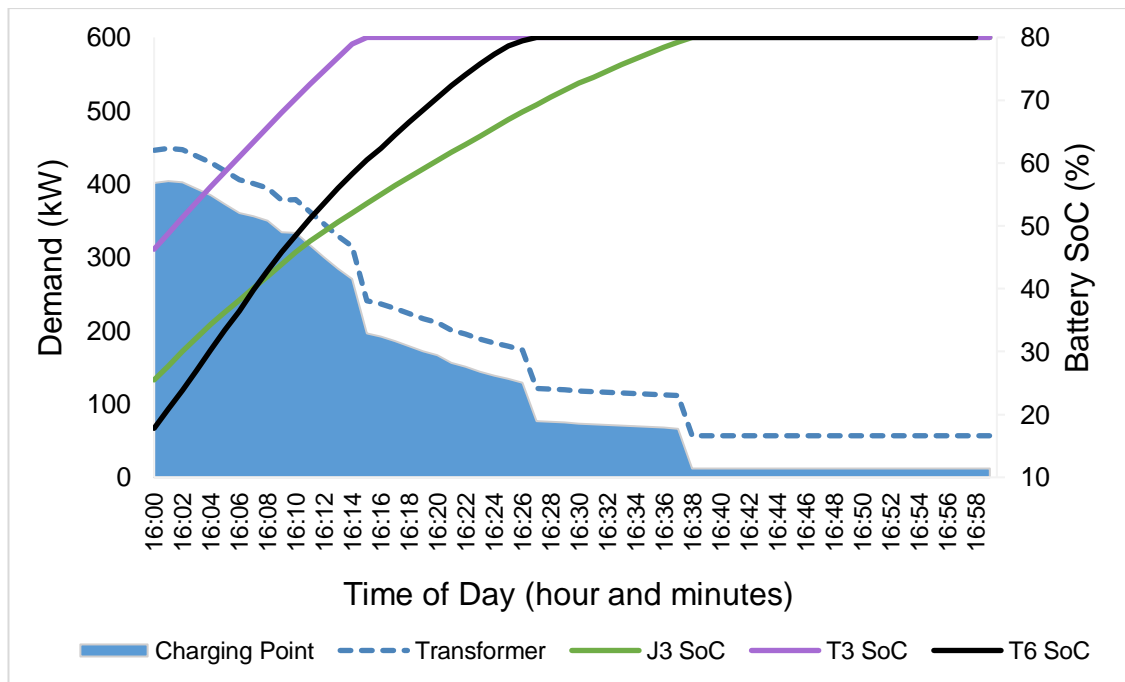
Figure 6.12: Fluctuation in the network peak demand between 16:00 and 17:00.

The graph illustrates the demand at the charging point and at the substation transformer (in kW) in the primary vertical axis, as a function of the battery SoC of the vehicles (in %) in the secondary vertical axis. It is plotted against real time (in hour and minutes) and shows how the peak demand varies between 16:00 and 17:00, when J3, T3, and T6 begin charging with 25.5%, 46.3%, and 17.8% SoC levels, respectively.

At the beginning of charging and hour, J3, T3, and T6 draw around 103 kW, 147 kW, and 139 kW, respectively, increasing the demand at the charging point and at the substation transformer to around 400 kW and 446 kW. J3's power consumption decreases gradually, whereas T3 and T6's power consumption increases until they reach 50% battery SoC. The peak demand of 404 kW and 448.7 kW occurs at 16:02 at the charging point and at the substation transformer, respectively. This peak demand only lasts less than a minute, which is used to represent the maximum peak demand as seen in **Figure 6.11**.

At 16:14, when the first vehicle (T3) reaches 80% battery SoC and stops charging, the overall network demand begins to decrease dramatically. The charging session for the second vehicle (T6) and the third vehicle (J3) concludes at approximately 16:26 and 16:37, respectively. Once all vehicles are charged to their target SoC of 80%, the demand at the charging station and the substation transformer will equal the baseload peak demand of 12 kW and 56.7 kW, respectively. The demand then remains constant until the beginning of the next hour, when it is anticipated that more vehicles will arrive and charge at the station. The minute-by-minute demand analysis of the next hour is shown in Figure 6.13.
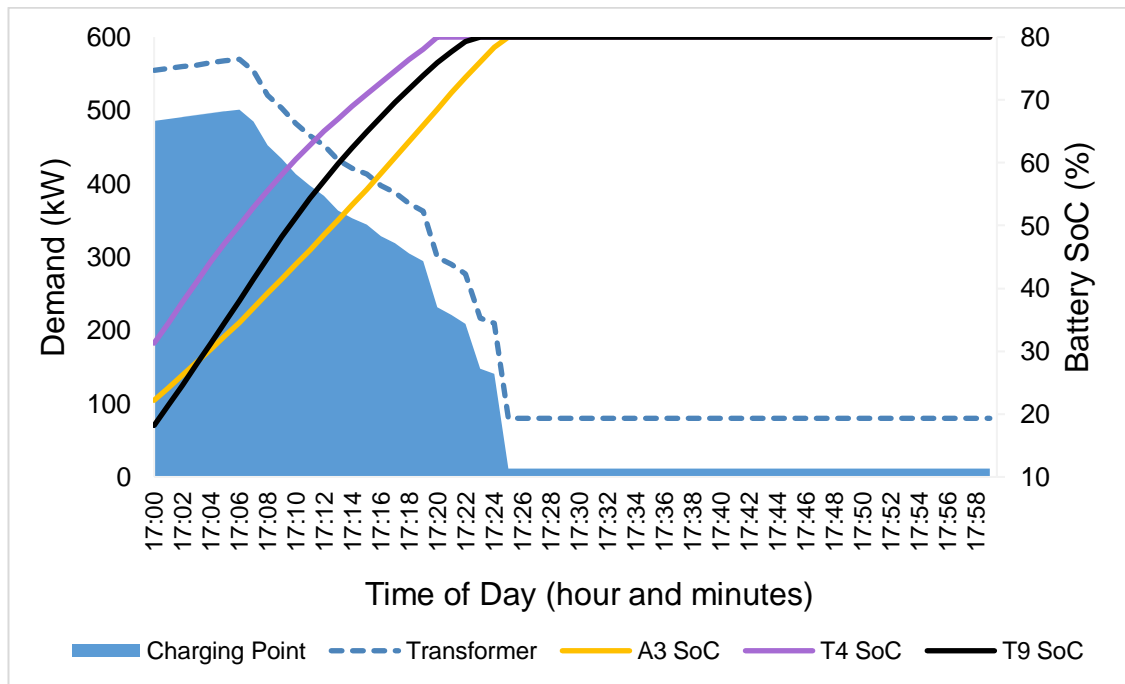
Figure 6.13: Fluctuation in the network peak demand between 17:00 and 18:00.

The graph illustrates the demand at the charging point and at the substation transformer (in kW) in the primary vertical axis, as a function of the battery SoC of the vehicles (in %) in the secondary vertical axis. It is plotted against real time (in hour and minutes) and shows how the peak demand varies between 17:00 and 18:00, when A3, T4, and T9 begin charging with 22.2%, 31.3%, and 18.2% SoC levels, respectively.

A3, T4, and T9 draw up to 147 kW, 150 kW, and 194 kW, respectively, between 17:04 and 17:06, which corresponds to the peak demand of 501 kW at the charging point and 570 kW at the substation transformer (also seen in **Figure 6.11**). After this point, network demand steadily decreases as the charging rates of Tesla vehicles gradually decrease when their batteries are between 40 to 45% full. At 17:20, T4 achieves its target SoC of 80%, resulting in a reduction in the peak demand in the network. Additionally, T9 and A2 reach their target SoCs at 17:22 and 17:24, respectively, and hence bringing down the demand at the charging point and at the substation transformer to 11.3 kW and 80 kW, respectively.

Two afternoon peak intervals of the day are shown in Figure 6.12 and Figure 6.13 to represent the charging characteristics of different EV models and to show how the interaction between different models affect and contribute to the increase in the network's peak demand. It should be noted that other intervals' minute-by-minute load profiles are not analysed and demonstrated since the same rationale applies with individual effect of charging on load profiles. These minute-by-minute demand profiles are also used when developing different discharge profiles for physical lithium-ion battery packs resembling a stationary battery energy storage unit in **Chapter 7**. This is to determine how much capacity of a typical stationary on-site battery energy storage can be used to support vehicle charging demand under various charging profiles. This also enables analysis of whether the battery's discharge end voltage has been reached.

6.5.3 Peak Load Reduction with V2G Chargers and Battery Energy Storage Units

The simulation results indicate that rapid and ultra-rapid devices significantly increase the peak demand of the feeder, particularly between 16:00 and 19:00 due to the higher likelihood of charging events taking place and higher residential demand in the network. The addition of two V2G chargers near the residential households at Node N11, and the connection of an on-site stationary battery energy storage unit at the charging point are proposed to reduce the feeder's peak demand.

For the V2G scenario, two 7.5-kW rated V2G chargers are connected near the network and the sizing is chosen to represent a typical device rating for a residential bidirectional charger from the UK trials [202]. The energy stored in the V2G charger is discharged back to the grid between 11:00–13:00 and 16:00–20:00 since these are the periods with the highest peak demand (see **Figure 6.11**). The impact of this small-scale V2G charger on the feeder's hourly peak demand is demonstrated in Figure 6.14.
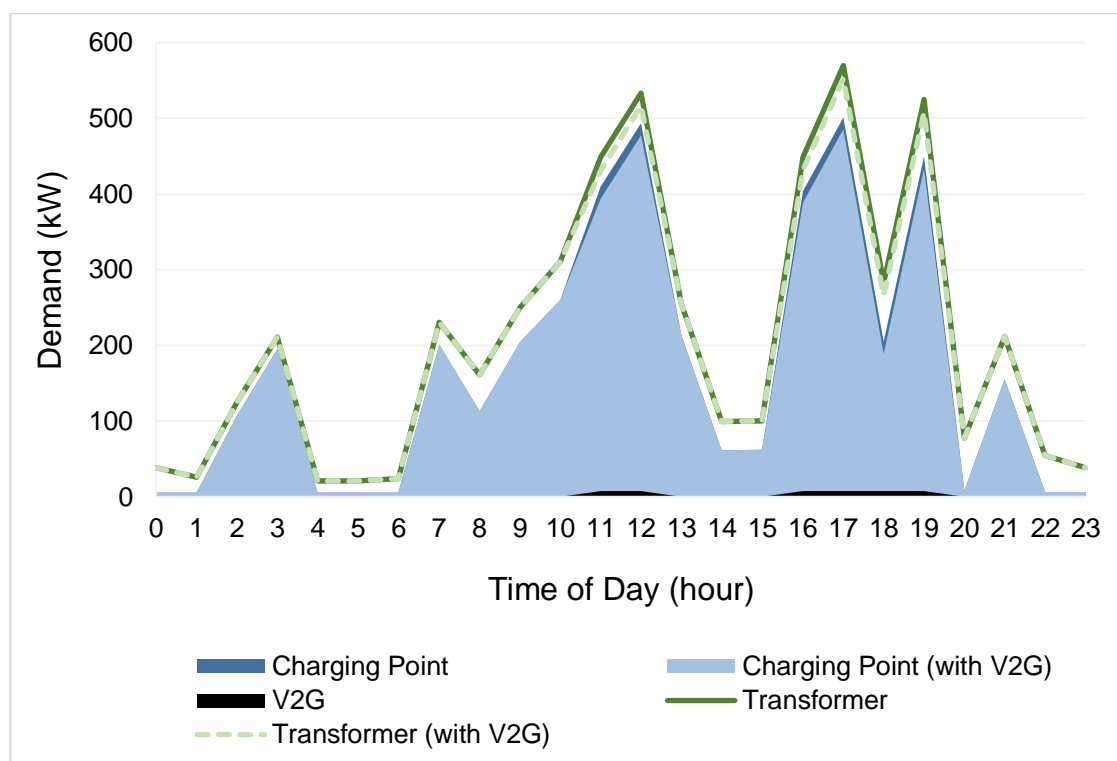
Figure 6.14: Effect of small-scale V2G chargers on the hourly peak demand.

The graph shows the hourly peak demand profile (in kW) at the charging point and at the substation transformer without and with the addition of two V2G chargers. V2G chargers are only providing energy between two intervals – represented by the small black areas at the bottom of the graph. Overall, the peak demand reduction achieved by the 7.5-kW V2G charger is not significant since the size of V2G chargers is small in comparison to rapid (50 kW) and ultra-rapid (100–350 kW) chargers.

To reduce peak demand, this chapter proposes to connect stationary battery energy storage units with larger energy capacity. Two operational scenarios for battery energy storage units are considered. Initially, a stationary grid-charged battery is connected to the charging point to reduce the peak demand. This scenario assumes that the stationary battery energy storage unit has a rated power of 50 kW between 11:00 and 13:00, and between 16:00 and 20:00.

In the second scenario, the effect of regulating the discharge rate of the battery energy storage unit is investigated. The second scenario assumes a larger storage unit is connected, and its capacity is governed based on the magnitude of the network's peak demand.

Figure 6.15 and Figure 6.16 depict the simulation results for the effect of battery energy storage units in the first and second scenarios, respectively.
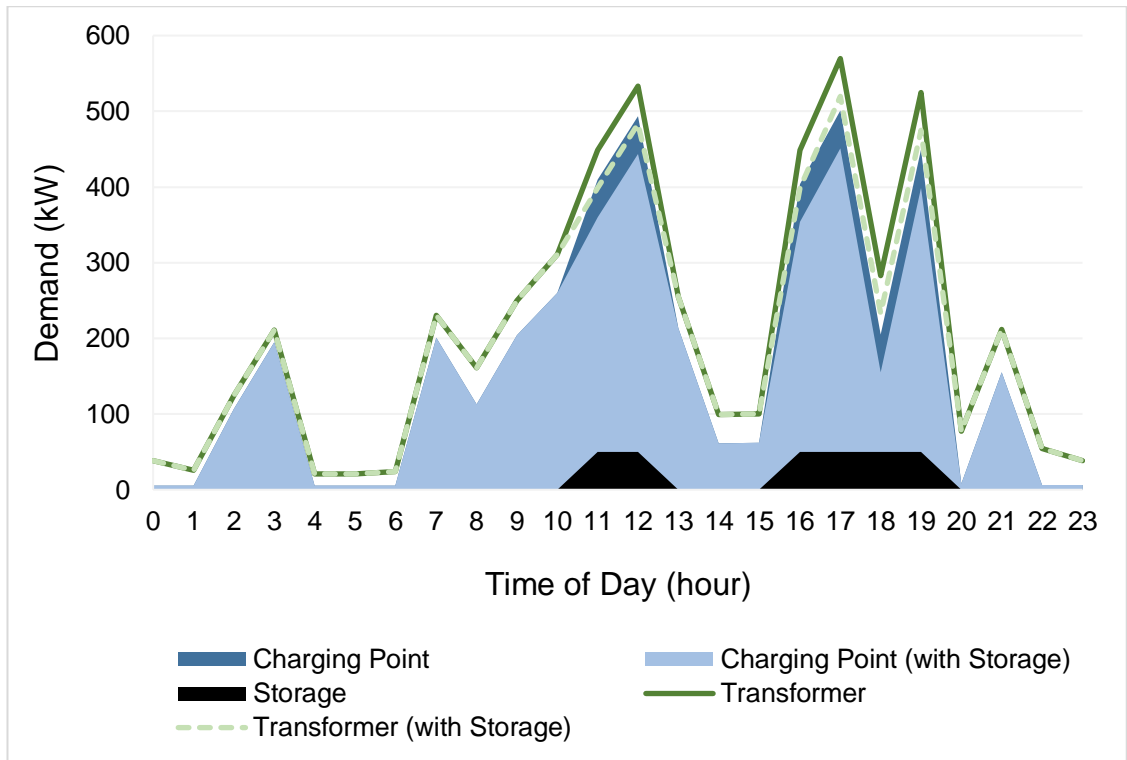
Figure 6.15: Effect of large-scale battery energy storage unit on the hourly peak demand.

The graph shows the hourly peak demand (in kW) at the charging point and at the substation transformer without and with a battery energy storage unit. The storage unit only discharges its energy during the intervals represented by the black areas at the bottom of the graph. This storage unit reduces peak demand by up to 10%, nearly 7% more than the V2G chargers were able to accomplish.
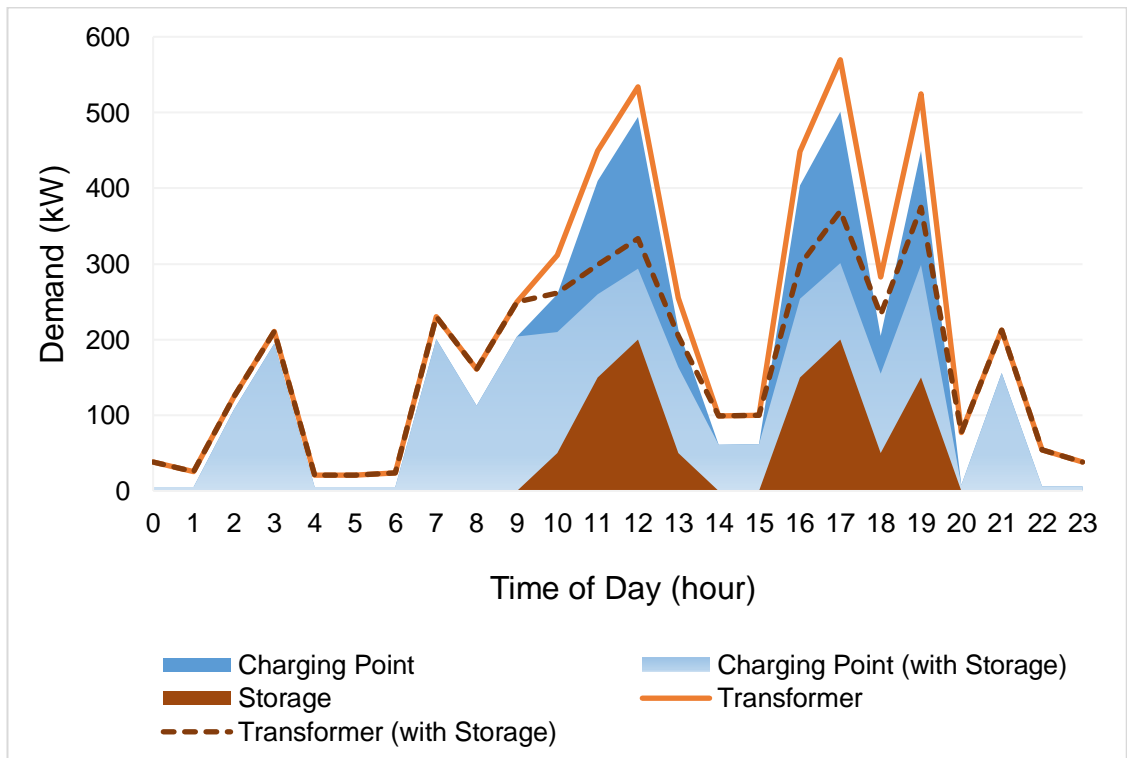
Figure 6.16: Effect of controlling the capacity of battery storage units on the hourly peak demand.

Figure 6.16 shows the effect of varying the output power of the battery energy storage unit on the peak demand. The discharge capability of the battery energy storage unit is varied from 0 to 200 kW for each interval. When the total charging demand is exceptionally high, the rated power output of the storage unit is increased to 200 kW. (e.g., at 12:00 and 17:00). In contrast, its capacity is reduced in response to a reduction in the aggregated charging demand to 150 kW (for example, at 11:00, 16:00, and 19:00) and to 50 kW (e.g., at 10:00, 13:00, and 18:00). Additionally, the storage unit is turned off when there is very little or no charging activity in the network.

6.5.4 Substation Transformer Loading Analysis

Each transformer (commonly referred to as a distribution transformer) that links a residential network to the higher-voltage grid is rated for a certain maximum demand. Once this value is exceeded, the transformer is said to be overloaded, which may result in deterioration of the insulating layers in the core, resulting in a shorter lifetime.

In this part of this chapter, the loading on the 11/0.433 kV substation transformer is analysed by measuring the full-load current on its secondary winding and then comparing to the simulated values during the maximum peak afternoon hours with the stochastic charging profiles. The full-load operation of the transformer, namely, the point at which the transformer runs at the maximum permitted secondary current, is initially determined using (6.8).

$$I_s = \frac{S_{tx}}{\sqrt{3}V_{L-L_s}}$$
(6.8)

Where:

I_s is the secondary winding full-load (threshold) current (A),

S_{tx} is the transformer rating (500 kVA),

V_{L-L_s} is the secondary winding line-to-line RMS voltage (V).

The secondary winding full-load current is determined as 667 A using the transformer's rated secondary winding voltage of 433 V. The transformer's loading is analysed between the main afternoon peak periods (16:00–18:00) because this is the time when the worst-case scenario's maximum peak demand is observed from the simultaneous charging of Audi, Jaguar, and Tesla vehicles in the studied network (see **Figure 6.11**). The loading analysis on the substation transformer between 16:00–17:00 and 17:00–18:00 is shown in Figure 6.17 and Figure 6.19, respectively.
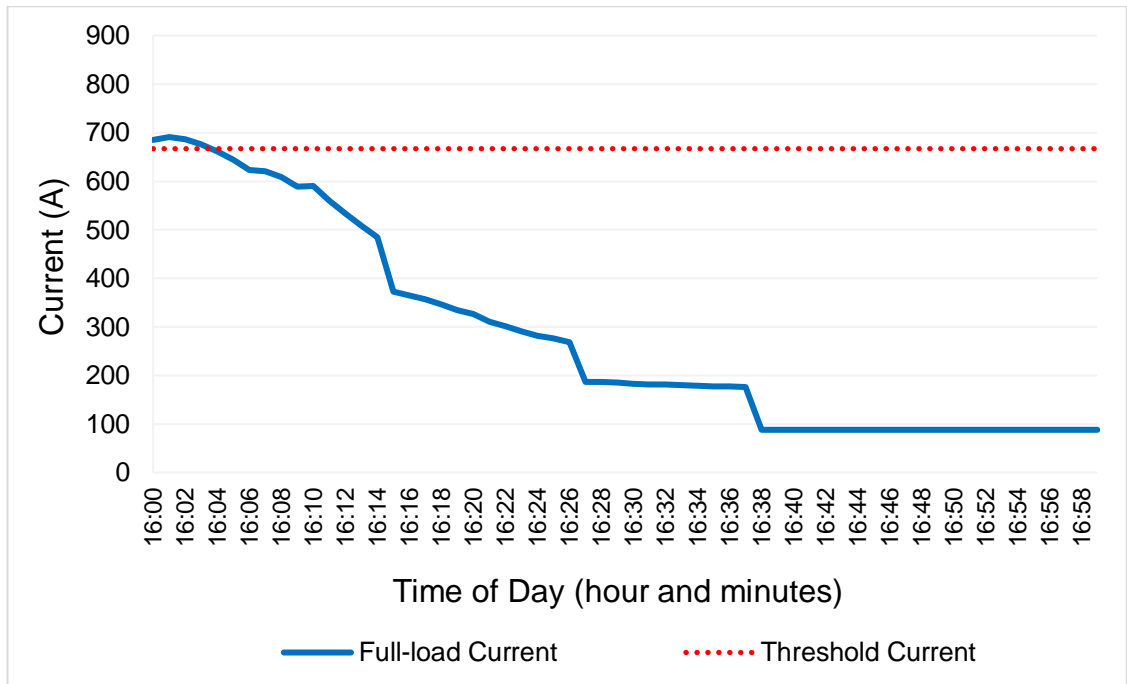
Figure 6.17: Substation transformer loading between 16:00 and 17:00.

On the vertical axis, the graph displays the measured full-load current (in A) at the secondary side of the transformer. The threshold current, which is the full-load current at which the transformer operates at full capacity, is also depicted as a dashed red line in the diagram. It is seen that the transformer's rated capacity is exceeded during the first four minutes. As the charging demand of the vehicles decreases, the substation transformer's load gradually decreases in the network. The effect of using a battery energy storage unit to reduce the transformer loading is seen in Figure 6.18.
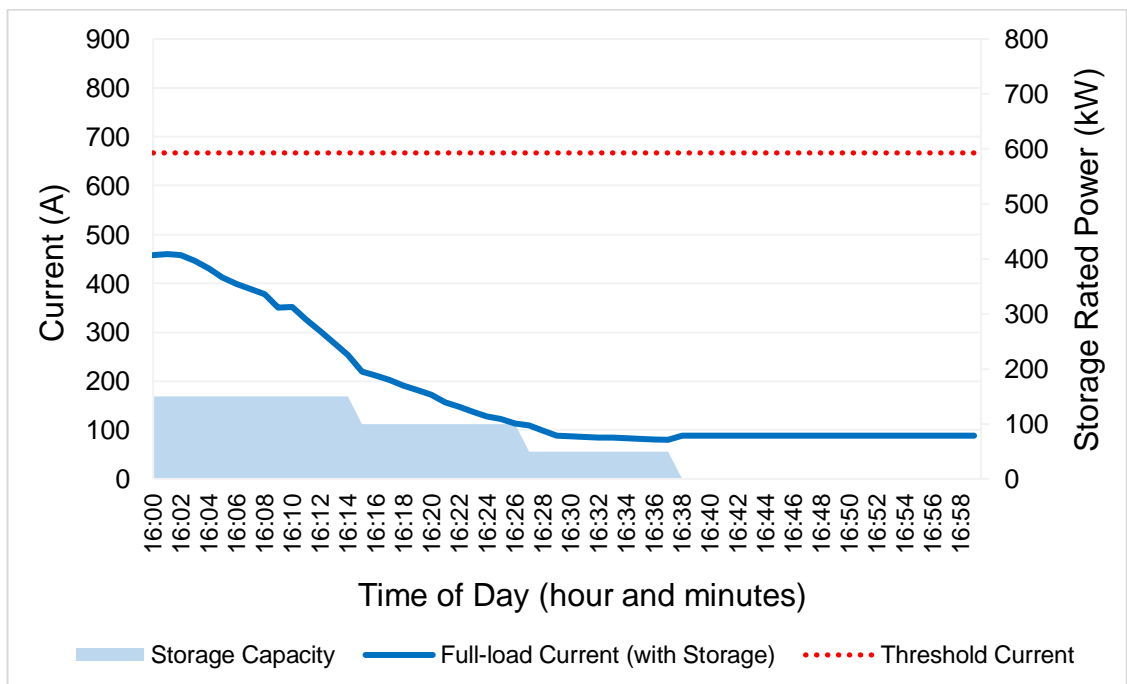
Figure 6.18: Substation transformer loading with a storage unit between 16:00 and 17:00.

The primary vertical axis in Figure 6.18 shows the measured full-load current (in A) at the secondary side of the transformer with a battery energy storage unit. The secondary vertical axis indicates the rated power of the controlled battery energy storage unit (in kW). The storage unit's rated power output is fixed between 16:00 and 16:14 at 150 kW. At 16:15, when T3 completes its charging cycle, its capacity is reduced to 100 kW, and then to 50 kW when T6 completes its charging session (see **Figure 6.12**). It should be clarified that the transformer loading increases very slightly at 16:37, when the battery energy storage unit is turned off after all vehicles have reached their target SoC levels. However, this increase is negligibly small and does not affect the operation of the transformer. Overall, the results demonstrate that utilising the battery energy storage unit to its maximum capacity reduces transformer loading by as much as 40%.
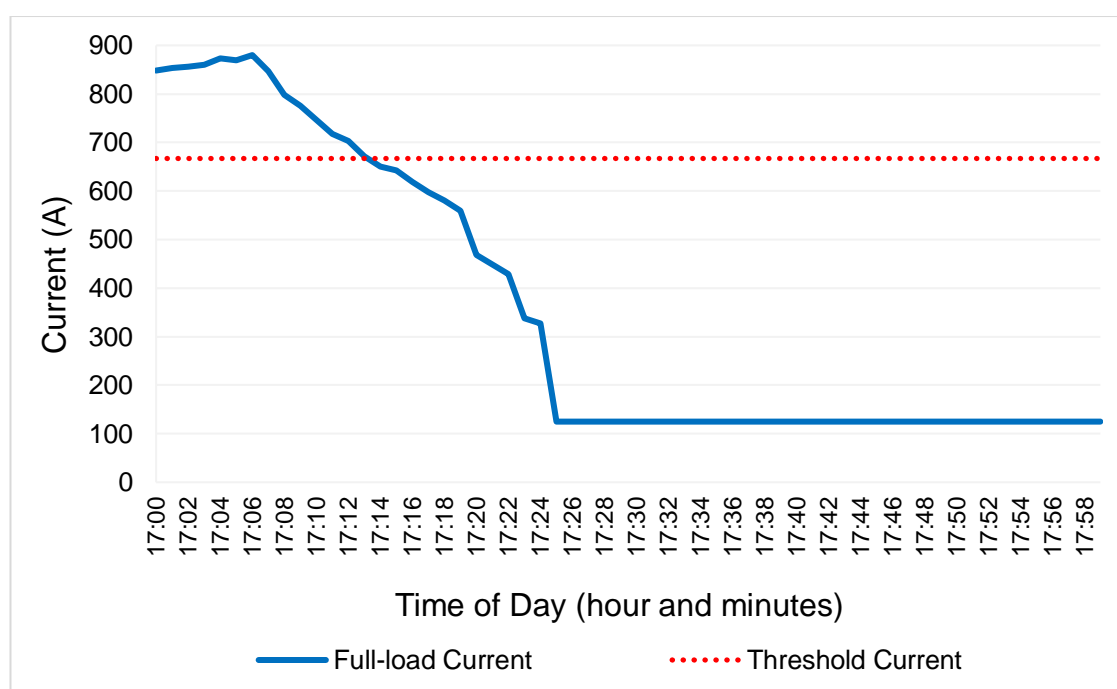
Figure 6.19: Substation transformer loading between 17:00 and 18:00.

Between 17:00 and 18:00, the substation transformer is approximately 21% more heavily loaded than between 16:00 and 17:00. This is due to the increased aggregated charging demand, which is primarily attributable to the Audi vehicle. Until 17:13, the transformer remains overloaded and operates beyond its maximum rated capacity. Results indicate that the substation transformer cannot simultaneously charge two Tesla vehicles and one Audi vehicle without being subjected to critical conditions.

For the last analysis, the effect of using a battery energy storage unit between 17:00 and 18:00 is shown on the substation transformer loading in Figure 6.20.
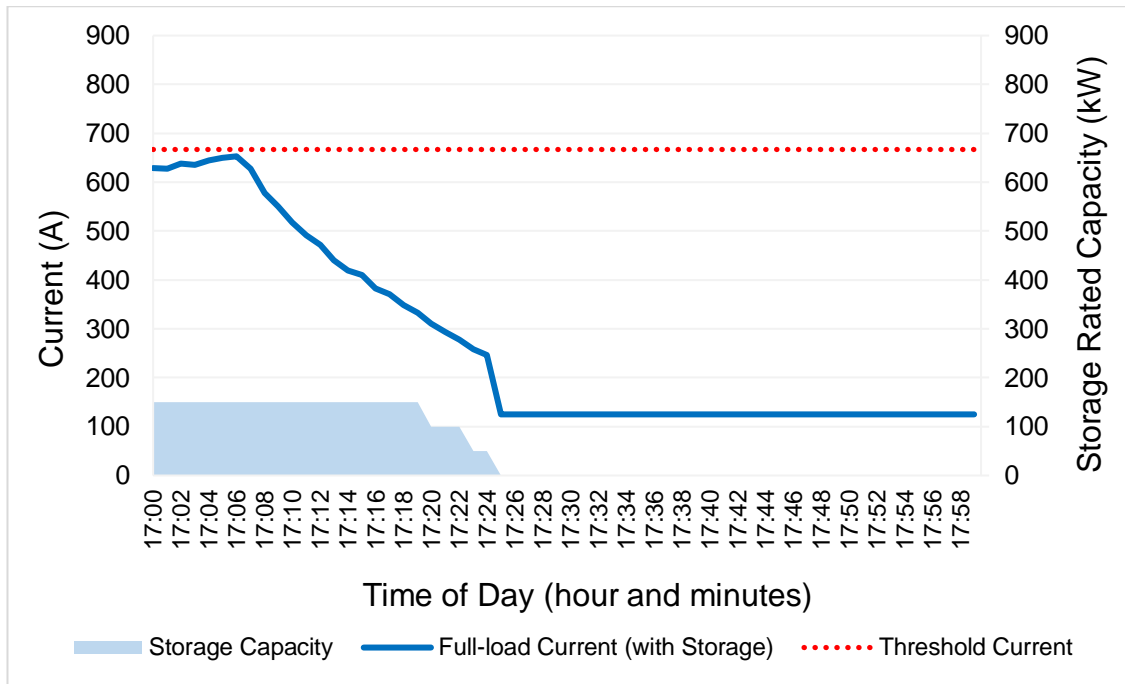
Figure 6.20: Substation transformer loading with a storage unit between 17:00 and 18:00.

The storage unit's rated power output is fixed between 17:00 and 17:19 at 150 kW. At 17:20, when T4 completes its charging cycle, its capacity is reduced to 100 kW, and then to 50 kW when T9 completes its charging session at 17:23 (see **Figure 6.13**). In the first eight minutes, as shown in Figure 6.20, the storage unit prevents the transformer from exceeding its rated capacity by a narrow margin.

6.5.5 Hosting Capacity of the Substation Transformer

Using the stochastic charging profiles from the worst-case scenario, the final section of this chapter determines the hosting capacity of the substation transformer serving the low-voltage distribution network and analyses how often the substation transformer's maximum rated capacity is exceeded due to EV demand. Moreover, the minimum required power that must be injected by the battery energy storage unit and the minimum transformer size required to handle EV charging activities without exceeding its maximum rated capacity are determined. This analysis is very significant because it focuses on the successful design of a low-voltage distribution network to account for the worst-case scenario.

The timely distribution of EVs (see **Table 6.7**), the stochastic charging requirements of EVs (see **Table 6.9**), and the total peak demand from EV charging (see **Figure 6.11**) are used to obtain the peak full-load current of the substation transformer for each hour based on the worst-case scenario. Simulation results are demonstrated in Figure 6.21.
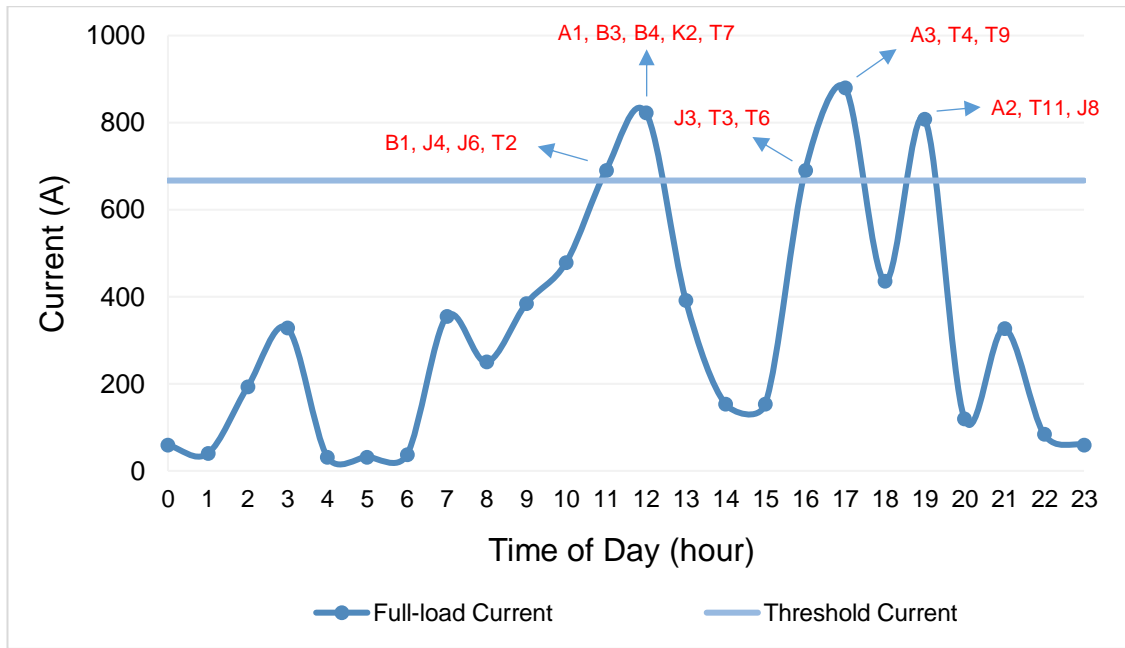
Figure 6.21: Loading profile of the substation transformer in the worst-case scenario.

The graph depicts the measured full-load current (in A) and the threshold current (in A), i.e., the point at which the transformer runs at the maximum rated capacity, under the worst-case scenario. The horizontal axis shows the time in the top-of-the-hour format.

The 500-kVA substation transformer is observed to exceed its maximum rated capacity at 11:00, 12:00, 16:00, 17:00, and 19:00 during simultaneous charging of different group of vehicles. Additionally, the graph depicts the EVs that are connected to the network at these intervals. During these times, the transformer is loaded to a maximum of 3.5%, 20.9%, 3.5%, 27.5%, and 19.1%, respectively. In addition to the number of EVs simultaneously connected to the network, their model and charging characteristics also affect the load intensity. For example, four EVs are connected between 11:00 and 12:00 (e.g., B1, J4, J6, and T2), but since the aggregated charging demand of A3, T4, and T9 (between 17:00 and 18:00) and A2, T11, and J8 (between 19:00 and 20:00), is greater, the substation transformer is more loaded. Furthermore, the SoC of the vehicles prior to charging and the baseload of the substation transformer at different time intervals also impact the severity of loading.

This section proposes the installation of battery energy storage units to power the additional demand between the substation transformer's peak load capacity and the point at which the transformer's maximum rated capacity is exceeded. Alternatively, since the substation transformer is not sized to accommodate the charging demand of EVs on rapid and ultra-rapid devices, its optimal size (in kVA) can be determined based on the peak current and peak demand in order to design a network for the worst-case scenario. **Section 6.5.5.1** and **Section 6.5.5.2** address the minimum required power from the storage and minimum required sizing of substation transformer, respectively.

6.5.5.1 Determination of Minimum Power Required by the Storage Unit

Since the purpose of this section is to design a network based on the stochastic charging profiles of the worst-case scenario, the maximum peak period between 17:00 and 18:00 is analysed. The minute-by-minute total charging demand from **Figure 6.13** and the magnitude of full-load current from **Figure 6.19** are used to determine the maximum power that substation transformer can deliver without operating beyond its maximum rated capacity.

As depicted in **Figure 6.19**, the substation transformer is overloaded between 17:00 and 17:12 because the full-load current exceeds the threshold current of 667 A. At 17:12, the substation transformer provides 452.4 kW of total demand, and the full-load current on its secondary winding is 697 A. As vehicles complete their charging sessions, the demand for charging and the transformer's load decrease. The transformer is no longer overloaded from 17:13 until the beginning of the next hour. At 17:13, the transformer at the substation supplies 432.2 kW and has a full-load current of 666 A. This indicates that the substation transformer can accommodate a peak demand of approximately 432 kW during the worst-case scenario's peak demand period without being overloaded. The peak demand that the substation transformer can accommodate without being subjected to overloaded conditions will vary for each interval based on the charging requirements and types of EVs. Table 6.11 depicts the additional power that must be injected from the battery energy storage unit between 17:00 and 17:12 to prevent substation from being operated above its maximum rated capacity.

Table 6.11: Minimum power required by the storage unit between 17:00 and 17:12

Time (hour)	Transformer Demand (kW)	Threshold Peak Demand (kW)	Additional Power Needed by the Storage Unit (kW)
17:00	554.2	433	121.2
17:01	557.3	433	124.3
17:02	559.7	433	126.7
17:03	562	433	129
17:04	564.7	433	131.7
17:05	567.5	433	134.5
17:06	569.7	433	136.7
17:07	553.6	433	120.6
17:08	520.9	433	87.9
17:09	503.1	433	70.1
17:10	481.7	433	48.7
17:11	465.8	433	32.8
17:12	452.4	433	19.4

The results indicate that as time passes, the additional power that must be injected from the battery energy storage unit decreases, as EVs approach the end of their charging sessions and the network demand decreases accordingly. After 17:12, the minimum power that must be injected by the storage unit is not determined and hence shown in the table because the substation transformer already operates below its rated maximum capacity. After 12 minutes, the total power that must be injected by the storage unit totals 1283.6 kW. This results in a minimum energy capacity requirement for the battery energy storage unit of 256.7 kWh ($1283.6\ kW \times 12\ minutes/60\ minutes$).

6.5.5.2 Determination of Minimum Required Transformer Size

Calculating the kVA is essential when selecting and sizing transformers. This represents the maximum apparent power a transformer can handle. This value is determined based on the maximum full-load current exhibited during the worst-case scenario. In the previous section, it is shown that the substation transformer experiences the largest loading condition at 17:06 (see **Table 6.11**). Using (**6.8**), the minimum required sizing of the substation transformer is determined as 660 kVA based on the maximum full-load current of 880 A. The timely distribution of EVs (see **Table 6.7**), the stochastic charging requirements of EVs (see **Table 6.9**), and the total peak demand from EV charging (see **Figure 6.11**) are used to obtain the peak full-load current of the substation transformer for each hour based on the worst-case scenario. Simulation results are demonstrated in Figure 6.22.
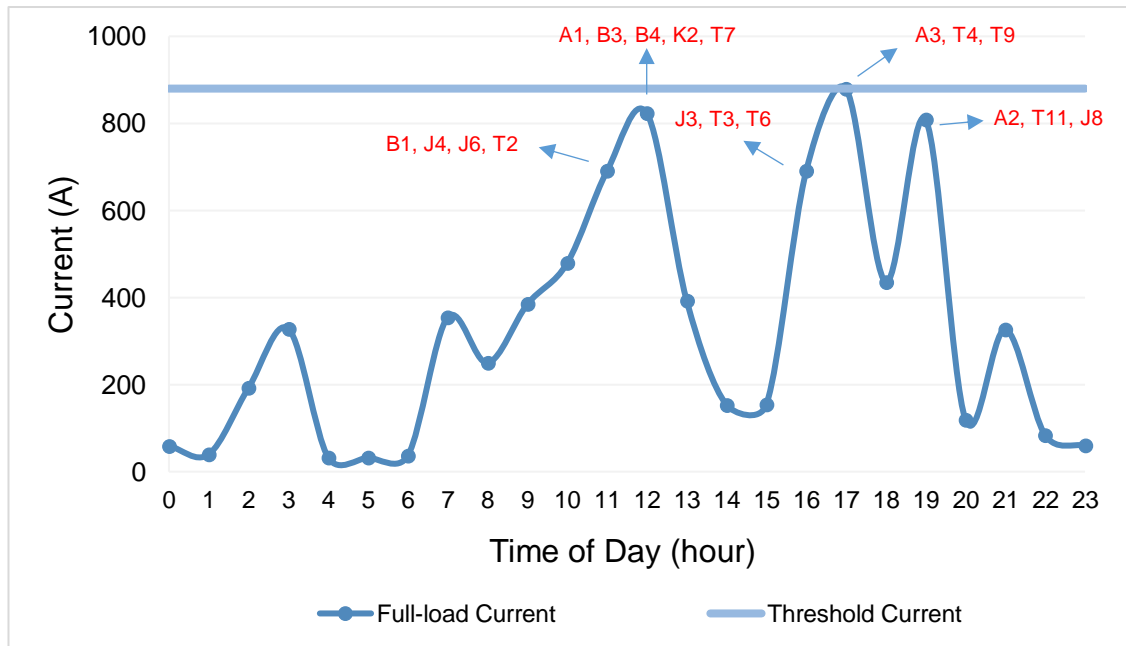
Figure 6.22: Loading profile of the 660-kVA substation transformer in the worst-case scenario.

The substation transformer's loading profile has not changed, as all network charging profiles remain unchanged. In spite of this, the results indicate that increasing the substation transformer's size from 500 kVA to 660 kVA enables the safe integration of all EVs in the worst-case scenario, even without the installation of a battery energy storage unit. Increasing the size of the substation transformer increases the system's capacity, enabling simultaneous charging of high-power EVs at 11:00, 12:00, 16:00, 17:00, and 19:00.

6.6 Summary

Considering various EV models and real-world data, a stochastic model is developed in this chapter. Simulation cases of the timely distribution of charging events to a multi-charger station using real data obtained from Zap Map is produced. The algorithm is then used to generate stochastic and non-linear SoC-dependent charging profiles for various EV models. Utilising non-linear charging profiles enables the accurate calculation of EVs' charging duration and energy consumption from many stochastic scenarios. Based on the maximum charging demand and energy consumption of randomly generated vehicle patterns, twenty scenarios are considered, and the worst-case scenario is identified. The impact of installing small-scale V2G chargers and large-scale battery energy storage units is examined on peak load reduction.

The hosting capacity of the substation transformer serving the low-voltage distribution network is initially determined to design a network for the worst-case scenario. It is also determined how often the maximum rated capacity of the substation transformer is exceeded due to EV demand. In addition, the minimum required power that must be injected by the battery energy storage unit and the minimum transformer size required to accommodate EV charging activities without exceeding the transformer's maximum rated capacity are calculated.

The results indicated that the network is most in demand during the late afternoon peak periods, particularly between 16:00 and 20:00, due to residential activities and high likelihood of public charging events. Between 16:00 and 17:00, the simultaneous charging of one Jaguar and two Tesla vehicles increased the peak demand at the charging station from 12 kW to 404 kW, and the peak demand at the substation transformer from 56.7 kW to 447.7 kW. In addition, between 17:00 and 18:00, the simultaneous charging of one Audi and two Tesla vehicles increased the peak demand to 501 kW at the charging station and 570 kW at the substation transformer.

This chapter continued by proposing the connection of small-scale V2G chargers and the integration of battery energy storage units to support the charging demand of vehicles. The latter is demonstrated to be more effective than the former due to its higher power density capability. A battery energy storage unit rated at 150 kW lowered the peak demand of the feeder by up to 30% and the peak load of the substation transformer by up to 40%. Not only are battery energy storage devices capable of lowering peak demand, but they also provide additional benefits, such as relieving strain on distribution network equipment. It is essential, however, to size and position these units appropriately.

During the worst-case scenario's peak demand period, simulation results demonstrated that the substation transformer can accommodate a peak demand of approximately 432 kW without becoming overloaded. Depending on the charging requirements and types of EVs, the maximum demand that a substation transformer can accommodate without being subject to overload conditions will vary for each interval. In addition, the optimal battery energy storage unit size for preventing substation transformer overload between 17:00 and 17:12 is calculated to be 256.7 kWh. In conclusion, it has been demonstrated that increasing the kVA rating of the substation transformer from 500 kVA to 660 kVA enables the safe integration of all EVs in the worst-case scenario.

The case studies and conclusions reported in this chapter instil confidence in the ability of multi-charger hubs to be enhanced and expanded globally to accommodate the rapid adoption of EVs. Although this comes at the expense of high costs for DNOs, the results indicate that the recommended course of action to safely integrate rapid and ultra-rapid devices in medium-voltage distribution networks is to expand the hosting capacity of local distribution grids by installing larger transformers and implementing large-scale battery energy storage units during periods with a high probability of charging occurrences. All the simulated instances in this research are based on a real case, notably the deployment of a battery energy storage unit, which was inspired by the UK's first hub-based electric forecourt in [78], [79], and [91].

CHAPTER 7

7. State of Charge Estimation of Lithium-Ion Batteries Under Discharge Tests

7.1 Introduction

The value of battery energy storage units has been described extensively in the literature review of this thesis. In addition, **Chapter 6** has demonstrated that properly sized battery energy storage units can effectively reduce peak loads and prevent substation transformers from exceeding their rated capacities. Nevertheless, it is essential to analyse the operating characteristics of these storage units under various discharge profiles. This is because battery energy storage units simply release their stored energy to alleviate the network's peak demand, thereby reducing the strain on the grid. In some instances, the remaining usable energy in the storage unit can be used to support other network loads.

The stochastic distribution of EV models influences the magnitude of peak demand at various times of the day, as demonstrated in **Chapter 6**. This chapter is relevant because it develops various discharge profiles for the storage units based on the stochastically developed EV charging profiles and the time and size of the network's peak demand. Then, these discharge profiles are incorporated into a physical battery charger and analyser unit employing lithium-ion batteries to determine the relationship between the cell voltage and discharged capacity under various scenarios brought about by the stochastic allocation of charging events. The relationship between cell voltage and discharged capacity is used to estimate the battery SoC and DoD. Estimating these parameters allows for the determination of the available and usable battery capacity if these storage units were used to meet the charging demand of various EV models.

7.1.1 Chapter Structure

Section 7.2 details lithium-ion battery specifications and test limitations.

Section 7.3 develops different discharging profiles for these batteries in Microsoft Excel. These profiles are then implemented into the MC3000's battery charger and analyser unit to obtain the relationship between the cell voltage and discharged capacity of the batteries. This relationship is then used to estimate the SoC, DoD, and useable capacity of lithium-ion batteries under different discharge scenarios.

Section 7.4 presents the key findings and conclusions of the chapter.

7.2 Characteristics of Battery Packs

LG INR18650 HG2 rechargeable lithium-ion battery packs are used for the experimental tests. The physical design of these rechargeable LG batteries under investigation is shown in Figure 7.1.
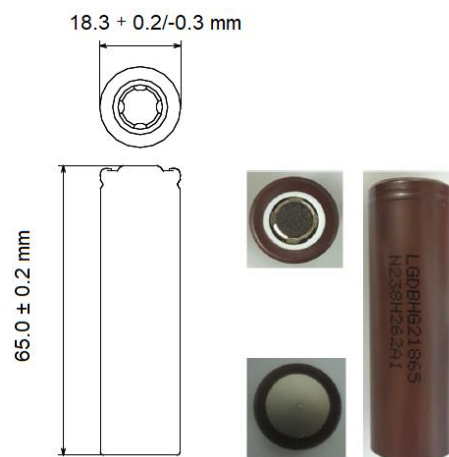
Figure 7.1: LG 18650 HG2 battery model [292].

From 18650 to 2170, cylindrical lithium-ion batteries appear to be gaining increasing acceptance. Nissan and Chevrolet Volt, the two largest electric car manufacturers in the world, use a different type of battery than Tesla, which uses 18650 cylindrical batteries [293]. The LG 18650 HG2 model used in this thesis has several positive characteristics and is one of 2015's finest cells. The LG HG2 has a maximum discharge rating of 20 A, which is excellent and sufficient for most of the high-current applications. This, along with the cell's capacity (3000 mAh), makes it a feasible energy storage device for various applications. The main specifications of these LG battery packs are detailed in Table 7.1.

Table 7.1: Specifications of the LG 18650 battery cells

Manufacturer	LG Chemical
Model	INR18650HG2
Rechargeable	Yes
Nominal Energy Capacity	3000 mAh or 3 Ah
Nominal Voltage	3.6 V
Discharge End Voltage	2.5 V
Charging Voltage	4.20 +/− 0.05 V
Standard Charging Current	1.5 A
Max. Continuous Discharge Current	20 A
Maximum Weight	48 g

These LG batteries typically have a nominal capacity of up to 3000 mAh. Each cell has a nominal voltage of around 3.6 V and a maximum charging voltage of up to 4.20 V with a plus and minus 0.05 V. The discharge end voltage for these batteries is 2.5 V. The minimum discharge voltage varies between various datasheets, but 2.7 – 3 V is an empirical value. If discharged below this voltage, the battery could be irreparably harmed.

The most common Tesla battery pack consists of 7,104 cells organised into 16 modules containing 444 cells each (recent improvements brought the number of cells to 8,256). These Tesla batteries have an inherent energy storage capacity of up to 85 kWh (recently improved up to 100 kWh). In 2015, Panasonic updated the anode design, which resulted in a 6% increase in cell capacity. This is a significant increase for a company that produces batteries for an EV manufacturer whose revenue optimisation depends on technological innovation [275].

It should be clarified that the characteristics of a typical EV battery have been scaled down to match those of a single LG cell since it is impractical to employ many cells in the lab setting for this experiment. In addition, the physical battery charger unit can only charge and discharge up to four cells simultaneously. However, the discharge current is limited by the unit and decreases if more cells are being charged and/or discharged simultaneously. Single slot is thus utilised to take advantage of the maximum discharging current capability of the charger and to simplify battery monitoring. The results from the single slot are then scaled up to make a comparison to a typical EV battery.

7.3 Development of Discharge Profiles

Chapter 6 demonstrated via simulation that battery energy storage can compensate for the charging demand of EVs while smoothing out the peak demand, and that their capacity can also be regulated to meet the fluctuating demand for EVs. Batteries perform these functions by discharging their stored energy. Using the specifications of the LG battery, various discharge profiles are established, and the relationship between battery voltage and discharged capacity is determined. It should be clarified that manufacturer discharge curves are not used for these tests because discharge profiles are developed based on stochastic charging profiles from **Chapter 6**'s worst-case scenario. Since each EV model has a unique charging curve, distinct discharge profiles are developed based on the type and charging profile of the randomly selected EV model.

For example, J3, T3, and T6 all charge simultaneously during the worst-case scenario between 16:00 and 17:00 (see **Table 6.7**). Using the minute-by-minute charging profiles of these vehicles, a discharge profile is developed to reduce the network's peak demand and the amount of energy supplied to the vehicles from the grid.

Secondly, different discharge profiles are also developed when A3, T4, and T9 charge simultaneously between 17:00 and 18:00 (see **Table 6.7**). Two distinct afternoon peak periods are chosen to broaden the scope of this work with the simultaneous charging of different EV models.

7.3.1 Estimation of Battery SoC and Battery DoD

Since estimating the SoC of a battery is a difficult process that depends on the battery type and the application for which the battery is intended, much development and research have been conducted in recent years to increase the accuracy of estimations. Accurate SoC estimation is one of the most important aspects of battery management systems, which will assist in enhancing the system's functionality and dependability, as well as extending the lifespan of the batteries and preventing them from being overcharged and deep discharged [294, 295].

The most used methodology for estimating the SoC is the coulomb counting method [294, 295]. This method is also known as ampere hour counting and current integration. This approach calculates SoC values by mathematically integrating battery current (I_{bat}) data across the use time, given by (7.1):

$$SoC = SoC_{(0)} + \frac{1}{S_r} \int I_{bat}\, dt \qquad (7.1)$$

Where:

$SoC_{(0)}$ is the initial SoC of the LG battery cell (%),

S_r is the rated energy capacity of the LG cell (Ah).

The coulomb counting technique measures the battery's remaining capacity by simply adding or subtracting the amount of charge moved into or out of the battery. With a known battery capacity, the SoC is determined by measuring the discharging current of a battery and integrating the discharging current over time. Losses always occur during the charging and discharging cycle because the available charge is always less than the stored charge [294].

For more precise SoC estimation, the declination of the releasable battery capacity (C_r) should be considered [294]. The SoC is defined as the proportion of the releasable battery capacity to the battery's rated energy capacity, given by (7.2):

$$SoC = (SoC_{(0)} - \frac{C_r}{S_r}) \times 100\% \qquad (7.2)$$

Additionally, the DoD, which refers to how much energy is cycled into and out of the battery (discharge depth), can also be expressed as a percentage of the total capacity of the battery that has been discharged relative to its rated capacity [294, 296]:

$$DoD = \frac{C_{di}}{S_r} \times 100\% \tag{7.3}$$

Where:

C_{di} is the capacity discharged by any amount of current (mAh).

To estimate the DoD and SoC of the LG battery, the relationship between the battery voltage and discharged capacity is determined using various discharge profiles. The development of discharge profiles is elaborated upon in the following section.

7.3.2 Discharge Tests Between 16:00 and 17:00

In the first scenario, a discharge profile is developed between 16:00 and 17:00 during the simultaneous charging of J3, T3, and T6. For the development of discharge profiles, the relationship between the charging demand and the SoC of the vehicle is essential. Figure 7.2 shows the individual charging profiles of these vehicles during this period.
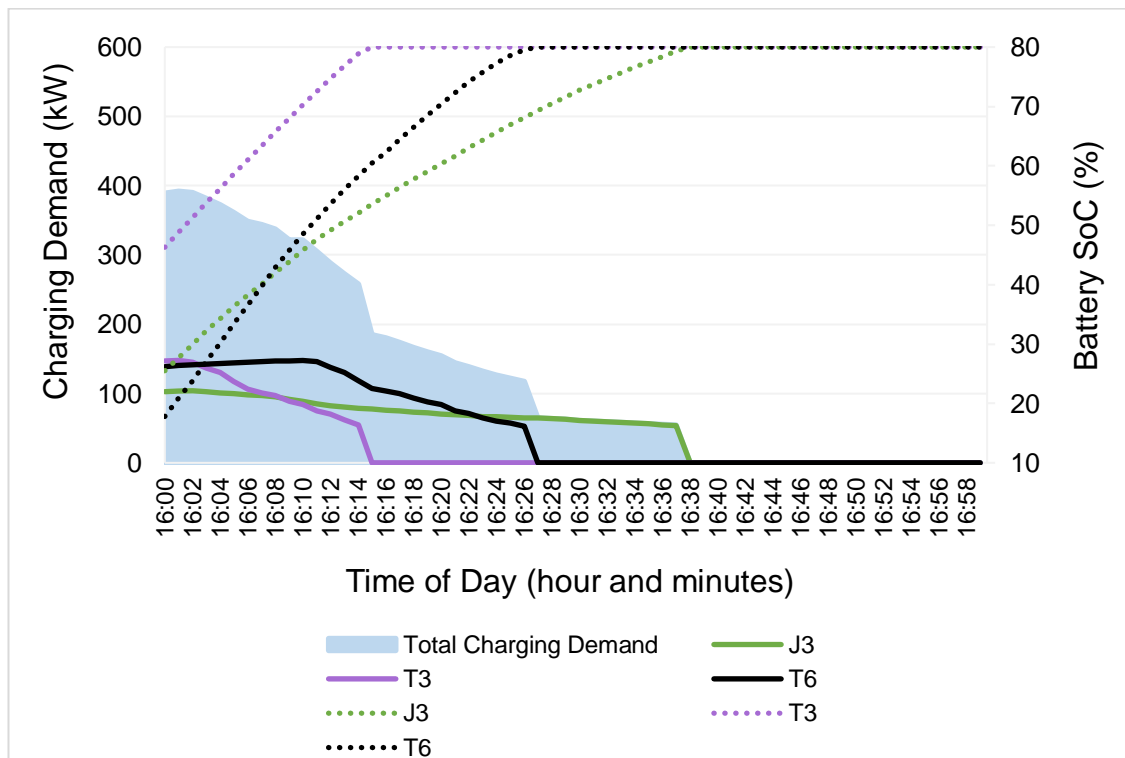
Figure 7.2: Individual charging profiles of J3, T3, and T6 between 16:00 and 17:00.

The graph's primary vertical axis shows the total and individual charging demand of J3, T3, and T6 (in kW). The secondary vertical axis depicts the battery SoC (in %) of these vehicles (represented by the dashed lines).

A pre-charged LG battery cell is used, and a battery discharge profile is developed based on the individual charging demand of one of the three vehicles. The developed discharge profile is shown in Table 7.2.

Table 7.2: Battery discharge profile between 16:00 and 17:00

Time	C_d (kW)	$J3_d$ (kW)	B_r (kW)	S_p (kW)	S_d (%)	S_s (A)	S_i (A)
16:00	389.3	103.1	150	102	0.68	2.04	0.68
16:01	392	103.5	150	102	0.68	2.04	0.68
16:02	390	104	150	102	0.68	2.04	0.68
16:03	381.6	102.4	150	102	0.68	2.04	0.68
16:04	372.7	101	150	102	0.68	2.04	0.68
16:05	361	99.6	150	102	0.68	2.04	0.68
16:06	348.8	98	150	93	0.62	1.86	0.62
16:07	344	97	150	93	0.62	1.86	0.62
16:08	337.6	95	150	93	0.62	1.86	0.62
16:09	322.1	92	150	93	0.62	1.86	0.62
16:10	321.7	89	150	93	0.62	1.86	0.62
16:11	305.2	85	150	93	0.62	1.86	0.62
16:12	288.5	82	150	78	0.52	1.56	0.52
16:13	272.7	80.8	150	78	0.52	1.56	0.52
16:14	258.3	79	150	78	0.52	1.56	0.52
16:15	184.5	77.5	150	78	0.52	1.56	0.52
16:16	180	76	150	78	0.52	1.56	0.52
16:17	174	74.5	150	78	0.52	1.56	0.52
16:18	166.5	73	150	69	0.46	1.38	0.46
16:19	160	72	150	69	0.46	1.38	0.46
16:20	154.6	70.5	150	69	0.46	1.38	0.46
16:21	144.3	69	150	69	0.46	1.38	0.46
16:22	138.6	68	150	69	0.46	1.38	0.46
16:23	131.8	67	150	69	0.46	1.38	0.46
16:24	126.3	66	150	64.5	0.43	1.29	0.43
16:25	122	65.5	150	64.5	0.43	1.29	0.43
16:26	117	65	150	64.5	0.43	1.29	0.43
16:27	64.3	64.3	150	64.5	0.43	1.29	0.43
16:28	63.5	63.5	150	64.5	0.43	1.29	0.43
16:29	62.5	62.5	150	64.5	0.43	1.29	0.43
16:30	61.3	61.3	150	60	0.40	1.2	0.40
16:31	60.3	60.3	150	60	0.40	1.2	0.40
16:32	59.3	59.3	150	60	0.40	1.2	0.40
16:33	58.3	58.3	150	60	0.40	1.2	0.40
16:34	57.5	57.5	150	60	0.40	1.2	0.40
16:35	56.5	56.5	150	60	0.40	1.2	0.40
16:36	55.5	55.5	150	55	0.37	1.11	0.37
16:37	54.5	54.5	150	55	0.37	1.11	0.37
16:38	0	0	0	0	0	0	0

Where:

C_d is the total charging demand at each minute (kW),

$J3_d$ is the charging demand of J3 at each minute (kW),

B_r is the rated power output of the battery energy storage unit (kW),

S_p is the power injected by the battery energy storage unit (kW),

S_d is the discharge rate of the battery energy storage unit (%),

S_s is the scaled down discharge current of the LG battery for tests (A),

S_i is the scaled down discharge current for the MC3000 device (A).

The discharge rate of the battery energy storage unit (S_d), the scaled down discharge current of the LG battery (S_s), and the scaled down discharge current for the MC3000 device (S_i) are determined as follows, respectively:

$$S_d\ (\%) = \frac{S_p}{B_r} \tag{7.4}$$

$$S_s\ (A) = S_d \times S_r \tag{7.5}$$

$$S_i\ (A) = \frac{S_s}{S_r} \tag{7.6}$$

It should be clarified that (7.4) is used to determine the discharge rate of the battery energy storage unit based on the individual charging demand of the vehicle. In addition, (7.6) is used to convert the discharge current of the LG battery to fit the maximum discharge capability of the physical battery charger and analyser unit.

As shown in **Figure 7.2**, T3 and T6 arrive at their respective SoCs before 16:15 and 16:27, while J3 remains connected to the charger until 16:37. This scenario assumes the storage unit is connected to offset J3's charging requirements. In this discharge profile, the discharge rate of the LG cell decreases gradually as the SoC of J3 rises (since J3 draws less power from the grid at higher SoCs). Table 7.2 demonstrates that the discharge rate is regulated and calculated every six minutes based on the average charging demand of J3. Each change in the discharge rate is represented in the table by a font colour. Note that since J3 finishes charging at 16:37, the storage unit has been turned off, and therefore all the values in the table are 0 at 16:38.

The effect of this discharge profile is analysed to determine the relationship between the LG cell's voltage and its discharged capacity. Figure 7.3 illustrates this correlation.
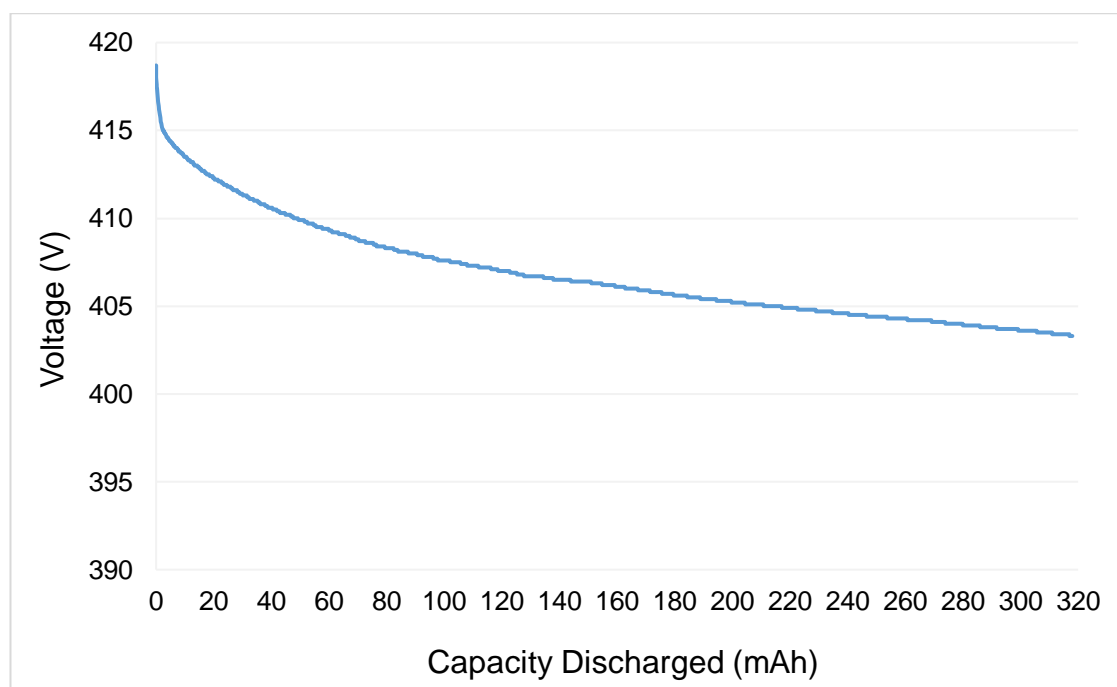
Figure 7.3: Relationship between battery voltage and capacity discharged.

The graph's vertical axis illustrates the upscaled voltage of the LG cell (in V), whereas the horizontal axis depicts time the total discharged capacity of the LG cell with respect to time.

The 18650 lithium-ion batteries that have been used in this research are charged up to 4.20 V and then discharged based on the current calculations. Figure 7.3 shows that the decrease in battery voltage is proportional to the decrease in discharge current from Table 7.3. At higher discharge current settings, battery voltage reduces at a faster rate. At the conclusion of the discharge test, after 38 minutes, the battery's voltage falls 4% below the fully charged voltage and reaches 403.3 V.

In addition, the capacity of the LG battery has been determined to be 320 mAh at the conclusion of the test. Given that the LG cell is rated at 3000 mAh, the LG battery has approximately 2680 mAh of energy remaining after 38 minutes of charging J3. Additionally, because LG batteries are charged to 4.20 V prior to the discharge tests, their initial SoC is assumed to be 100%. As a result of this discharge test, using (7.2) and (7.3), the LG cell has a DoD of 10.7% and a remaining SoC of 89.3%.

7.3.3 Discharge Tests Between 17:00 and 18:00

In the second scenario, three distinct discharge profiles are developed between 17:00 and 18:00 during the simultaneous charging of A3, T4, and T9. The relationship between the charging demand and the SoC of the vehicle is initially presented in Figure 7.4.
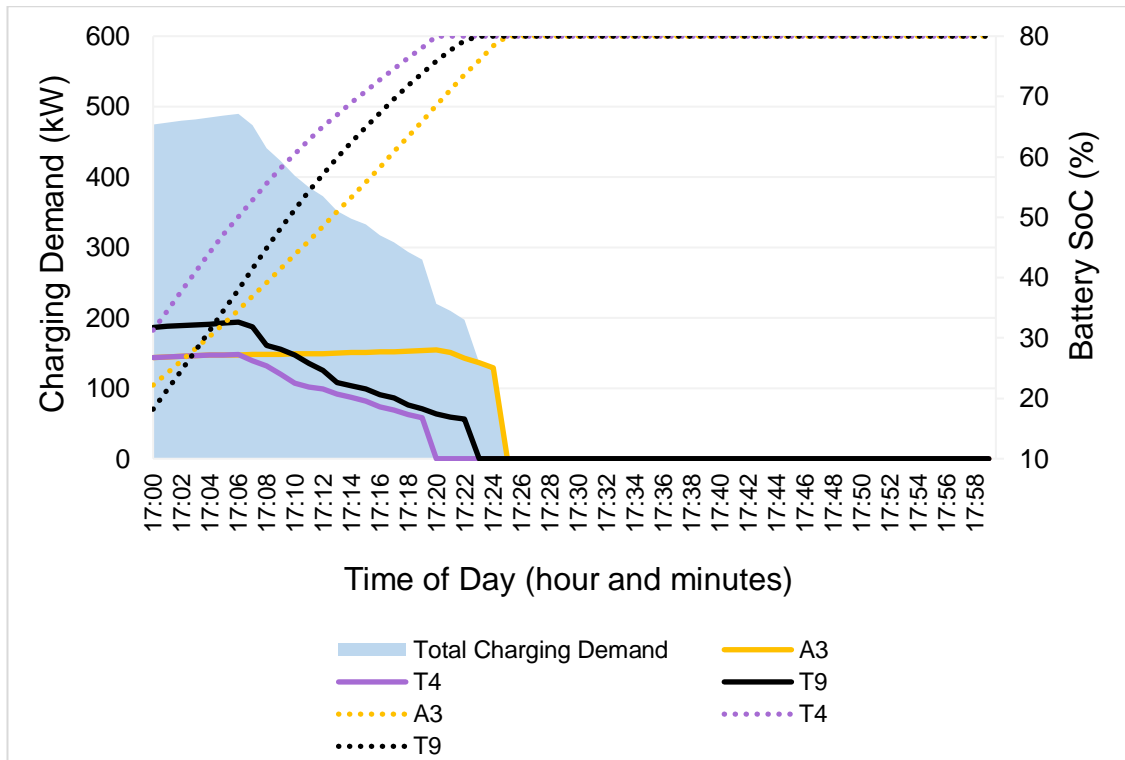
Figure 7.4: Individual charging profiles of A3, T4, and T9 17:00 and 18:00.

The primary vertical axis of the graph depicts the total and individual charging demand (in kW) for A3, T4, and T9 between 17:00 and 18:00. The secondary vertical axis illustrates the battery SoC (in %) for these vehicles (represented by the dashed lines).

T4 and T9 arrive at their respective SoCs at around 17:19 and 17:22, respectively. In addition, A3 remains connected to the network for charging until 17:24. In this case study, the battery energy storage unit's rated power output is increased to 500 kW. This value is determined by the maximum total charging demand of three vehicles at around 17:06, but it is only used as a starting point to determine the storage unit's discharge rate. This period is used to conduct three case studies by developing three distinct discharge profiles.

In the first case study (C1), the storage unit is connected to account for the A3's charging demand. The second case study (C2) uses the storage unit to facilitate the simultaneous charging of both Tesla vehicles. In the last case study (C3), the storage unit is designed to accommodate the demand for charging all three vehicles between 17:00 and 18:00. This analysis broadens the scope of this study and permits a general comparison of the performance and efficacy of lithium-ion batteries under varying vehicle charging requirements.

The developed discharge profiles for C1, C2, and C3 are presented in Table 7.3, Table 7.4, and Table 7.5, respectively.

Table 7.3: Battery discharge profile between 17:00 and 18:00 (C1)

Time	C_d (kW)	$A3_d$ (kW)	B_r (kW)	S_p (kW)	S_d (%)	S_s (A)	S_i (A)
17:00	474.2	144	500	145.5	0.29	0.87	0.29
17:01	477.3	144.6	500	145.5	0.29	0.87	0.29
17:02	479.7	145.5	500	145.5	0.29	0.87	0.29
17:03	482	146.3	500	145.5	0.29	0.87	0.29
17:04	484.7	147	500	145.5	0.29	0.87	0.29
17:05	487.5	147.4	500	148	0.3	0.9	0.3
17:06	489.7	147.7	500	148	0.3	0.9	0.3
17:07	473.6	148	500	148	0.3	0.9	0.3
17:08	440.9	148.4	500	148	0.3	0.9	0.3
17:09	423.1	148.6	500	148	0.3	0.9	0.3
17:10	401.7	148.7	500	149.5	0.3	0.9	0.3
17:11	385.8	148.8	500	149.5	0.3	0.9	0.3
17:12	372.4	148.9	500	149.5	0.3	0.9	0.3
17:13	352.2	150.2	500	149.5	0.3	0.9	0.3
17:14	341.2	150.7	500	149.5	0.3	0.9	0.3
17:15	332.9	151.2	500	152	0.3	0.9	0.3
17:16	317.4	151.6	500	152	0.3	0.9	0.3
17:17	307.7	152.2	500	152	0.3	0.9	0.3
17:18	293.2	152.7	500	152	0.3	0.9	0.3
17:19	282.8	153.3	500	152	0.3	0.9	0.3
17:20	220	154.5	500	143	0.29	0.9	0.29
17:21	210	151.1	500	143	0.29	0.87	0.29
17:22	197.3	142.9	500	143	0.29	0.87	0.29
17:23	136.6	136.6	500	143	0.29	0.87	0.29
17:24	129.4	129.4	500	143	0.29	0.87	0.29
17:25	0	0	0	0	0	0	0

In this case study, the discharge rate is calculated based on the A3's individual charging demand ($A3_d$). It is seen in the table that the discharge rate is regulated every five minutes between 17:00 and 17:25. For example, the average charging demand for A3 over the first five minutes is 145.5 kW. This is used to determine the amount of power the battery energy storage unit must inject into the network (S_p). It should be noted that once the Audi vehicle reaches 80% battery SoC after 17:24, the battery energy storage unit is turned off (and hence why all the values are 0 in the table).

In addition, it is seen that the discharge rate is nearly constant and ranges between 29% and 30%. This is because the charging profile of Audi vehicles is linear, and the charging power varies very little in relation to the battery SoC (this can also be seen in **Figure 6.4**).

Table 7.4: Battery discharge profile between 17:00 and 18:00 (C2)

Time	C_d (kW)	$T4_d$ (kW)	$T9_d$ (kW	B_r (kW)	S_p (kW)	S_d (%)	S_s (A)	S_i (A)
17:00	474.2	143.5	186.7	500	334	0.67	2.01	0.67
17:01	477.3	144.4	188.3	500	334	0.67	2.01	0.67
17:02	479.7	145.4	188.8	500	334	0.67	2.01	0.67
17:03	482	146.2	189.5	500	334	0.67	2.01	0.67
17:04	484.7	147	190.7	500	334	0.67	2.01	0.67
17:05	487.5	147.4	192.7	500	315	0.63	1.89	0.63
17:06	489.7	148	194	500	315	0.63	1.89	0.63
17:07	473.6	138.5	187.1	500	315	0.63	1.89	0.63
17:08	440.9	131.5	161	500	315	0.63	1.89	0.63
17:09	423.1	119.9	154.6	500	315	0.63	1.89	0.63
17:10	401.7	106.5	146.5	500	221	0.44	1.32	0.44
17:11	385.8	101.8	135.2	500	221	0.44	1.32	0.44
17:12	372.4	98.8	124.7	500	221	0.44	1.32	0.44
17:13	352.2	93	109	500	221	0.44	1.32	0.44
17:14	341.2	87	103.5	500	221	0.44	1.32	0.44
17:15	332.9	82.3	99.4	500	155	0.31	0.93	0.31
17:16	317.4	74.5	91.3	500	155	0.31	0.93	0.31
17:17	307.7	69.3	86.2	500	155	0.31	0.93	0.31
17:18	293.2	63.5	77	500	155	0.31	0.93	0.31
17:19	282.8	58	71.5	500	155	0.31	0.93	0.31
17:20	220	0	65.5	500	60	0.12	0.36	0.12
17:21	210	0	58.9	500	60	0.12	0.36	0.12
17:22	197.3	0	54.4	500	60	0.12	0.36	0.12
17:23	136.6	0	0	500	0	0	0	0
17:24	129.4	0	0	500	0	0	0	0
17:25	0	0	0	0	0	0	0	0

In the second case study, the discharge rate is now calculated based on the aggregated charging demand of T4 ($T4_d$) and T9 ($T9_d$). The power injected by the battery energy storage unit is determined by adding the average charging power of T4 and T9 every five minutes. In the first five minutes, the average charging power for T4 and T9 vehicles is respectively 145.3 kW and 188.8 kW. This totals 334.1 kW, and the injected power is determined accordingly in Table 7.4. It is seen that T4 is fully charged prior to 17:20; consequently, the injected power by the storage unit is determined solely by the charging demand of T9 between 17:20 and 17:25.

The discharge rate in this case study is more flexible and goes higher in this case study due to the charging nature of Tesla vehicles. This rate ranges between 67% and 12%.

Table 7.5: Battery discharge profile between 17:00 and 18:00 (C3)

Time	C_d (kW)	$A3_d$ (kW)	$T4_d$ (kW)	$T9_d$ (kW	B_r (kW)	S_p (kW)	S_d (%)	S_s (A)	S_i (A)
17:00	474.2	144	143.5	186.7	500	480	0.96	2.88	0.96
17:01	477.3	144.6	144.4	188.3	500	480	0.96	2.88	0.96
17:02	479.7	145.5	145.4	188.8	500	480	0.96	2.88	0.96
17:03	482	146.3	146.2	189.5	500	480	0.96	2.88	0.96
17:04	484.7	147	147	190.7	500	480	0.96	2.88	0.96
17:05	487.5	147.4	147.4	192.7	500	463	0.93	2.79	0.93
17:06	489.7	147.7	148	194	500	463	0.93	2.79	0.93
17:07	473.6	148	138.5	187.1	500	463	0.93	2.79	0.93
17:08	440.9	148.4	131.5	161	500	463	0.93	2.79	0.93
17:09	423.1	148.6	119.9	154.6	500	463	0.93	2.79	0.93
17:10	401.7	148.7	106.5	146.5	500	371	0.74	2.22	0.74
17:11	385.8	148.8	101.8	135.2	500	371	0.74	2.22	0.74
17:12	372.4	148.9	98.8	124.7	500	371	0.74	2.22	0.74
17:13	352.2	150.2	93	109	500	371	0.74	2.22	0.74
17:14	341.2	150.7	87	103.5	500	371	0.74	2.22	0.74
17:15	332.9	151.2	82.3	99.4	500	307	0.61	1.83	0.61
17:16	317.4	151.6	74.5	91.3	500	307	0.61	1.83	0.61
17:17	307.7	152.2	69.3	86.2	500	307	0.61	1.83	0.61
17:18	293.2	152.7	63.5	77	500	307	0.61	1.83	0.61
17:19	282.8	153.3	58	71.5	500	307	0.61	1.83	0.61
17:20	220	154.5	0	65.5	500	203	0.41	1.23	0.41
17:21	210	151.1	0	58.9	500	203	0.41	1.23	0.41
17:22	197.3	142.9	0	54.4	500	203	0.41	1.23	0.41
17:23	136.6	136.6	0	0	500	203	0.41	0	0.41
17:24	129.4	129.4	0	0	500	203	0.41	0	0.41
17:25	0	0	0	0	0	0	0	0	0

In the last case study, the battery energy storage unit is now used to inject power based on the charging demand of all three vehicles: A3 ($A3_d$), T4 ($T4_d$) and T9 ($T9_d$). The power injected by the storage unit is determined by adding the average charging power of these vehicles every five minutes. In the first five minutes, the average charging power for A3, T4 and T9 vehicles is respectively 145.5 kW, 145.3 kW and 188.8 kW. This totals 480 kW, and the injected power is determined accordingly in Table 7.5 This is performed every five minutes until all vehicles on the network have completed charging. The discharge rate in this case study ranges from 97% to 41%.

The effect of all three discharge profiles from C1 to C3 is analysed to determine the relationship between the LG cell's voltage and its discharged capacity. Figure 7.5 demonstrates the results.
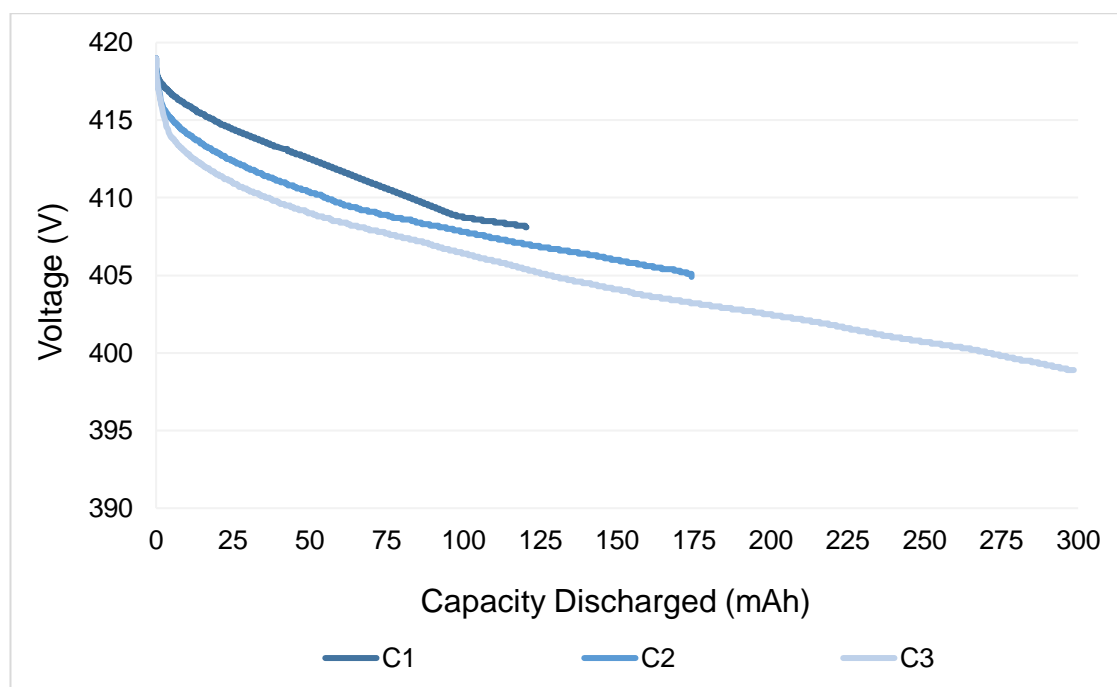
Figure 7.5: Relationship between battery voltage and capacity discharged.

The vertical axis of the graph depicts the increased cell voltage (in V) of the LG battery in three cases (represented by C1, C2, and C3). The horizontal axis represents the experimental time between 17:00 and 17:25 (in hours, minutes, and seconds). The remainder of the hour is not analysed because the storage unit operates only until 17:25 and the vehicles have finished charging by that time in the network.

The 18650 lithium-ion batteries that have been used in this research are charged up to a maximum charging voltage of 4.20 V. Due to a greater discharge rate throughout the experiment, the rate of decrease in battery voltage (represented by the steeper curve in Figure 7.5) for the third case study is faster than the first two case studies. At the conclusion of the discharge test, the battery voltage reaches 408.1 V for C1, 405 V for C2, and 399 V for C3 after 25 minutes. In three separate case studies, the battery voltage drops by 2.8%, 3.6%, and 5%, respectively, below the fully charged voltage.

In addition, 121 mAh was determined to be the total discharged capacity of the LG battery at the conclusion of the test in the first case study. In the second and third case studies, respectively, the capacity of the LG battery has been determined to be 174 mAh and 300 mAh. The LG cells retain majority of their capacities after 25 minutes of supporting the charging demand of vehicles. As a result of three discharge tests for C1, C2, and C3, using (7.2) and (7.3), the LG cell has a DoD of 4%, 5.8%, and 10%, respectively. In addition, this yields the following SoC levels for the LG cells under the respective tests: 96%, 94.2%, and 90%.

7.4 Summary

Different battery discharge profiles are developed based on the relationship between the **Chapter 6**'s developed stochastic charging profiles and battery SoCs from the maximum peak periods. **Chapter 6** dealt with the installation of stationary battery energy storage units to assist in reducing network and transformer peak loads. In this chapter, small-scale physical battery chargers are used, and the operating characteristics of lithium-ion batteries are examined under different discharge tests. Experiments were conducted to complement simulation results, specifically to demonstrate the efficacy of battery energy storage units and provide confidence in their viability for reducing peak demand and meeting the rising demand for high-energy consumer vehicles (such as Audi, Jaguar, and Tesla).

To estimate their SoC and DoD under different conditions, the relationship between the cell voltage of LG batteries and the current used to discharge them, as well as the relationship between the cell voltage and their total discharged capacity, were determined. For 38 minutes and 25 minutes of compensating for the charging demand of Jaguar and Audi vehicles, the battery voltage drops to within 4% and 5% of its fully charged level, respectively, according to experimental findings. Despite taking 1.5 times less time to reach its SoC, the Audi vehicle draws more energy from the storage unit due to its greater power drawing capability. In addition, the results indicate that the end-of-discharge voltage of 250 V for the batteries is never reached, and that they retain more than 85% of their capacities once the Jaguar and Audi vehicles have completed charging during peak periods.

Due to the high energy density of lithium-ion batteries, their ability to support the simultaneous charging of three vehicles was also evaluated. The SoC and DoD estimations of the batteries under various loading scenarios and discharge ratings have shown that they will still contain a substantial amount of usable energy once the associated vehicles reach their target SoCs. This is advantageous, especially if the same storage unit must be used to support the charging demand of other vehicles at the charging station prior to being charged to its maximum voltage. To maximise the benefit at scale, it is essential, however, to properly size these units.

Overall, the discharge tests demonstrate that lithium-ion batteries are highly practical as grid-level storage devices due to their high energy density. These devices can also be used to facilitate the simultaneous charging of multiple vehicles without their end-of-discharge voltage exceeding or falling below the specified SoC limits.

CHAPTER 8

8. Conclusions and Recommendations for Future Work

8.1 Discussion

The growing EV penetration places a strain on the grid, particularly during peak periods of demand. The hosting capacity of substations may be surpassed, leading to increased power losses and voltage violations, and overloaded distribution network equipment. This thesis has focused on the development of novel schemes for facilitating the connection of EV charging loads (particularly rapid and ultra-rapid chargers) with robust network measures. The following research questions have been addressed:

Q1. To what extent does the integration of EVs influence the operational characteristics of power networks at the transmission and distribution level? And What is the effect of increasing the uptake level of uncontrolled EV chargers?

A1. Load flow analysis is performed using static EV load profiles in IPSA+ Power simulation software and the effects of increasing the uptake level of EV chargers on the voltage drops and power losses are studied in **Chapter 3**. In **Chapter 4**, dynamic battery models are developed to investigate the combined effect of slow-speed, fast-speed, and rapid-speed EV chargers on voltage deviations, power losses, cable loading, and transformer loading in **Chapter 5**.

Q2. What technologies are feasible for connecting EVs without jeopardising the operational characteristics of distribution networks? And how can the impact of EV charging loads on distribution networks be mitigated?

A2. The installation of OLTCs in grid transformers, and the optimum placement of DG units and the optimum sizing of SVC devices near critical substations and busbars significantly reduce voltage deviations and active power losses in medium-voltage distribution networks. In addition, it is demonstrated that the utilisation of coordinated charging techniques, the integration of V2G chargers, and the optimum sizing and placement of battery energy storage units play a key role in relieving the stress on the grid and reducing the peak load on substation transformers in a low-voltage distribution network.

Q3. i) How can the hourly peak demand and energy consumption required by different EV models on rapid and ultra-rapid devices be estimated? ii) How often is the rated capacity of the substation transformer exceeded? iii) In the worst-case scenario, what is the minimum size of a battery energy storage unit required for the network to operate safely? iv) What is the minimum substation transformer size required to accommodate EV demand without becoming overloaded?

A3. The energy consumption of an EV depends on the model, battery capacity, battery SoC prior to charging, target SoC, duration of charging, and rating of chargers. In **Chapter 6**, a stochastic model to generate charging profiles for various EV models is developed. These profiles are then incorporated into a low-voltage distribution network to quantify the hourly peak demand and determine the substation transformer's peak demand. The frequency with which the maximum rated capacity of the substation transformer is exceeded due to EV demand is determined by calculating the full-load current on the secondary winding of the transformer and comparing it to the maximum threshold current at which the transformer is permitted to operate. In addition, the minimum required power that must be injected by the battery energy storage unit and the minimum transformer size required to accommodate EV charging activities without exceeding the system's hosting capacity are calculated to design a network to operate safely during the worst-case scenario.

Q4. i) How do the operating characteristics of lithium-ion batteries change under various discharge profiles? ii) How can the battery SoC and DoD be estimated? iii) How much battery energy storage capacity remains when it is used to charge a group of EVs with different charging needs?

A4. This question is addressed by combining the stochastic model for EVs, simulation of hourly peak demand for EVs, and discharge characteristics of lithium-ion batteries. Initially, various discharge profiles for the storage units based on stochastically developed EV charging profiles are developed based on the network's peak demand time and size. Then, these discharge profiles are incorporated into a physical battery charger and analyser unit employing lithium-ion batteries to experimentally determine the relationship between their cell voltage and discharged capacity under a variety of circumstances. Finally, the relationship between cell voltage and discharged capacity is used to estimate the battery SoC and DoD, as well as the available and usable battery capacity under various discharge profiles. Notably, discharge profiles are developed based on the charging needs of one, two, and three EVs simultaneously.

8.2 Thesis Contributions

This thesis made the following major contributions to the existing research to address the research questions:

1. This thesis proposes to use a combination of voltage control measures, particularly the installation of OLTCs on grid transformers, the placement of DGs in optimal locations, and the placement of SVCs in optimal locations, to safely accommodate the increased uptake level of rapid EV chargers in a HV/MV distribution network.

2. Numerous studies model EVs as static loads in distribution networks and view them as uncontrollable charging loads. Since network demand is constantly changing due to variations in customer load profiles, the battery dynamics should be developed in detail and integrated into different parts of the network based on customer type, as different customers have different charging needs. This thesis investigates the interaction of slow-speed, fast-speed, and rapid-speed charges on a real low-voltage distribution network. Also investigated are the effects of V2G and the combined effects of controllable and uncontrollable charging methods to mitigate and smooth out peak loads in the network.

3. A stochastic model is developed with real vehicle and charging time data to produce stochastic charging profiles for i) estimating the individual charging demand, ii) calculating the charging duration, and iii) determining the energy consumption of different EV models from the UK market with varying battery specifications and non-uniform charging characteristics. Collaboration is also made with Zap Map to obtain relevant data to model the timely distribution of vehicles at public charging hubs. The influence of battery energy storage units on the peak demand of the network and substation transformer is analysed. In the worst-case scenario, the frequency with which the charging demand exceeds the system's capacity is also determined. This allowed for the calculation of the optimal sizing of battery energy storage units and the determination of the minimum required kVA rating of substation transformers to operate the distribution network within safe and secure limits.

4. The SoC of an EV battery is an important parameter that reflects the battery performance. An accurate estimation of SoC does not only protect the battery from overcharging or deep discharging, but also extends its life. In this thesis, different discharge profiles are developed based on the stochastic charging profiles. These discharge profiles are then used to estimate the SoC and DoD of physical lithium-ion battery cells, which are then upscaled to represent the typical operating characteristic of a grid-connected battery energy storage unit. The effective utilisation of stationary battery energy storage units to meet the demand of EVs at public charging stations is studied with different EV models.

8.3 Overview of Study Chapters

This thesis proposed feasible technologies and measures to facilitate the connection of EVs and their charging technologies near strategic locations in distribution networks. The main findings for each study chapter are summarised in this section.

8.3.1 Chapter 3: Effect of Increasing the Uptake Level of Electric Vehicles on HV/MV Distribution Network

This chapter examined the impact of increasing the penetration rate of rapid EV chargers and implementing various voltage control measures on the steady-state operating characteristics of a generic HV/MV distribution network. The main findings and conclusions are summarised as follows:

1. Increasing the uptake level of EVs introduced voltage violations and increased active power losses in the network.
2. Even though the installation of OLTCs on grid transformers improved voltage profiles, voltage violations in some busbars were not completely eliminated at higher uptake levels of EV integration.
3. The optimal positioning of four DG units and four SVC devices eliminated all voltage violations and reduced network power losses by up to 15.6% and 26.0%, respectively.

8.3.2 Chapter 4: Computational Modelling and Simulation, and Experimental Testing of Batteries and Chargers

This chapter is considered as a methodological part for the modelling of battery dynamics and the choice of relevant experimental equipment. The main conclusions are summarised as follows:

1. Computational simulation of battery chargers was conducted by varying the power delivered to the Shepherd battery pack. It is shown that switching the charger's operation between charging (G2V) and discharging (V2G) modes affects the direction of power flow at the point of charging.
2. Experimental charging of batteries was carried out by varying the current delivered to the lithium-ion cells.

8.3.3 Chapter 5: Impact of Integrating Different Battery Chargers on a Low-Voltage Distribution Network Feeder

This chapter modelled a low-voltage distribution network feeder comprised of various residential and commercial buildings, as well as various battery chargers, categorised by their speed and rating. The main findings and conclusions are summarised as follows:

1. When and where EV charging loads are charged and connected to distribution networks, respectively, have a significant impact on the severity of grid issues. Additionally, the rating of the charger influences the severity of grid issues.
2. The supply cables were not designed to withstand the connection of a 150-kW charger during the peak demand (between 18:00 and 21:00). Two cables were severely overloaded at and near the point of charging.
3. The total daily costs associated with power losses increased from £47.4 in the absence of EV chargers to £285.9 with the presence of EV chargers.
4. Cable loading was reduced by (i) increasing the size of supply cables, (ii) using small-scale domestic V2G chargers rated at 7.5 kW each, and (iii) applying coordinated charging strategies. Coordinated charging was the most effective method, decreasing cable loading and peak demand by 45.7% and 47%, respectively. Using the coordinated charging method, power losses were also reduced by up to 70% at the point of charging.

8.3.4 Chapter 6: Estimation of Demand and Energy Consumption of Electric Vehicles at Rapid Chargers

This chapter developed a stochastic model to estimate the energy consumption of popular BEV models from the UK market (such as Audi e-Tron, BMW i3, Jaguar I-Pace, Kia e-Niro, and Tesla Model 3), and to estimate the hourly and minute-by-minute peak demand on the network and substation transformer, respectively. The main findings are summarised as follows:

1. While Kia models consume less energy than Audi, Jaguar, and Tesla models, it takes them longer to reach 80% battery SoC. BMW models require the least amount of energy to achieve 80% battery SoC, but their average charging times are longer than Audi and Tesla models. The increased range and relatively rapid recharging times of Tesla vehicles set them apart not only from other models in this study, but also from other vehicles on the market. This demonstrates why Tesla vehicles are currently the market leaders.

2. Due to the increased likelihood of rapid and ultra-rapid charger operations occurring between 12:00 and 21:00 in the UK, distribution grids and substation transformers are anticipated to experience more pulsating loads and be more heavily loaded.

3. Under the worst-case scenario, the peak demand on the distribution network increased from 12 kW to 404 kW and on the substation transformer from 56.7 kW to 447.7 kW between 17:00 and 18:00.

4. To reduce peak demand, the connection of two small-scale V2G chargers (rated at 7.5 kW) and one large-scale battery energy storage unit (rated at 150 kW) has been proposed. The storage unit reduced the distribution network feeder's and substation transformer's peak demand by up to 30% and 40%, respectively.

5. Simulation results revealed that the substation transformer can accommodate a peak demand of approximately 432 kW during the worst-case scenario without becoming overloaded. However, the optimal sizing of the battery energy storage unit to prevent substation transformer overload between 17:00 and 17:12 must be 256.7 kWh to power the additional demand between the substation transformer's peak load capacity and the point at which the transformer reaches its maximum rated capacity.

6. The 500-kVA substation transformer was exceeding its maximum rated capacity at 11:00, 12:00, 16:00, 17:00, and 19:00 under the worst-case scenario. During these times, the transformer was loaded to a maximum of 3.5%, 20.9%, 3.5%, 27.5%, and 19.1%, respectively. To accommodate the simultaneous connection of A3, T4, and T9 vehicles securely to the network between 17:00 and 18:00, the transformer was sized to a minimum of 660 kVA based on the maximum full-load current and maximum peak demand of 880 A and 570 kW, respectively.

8.3.5 Chapter 7: State of Charge Estimation of Lithium-Ion Batteries Under Discharge Tests

This chapter developed different battery discharge profiles to determine the relationship between i) cell voltage and charging current, and ii) cell voltage and total discharged capacity of lithium-ion batteries. The findings of the chapter are summarised as follows:

1. The end-of-discharge voltages of 2.5 V for the lithium-ion battery cell and 250 V for the stationary battery energy storage unit were not reached under different discharge tests. The lithium-ion batteries retained more around 90% of their capacities once the Audi and Tesla vehicles have completed their charging sessions during the peak periods.

2. Due to the high energy density of lithium-ion batteries, the SoC estimations from various discharge profiles and scenarios revealed that they contain a substantial amount of reusable energy even if they were used to support the simultaneous charging of three high-power EVs.

3. It is essential to size the battery storage units adequately to maximise the grid-scale benefits.

8.4 Suggestions for Future Work

The work presented in this thesis can be extended in the following ways:

- Dynamic demand profiles can be used to do a more detailed impact study at the transmission side of HV/MV distribution networks.

- The optimum sizing of DG units can be included within the optimum placement of them.

- The Shepherd battery model may be improved and the effect of charging on the internal battery temperatures could be analysed throughout a range of charging and discharging cycles to study the likelihood of battery performance deterioration and ageing.

- Since the ability to use V2G on a commercial scale is yet to develop at the time of conducting this research, future work may explore the effects of larger scale V2G chargers on cable loading, transformer loading, and power losses.

- The stochastic model may be updated with newer vehicle models from the market.

- A solar PV system may be combined with an on-site battery energy storage unit to assist in reducing network's peak demand and lowering the costs of charging.

- The other physical operating characteristics of the lithium-ion battery cells may be monitored. For example, different discharge tests can be run at different ambient temperatures to investigate how the battery performance and battery SoC/DoD are affected under different settings. In addition, the state of health of the batteries may be estimated.

- Due to budgetary constraints, a larger (in size and rating) battery charger and analyser unit could not be purchased and utilised for more comprehensive testing in this thesis. However, a larger physical battery charger (in rating and size) with the capacity to analyse an entire battery pack could be utilised for further analysis.

8.5 Research Benefits

Widespread use of EVs is achieved through the availability of rapid charging stations. Not only will these stations reduce range anxiety but also minimise service and waiting times, preserve smoother traffic operation, and enable drivers to charge their vehicles at conveniently accessible public outlets (such as motorway junctions and at car parks of shopping malls). At the time of conducting this research, the shift towards ultra-high speed DC chargers is still in relatively slow phase, owing to the limitations in the battery technology. For this reason, there is a limited amount of work quantifying the impacts of ultra-rapid chargers on distribution grids. This thesis puts a greater emphasis on the modelling, operation, and control principles of high-powered DC chargers. Several actors, based on the principles of this study, could benefit from this thesis:

First and foremost, the energy suppliers and DNOs may benefit from this research in different ways. At the transmission and distribution levels, there will be an increase in peak demand with the rapid uptake of EVs. The minimum generation capacity required to ensure demand is met, has been continuously rising. The maximum currents carried by the transmission, as well as the distribution networks are also increasing. The proposed framework for analysing the impact of EVs includes a national and local approach by using a generic and an existing real distribution network, respectively. The findings (particularly subjected overloading conditions on cables and transformers) raise awareness for the potential risk in the operation of existing distribution networks in urban and populated areas. DNOs may show tendency towards the reinforcement of distribution networks by upgrading the sizes of cables and transformers. However, this comes at the expense of increased costs.

Charge point operators, who build and maintain charging stations for electric car owners, may also benefit from this research. The results from the estimation of the EV demand on rapid and ultra-rapid chargers showed that on-site supplementary battery energy storage units will play a key role to help reduce network demand. These storage units even provide other ancillary services to reduce network costs and improve network reliability.

The society and the environment may also benefit in a way to promote and accelerate the shift to the electric mobility. The increased awareness and knowledge among the society will be significant to help reduce transportation-related emissions as quick as possible and enable synergies with smart grid development across many other countries.

The Appendices

A. HV/MV Generic British Distribution Network

This section presents the parameters used in the modelling of the HV/MV British generic distribution network in **Chapter 3** (see **Figure 3.1**). Additionally, it outlines the formulation problem for the optimum allocation of the DG units near critical feeders.

This generic distribution network is modelled by using the constant and average PQ demand of load busbars derived from [44]. The data is provided by the Excel spreadsheet that specifies the United Kingdom Generic Distribution System (UKGDS) Phase One Extra High Voltage Number 3 generic model in the UKGDS Phase One standard format. The Extra High Voltage Number 3 generic model represents a suburban area with mixed construction. The topology is mostly radial but with some interconnection within the network and links to neighbouring 33-kV networks.

Since the network's variable load profiles were not available in the dataset, one-time step demand data was used to evaluate the network's steady-state operational characteristics under various case studies. Simulation results are obtained by using the Newton-Raphson method.

A.1 Cable and Line Data

Table A.1 contains the line data (resistance, reactance, and susceptance) for the HV/MV distribution network. The abbreviations for the line data are defined below as well.

Where:

C_{R1} is the positive and negative sequence resistance of the branch (p.u.),

C_{X1} is the positive and negative sequence reactance of the branch (p.u.),

C_{B1} is the positive and negative sequence susceptance of the branch (p.u.),

C_{R0} is the zero-sequence resistance of the branch (p.u.),

C_{X1} is the zero-sequence reactance of the branch (p.u.),

C_{B1} is the zero-sequence susceptance of the branch (p.u.).

Table A.1: Line data for the HV/MV distribution network

From	To	C_{R1} (p.u.)	C_{X1} (p.u.)	C_{B1} (p.u.)	C_{R0} (p.u.)	C_{X0} (p.u.)	C_{B0} (p.u.)	Length (km)
101	102	0.0046	0.0228	0.0105	0.0121	0.0576	0.0105	5.865
101	103	0.0041	0.0203	0.0094	0.0107	0.0513	0.0094	0.087
101	106	0.0171	0.0374	0.0428	0.0352	0.0957	0.0428	11.754
101	107	0.0149	0.0326	0.0387	0.0307	0.0834	0.0387	0.153
101	108	0.0004	0.0008	0.0015	0.0008	0.0020	0.0015	0.02
101	109	0.0004	0.0010	0.0022	0.0009	0.0023	0.0022	0.352
101	110	0.0062	0.0133	0.0328	0.0171	0.0340	0.0328	4.293
101	111	0.0065	0.0140	0.0353	0.0180	0.0358	0.0353	6.183
101	116	0.0122	0.0275	0.0098	0.0255	0.0700	0.0098	7.066
102	104	0.0009	0.0012	0.0397	0.0076	0.0025	0.0397	1.853
103	105	0.0008	0.0011	0.0349	0.0067	0.0022	0.0349	0.466
103	117	0.0021	0.0049	0.0011	0.0043	0.0124	0.0011	1.493
106	112	0.0003	0.0008	0.0002	0.0007	0.0020	0.0002	0.234
106	114	0.0065	0.0220	0.0082	0.0144	0.0626	0.0082	3.364
107	113	0.0003	0.0007	0.0002	0.0007	0.0019	0.0002	0.208
107	115	0.0069	0.0234	0.0088	0.0154	0.0665	0.0088	7.337
307	341	0.0178	0.0220	0	0.0533	0.0659	0	0.124
313	308	0.0571	0.0540	0	0.1712	0.1621	0	2.729
313	309	0.0791	0.1078	0	0.2372	0.3233	0	2.347
313	362	0.0010	0.0013	0	0.0031	0.0038	0	0.021
313	363	0.0006	0.0012	0	0.0019	0.0035	0	0.019
314	315	0.0187	0.0177	0	0.0561	0.0532	0	0.521
315	345	0.0707	0.0624	0	0.2121	0.1872	0	1.105
316	314	0.0340	0.0342	0	0.1021	0.1027	0	3.811
316	315	0.0691	0.0490	0	0.2072	0.1469	0	2.911
316	315	0.0520	0.0479	0	0.1561	0.1437	0	2.154
316	315	0.0738	0.0523	0	0.2214	0.1568	0	3.801
316	317	0.0055	0.0051	0	0.0166	0.0154	0	0.383
316	318	0.0056	0.0049	0	0.0169	0.0147	0	0.077
316	353	0.0322	0.0296	0	0.0965	0.0888	0	1.379
316	354	0.0394	0.0200	0	0.1182	0.0601	0	0.085
327	326	0.0839	0.0870	0	0.2518	0.2610	0	1.369
332	325	0.0199	0.0181	0	0.0596	0.0542	0	1.24
334	327	0.0420	0.0812	0	0.1261	0.2435	0	1.276
334	332	0.0225	0.0198	0	0.0676	0.0593	0	1.944
336	332	0.0334	0.0371	0	0.1001	0.1112	0	0.974
337	333	0.0399	0.0317	0	0.1197	0.0952	0	1.787
337	336	0.0000	0.0000	0	0	0	0	0
338	305	0.0453	0.0774	0	0.1359	0.2322	0	1.605
338	306	0.0571	0.0899	0	0.1712	0.2698	0	2.693
338	330	0.1025	0.1275	0	0.3075	0.3824	0	1.173
338	331	0.1111	0.1397	0	0.3332	0.4191	0	3.847
338	334	0.0630	0.1033	0	0.1889	0.3100	0	1.566
338	339	0.0008	0.0011	0	0.0025	0.0033	0	0.096
338	340	0.0005	0.0007	0	0.0014	0.0020	0	0.048
338	341	0.0434	0.0716	0	0.1301	0.2147	0	2.617
338	346	0.0181	0.0162	0	0.0544	0.0485	0	1.396
338	347	0.0168	0.0149	0	0.0505	0.0447	0	0.497
338	360	0.0403	0.0370	0	0.1208	0.1110	0	3.612

338	361	0.0352	0.0323	0	0.1055	0.0969	0	1.081
342	319	0.0169	0.0160	0	0.0508	0.0480	0	0.432
342	320	0.0123	0.0125	0	0.0369	0.0375	0	0.694
342	335	0.0432	0.0349	0	0.1295	0.1047	0	2.627
342	336	0.0394	0.0472	0	0.1182	0.1417	0	3.61
342	337	0.0658	0.0817	0	0.1973	0.2451	0	0.045
342	343	0.0099	0.0092	0	0.0298	0.0277	0	0.667
342	344	0.0077	0.0071	0	0.0231	0.0213	0	0.422
342	350	0.0150	0.0108	0	0.0449	0.0323	0	0.984
342	351	0.0131	0.0094	0	0.0392	0.0281	0	0.094
348	324	0.1077	0.1074	0	0.3231	0.3222	0	4.722
348	327	0.2730	0.3717	0	0.8190	1.1152	0	5.458
348	328	0	0	0	0	0	0	0
348	329	0	0	0	0	0	0	0
353	352	0.0287	0.0244	0	0.0860	0.0731	0	0.299
353	357	0.0149	0.0130	0	0.0447	0.0389	0	0.071
357	301	0.0333	0.0313	0	0.0998	0.0938	0	0.992
357	303	0.0351	0.0311	0	0.1052	0.0934	0	3.44
357	311	0.0178	0.0157	0	0.0534	0.0472	0	0.307
357	312	0.0195	0.0173	0	0.0584	0.0520	0	1.058
357	321	0.0081	0.0097	0	0.0244	0.0292	0	0.236
357	322	0.0091	0.0108	0	0.0272	0.0325	0	0.793
357	355	0.0243	0.0230	0	0.0730	0.0691	0	0.479
357	356	0.0369	0.0380	0	0.1106	0.1141	0	1.215
357	358	0.0015	0.0014	0	0.0044	0.0042	0	0.004

It should be clarified that all the line data for the HV/MV distribution network is expressed in per unit on system base.

A.2 Transformer Data

Table A.2 presents the transformer data concerning resistance, reactance, earthing resistance, and earthing reactance for the network. The abbreviations for the line data are defined below as well.

Where:

T_{R1} is the positive and negative sequence resistance of the transformer (p.u.),

T_{X1} is the positive and negative sequence reactance of the transformer (p.u.),

T_{B1} is the positive and negative sequence susceptance of transformer (p.u.),

T_{R0} is the zero-sequence resistance of the transformer (p.u.),

T_{X1} is the zero-sequence reactance of the transformer (p.u.),

T_{B1} is the zero-sequence susceptance of the transformer (p.u.).

Table A.2: Transformer data for the HV/MV distribution network

From	To	T_{R1} (p.u.)	T_{X1} (p.u.)	T_{R0} (p.u.)	T_{X0} (p.u.)	T_{RE} (p.u.)	T_{XE} (p.u.)	Winding
99	101	0	0.1	0	0.1	0	0	YY
99	101	0	0.1	0	0.1	0	0	YY
104	316	0.0056	0.1720	0	0.1463	1.0006	0.3602	YD
105	316	0.0054	0.1706	0	0.1451	1.0006	0.3602	YD
108	338	0.0092	0.1946	0	0.1655	1.4470	0.5209	YD
109	338	0.0090	0.1949	0	0.1658	1.4470	0.5209	YD
109	338	0.0092	0.1984	0	0.1689	1.4470	0.5209	YD
110	342	0.0107	0.2235	0	0.1902	1.6739	0.6026	YD
111	342	0.0107	0.2246	0	0.1911	1.6739	0.6026	YD
112	348	0.0132	0.3024	0	0.2573	2.2200	0.7991	YD
113	348	0.0132	0.2946	0	0.2507	2.2200	0.7991	YD
114	313	0.0069	0.2351	0	0.2000	0.9876	0.3555	YD
115	313	0.0061	0.2371	0	0.2016	0.9876	0.3555	YD
116	357	0.0108	0.2281	0	0.1941	1.6873	0.6074	YD
117	357	0.0108	0.2253	0	0.1917	1.6873	0.6074	YD
301	6601	0.0374	0.9718	0	0.8260	7.6696	2.7609	DY
303	6601	0.0374	0.9718	0	0.8260	7.6696	2.7609	DY
305	6602	0.0438	1.0962	0	0.9318	13.5442	4.8756	DY
306	6602	0.0438	1.0962	0	0.9318	13.5442	4.8756	DY
307	6602	0.0438	1.0962	0	0.9318	13.5442	4.8756	DY
308	6603	0.0372	0.9288	0	0.7895	7.6240	2.7444	DY
309	6603	0.0372	0.9288	0	0.7895	7.6240	2.7444	DY
311	6604	0.0411	1.0279	0	0.8738	8.4374	3.0373	DY
312	6604	0.0411	1.0279	0	0.8738	8.4374	3.0373	DY
314	6605	0.0393	1.0221	0	0.8688	7.5150	2.7052	DY
314	6605	0.0393	1.0221	0	0.8688	7.5150	2.7052	DY
315	6606	0.0407	1.0163	0	0.8638	8.3416	3.0028	DY
315	6606	0.0407	1.0163	0	0.8638	8.3416	3.0028	DY
316	6615	0.0381	0.9918	0	0.8430	7.8480	2.8251	DY
316	6615	0.0381	0.9918	0	0.8430	7.8480	2.8251	DY
317	6607	0.0432	1.0804	0	0.9184	8.8682	3.1923	DY
318	6607	0.0432	1.0804	0	0.9184	8.8682	3.1923	DY
319	6608	0.0373	0.9320	0	0.7922	7.6699	2.7610	DY
320	6608	0.0373	0.9320	0	0.7922	7.6699	2.7610	DY
321	6609	0.0428	1.0701	0	0.9096	8.7835	3.1618	DY
322	6609	0.0428	1.0701	0	0.9096	8.7835	3.1618	DY
324	1101	0.0426	1.0639	0	0.9043	5.2532	1.8910	DY
325	1102	0.0401	1.0420	0	0.8857	4.9473	1.7809	DY
326	1102	0.0401	1.0420	0	0.8857	4.9473	1.7809	DY
328	1103	0.0422	1.0557	0	0.8973	5.2126	1.8764	DY
329	1103	0.0422	1.0557	0	0.8973	5.2126	1.8764	DY
330	1104	0.0387	0.9683	0	0.8231	4.7814	1.7212	DY
331	1104	0.0387	0.9683	0	0.8231	4.7814	1.7212	DY
332	1105	0.0405	1.0125	0	0.8606	4.9995	1.7997	DY
333	1105	0.0405	1.0125	0	0.8606	4.9995	1.7997	DY
336	1106	0.0377	0.9809	0	0.8338	4.6573	1.6765	DY
337	1106	0.0377	0.9809	0	0.8338	4.6573	1.6765	DY
339	6610	0.0435	1.0882	0	0.9249	8.9551	3.2236	DY
340	6610	0.0435	1.0882	0	0.9249	8.9551	3.2236	DY

341	6611	0.0383	0.9963	0	0.8469	7.8842	2.8381	DY
341	6611	0.0383	0.9963	0	0.8469	7.8842	2.8381	DY
343	6612	0.0386	0.9641	0	0.8195	7.9340	2.8560	DY
344	6612	0.0386	0.9641	0	0.8195	7.9340	2.8560	DY
346	1107	0.0393	0.9814	0	0.8342	4.8460	1.7444	DY
347	1107	0.0393	0.9814	0	0.8342	4.8460	1.7444	DY
350	1108	0.0415	1.0780	0	0.9163	5.1180	1.8424	DY
351	1108	0.0415	1.0780	0	0.9163	5.1180	1.8424	DY
352	6613	0.0375	0.9760	0	0.8296	7.7029	2.7728	DY
354	6613	0.0375	0.9760	0	0.8296	7.7029	2.7728	DY
355	6614	0.0364	0.9464	0	0.8044	7.4690	2.6886	DY
356	6614	0.0364	0.9464	0	0.8044	7.4690	2.6886	DY
358	6616	0.0406	1.0149	0	0.8626	8.3302	2.9987	DY
359	6616	0.0406	1.0149	0	0.8626	8.3302	2.9987	DY
360	6617	0.0419	1.0482	0	0.8909	8.6034	3.0970	DY
361	6617	0.0419	1.0482	0	0.8909	8.6034	3.0970	DY
362	1109	0.0416	1.0399	0	0.8839	5.1350	1.8485	DY

It should be clarified that all the transformer data for the HV/MV distribution network is expressed in per unit on a system base.

A.3 Busbar and Line Data for Optimisation Model

With reference to the schematic diagram of the distribution network presented in Figure A.1, the busbar and line data used to determine the optimum placement of DG units are shown in Table A.3 and Table A.4, respectively.
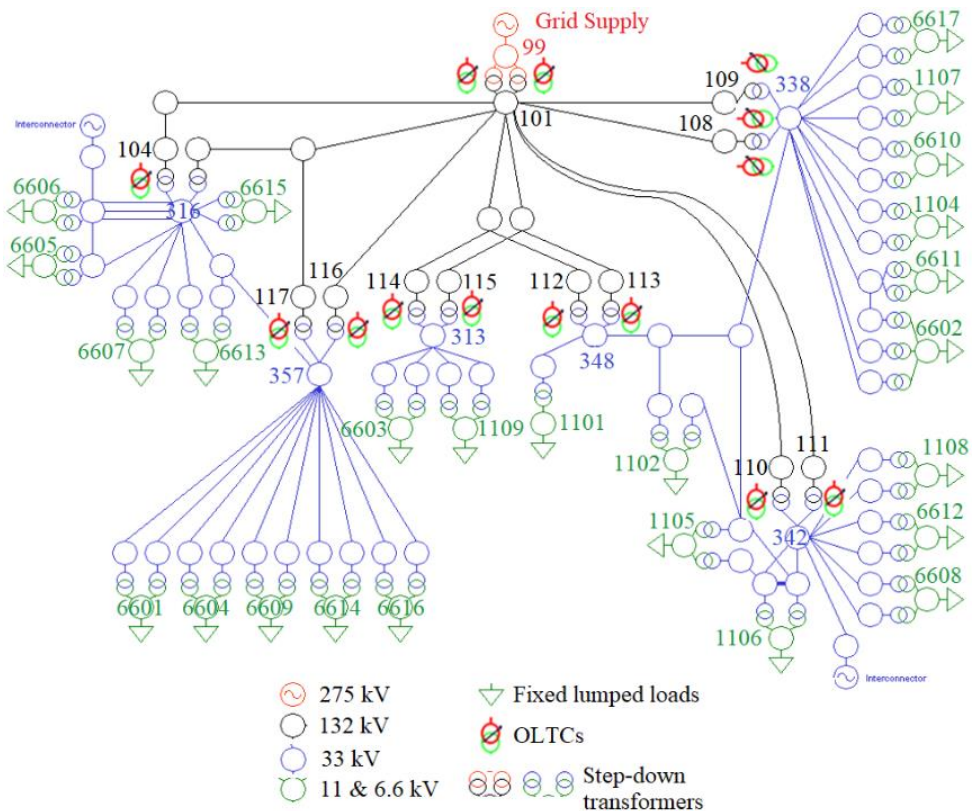
Figure A.1: Schematic diagram of the HV/MV generic distribution network.

Table A.3: Busbar data of the HV/MV distribution network for the MATLAB codes

Busbar Name	Busbar Label	Busbar Type: 1: Slack 2: PV 3: PQ	Generation (MW)	Generation (MVAr)	Minimum Reactive Power (MVAr)	Maximum Reactive Power (MVAr)
99	1	1	0.0	206.8	1000.0	-1000.0
101	2	3	0.0	0.0	0.0	0.0
102	3	3	0.0	0.0	0.0	0.0
103	4	3	0.0	0.0	0.0	0.0
104	5	3	0.0	0.0	0.0	0.0
105	6	3	0.0	0.0	0.0	0.0
106	7	3	0.0	0.0	0.0	0.0
107	8	3	0.0	0.0	0.0	0.0
108	9	3	0.0	0.0	0.0	0.0
109	10	3	0.0	0.0	0.0	0.0
110	11	3	0.0	0.0	0.0	0.0
111	12	3	0.0	0.0	0.0	0.0
112	13	3	0.0	0.0	0.0	0.0
113	14	3	0.0	0.0	0.0	0.0
114	15	3	0.0	0.0	0.0	0.0
115	16	3	0.0	0.0	0.0	0.0
116	17	3	0.0	0.0	0.0	0.0
117	18	3	0.0	0.0	0.0	0.0
301	19	3	0.0	0.0	0.0	0.0
303	20	3	0.0	0.0	0.0	0.0
305	21	3	0.0	0.0	0.0	0.0
306	22	3	0.0	0.0	0.0	0.0
307	23	3	0.0	0.0	0.0	0.0
308	24	3	0.0	0.0	0.0	0.0
309	25	3	0.0	0.0	0.0	0.0
311	26	3	0.0	0.0	0.0	0.0
312	27	3	0.0	0.0	0.0	0.0
313	28	3	0.0	0.0	0.0	0.0
314	29	3	0.0	0.0	0.0	0.0
315	30	3	0.0	0.0	0.0	0.0
316	31	3	0.0	0.0	0.0	0.0
317	32	3	0.0	0.0	0.0	0.0
318	33	3	0.0	0.0	0.0	0.0
319	34	3	0.0	0.0	0.0	0.0
320	35	3	0.0	0.0	0.0	0.0
321	36	3	0.0	0.0	0.0	0.0
322	37	3	0.0	0.0	0.0	0.0
324	38	3	0.0	0.0	0.0	0.0
325	39	3	0.0	0.0	0.0	0.0
326	40	3	0.0	0.0	0.0	0.0
327	41	3	0.0	0.0	0.0	0.0
330	42	3	0.0	0.0	0.0	0.0

331	43	3	0.0	0.0	0.0	0.0
332	44	3	0.0	0.0	0.0	0.0
333	45	3	0.0	0.0	0.0	0.0
334	46	3	0.0	0.0	0.0	0.0
335	47	2	0.0	23.4	30.0	-30.0
336	48	3	0.0	0.0	0.0	0.0
337	49	3	0.0	0.0	0.0	0.0
338	50	3	0.0	0.0	0.0	0.0
339	51	3	0.0	0.0	0.0	0.0
340	52	3	0.0	0.0	0.0	0.0
341	53	3	0.0	0.0	0.0	0.0
342	54	3	0.0	0.0	0.0	0.0
343	55	3	0.0	0.0	0.0	0.0
344	56	3	0.0	0.0	0.0	0.0
345	57	2	0.0	26.8	20.0	-20.0
346	58	3	0.0	0.0	0.0	0.0
347	59	3	0.0	0.0	0.0	0.0
348	60	3	0.0	0.0	0.0	0.0
350	61	3	0.0	0.0	0.0	0.0
351	62	3	0.0	0.0	0.0	0.0
352	63	3	0.0	0.0	0.0	0.0
353	64	3	0.0	0.0	0.0	0.0
354	65	3	0.0	0.0	0.0	0.0
355	66	3	0.0	0.0	0.0	0.0
356	67	3	0.0	0.0	0.0	0.0
357	68	3	0.0	0.0	0.0	0.0
358	69	3	0.0	0.0	0.0	0.0
359	70	3	0.0	0.0	0.0	0.0
360	71	3	0.0	0.0	0.0	0.0
361	72	3	0.0	0.0	0.0	0.0
362	73	3	0.0	0.0	0.0	0.0
363	74	3	0.0	0.0	0.0	0.0
1101	75	3	10.1	0.0	0.0	0.0
1102	76	3	4.0	0.0	0.0	0.0
1104	77	3	9.3	0.0	0.0	0.0
1105	78	3	3.3	0.0	0.0	0.0
1106	79	3	2.1	0.0	0.0	0.0
1107	80	3	3.3	0.0	0.0	0.0
1108	81	3	1.0	0.0	0.0	0.0
1109	82	3	9.8	0.0	0.0	0.0
6601	83	3	5.0	0.0	0.0	0.0
6602	84	3	6.7	0.0	0.0	0.0
6603	85	3	4.8	0.0	0.0	0.0
6604	86	3	5.9	0.0	0.0	0.0
6605	87	3	4.3	0.0	0.0	0.0
6606	88	3	5.4	0.0	0.0	0.0
6607	89	3	7.2	0.0	0.0	0.0
6608	90	3	8.6	0.0	0.0	0.0

6609	91	3	0.5	0.0	0.0	0.0
6610	92	3	7.2	0.0	0.0	0.0
6611	93	3	2.9	0.0	0.0	0.0
6612	94	3	8.6	0.0	0.0	0.0
6613	95	3	4.8	0.0	0.0	0.0
6614	96	3	5.7	0.0	0.0	0.0
6615	97	3	4.3	0.0	0.0	0.0
6616	98	3	6.3	0.0	0.0	0.0
6617	99	3	0.3	0.0	0.0	0.0

Table A.4: Line data of the HV/MV distribution network for the MATLAB codes

From Busbar	To Busbar	C_{R1} (p.u.)	C_{X1} (p.u.)	C_{B1} (p.u.)	Tap setting (a)
1	2	0.0	0.1	0.0	1
1	2	0.0	0.1	0.0	1
2	3	0.00456	0.02278	0.00526	1
3	5	0.00088	0.00123	0.01987	1
2	4	0.00407	0.02030	0.00468	1
2	10	0.0043	0.00097	0.00108	1
2	9	0.00036	0.00082	0.00075	1
2	7	0.01709	0.03743	0.02139	1
2	8	0.01492	0.03264	0.01936	1
2	17	0.01219	0.02745	0.00488	1
4	6	0.00077	0.00108	0.01745	1
4	18	0.00214	0.00487	0.00053	1
17	68	0.01079	0.22809	0.01738	1
18	68	0.01079	0.22528	0.00502	1
6	31	0.00538	0.17062	0.01572	1
5	31	0.00556	0.17199	0.04060	1
31	97	0.03815	0.99178	0.00874	1
31	97	0.03815	0.99178	0.00874	1
31	30	0.06905	0.04896	0.0	1
31	30	0.05204	0.04789	0.0	1
31	30	0.07379	0.05227	0.0	1
30	57	0.07071	0.06239	0.01816	1
30	88	0.04065	1.01627	0.0	1
30	88	0.04065	1.01627	0.0	1
31	29	0.00553	0.00515	0.0	1
29	30	0.01869	0.01772	0.05020	1
29	87	0.03931	1.02212	0.0	1
29	87	0.03931	1.022212	0.0	1
31	32	0.00553	0.00515	0.0	1
31	33	0.00562	0.00491	0.0	1
31	65	0.03942	0.02002	0.0	1
31	64	0.03216	0.02962	0.0	1
64	68	0.01489	0.01296	0.0	1
63	95	0.03754	0.97599	0.0	1
65	95	0.03754	0.97599	0.0	1
64	63	0.02866	0.02438	0.0	1
32	89	0.03738	0.97178	0.0	1
33	89	0.03738	0.97178	0.0	1
10	50	0.00916	0.19837	0.0	1
10	50	0.00898	0.19486	0.0	1
9	50	0.00916	0.19458	0.0	1
7	15	0.00646	0.02204	0.00412	1
7	13	0.00033	0.00075	0.0008	1
8	16	0.00687	0.02342	0.00438	1
8	14	0.00033	0.00074	0.00008	1

15	28	0.00690	0.23512	0.0	1
16	28	0.00614	0.23710	0.0	1
28	24	0.05708	0.05404	0.0	1
28	25	0.07907	0.10776	0.0	1
24	85	0.03715	0.92884	0.0	1
25	85	0.03715	0.92884	0.0	1
28	73	0.00102	0.00128	0.0	1
28	74	0.00064	0.00118	0.0	1
73	82	0.04160	1.03994	0.0	1
74	82	0.04160	1.03994	0.0	1
68	19	0.03327	0.03128	0.0	1
68	20	0.03506	0.03115	0.0	1
19	83	0.03738	0.97178	0.0	1
19	83	0.03738	0.97178	0.0	1
68	26	0.01781	0.01573	0.0	1
68	27	0.01946	0.01732	0.0	1
26	86	0.04112	1.02795	0.0	1
27	86	0.04112	1.02795	0.0	1
68	36	0.00812	0.00973	0.0	1
68	37	0.00905	0.01085	0.0	1
36	91	0.04280	1.07011	0.0	1
37	91	0.04280	1.07011	0.0	1
68	66	0.02434	0.02303	0.0	1
68	67	0.03688	0.03804	0.0	1
66	96	0.03640	0.94636	0.0	1
67	96	0.03640	0.94636	0.0	1
68	69	0.00146	0.00139	0.0	1
68	70	0.00148	0.00141	0.0	1
69	98	0.04060	1.01488	0.0	1
70	98	0.04060	1.01488	0.0	1
50	72	0.03516	0.03231	0.0	1
50	71	0.04027	0.03701	0.0	1
72	99	0.04193	1.04817	0.0	1
71	99	0.04193	1.04817	0.0	1
50	59	0.01682	0.01489	0.0	1
50	58	0.01813	0.01616	0.0	1
59	80	0.03926	0.98142	0.0	1
58	80	0.03926	0.98142	0.0	1
50	52	0.00047	0.00065	0.0	1
50	51	0.00093	0.00111	0.0	1
52	92	0.04353	1.08815	0.0	1
51	92	0.04353	1.08815	0.0	1
50	43	0.11105	0.09660	0.0	1
50	42	0.10250	0.12748	0.0	1
43	77	0.03873	0.96832	0.0	1
42	77	0.03873	0.96832	0.0	1
50	53	0.04338	0.07157	0.0	1
23	53	0.01777	0.02198	0.0	1

53	93	0.03832	0.99635	0.0	1
53	93	0.03832	0.99635	0.0	1
50	22	0.05707	0.08994	0.0	1
50	21	0.04531	0.07740	0.0	1
23	84	0.04385	1.09623	0.0	1
22	84	0.04385	1.09623	0.0	1
21	84	0.04385	1.09623	0.0	1
2	11	0.00617	0.01328	0.01638	1
2	12	0.00650	0.01399	0.01763	1
11	54	0.01070	0.22350	0.0	1
12	54	0.01070	0.22350	0.0	1
54	62	0.01306	0.00936	0.0	1
54	61	0.01498	0.01077	0.0	1
62	81	0.04146	1.07797	0.0	1
61	81	0.00771	1.07797	0.0	1
54	55	0.00994	0.00922	0.0	1
54	56	0.00771	0.00709	0.0	1
56	94	0.03856	0.96407	0.0	1
55	94	0.03856	0.96407	0.0	1
54	35	0.01229	0.01250	0.0	1
54	34	0.01693	0.01601	0.0	1
35	90	0.03728	0.98198	0.0	1
34	90	0.03728	0.93198	0.0	1
54	47	0.04317	0.03490	0.0	1
54	48	0.03939	0.04722	0.0	1
13	60	0.01317	0.30238	0.0	1
14	60	0.01317	0.30238	0.0	1
50	46	0.06296	0.10334	0.0	1
60	41	0.27301	0.37173	0.0	1
60	38	0.10769	0.10741	0.0	1
38	75	0.04256	1.06387	0.0	1
46	41	0.04203	0.08116	0.0	1
49	79	0.03773	0.98093	0.0	1
48	79	0.03773	0.98093	0.0	1
49	45	0.03991	0.03175	0.0	1
45	78	0.04050	1.01250	0.0	1
44	78	0.04050	1.01250	0.0	1
46	44	0.02255	0.01976	0.0	1
48	44	0.03335	0.03706	0.0	1
54	49	0.06576	0.08171	0.0	1
44	39	0.01986	0.01806	0.0	1
41	40	0.08393	0.08699	0.0	1
40	76	0.04008	1.04200	0.0	1
39	76	0.04008	1.04200	0.0	1

A.4 MATLAB Codes

The establishment of the structure of inputs and objects in the developed MATLAB code is presented in this part. The functions to input the busbar data in the matrix form is shown in the next page.

```
function busdt = busdatas(num)

%| Bus | Type |  Vsp  | theta | PGi |  QGi | PLi | QLi  | Qmin | Qmax |
busdat99 =
[1     1   1.000   0.0   371.4   206.8    0.0    0.0  -1000   1000
 2     3   1.000  -9.9    0.0     0.0     0.0    0.0    0.0    0.0
 3     3   0.995 -10.4    0.0     0.0     0.0    0.0    0.0    0.0
 4     3   0.994 -10.7    0.0     0.0     0.0    0.0    0.0    0.0
 5     3   0.995 -10.5    0.0     0.0     0.0    0.0    0.0    0.0
 6     3   0.994 -10.7    0.0     0.0     0.0    0.0    0.0    0.0
 7     3   0.989 -10.4    0.0     0.0     0.0    0.0    0.0    0.0
 8     3   0.990 -10.3    0.0     0.0     0.0    0.0    0.0    0.0
 9     3   1.000  -9.9    0.0     0.0     0.0    0.0    0.0    0.0
10     3   1.000  -9.9    0.0     0.0     0.0    0.0    0.0    0.0
11     3   0.997 -10.1    0.0     0.0     0.0    0.0    0.0    0.0
12     3   0.997 -10.2    0.0     0.0     0.0    0.0    0.0    0.0
13     3   0.989 -10.4    0.0     0.0     0.0    0.0    0.0    0.0
14     3   0.990 -10.3    0.0     0.0     0.0    0.0    0.0    0.0
15     3   0.985 -10.6    0.0     0.0     0.0    0.0    0.0    0.0
16     3   0.986 -10.5    0.0     0.0     0.0    0.0    0.0    0.0
17     3   0.992 -10.3    0.0     0.0     0.0    0.0    0.0    0.0
18     3   0.992 -10.8    0.0     0.0     0.0    0.0    0.0    0.0
19     3   0.977  15.2    0.0     0.0     0.0    0.0    0.0    0.0
20     3   0.977  15.2    0.0     0.0     0.0    0.0    0.0    0.0
21     3   0.990  16.5    0.0     0.0     0.0    0.0    0.0    0.0
22     3   0.989  16.2    0.0     0.0     0.0    0.0    0.0    0.0
23     3   0.984  16.3    0.0     0.0     0.0    0.0    0.0    0.0
24     3   0.986  16.9    0.0     0.0     0.0    0.0    0.0    0.0
25     3   0.982  16.7    0.0     0.0     0.0    0.0    0.0    0.0
26     3   0.979  15.2    0.0     0.0     0.0    0.0    0.0    0.0
27     3   0.978  15.2    0.0     0.0     0.0    0.0    0.0    0.0
28     3   0.993  17.1    0.0     0.0     0.0    0.0    0.0    0.0
29     3   0.982  14.9    0.0     0.0     0.0    0.0    0.0    0.0
30     3   0.983  14.9    0.0     0.0     0.0    0.0    0.0    0.0
31     3   0.987  15.2    0.0     0.0     0.0    0.0    0.0    0.0
32     3   0.986  15.2    0.0     0.0     0.0    0.0    0.0    0.0
33     3   0.986  15.2    0.0     0.0     0.0    0.0    0.0    0.0
34     3   0.990  15.8    0.0     0.0     0.0    0.0    0.0    0.0
35     3   0.990  15.8    0.0     0.0     0.0    0.0    0.0    0.0
36     3   0.981  15.2    0.0     0.0     0.0    0.0    0.0    0.0
37     3   0.981  15.2    0.0     0.0     0.0    0.0    0.0    0.0
38     3   0.979  17.7    0.0     0.0     0.0    0.0    0.0    0.0
39     3   0.976  15.8    0.0     0.0     0.0    0.0    0.0    0.0
40     3   0.970  15.8    0.0     0.0     0.0    0.0    0.0    0.0
41     3   0.985  16.1    0.0     0.0     0.0    0.0    0.0    0.0
42     3   0.985  16.7    0.0     0.0     0.0    0.0    0.0    0.0
43     3   0.984  16.7    0.0     0.0     0.0    0.0    0.0    0.0
44     3   0.982  15.8    0.0     0.0     0.0    0.0    0.0    0.0
45     3   0.978  15.3    0.0     0.0     0.0    0.0    0.0    0.0
46     3   0.986  15.9    0.0     0.0     0.0    0.0    0.0    0.0
47     2   1.000  15.2    0.0    23.4     0.0    0.0   30.0  -30.0
48     3   0.985  15.8    0.0     0.0     0.0    0.0    0.0    0.0
49     3   0.981  15.4    0.0     0.0     0.0    0.0    0.0    0.0
50     3   0.995  16.7    0.0     0.0     0.0    0.0    0.0    0.0
51     3   0.995  16.7    0.0     0.0     0.0    0.0    0.0    0.0
52     3   0.995  16.7    0.0     0.0     0.0    0.0    0.0    0.0
53     3   0.986  16.3    0.0     0.0     0.0    0.0    0.0    0.0
54     3   0.992  15.8    0.0     0.0     0.0    0.0    0.0    0.0
55     3   0.990  15.8    0.0     0.0     0.0    0.0    0.0    0.0
56     3   0.991  15.8    0.0     0.0     0.0    0.0    0.0    0.0
57     2   1.000  13.8    0.0    26.8     0.0    0.0   20.0  -20.0
58     3   0.994  16.7    0.0     0.0     0.0    0.0    0.0    0.0
59     3   0.994  16.7    0.0     0.0     0.0    0.0    0.0    0.0
60     3   1.013  17.7    0.0     0.0     0.0    0.0    0.0    0.0
61     3   0.991  15.8    0.0     0.0     0.0    0.0    0.0    0.0
62     3   0.991  15.8    0.0     0.0     0.0    0.0    0.0    0.0
63     3   0.979  15.2    0.0     0.0     0.0    0.0    0.0    0.0
```

```
64   3   0.982  15.2    0.0   0.0    0.0   0.0   0.0   0.0
65   3   0.983  15.2    0.0   0.0    0.0   0.0   0.0   0.0
66   3   0.978  15.2    0.0   0.0    0.0   0.0   0.0   0.0
67   3   0.977  15.2    0.0   0.0    0.0   0.0   0.0   0.0
68   3   0.981  15.2    0.0   0.0    0.0   0.0   0.0   0.0
69   3   0.981  15.2    0.0   0.0    0.0   0.0   0.0   0.0
70   3   0.981  15.2    0.0   0.0    0.0   0.0   0.0   0.0
71   3   0.992  16.6    0.0   0.0    0.0   0.0   0.0   0.0
72   3   0.992  16.6    0.0   0.0    0.0   0.0   0.0   0.0
73   3   0.993  17.1    0.0   0.0    0.0   0.0   0.0   0.0
74   3   0.993  17.1    0.0   0.0    0.0   0.0   0.0   0.0
75   3   0.819 -23.9    0.0   0.0   15.6  10.1   0.0   0.0
76   3   0.949 -19.2    0.0   0.0   15.6   4.0   0.0   0.0
77   3   0.934 -15.5    0.0   0.0    7.8   3.3   0.0   0.0
78   3   0.956 -19.1    0.0   0.0   15.0   3.3   0.0   0.0
79   3   0.969 -17.5    0.0   0.0   10.4   2.1   0.0   0.0
80   3   0.979 -17.0    0.0   0.0   12.7   3.3   0.0   0.0
81   3   0.985 -15.9    0.0   0.0    5.2   1.0   0.0   0.0
82   3   0.929 -18.6    0.0   0.0   17.8   9.8   0.0   0.0
83   3   0.945 -19.4    0.0   0.0   15.4   5.0   0.0   0.0
84   3   0.958 -17.4    0.0   0.0   17.4   6.7   0.0   0.0
85   3   0.953 -18.3    0.0   0.0   17.9   4.8   0.0   0.0
86   3   0.938 -20.4    0.0   0.0   17.7   5.9   0.0   0.0
87   3   0.952 -19.9    0.0   0.0   15.5   4.3   0.0   0.0
88   3   0.943 -21.8    0.0   0.0   21.5   5.4   0.0   0.0
89   3   0.929 -22.7    0.0   0.0   23.5   7.2   0.0   0.0
90   3   0.941 -18.6    0.0   0.0   15.5   8.6   0.0   0.0
91   3   0.977 -15.6    0.0   0.0    2.5   0.5   0.0   0.0
92   3   0.945 -18.9    0.0   0.0   17.5   7.2   0.0   0.0
93   3   0.968 -15.9    0.0   0.0    7.6   2.9   0.0   0.0
94   3   0.935 -21.0    0.0   0.0   23.0   8.6   0.0   0.0
95   3   0.950 -19.3    0.0   0.0   15.1   4.8   0.0   0.0
96   3   0.942 -19.4    0.0   0.0   15.9   5.7   0.0   0.0
97   3   0.962 -16.7    0.0   0.0    6.7   4.3   0.0   0.0
98   3   0.940 -18.5    0.0   0.0   15.2   6.3   0.0   0.0
99   3   0.983 -18.5    0.0   0.0   16.4   0.3   0.0   0.0];
switch num
case 99
busdt = busdat99;
end
```

The functions to input the line and transformer data in the matrix form is shown below.

```
%          |From| To |  R   |  X   |  B/2  | X'mer |
%          |Bus | Bus|  pu  |  pu  |  pu   | TAP (a)|
linedat99 =
        [ 1   2   0.0     0.1      0.0        1
          1   2   0.0     0.1      0.0        1
          2   3   0.00456 0.02278  0.00526    1
          3   5   0.00088 0.00123  0.01987    1
          2   4   0.00407 0.02030  0.00468    1
          2  10   0.00043 0.00097  0.00108    1
          2   9   0.00036 0.00082  0.00075    1
          2   7   0.01709 0.03743  0.02139    1
          2   8   0.01492 0.03264  0.01936    1
          2  17   0.01219 0.02745  0.00488    1
          4   6   0.00077 0.00108  0.01745    1
          4  18   0.00214 0.00487  0.00053    1
         17  68   0.01079 0.22809  0.01738    1
         18  68   0.01079 0.22528  0.00502    1
          6  31   0.00538 0.17062  0.01572    1
          5  31   0.00556 0.17199  0.04060    1
         31  97   0.03815 0.99178  0.00874    1
         31  97   0.03815 0.99178  0.00874    1
         31  30   0.06905 0.04896  0.0        1
         31  30   0.05204 0.04789  0.0        1
         31  30   0.07379 0.05227  0.0        1
         30  57   0.07071 0.06239  0.01816    1
         30  88   0.04065 1.01627  0.0        1
         30  88   0.04065 1.01627  0.0        1
         31  29   0.00553 0.00515  0.0        1
         29  30   0.01869 0.01772  0.05020    1
         29  87   0.03931 1.02212  0.0        1
         29  87   0.03931 1.02212  0.0        1
         31  32   0.00553 0.00515  0.0        1
         31  33   0.00562 0.00491  0.0        1
         31  65   0.03942 0.02002  0.0        1
         31  64   0.03216 0.02962  0.0        1
         64  68   0.01489 0.01296  0.0        1
         63  95   0.03754 0.97599  0.0        1
         65  95   0.03754 0.97599  0.0        1
         64  63   0.02866 0.02438  0.0        1
         32  89   0.03738 0.97178  0.0        1
         33  89   0.03738 0.97178  0.0        1
         10  50   0.00916 0.19837  0.0        1
         10  50   0.00898 0.19486  0.0        1
          9  50   0.00916 0.19458  0.0        1
          7  15   0.00646 0.02204  0.00412    1
          7  13   0.00033 0.00075  0.00008    1
          8  16   0.00687 0.02342  0.00438    1
          8  14   0.00033 0.00074  0.00008    1
         15  28   0.00690 0.23512  0.0        1
         16  28   0.00614 0.23710  0.0        1
         28  24   0.05708 0.05404  0.0        1
         28  25   0.07907 0.10776  0.0        1
         24  85   0.03715 0.92884  0.0        1
         25  85   0.03715 0.92884  0.0        1
         28  73   0.00102 0.00128  0.0        1
         28  74   0.00064 0.00118  0.0        1
         73  82   0.04160 1.03994  0.0        1
         74  82   0.04160 1.03994  0.0        1
         68  19   0.03327 0.03128  0.0        1
         68  20   0.03506 0.03115  0.0        1
         19  83   0.03738 0.97178  0.0        1
         19  83   0.03738 0.97178  0.0        1
         68  26   0.01781 0.01573  0.0        1
         68  27   0.01946 0.01732  0.0        1
         26  86   0.04112 1.02795  0.0        1
         27  86   0.04112 1.02795  0.0        1
         68  36   0.00812 0.00973  0.0        1
         68  37   0.00905 0.01085  0.0        1
         36  91   0.04280 1.07011  0.0        1
         37  91   0.04280 1.07011  0.0        1
         68  66   0.02434 0.02303  0.0        1
         68  67   0.03688 0.03804  0.0        1
         66  96   0.03640 0.94636  0.0        1
         67  96   0.03640 0.94636  0.0        1
         68  69   0.00146 0.00139  0.0        1
```

```
       68   70   0.00148   0.00141   0.0             1
       69   98   0.04060   1.01488   0.0             1
       70   98   0.04060   1.01488   0.0             1
       50   72   0.03516   0.03231   0.0             1
       50   71   0.04027   0.03701   0.0             1
       72   99   0.04193   1.04817   0.0             1
       71   99   0.04193   1.04817   0.0             1
       50   59   0.01682   0.01489   0.0             1
       50   58   0.01813   0.01616   0.0             1
       59   80   0.03926   0.98142   0.0             1
       58   80   0.03926   0.98142   0.0             1
       50   52   0.00047   0.00065   0.0             1
       50   51   0.00083   0.00111   0.0             1
       52   92   0.04353   1.08815   0.0             1
       51   92   0.04353   1.08815   0.0             1
       50   43   0.11105   0.09660   0.0             1
       50   42   0.10250   0.12748   0.0             1
       43   77   0.03873   0.96832   0.0             1
       42   77   0.03873   0.96832   0.0             1
       50   53   0.04338   0.07157   0.0             1
       23   53   0.01777   0.02198   0.0             1
       53   93   0.03832   0.99635   0.0             1
       53   93   0.03832   0.99635   0.0             1
       50   22   0.05707   0.08994   0.0             1
       50   21   0.04531   0.07740   0.0             1
       23   84   0.04385   1.09623   0.0             1
       22   84   0.04385   1.09623   0.0             1
       21   84   0.04385   1.09623   0.0             1
        2   11   0.00617   0.01328   0.01638         1
        2   12   0.00650   0.01399   0.01763         1
       11   54   0.01070   0.22350   0.0             1
       12   54   0.01070   0.22350   0.0             1
       54   62   0.01306   0.00936   0.0             1
       54   61   0.01498   0.01077   0.0             1
       62   81   0.04146   1.07797   0.0             1
       61   81   0.04146   1.07797   0.0             1
       54   56   0.00771   0.00709   0.0             1
       54   55   0.00994   0.00922   0.0             1
       56   94   0.03856   0.96407   0.0             1
       55   94   0.03856   0.96407   0.0             1
       54   35   0.01229   0.01250   0.0             1
       54   34   0.01693   0.01601   0.0             1
       35   90   0.03728   0.93198   0.0             1
       34   90   0.03728   0.93198   0.0             1
       54   47   0.04317   0.03490   0.0             1
       54   48   0.03939   0.04722   0.0             1
       13   60   0.01317   0.30238   0.0             1
       14   60   0.01317   0.30238   0.0             1
       50   46   0.06296   0.10334   0.0             1
       60   41   0.27301   0.37173   0.0             1
       60   38   0.10769   0.10741   0.0             1
       38   75   0.04256   1.06387   0.0             1
       46   41   0.04203   0.08116   0.0             1
       49   79   0.03773   0.98093   0.0             1
       48   79   0.03773   0.98093   0.0             1
       49   45   0.03991   0.03175   0.0             1
       45   78   0.04050   1.01250   0.0             1
       44   78   0.04050   1.01250   0.0             1
       46   44   0.02255   0.01976   0.0             1
       48   44   0.03335   0.03706   0.0             1
       54   49   0.06576   0.08171   0.0             1
       44   39   0.01986   0.01806   0.0             1
       41   40   0.08393   0.08699   0.0             1
       40   76   0.04008   1.04200   0.0             1
       39   76   0.04008   1.04200   0.0            1];

switch num
    case 99
        linedt = linedat99;
end
```

The following shows the lines concerning the initialisation of the power flow.

```
%Line Power Flows.
 for m = 1:nb (number of buses)
     for n = 1:nb
         if m ~= n
             Sij(m,n) = Vm(m)*conj(Iij(m,n))*BMva;
end
 Pij = real(Sij);
 Qij = imag(Sij);

 %Line Losses.
 Lij = zeros(nl,1);
 for m = 1:nl
     p = fb(m); q = tb(m);
     Lij(m) = Sij(p,q) + Sij(q,p);
 end
Lpij = real(Lij);
Lqij = imag(Lij);

%Bus Power Injections.
Si = zeros(nb,1);
for i = 1:nb
    for k = 1:nb
        Si(i) = Si(i) + conj(Vm(i))* Vm(k)*Y(i,k)*BMva;
    end
end
Pi = real(Si); Qi = -imag(Si); Pg = Pi+Pl; Qg = Qi+Ql;
```

The calculation of the power flows and the returned output functions are demonstrated below.

```
%Calculate Active Power (P) and Reactive Power (Q)
    for i = 1:nbus
        for k = 1:nbus
            P(i) = P(i) + V(i)* V(k)*(G(i,k)*cos(del(i)-del(k)) + B(i,k)*sin(del(i)-del(k)));
            Q(i) = Q(i) + V(i)* V(k)*(G(i,k)*sin(del(i)-del(k)) - B(i,k)*cos(del(i)-del(k)));
        end
    end
%Checking violations for reactive power
    if Iter <= 7 && Iter > 2    % Only checked up to 7th iterations.
        for n = 2:nbus
            if type(n) == 2
                QG = Q(n)+Ql(n);
                if QG < Qmin(n)
                    V(n) = V(n) + 0.01;
                elseif QG > Qmax(n)
                    V(n) = V(n) - 0.01;
                end
```

```
        end
      end
   end
disp('                          Newton Raphson Load-flow Analysis ');
disp('| Bus |    V   |  Angle  |     Injection    |    Generation   |       Load      |');
disp('| No  |   pu   |  Degree |   MW   |  MVar  |   MW   |  Mvar   |      MW     |    MVar  |
');
for m = 1:nb
    fprintf('%3g', m); fprintf('  %8.4f', V(m)); fprintf('   %8.4f', Del(m));
    fprintf('  %8.2f', Pi(m)); fprintf('    %8.2f', Qi(m));
    fprintf('  %8.2f', Pg(m)); fprintf('    %8.2f', Qg(m));
    fprintf('  %8.2f', Pl(m)); fprintf('    %8.2f', Ql(m)); fprintf('\n');
end
fprintf(' Total                   ');fprintf('  %8.3f', sum(Pi)); fprintf('    %8.3f', sum(Qi));
fprintf('  %8.3f', sum(Pi+Pl)); fprintf('    %8.3f', sum(Qi+Ql));
fprintf('  %8.3f', sum(Pl)); fprintf('    %8.3f', sum(Ql)); fprintf('\n');


disp('                          Line Flow and Losses ');
disp('|From|To |    P    |    Q    | From| To |    P    |    Q    |      Line Loss      |');
disp('|Bus |Bus|   MW    |   MVar  | Bus | Bus|   MW    |   MVar  |    MW   |    MVar  |');
for m = 1:nl
    p = fb(m); q = tb(m);
fprintf('%4g', p); fprintf('%4g', q); fprintf('  %8.2f', Pij(p,q)); fprintf('   %8.2f', Qij(p,q));
fprintf('    %4g', q); fprintf('%4g', p); fprintf('    %8.2f', Pij(q,p)); fprintf('    %8.2f',
Qij(q,p));
fprintf('  %8.2f', Lpij(m)); fprintf('    %8.2f', Lqij(m));
fprintf('\n');
end
fprintf('    Total Loss                                      ');
fprintf('  %8.3f', sum(Lpij)); fprintf('    %8.3f', sum(Lqij));  fprintf('\n');
```

B. Mathematical Modelling of Battery Chargers

This section presents the characteristics and data that were utilised in **Chapter 4** to model grid-connected battery charger systems. Additionally, the derivation of the phase-angle tracking PLL mechanism, the outer and inner current controller loops, as well as the design criteria of grid-connected filters are presented. It should be mentioned that the procedure for designing the equivalent Shepherd model is acquired from the *Manitoba Hydro International Limited's Power Systems Technology Centre* in [45, 46].

B.1 Shepherd Battery Model Specifications

The ideal open-circuit voltage regulated battery employed in this research is a generic Shepherd battery model available in the PSCAD/EMTDC simulation software library. The generic model's details may be found in [46]. The following assumptions and limitations have been considered for the ideal equivalent Shepherd battery model circuit (as seen in **Figure 4.7**) throughout the computer-based simulation cases:

Assumptions:

- The internal resistance of the battery is constant during charging and discharging cycles.

- The charging and discharging characteristics of the battery are assumed to be the same.

- The battery model's behaviour is not affected by the temperature.

- The battery may be simulated many times without losing its capacity (no deterioration).

- The battery cannot self-charge or discharge.

- The nominal voltage, rated capacity, initial state of charge, and loss of capacity at nominal current in an hour can be adjusted prior to simulation.

Limitations:

- The battery voltage cannot be negative, and the maximum battery voltage is not limited.

- The capacity of the battery cannot be negative, and hence the maximum capacity is not limited.

Default internal parameters of the Shepherd battery model used for charging and discharging are shown in Table B.1.

Table B.1: Shepherd battery model internal parameters

Nominal Capacity (p.u.)	Resistive Drop (p.u.)	Voltage at Exponential Point (p.u.)	Capacity at Exponential Point (p.u.)	Fully Charged Voltage (p.u.)
0.95	0.005	1.03	0.4	1.15

B.2 Phase-Locked Loop

The PLL operates on the fundamental principle of a feedback system with a proportional-integral (PI) regulator monitoring the phase angle (ϕ) at the PCC [264]. Synchronous reference frame (SRF) based PLL is widely used approach in three-phase applications due to its popularity and simplicity of implementation [265]. The schematic diagram of a standard SRF-PLL system is shown in Figure B.1.
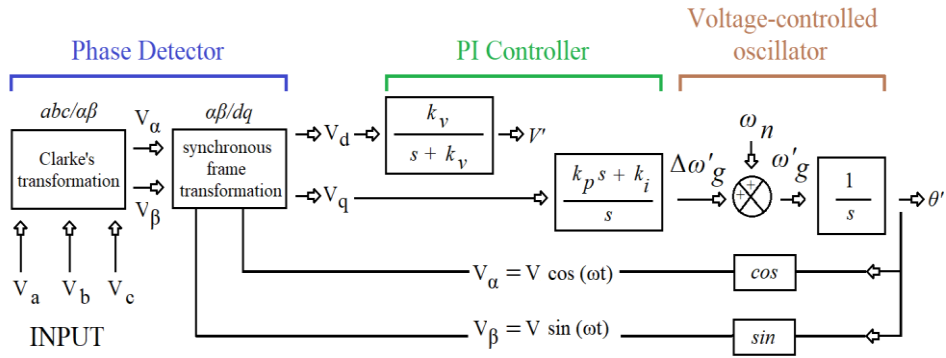
Figure B.1: Basic structure for the SRF based PLL system.

The SRF-PLL incorporates a phase detector, a loop filter made up of PI controller blocks with tuneable proportional (k_p) and integral gain (k_i) variables, and a voltage-controlled oscillator. The phase detector is implemented by applying the Clarke's transformation to the input three-phase grid voltages, followed by Park's transformation. The PLL aligns the *d-axis* with the grid voltage, and the phase detector's output (V_q) is sent into the PI controller. The PI controller generates an estimated frequency signal, which is then sent through the voltage-controlled oscillator to generate the estimated phase angle (ϕ′) from the PCC [265]. The three phases of the grid voltages are fed into the PLL, and the output is the phase angle of one of the three phases.

The *abc* to *dq* transformation is deduced mathematically. Let the voltages on the three-phase grid side be represented by (B.1) to (B.3).

$$V_a(t) = V_{amp}\cos(\phi) \tag{B.1}$$

$$V_b\ (t) = V_{amp}\ \ (\phi - \frac{2\pi}{3})$$ (B.2)

$$V_c\ (t) = V_{amp}\ \ (\phi + \frac{2\pi}{3})$$ (B.3)

Where:

V_{amp} is the amplitude of the three-phase voltage signals (V).

Considering the Clarke's and Park's transformations as:

$$T_{abc \to \alpha\beta} = \frac{2}{3}\begin{bmatrix} 1 & -\frac{1}{2} & -\frac{1}{2} \\ 0 & -\frac{\sqrt{3}}{2} & \frac{\sqrt{3}}{2} \end{bmatrix}$$ (B.4)

$$T_{\alpha\beta \to dq} = \begin{bmatrix} cos\ (\phi') & sin\ (\phi') \\ -sin(\phi') & cos\ (\phi') \end{bmatrix}$$ (B.5)

Where:

ϕ' is the estimated phase angle and output of the oscillator.

Equations (B.4) and (B.5) may be inserted into (B.3) by carrying out the following multiplication:

$$V_{\alpha\beta} = T_{\alpha\beta} V_{abc}$$ (B.6)

The *dq* frame voltage variables are obtained as:

$$V_d\ (t) = V_{amp}\ cos\ (\phi - \phi')$$ (B.7)

$$V_q\ (t) = V_{amp}\ sin\ (\phi - \phi')$$ (B.8)

Where:

$$\phi = \int \omega_g dt = \int (\omega_n + \Delta\omega_g) dt$$ (B.9)

$$\phi' = \int \omega'_g dt = \int (\omega_n + \Delta\omega'_g) dt$$ (B.10)

Where:

ω'_g is the estimated frequency by the PLL (Hz),

ω_n is the nominal frequency (Hz),

$\Delta\omega'_g$ is the damped transient response in the estimated frequency (Hz).

Substituting (B.10) into (B.9) yields the following expressions for d and q frame voltages.

$$V_d\,(t) = V\cos\,(\Delta\phi - \phi') \approx V \tag{B.11}$$

$$V_q\,(t) = V\sin\,(\Delta\phi - \phi') \approx V\,(\Delta\phi - \phi'). \tag{B.12}$$

The output of the phase detector, notable V_q, contains the phase error information that passes through the PI controllers, whereas signal V_d is a measure of the amplitude of the three-phase signals. More explanation and performance of other PLL systems are given in [259, 260].

B.3 Outer Controllers

Outer controllers have four input signals: AC voltage (V_{AC}), active power (P_{AC}), reactive power (Q_{AC}) and DC voltage (V_{DC}). These controller loops generate two-phase *dq* frame reference current variables: $I*_d$ and $I*_q$, as represented in Figure B.2 and Figure B.3, respectively.
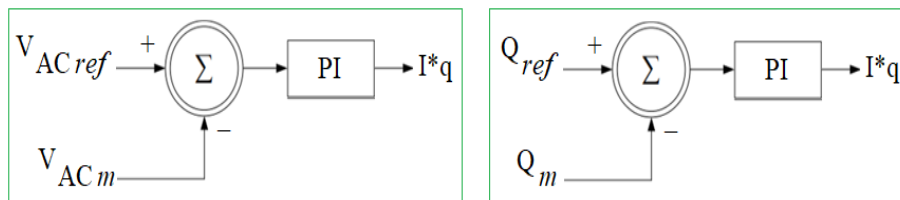
Figure B.2: Outer controller loops that produce $I*_q$.
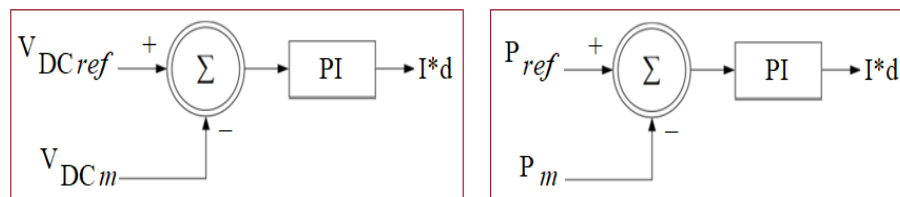
Figure B.3: Outer controller loops that produce $I*_d$.

The first loop on the left computes the difference between reference AC voltage ($V_{AC\,ref}$) and measured AC voltage ($V_{AC\,m}$), whereas the second loop computes the error signal between reference reactive power (Q_{ref}) and measured reactive power (Q_m) from the PCC in Figure B.2. Because both loops produce the same output: $I*_q$, only one of the AC voltage or reactive power loops is modelled at once [261, 262].

The third and fourth loops compare reference DC voltage ($V_{DC\,ref}$) with measured DC voltage ($V_{DC\,m}$), and reference active power (P_{ref}) with measured active power (P_m), respectively. These loops are used to produce $I*_d$.

B.4 Inner Current Controller Loops

Inner controllers have six input signals: *d* and *q* frame current and voltage variables (I_d, I_q, V_d, V_q), and the outputs of the outer controller loops ($I*_d$ and $I*_q$). Inner loops produce two-phase reference voltage variables: $V*_d$ and $V*_q$, as seen in Figure B.4.
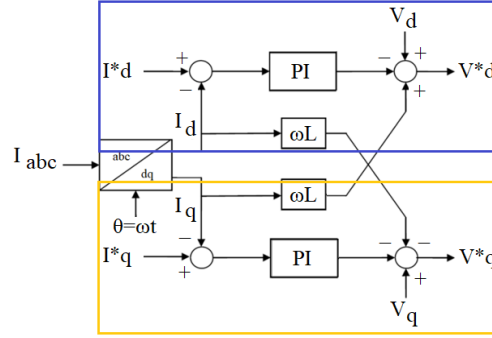
Figure B.4: Schematic of inner current controller loops.

The upper and lower loops compute the difference between $I*_d$ and I_d, and $I*_q$ and I_q, respectively. They are then sent into the PI controllers to obtain error signals. These error signals are subtracted from the summation of $V_d + I_q\omega L$ and $V_q - I_d\omega L$ to produce $V*_d$ and $V*_q$ for the upper and lower loops, respectively. Inner controller loops may be mathematically modelled by applying Kirchhoff's voltage law along the PCC line. As a result, the three-phase grid voltages are as follows:

$$V_{abc} = V_{abc\_con} + Ri_{abc} + L\frac{d}{dt}i_{abc} \tag{B.13}$$

Where:

V_{abc_con} is the input terminal voltage of the rectifier,

R and L are the resistance and inductance along the PCC line, respectively.

Three-phase grid voltages are transformed to two-phase *αβ* frame and then to two-phase *dq* frame variables. Equation (B.13) may be rewritten as:

$$V_{\alpha\beta} = V_{\alpha\beta\_con} + Ri_{\alpha\beta} + L\frac{d}{dt}i_{\alpha\beta} \tag{B.14}$$

Given that the *dq* frame variables rotate with angular frequency (ω), the position of these with respect to *αβ* determines the angular position with respect to time (ωt) [261, 262]. As a result of Park's transformation, the following expression is obtained in (B.15):

$$V_{dq}e^{j\omega t} = V_{dq\_con}e^{j\omega t} + Ri_{dq}e^{j\omega t} + L\frac{d}{dt}i_{dq}e^{j\omega t} \tag{B.15}$$

To simplify, the $e^{j\omega t}$ terms may be omitted:

$$V_{dq} = V_{dq\_con} + Ri_{dq} + L\frac{d}{dt}i_{dq} + j\omega L i_{dq} \tag{B.16}$$

Further simplification is possible by decoupling the *dq* variables [262, 263]:

$$\begin{bmatrix} V*_d \\ V*_q \end{bmatrix} = \begin{bmatrix} v_d \\ v_q \end{bmatrix} + R\begin{bmatrix} i_d \\ i_q \end{bmatrix} + L\frac{d}{dt}\begin{bmatrix} i_d \\ i_q \end{bmatrix} + \omega L \begin{bmatrix} 0 & 1 \\ -1 & 0 \end{bmatrix}\begin{bmatrix} i_d \\ i_q \end{bmatrix} \tag{B.17}$$

By solving for the matrix, the following equations are obtained:

$$V*_d = V_d + Ri_d + L\frac{d}{dt}i_d + \omega L i_q \tag{B.18}$$

$$V*_q = V_q + Ri_q + L\frac{d}{dt}i_q - \omega L i_d \tag{B.19}$$

As also illustrated in the modelling of inner current controller loops (see **Figure B.4**), (B.18) and (B.19) are related via the decoupling terms of $\omega L i$ and Ri.

B.5 Buck–boost Converter Controller Loops

The charging and discharging of buck–boost converters are shown in Figure B.5.
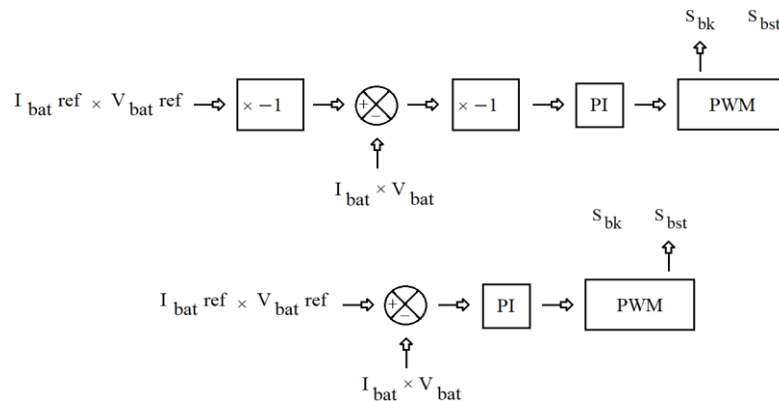
Figure B.5: Controller loops for buck (top) and boost (below) switching.

The control system can be manually controlled to charge and discharge the battery and regulate the amount of power during charging and discharging modes. When the converter is in charging mode, the buck converter is active, and the reference power ($P_{ref} = I_{bat\_ref} \times V_{bat\_ref}$) is compared to the battery side power ($P_{bat} = I_{bat} \times V_{bat}$).

When the converter is in discharging mode, the boost converter is active, but in the reversed current direction, dictated by $P_{ref} - P_{bat}$ in the loop arrangement schematic. Both loops generate error signals that are supplied to the PI controllers in order to define the mode of operation through the PWM scheme [270, 271].

B.6 Filtering of Battery Chargers

Since battery charger systems are made up of a variety of different power electronic devices and components, they may affect the operating features of distribution grids and introduce various power quality issues. By including an active power factor correction converter, the line current is reshaped proportionate to the input voltage and the line current harmonics are reduced to acceptable levels. Another widely used harmonic mitigation approach in the literature is using a resonant filter. It is often employed in high-power systems when the cost of an active power factor correction is excessively high and impairs system reliability. Active power factor correction strategy uses semiconductor switches and energy storage components (inductors and/or capacitors) to monitor the input voltage and provide a semi-regulated output voltage [297].

This thesis adapts the latter method and designs a filter located within the charger circuitry. The design requirements for the filter are also available in [298]. The design of an appropriate LC filter circuit (consisting of inductors and capacitors) is an effective method for mitigating harmonic distortion, eliminating undesirable frequency components, and suppressing unwanted noise (high frequency signal) introduced into the grid. This method is widely used in grid-connected applications and this thesis presents a strategy for designing LCL filters for AC and DC battery chargers.

The first 'L', notably, the rectifier side inductance (L_{rec}) in an LCL filter for a three-phase grid-connected rectifier is determined initially using (B.20) [297–301]:

$$L_{rec} = \frac{V_{DC}}{8 \times f_{sw} \times I_{pp}} \tag{B.20}$$

Where:

f_{sw} is the rectifier's switching frequency (kHz),

I_{pp} is the peak-to-peak amplitude of the ripple current (kA).

The carrier frequency (C_{freq}) as multiple of fundamental frequencies is related to the switching frequency and is calculated according to (B.21).

$$C_{freq} = \frac{f_{sw}}{f} \tag{B.21}$$

Where:

f is the nominal system frequency (Hz).

The switching frequency, which usually varies between a few kHz and a few MHz, is the rate at which the IGBT switches are turned on and off [300]. Once the switching frequency of the rectifier is determined, the peak-to-peak current is also determined [298], as given by (B.22):

$$I_{pp} = \frac{S_{base}}{\sqrt{3} \times V_{L-L,rms}} \times \sqrt{2} \times 20\% \tag{B.22}$$

Where:

S_{base} is the rectifier's rated power (MVA),

$V_{L-L,rms}$ is the RMS line-to-line voltage at the connection point (kV).

The multiplication of the peak-to-peak current with 20% is also performed, since the amplitude of the ripple current is assumed to be 20% of the rated current as per design criteria highlighted in [298, 299, 301]. The peak maximum current is also calculated by multiplying the amplitude of the ripple current by the square root of two.

A cut-off frequency (f_{co}) is chosen to provide adequate filtering up to the nth order and to filter any frequencies greater than the 'n[th]' order harmonic. Equation (B.23) is used to calculate the filter capacitance (C_{filter}) required to achieve a certain cut-off frequency:

$$C_{filter} = \frac{1}{(2 \times \pi \times f_{co})^2 \times L_{rec}} \tag{B.23}$$

The frequency of 200 Hz is selected as the cut-off frequency in this thesis, which is also a frequent design requirement for battery charger-based applications [298]. Additional design criteria, including the employment of a damping circuit with damping capacitance (C_{damp}), damping inductance (L_{damp}), and damping resistance (R_{damp}), is also used to minimise oscillations in the output waveforms [298, 301]. These damping parameters are determined as follows:

$$C_{damp} = \frac{C_{filter}}{2} \tag{B.24}$$

$$L_{damp} = L_{rec} \times 5 \tag{B.25}$$

$$R_{damp} = \sqrt{\frac{L_{damp}}{C_{damp}}} \tag{B.26}$$

The data for harmonic filtering that is included within the charging circuit is presented in Table B.4. The design requirements for the filter are available in [298].

Table B2: Calculated filter parameters for chargers

L_{rec} (mH)	f_{sw} (kHz)	I_{pp} (kA)	f_{co} (kHz)	C_{filter} (μF)	C_{damp} (μF)	L_{damp} (mH)	R_{damp} (Ω)
0.46	3.35	0.083	0.2	1380	690	2.3	1.83

B.7 Switching Parameters for Controller Loops

The data for the semiconductor switches and other power electronic components for the modelling of single-phase and three-phase battery chargers are obtained from [45]. The high-frequency IGBT switches and diodes are sufficiently sized to achieve high-power charging from the battery. Table B.3 and Table B.4 present the data for power electronics and switching for AC/DC converters and DC/DC converters, respectively.

Table B.3: Switching data for AC/DC converters

IGBT Label	IGBT Rating	Diode Label	Diode Rating
Thyristor ON Resistance	0.0005 Ω	Thyristor ON Resistance	0.0005 Ω
Thyristor OFF Resistance	1.0E8 Ω	Thyristor OFF Resistance	1.0E8 Ω
Forward Voltage Drop	0 kV	Forward Voltage Drop	0 kV
Forward Breakover Voltage	1.0E5 kV	Forward Breakover Voltage	1.0E5 kV
Reverse Withstand Voltage	1.0E5 kV	Reverse Withstand Voltage	1.0E5 kV

Table B.4: Switching data for DC/DC converters

IGBT Label	IGBT Rating	Diode Label	Diode Rating
Thyristor ON Resistance	1.4e−4 Ω	Thyristor ON Resistance	1.4e−4 Ω
Thyristor OFF Resistance	1.0E6 Ω	Thyristor OFF Resistance	1.0E6 Ω
Forward Voltage Drop	1.9e−3 kV	Forward Voltage Drop	1.2e−3 kV
Forward Breakover Voltage	17 kV	Forward Breakover Voltage	12 kV
Reverse Withstand Voltage	17 kV	Reverse Withstand Voltage	12 kV

C. Low-Voltage British Distribution Network

This section presents the parameters and data that were used in **Chapter 5** to model and analyse the MV/LV distribution network feeder utilising the line and demand profiles of residential and commercial customers acquired from [47].

C.1 Schematic Diagram

The top and bottom structures of the low-voltage network diagram supplied by WPD, now National Grid Distribution are shown in Figure C.1 and Figure C.2, respectively.

Figure C.1: Upper section of the low-voltage network showing the locations of Nodes N1 to N8.
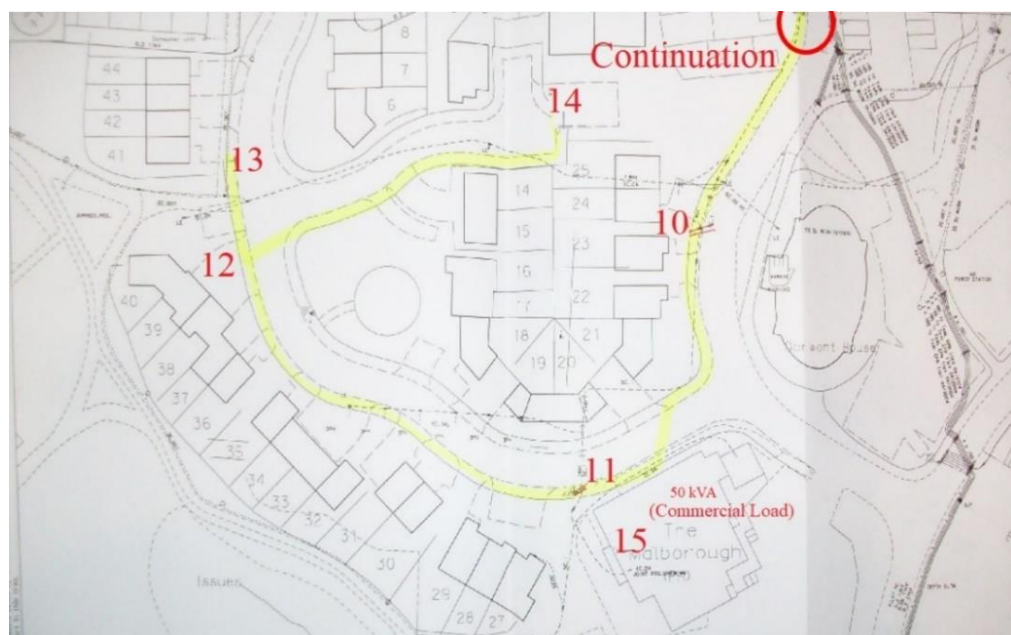
Figure C.2: Lower section of the low-voltage network showing the locations of Nodes N10 to N15.

C.2 Underground Cable Data

Table C.1 contains the cable specification provided by the National Grid Distribution for the low-voltage network feeder under examination.

Table C.1: Low-voltage distribution network cable specification

Between Nodes	Type	Length (m)	Size (in^2)	Size (mm^2)
Substation and 1	Copper	10	0.3	193.548
1 and 2	Copper	10	0.3	193.548
2 and 3	Copper	30	0.1	64.516
3 and 4	Copper	30	0.1	64.516
4 and 5	Copper	30	0.06	38.7096
3 and 6	Copper	30	0.06	38.7096
4 and 7	Copper	35	0.06	38.7096
5 and 8	Copper	50	0.06	38.7096
2 and 10	Copper	65	0.3	193.548
10 and 11	Wavecon	40	0.14725	95
11 and 12	Wavecon	70	0.14725	95
12 and 13	Wavecon	30	0.04	25.8064
12 and 14	Wavecon	40	0.14725	95
11 and 15	Copper	20	0.04	25.8064

C.3 Updated Cable Data for Loading Mitigation

Following the overloading of two cables, namely C10-11 and C11-15, the initial loading mitigation solution used increased conductor sizes. Low-voltage service cables are often installed underground to link residential and business premises to the grid [302] in compliance with BS7870. Due to the lack of existing cable design and installation procedures, WPD's Standard Technique: Relating to Low Voltage Underground Cable Ratings [48] was utilised to establish the new cable size. The installation parameters for an urban British distribution network are shown in Table C.2.

Table C.2: Considered cable installation conditions and parameters for the network

Rating	Depth (m)	Ambient Temperature (°C)	Ground Temperature (°C)	Conductor Temperature (°C)	Resistivity (°C m/W)
Distribution	0.5	10	10	90 XLPE 70 PVC	0.9

Distribution ratings are considered for stated conditions that are often encountered in distribution networks. Other parameters were specified based on distribution ratings for the winter season, when demand is greater than in the summer [277]. Additionally, it was assumed that the cables were put in multicore arrangement in open air since the design criteria for the installation approach in [48] were quite identical and hence comparable to the original cable specifications provided by the WPD.

D. Charging Curves and Algorithm Development

This part presents the charging profiles used to calculate the average charging power and energy consumption of vehicles. Additionally, the script for introduction of the structure, and randomisation and estimation of the vehicle parameters is presented.

The relevant data from [49] and [50] was acquired for calculating the daily distribution of charging events in the UK. The time distribution of charging events was used to generate stochastic charging profiles depending on the time of the day.

D.1 Real-World Charging Curves of the Electric Vehicle Models

BMW i3 (2019), Audi e-Tron (2020), Kia e-Niro 4 (2020), Jaguar I-Pace (2019), and Tesla Model 3 Performance (2021) were among the selected vehicles for the algorithm. The original charging profiles with respect to the battery SoC for BMW i3, Kia e-Niro, Audi e-Tron 55 quattro, Jaguar I-Pace and Tesla Model 3 models on their associated charging devices are presented in Figure D.1 through Figure D.5, respectively.
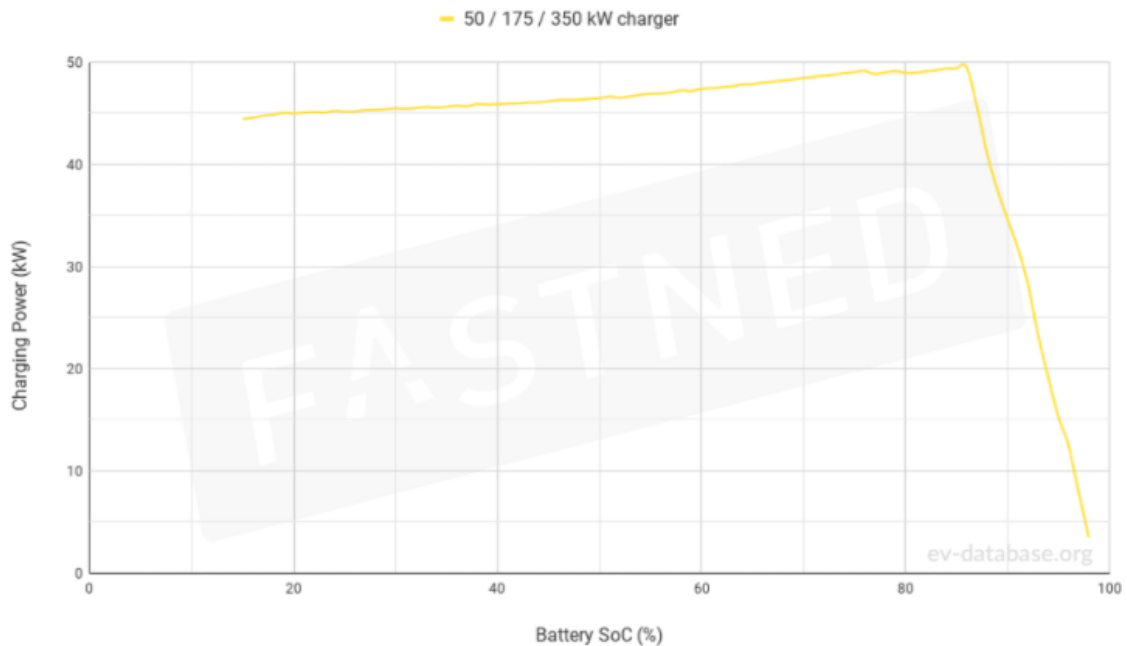
Figure D.1: Charging characteristics of BMW i3 models on different CCS devices [242].

All BMW i3 models, regardless of charger rating, have the identical charging behaviour on 50/175/350-kW CCS devices. Nevertheless, it should be emphasised that the charging characteristics of these BMW automobiles are prone to change as battery technology advances. This indicates that the maximum theoretical power the vehicle may get from each battery SoC interval can be improved.
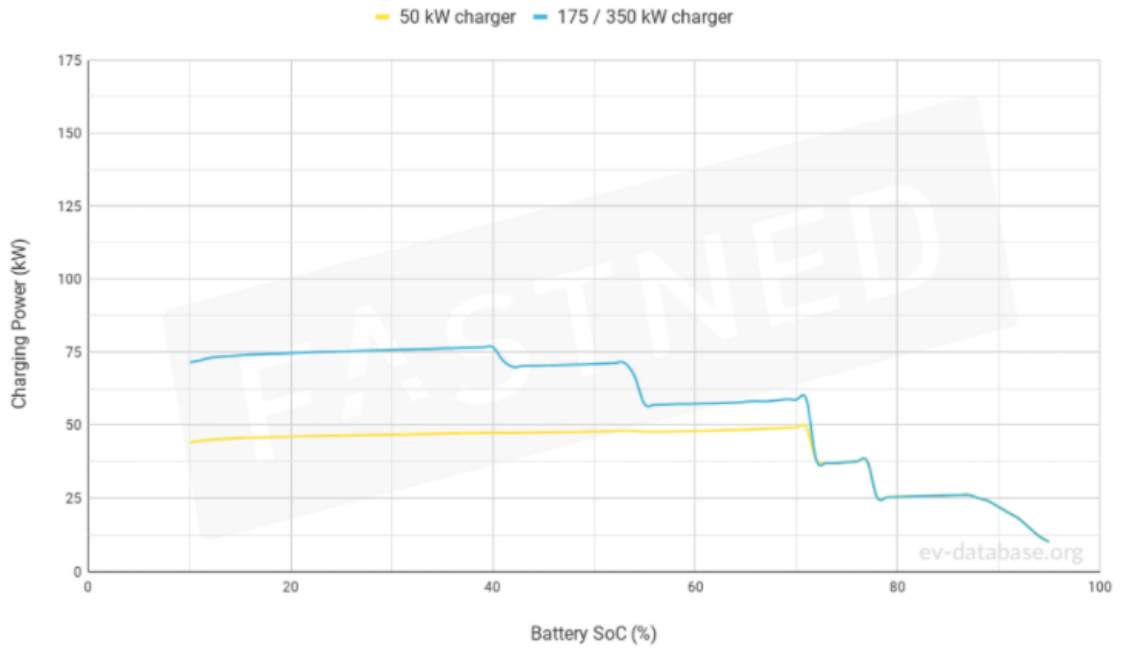
Figure D.2: Charging characteristics of Kia e-Niro 4 models on different CCS devices [242].

The Kia e-Niro 4 model can be charged at a CCS device of 50/175/350 kW. However, the theoretical power provided to the vehicle is limited to 75 kW on a 175- and 350-kW device. This study used the assumption that Kia models charged only using the 50-kW.
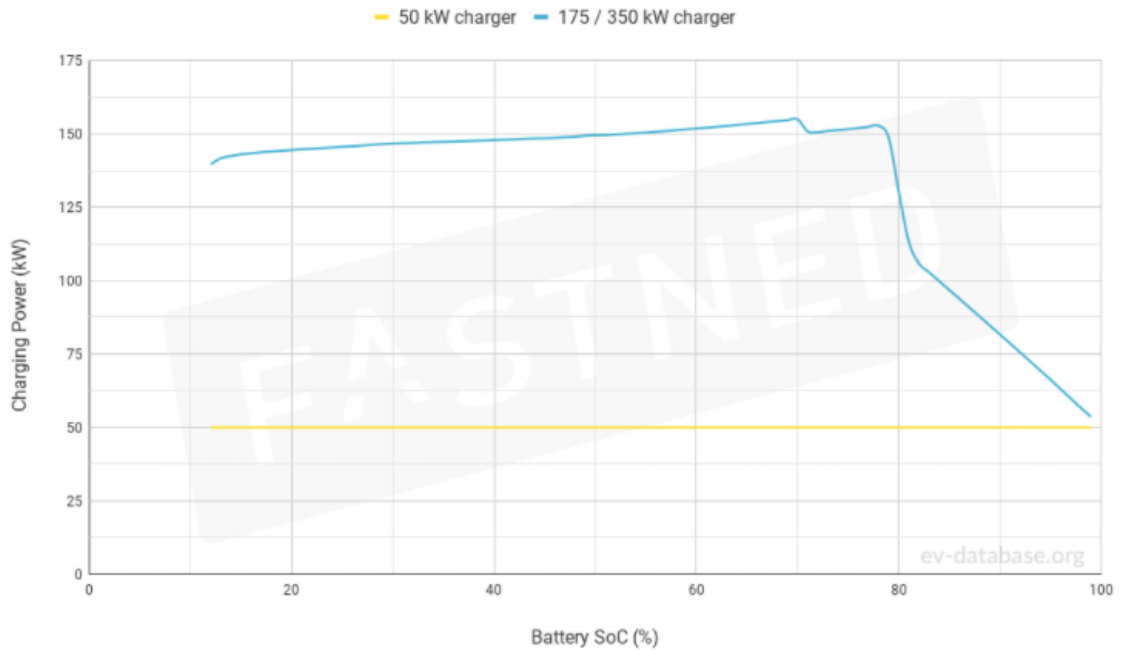
Figure D.3: Charging characteristics of Audi e-Tron 55 quattro on different CCS devices [242].
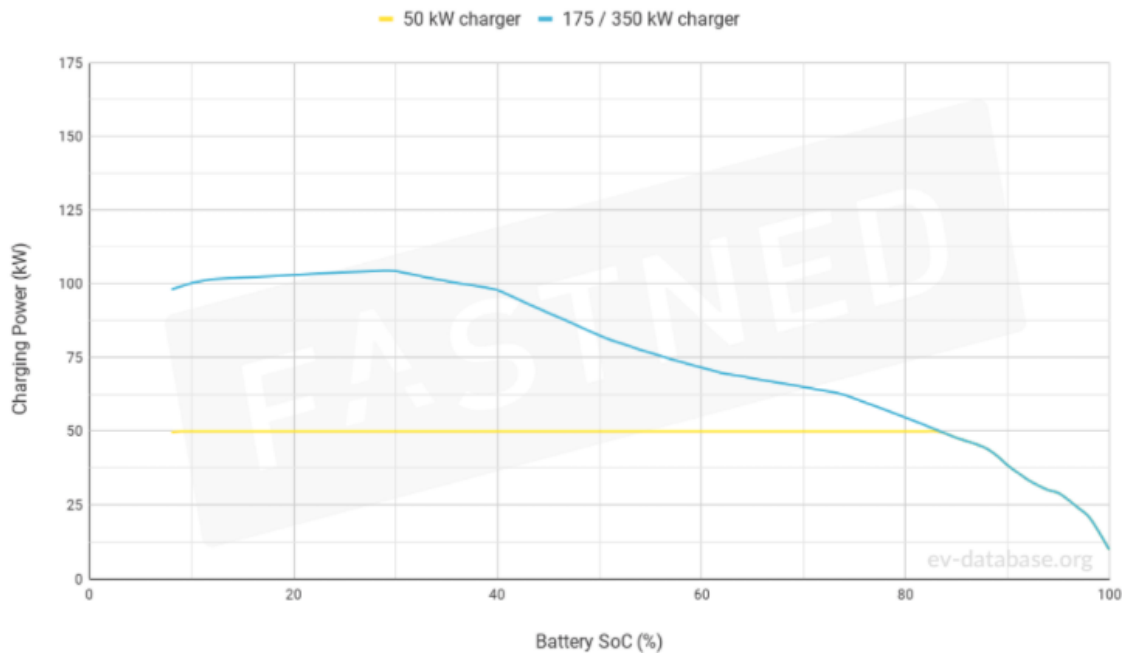
Figure D.4: Charging characteristics of Jaguar I-Pace on different CCS devices [242].

This study assumed that both Audi and Jaguar models charged only on the 175-kW device to add the operation of ultra-rapid chargers into the algorithm.
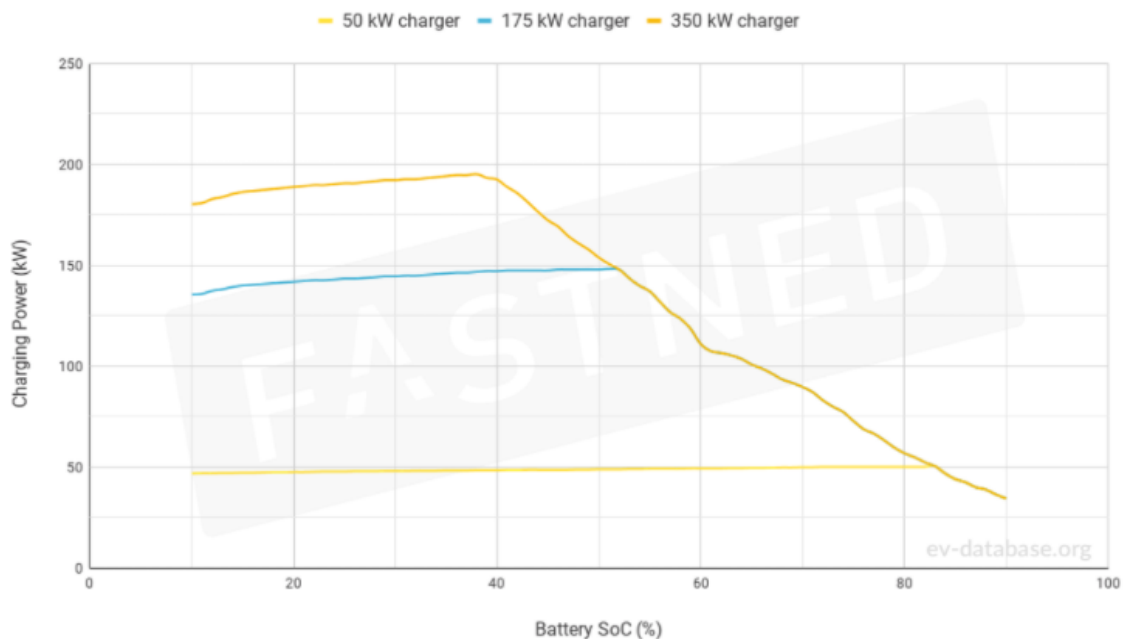
Figure D.5: Charging characteristics of Tesla Model 3 on different CCS devices [242].

Unlike the other four models, Tesla models have somewhat distinct charging profiles. Initially, the graph only shows charging power up to 90% of the battery's charge level. Additionally, it should be noted that each of these charging profiles represents a generic charging characteristic. As described in **Section 6.3.2**, various variables affect the speed of charging. It is anticipated that as battery and vehicle technology advances, charging profiles will be adjusted and cars will be able to take more power.

D.2 DENO Runtime Codes for the Algorithm

The establishment of the structure of inputs and objects in the algorithm script is presented in this part.

```typescript
import { Vehicle } from './Vehicle.ts';
import { VehicleData } from './typings/data.ts';

class VehicleFactory {
    make({
        amount,
        battery,
        make,
        range,
        tenToEightyChargingTime,
        power
    }: VehicleData): Array<Vehicle> {
        return Array(amount)
            .fill(null)
            .map(
                (_, idx) =>
                    new Vehicle(
                        battery,
                        idx + 1,
                        make,
                        range,
                        tenToEightyChargingTime,
                        power
                    )
            );
    }
}

export const vehicleFactory = new VehicleFactory();
```

```json
[
    {
        "amount": 4,
        "battery": { "average": 47, "capacity": 42 },
        "make": "BMW",
        "power": {
            "average": 44,
            "max": 47,
            "min": 40
        },
        "range": 310000,
        "tenToEightyChargingTime": 36
    },
```

```
{
    "amount": 6,
    "battery": { "average": 45, "capacity": 64 },
    "make": "Kia",
    "power": {
        "average": 45,
        "max": 45,
        "min": 45
    },
    "range": 453800,
    "tenToEightyChargingTime": 63
},
{
    "amount": 8,
    "battery": { "average": 85, "capacity": 90 },
    "make": "Jaguar",
    "power": {
        "average": 63,
        "max": 85,
        "min": 40
    },
    "range": 470000,
    "tenToEightyChargingTime": 44
},
{
    "amount": 5,
    "battery": { "average": 146, "capacity": 95 },
    "make": "Audi",
    "power": {
        "average": 146,
        "max": 146,
        "min": 146
    },
    "range": 436000,
    "tenToEightyChargingTime": 26
},
{
    "amount": 7,
    "battery": { "average": 121, "capacity": 79.5 },
    "make": "Tesla V2",
    "power": {
        "average": 100,
        "max": 124,
        "min": 75
    },
    "range": 507000,
    "tenToEightyChargingTime": 27
},
{
    "amount": 4,
```

```
        "battery": { "average": 145, "capacity": 79.5 },
        "make": "Tesla V3",
        "power": {
            "average": 112,
            "max": 148,
            "min": 75
        },
        "range": 507000,
        "tenToEightyChargingTime": 23
    }
]
```

The randomisation functions to return vehicle data is shown below.

```typescript
import { Die } from './Die.ts';
import { Interval } from './Interval.ts';
import { Vehicle } from './Vehicle.ts';
import { Visit } from './Visit.ts';
import { Visits } from './typings/values.ts';

export class VisitRandomizer {
    private _intervals: Array<Interval>;

    private _vehicles: Array<Vehicle>;

    constructor(intervals: Array<Interval>, vehicles: Array<Vehicle>) {
        this._intervals = intervals;
        this._vehicles = vehicles.slice();
    }

    randomize(): Visits {
        return this._intervals.reduce<Visits>((visits, interval) => {
            visits[interval.toString()] = [];

            while (interval.hasRemainingVisits()) {
                const rng = new Die(0, this._vehicles.length).roll();
                const vehicle = this._vehicles.splice(rng, 1)[0]; // this line

                vehicle.distance = new Die(
                    vehicle.minDistance,
                    vehicle.maxDistance
                ).roll();

                const at = new Die(interval.start, interval.end).roll();

                visits[interval.toString()].push(new Visit(at, vehicle));

                interval.decrementVisits();
            }

            visits[interval.toString()].sort((a, b) => a.at - b.at);
```

```
        return visits;
    }, {});
}
```

The equations, returned output functions, and the spread of results from twenty stochastic cases are obtained as follows:

```javascript
get chargeState() {
    return this.remainingRange * 100 / this._range;
}

get distanceInKm() {
    if (typeof this._distance !== 'number') {
        throw new Error('The distance must be set first.');
    }

    return Utils.round(Utils.km(this._distance), 1) + ' km';
}

get emptyToFullChargingTime() {
    return (this._battery.capacity / this._battery.average) * 60;
}

get energyConsumption() {
    return new EnergyConsumptionCalculator(this._power, this.estimatedChargingTime);
}
get estimatedChargingTime() {
    return (this._tenToEightyChargingTime * (80 - this.chargeState)) / 70;
}

get formattedChargeState() {
    return Utils.round(this.chargeState, 1) + '%';
}

get formattedEstimatedChargingTime() {
    return Utils.round(this.estimatedChargingTime, 1) + ' mins';
}

get maxDistance() {
    return this._range - (this._range * 10) / 100;
}

get minDistance() {
    return this._range - (this._range * 50) / 100;
}

get name() {
    return this._make + ' ' + this._id;
}
```

```
export const options = {
  scales: {
    x: {
      title: {
        display: true,
        text: "Time of Day (hour)",
      },
      min: 0,
      max: 24,
      ticks: {
        // forces step size to be 50 units
        stepSize: 3,
      },
    },
    y: {
      title: {
        display: true,
        text: "Battery State of Charge (%)",
      },
    },
  },
};

const generateDataSets = (ref, iterations) => {
  temp = {};
  newTest = {};
  let datasets: any[] = [];
  // console.log("latest graph dataset: ", vs);

  for (let i = 0; i < iterations; i++) {
    const visits: any[] = getVisits();
    const inerationOfData = [];
    Object.entries(visits).forEach(([key, val]) => {
      if (!(key in newTest)) newTest[key] = [];
      newTest[key] = newTest[key].concat(val);
      val.forEach((visit) => {
        visit.ds = i + 1;
        const vehicle: Vehicle = visit.vehicle;
        inerationOfData.push({
          name: vehicle.name,
          dayTime: visit.at,
          chargeState: vehicle.chargeState.toFixed(2),
          chargeTime: vehicle.estimatedChargingTime.toFixed(2),
        });
      });
    });
    temp[`dataSet${i + 1}`] = inerationOfData;
  }
```

D.3 Different Stochastic Scenarios

The stochastic model is run 20 times to let the stochasticity play out and draw a more general conclusion for the results. This section shows the detailed stochastic results obtained from the model. The stochastic distribution of 34 vehicles from 20 cases and their calculated data are shown in Table D.1 through Table D.18. The distribution of Case 11 and Case 15 is not presented since they have already been discussed in **Chapter 6**.

Table D.1: Timely distribution and calculated charging data of vehicles in Case 1

Time (hour)	Vehicle	SoC (%)	Estimated Recharge Time (mins)	Average Charge Power (kW)	Estimated Energy Consumption (kWh)
00:00	T2	14.1	25.4	123.8	52.4
04:00	A4	33.2	17.4	148.3	43.0
06:00	K1	16.4	57.3	45.6	43.5
07:00	K5	25.3	49.2	45.5	37.3
07:00	J8	18.7	38.5	83.2	53.4
09:00	T11	36.3	14.4	124.7	29.9
09:00	B2	47.2	16.9	47.7	13.4
09:00	T5	17.3	24.2	123.1	49.7
10:00	K2	21.2	52.9	45.6	40.2
10:00	T4	28.9	19.7	119	39.1
10:00	T7	13.5	25.7	124	53.1
11:00	K3	26.9	47.8	45.5	36.2
12:00	J2	16.2	40.1	84.1	56.2
12:00	T8	11.9	22.4	147.1	54.9
12:00	K4	45.7	30.9	44.5	22.9
13:00	T3	43.6	14	108.2	25.2
13:00	T10	13.1	22	146.6	53.8
13:00	T1	21.2	22.7	122	46.2
13:00	B1	45.8	17.6	47.7	14.0
14:00	B3	35.7	22.8	47.3	18.0
15:00	A5	42.2	14.1	148.4	34.9
16:00	K6	39	36.9	45	27.7
16:00	J5	47.7	20.3	68.7	23.2
16:00	B4	35.2	23.1	47.3	18.2
16:00	T6	26.5	20.6	120.3	41.3
17:00	J3	33.8	29	78.8	38.1
17:00	J1	21.5	36.8	82.6	50.7
19:00	J6	19.1	38.3	83.2	53.1
19:00	A2	38.3	15.5	148.4	38.3
19:00	A1	29.8	18.6	148.3	46.0
19:00	A3	33	17.4	148.3	43.0
20:00	T9	32.4	15.6	130.3	33.9
22:00	J7	29.1	32	79.4	42.3
23:00	J4	31.8	30.3	77.9	39.3

Table D.2: Timely distribution and calculated charging data of vehicles in Case 2

Time (hour)	Vehicle	SoC (%)	Estimated Recharge Time (mins)	Average Charge Power (kW)	Estimated Energy Consumption (kWh)
00:00	J2	42.7	23.4	71.6	27.9
05:00	B3	49	16	47.8	12.7
06:00	K3	18.7	55.1	45.6	41.9
08:00	K5	29.5	45.4	45.4	34.4
08:00	J7	19.9	37.8	82.9	52.2
09:00	A3	27.3	19.6	148.2	48.4
09:00	T6	30	19.3	118.5	38.1
09:00	T7	25.1	21.2	120.7	42.6
10:00	A2	45.1	13	148.4	32.2
11:00	T5	31.5	18.7	117.5	36.6
11:00	B2	13.5	34.2	46.6	26.6
11:00	J6	11.9	42.8	85.1	60.7
12:00	J8	47.7	20.3	68.7	23.2
12:00	T2	14	25.5	123.8	52.6
12:00	T11	31.6	15.9	130.3	34.5
13:00	J3	16.2	40.1	84.1	56.2
13:00	T3	14.7	25.2	123.6	51.9
13:00	K2	45.5	31.1	44.5	23.1
14:00	J4	18.8	38.5	83.2	53.4
14:00	T4	19.2	23.4	122.6	47.8
15:00	J1	29.1	32	79.4	42.3
16:00	B1	19.1	31.3	46.8	24.4
16:00	T9	21.7	19.2	140.5	45.0
16:00	T10	42.7	12.3	112.1	23.0
16:00	K4	37	38.8	45.1	29.2
16:00	K6	20	54.1	45.6	41.1
17:00	K1	39.4	36.5	45	27.4
18:00	A1	43.9	13.4	148.4	33.1
19:00	A4	10.7	25.7	146.7	62.8
19:00	A5	14.8	24.2	147.2	59.4
20:00	J5	19.6	38	82.9	52.5
20:00	B4	23.1	29.2	46.9	22.8
21:00	T8	46.5	11	105.6	19.4
23:00	T1	37.6	16.4	113.7	31.1

Table D.3: Timely distribution and calculated charging data of vehicles in Case 3

Time (hour)	Vehicle	SoC (%)	Estimated Recharge Time (mins)	Average Charge Power (kW)	Estimated Energy Consumption (kWh)
01:00	J7	35.6	27.9	75.7	35.2
05:00	T2	15.6	24.9	123.3	51.2
07:00	T10	10.7	22.8	147.6	56.1
08:00	B2	21.7	30	46.9	23.5
08:00	J5	37.5	26.7	74.6	33.2
09:00	A5	41.4	14.4	148.4	35.6
10:00	T4	13.6	25.6	123.8	52.8
10:00	J2	16.1	40.2	84.1	56.3
10:00	T1	17.4	24.1	123.1	49.4
11:00	B3	16.9	32.5	46.7	25.3
11:00	K3	36	39.6	45.2	29.8
11:00	J8	43.2	21.3	71.6	25.4
12:00	T6	17.9	24	122.9	49.2
12:00	K2	37.2	38.5	45.1	28.9
13:00	K1	14.4	59.1	45.5	44.8
13:00	J6	31.8	30.3	77.9	39.3
13:00	K6	31.1	44	45.4	33.3
14:00	B4	37.2	22	47.3	17.3
14:00	K5	43.5	32.9	44.6	24.5
14:00	B1	19.2	31.3	46.8	24.4
15:00	J1	11.1	43.3	85.3	61.6
15:00	A2	26.4	19.9	148.1	49.1
16:00	T8	21.8	19.1	140.5	44.7
16:00	T7	36.9	16.6	114.4	31.7
17:00	T11	17.9	20.4	143.5	48.8
17:00	J4	11	43.4	85.3	61.7
17:00	A4	32.6	17.6	148.3	43.5
18:00	J3	45.6	21.7	69.8	25.2
19:00	T9	41.9	12.5	114	23.8
19:00	T3	33.4	18	116.9	35.1
20:00	A3	46.5	12.5	148.4	30.9
20:00	K4	22	52.2	45.6	39.7
21:00	A1	32	17.8	148.3	44.0
23:00	T5	14.8	25.2	123.6	51.9

Table D.4: Timely distribution and calculated charging data of vehicles in Case 4

Time (hour)	Vehicle	SoC (%)	Estimated Recharge Time (mins)	Average Charge Power (kW)	Estimated Energy Consumption (kWh)
02:00	T7	15.7	24.8	123.3	51.0
03:00	J7	44.1	22.6	71	26.7
07:00	K5	44	32.5	44.6	24.2
08:00	T1	18.7	23.7	122.6	48.4
08:00	J1	31.9	30.2	77.9	39.2
09:00	J5	18.9	38.4	83.2	53.2
09:00	T2	42.8	14.4	109.3	26.2
09:00	B4	36.9	22.2	47.3	17.5
10:00	T8	22.3	19	121.7	38.5
11:00	J3	34.6	28.6	76.3	36.4
11:00	K4	31.6	43.5	45.3	32.8
11:00	A2	43.4	13.6	148.4	33.6
12:00	B2	26.7	27.4	47	21.5
12:00	T10	37.7	13.9	121.5	28.1
12:00	J2	45.6	21.6	69.8	25.1
13:00	T9	10.3	22.9	148	56.5
13:00	T6	31.6	18.7	117.5	36.6
14:00	A3	24	20.8	148	51.3
14:00	J4	19.5	38.1	82.9	52.6
14:00	K6	25.3	49.3	45.5	37.4
15:00	K2	46.7	29.9	44.5	22.2
16:00	J6	47.1	20.7	69.2	23.9
16:00	A1	32.2	17.8	148.3	44.0
16:00	B1	46.6	17.2	47.7	13.7
16:00	K3	45.9	30.7	44.5	22.8
17:00	J8	17	39.6	83.8	55.3
17:00	T3	28.2	20	119.4	39.8
18:00	A4	10.3	25.9	146.7	63.3
19:00	A5	14.9	24.2	147.2	59.4
20:00	T5	45.3	13.4	107.1	23.9
20:00	T11	43.5	12	110.3	22.1
20:00	T4	16	24.7	123.3	50.8
21:00	B3	25	28.3	46.9	22.1
21:00	K1	22.1	52.2	45.6	39.7

Table D.5: Timely distribution and calculated charging data of vehicles in Case 5

Time (hour)	Vehicle	SoC (%)	Estimated Recharge Time (mins)	Average Charge Power (kW)	Estimated Energy Consumption (kWh)
02:00	K3	36.9	38.8	45.1	29.2
04:00	A5	48.5	11.7	148.3	28.9
06:00	K6	32	43.2	45.3	32.6
08:00	A4	22.1	21.5	147.9	53.0
08:00	K4	31.3	43.8	45.4	33.1
09:00	T8	23.5	18.6	138.8	43.0
09:00	K2	10.4	62.7	45.4	47.4
09:00	B4	31.8	24.8	47.2	19.5
10:00	J5	18	39	83.5	54.3
10:00	T2	28.5	19.9	119	39.5
11:00	T1	31.2	18.8	118	37.0
11:00	T3	48	12.4	103.4	21.4
12:00	T4	13.4	25.7	124	53.1
12:00	J6	26.5	33.6	80.3	45.0
13:00	T7	20.6	22.9	122	46.6
13:00	K5	28.2	46.7	45.4	35.3
14:00	T9	43	12.1	112.1	22.6
14:00	A3	11.9	25.3	146.8	61.9
14:00	T11	21.1	19.4	141.3	45.7
14:00	J8	24.4	35	81.5	47.5
15:00	J1	24.3	35	81.5	47.5
16:00	T6	17.9	24	122.9	49.2
16:00	J4	20	37.7	82.9	52.1
17:00	J3	43.4	23	71.6	27.4
17:00	J7	35.7	27.8	75.7	35.1
17:00	K1	32	43.2	45.3	32.6
17:00	J2	33.4	29.3	77.4	37.8
18:00	B2	48.8	16	47.8	12.7
19:00	T10	40.5	13	115.9	25.1
20:00	B1	24.4	28.6	46.9	22.4
20:00	T5	16.2	24.6	123.3	50.6
20:00	A1	16.4	23.6	147.3	57.9
21:00	B3	31.4	25	47.1	19.6
23:00	A2	43.8	13.4	148.4	33.1

Table D.6: Timely distribution and calculated charging data of vehicles in Case 6

Time (hour)	Vehicle	SoC (%)	Estimated Recharge Time (mins)	Average Charge Power (kW)	Estimated Energy Consumption (kWh)
01:00	A2	28.6	19.1	148.2	47.2
04:00	J8	18.6	38.6	83.2	53.5
06:00	J7	40.5	24.8	72.8	30.1
07:00	T8	23	18.7	139.7	43.5
07:00	J6	17.2	39.5	83.8	55.2
09:00	T10	10	23	148	56.7
09:00	A5	14.4	24.4	147.1	59.8
10:00	J2	49.1	19.4	68.2	22.1
11:00	J1	15.7	40.5	84.1	56.8
11:00	K5	14.3	59.2	45.5	44.9
11:00	A4	43.8	13.5	148.4	33.4
11:00	T9	23.3	18.6	141.2	43.8
12:00	K1	32	43.2	45.3	32.6
12:00	B3	45.2	17.9	47.6	14.2
12:00	T7	25	21.2	120.7	42.6
13:00	T5	22.8	22.1	121.4	44.7
13:00	T11	30.6	16.2	131.6	35.5
13:00	T4	28.7	19.8	120.3	39.7
13:00	B1	49	15.9	47.8	12.7
14:00	B4	45.4	17.8	47.6	14.1
15:00	T1	36.9	16.6	114.4	31.7
16:00	K6	25.5	49	45.5	37.2
16:00	T2	36.1	16.9	115.1	32.4
16:00	K2	45.4	31.1	44.6	23.1
16:00	A3	24.1	20.8	148	51.3
17:00	T6	30.3	19.2	118.5	37.9
17:00	J4	35.7	27.8	75.7	35.1
18:00	T3	19.8	23.2	122.3	47.3
18:00	J3	34.9	28.4	76.3	36.1
18:00	K4	33.1	42.2	45.3	31.9
19:00	A1	29.5	18.8	148.3	46.5
19:00	J5	33.6	29.2	76.8	37.4
22:00	K3	15.8	57.8	45.6	43.9
22:00	B2	40.1	20.5	47.5	16.2

Table D.7: Timely distribution and calculated charging data of vehicles in Case 7

Time (hour)	Vehicle	SoC (%)	Estimated Recharge Time (mins)	Average Charge Power (kW)	Estimated Energy Consumption (kWh)
02:00	B4	31.5	25	47.2	19.7
03:00	T10	18.1	20.3	143.5	48.6
06:00	J7	22.7	36	81.9	49.1
06:00	T8	16.3	20.9	144.8	50.4
06:00	T7	49	12	102	20.4
09:00	K6	21.1	53	45.6	40.3
09:00	J2	15.1	40.8	84.3	57.3
09:00	A4	16.7	23.5	147.3	57.7
09:00	T6	38.1	16.2	113.7	30.7
10:00	A3	29.2	18.9	148.2	46.7
10:00	T3	31.9	18.6	117.5	36.4
10:00	A2	39.6	15	148.4	37.1
12:00	K2	40.6	35.4	44.9	26.5
12:00	T5	29.2	19.6	119	38.9
12:00	A5	12.4	25.1	146.8	61.4
13:00	T11	32.7	15.5	129	33.3
13:00	B3	46.8	17.1	47.7	13.6
14:00	T4	35.6	17.1	115.1	32.8
14:00	J1	17.9	39	83.5	54.3
14:00	B2	32.3	24.6	47.2	19.4
15:00	A1	22.1	21.5	147.9	53.0
15:00	T1	20.2	23.1	122.3	47.1
15:00	K5	40.7	35.4	44.9	26.5
16:00	J3	33.6	29.2	76.8	37.4
16:00	T9	48.1	10.5	104	18.2
17:00	J8	48.6	19.8	68.2	22.5
17:00	K4	12	61.2	45.5	46.4
18:00	B1	28	26.8	47	21.0
18:00	J6	34.9	28.3	76.3	36.0
18:00	K1	18.8	55.1	45.6	41.9
19:00	K3	25	49.5	45.5	37.5
19:00	T2	30.2	19.2	118.5	37.9
21:00	J4	27.9	32.7	79.9	43.5
23:00	J5	26	34	80.7	45.7

Table D.8: Timely distribution and calculated charging data of vehicles in Case 8

Time (hour)	Vehicle	SoC (%)	Estimated Recharge Time (mins)	Average Charge Power (kW)	Estimated Energy Consumption (kWh)
02:00	B3	12	35	46.6	27.2
03:00	T8	15.9	21.1	144.8	50.9
06:00	K6	43.5	32.8	44.6	24.4
07:00	T9	33.5	15.3	127.7	32.6
08:00	B1	43.5	18.8	47.6	14.9
09:00	J7	43	23.3	71.6	27.8
09:00	J4	14.2	41.4	84.6	58.4
09:00	K5	38.5	37.3	45	28.0
10:00	T3	34.5	17.5	115.7	33.7
10:00	J3	27.2	33.2	80.3	44.4
10:00	T10	15.7	21.1	144.8	50.9
11:00	J6	29	32.1	79.4	42.5
12:00	A1	32.1	17.8	148.3	44.0
13:00	T4	11	26.6	124.3	55.1
13:00	K1	19.8	54.2	45.6	41.2
13:00	A3	15.1	24.1	147.2	59.1
14:00	A4	26.8	19.8	148.2	48.9
14:00	T11	28.4	17	136.5	38.7
14:00	T6	22.5	22.2	121.4	44.9
14:00	J5	30.2	31.3	78.9	41.2
15:00	J8	48.8	19.6	68.2	22.3
15:00	B4	27.6	26.9	47	21.1
15:00	T5	42.2	14.6	110.3	26.8
16:00	J1	43.9	22.7	71	26.9
16:00	K2	24	50.4	45.9	38.6
17:00	A2	41	12.2	148.4	30.2
17:00	T7	37.6	16.4	113.7	31.1
18:00	T1	18.9	23.6	122.6	48.2
19:00	J2	29.7	31.7	78.9	41.7
19:00	K4	32.3	42.9	45.3	32.4
20:00	A5	23.2	21.1	147.9	52.0
20:00	B2	39.2	21	47.4	16.6
23:00	T2	42.4	14.5	110.3	26.7
23:00	K3	13.9	59.5	45.5	45.1

Table D.9: Timely distribution and calculated charging data of vehicles in Case 9

Time (hour)	Vehicle	SoC (%)	Estimated Recharge Time (mins)	Average Charge Power (kW)	Estimated Energy Consumption (kWh)
02:00	K3	23.4	51	45.5	38.7
05:00	J5	44.9	22.1	70.4	25.9
06:00	K2	27.4	47.4	45.5	35.9
07:00	J8	23.6	35.5	81.5	48.2
08:00	T3	35.3	17.2	115.7	33.2
09:00	T4	32.6	18.3	116.9	35.7
09:00	T1	11.5	26.4	124.1	54.6
10:00	T5	22.6	22.2	121.4	44.9
10:00	K6	48.7	28.2	44.1	20.7
10:00	A2	49.3	11.4	148.3	28.2
11:00	T11	18.4	20.3	143.5	48.6
11:00	T8	45	11.5	108.7	20.8
12:00	T10	24.8	18.2	137.9	41.8
13:00	B2	12.2	34.9	46.6	27.1
13:00	T7	23.3	21.9	121.4	44.3
13:00	B3	49.8	15.5	47.8	12.3
14:00	A1	48.4	11.8	148.4	29.2
14:00	J3	17	39.6	83.8	55.3
14:00	A3	21.8	21.6	147.9	53.2
14:00	K1	43.4	32.9	44.7	24.5
15:00	J7	22.4	36.2	82.3	49.7
15:00	T2	34.6	17.5	115.7	33.7
15:00	K4	43.8	32.6	44.6	24.2
16:00	B1	43	19	47.6	15.1
16:00	J1	43	23.3	71.6	27.8
17:00	B4	29.5	26	47.1	20.4
17:00	T6	27.2	20.4	119.9	40.8
18:00	J6	27.2	33.2	80.3	44.4
18:00	J2	47.3	20.6	69.2	23.8
18:00	K5	19.4	54.6	45.6	41.5
20:00	A5	21.5	21.7	147.9	53.5
20:00	J4	23.8	35.3	81.5	47.9
22:00	T9	30.8	16.2	131.6	35.5
23:00	A4	34.6	16.9	148.4	41.8

Table D.10: Timely distribution and calculated charging data of vehicles in Case 10

Time (hour)	Vehicle	SoC (%)	Estimated Recharge Time (mins)	Average Charge Power (kW)	Estimated Energy Consumption (kWh)
01:00	T6	36.1	17	115.1	32.6
05:00	B1	10.6	35.7	46.5	27.7
06:00	B2	32.4	24.5	47.2	19.3
06:00	T3	36.9	16.6	114.4	31.7
07:00	J5	14.1	41.4	84.6	58.4
09:00	B3	17.5	32.1	46.7	25.0
09:00	A2	45.5	12.8	148.4	31.7
10:00	K1	46.6	30.1	44.4	22.3
11:00	A3	44	13.4	148.4	33.1
11:00	J8	44.8	22.2	70.4	26.0
11:00	A5	21.6	21.7	147.9	53.5
11:00	T10	49.4	10.1	102.4	17.2
12:00	T11	40.1	13.1	117.8	25.7
12:00	T9	34.2	15	127.7	31.9
13:00	J4	37	27.1	75.2	34.0
13:00	K6	23.5	50.9	45.5	38.6
14:00	A1	19.2	22.6	147.6	55.6
14:00	K3	26.7	47.8	45.5	36.2
14:00	T4	49.7	11.7	100.4	19.6
14:00	A4	26.2	20	148.1	49.4
15:00	B4	45.8	17.6	47.7	14.0
16:00	J1	33.6	29.2	76.8	37.4
16:00	K4	17.1	56.6	45.6	43.0
16:00	J3	20.9	37.1	82.6	51.1
16:00	K2	35.8	39.8	46.6	30.9
17:00	T1	49.3	11.8	102	20.1
17:00	T5	18.5	23.7	122.6	48.4
18:00	J6	37.3	26.9	75.2	33.7
19:00	T2	33.2	18.1	116.9	35.3
20:00	J2	30.7	31	78.4	40.5
20:00	J7	10.2	43.9	85.4	62.5
20:00	K5	19	54.9	45.6	41.7
21:00	T7	40.1	15.4	112.1	28.8
22:00	T8	13.9	21.7	146	52.8

Table D.11: Timely distribution and calculated charging data of vehicles in Case 12

Time (hour)	Vehicle	SoC (%)	Estimated Recharge Time (mins)	Average Charge Power (kW)	Estimated Energy Consumption (kWh)
02:00	A2	49	11.5	148.3	28.4
05:00	T9	42	12.5	114	23.8
06:00	T3	40.6	15.2	111.2	28.2
07:00	T7	29.5	19.5	118.5	38.5
07:00	T1	49.4	11.8	102	20.1
09:00	K2	19.9	54.1	45.6	41.1
09:00	B3	34.3	23.5	47.2	18.5
10:00	T11	10.4	22.9	148	56.5
11:00	K4	16.3	57.4	45.6	43.6
11:00	B2	39.9	20.6	47.5	16.3
11:00	K5	24	50.5	45.5	38.3
11:00	T4	41.8	14.7	110.3	27.0
12:00	K1	44.7	31.7	44.6	23.6
12:00	J4	30.6	31	78.4	40.5
12:00	K6	27.6	47.2	45.5	35.8
12:00	B1	45.9	17.5	47.7	13.9
13:00	T6	47.2	12.7	104.7	22.2
13:00	A5	42.1	14.1	148.4	34.9
14:00	T2	45.1	13.5	107.1	24.1
14:00	J2	16.1	40.2	84.1	56.3
15:00	J6	29.9	31.5	78.9	41.4
15:00	T8	18.5	20.2	142.8	48.1
16:00	A1	28.8	19	148.2	46.9
16:00	K3	28.6	37.3	45.8	28.5
16:00	J3	10.3	43.8	85.5	62.4
17:00	J5	12.4	42.5	85.1	60.3
17:00	B4	43.3	18.9	47.6	15.0
18:00	A3	15.3	24	147.1	58.8
18:00	J8	32.9	29.6	77.4	38.2
19:00	T10	33.5	15.3	127.7	32.6
20:00	J7	18.6	38.6	83.2	53.5
20:00	A4	16.5	23.6	147.4	58.0
21:00	J1	13.7	41.7	84.6	58.8
21:00	T5	23.1	21.9	121.4	44.3

Table D.12: Timely distribution and calculated charging data of vehicles in Case 13

Time (hour)	Vehicle	SoC (%)	Estimated Recharge Time (mins)	Average Charge Power (kW)	Estimated Energy Consumption (kWh)
00:00	J7	40.6	24.7	72.8	30.0
04:00	K4	21.5	52.7	45.6	40.1
06:00	T9	21.4	19.3	141.3	45.5
06:00	T10	20.6	19.5	141.3	45.9
07:00	J4	30.6	31.1	78.4	40.6
09:00	T4	32.3	18.4	117.5	36.0
09:00	A2	24.3	20.7	148	51.1
10:00	A5	21.5	21.7	147.9	53.5
11:00	K6	37.9	37.9	45.1	28.5
11:00	A4	44.5	13.2	148.4	32.6
11:00	K3	25.3	49.2	45.5	37.3
11:00	T8	30.2	16.4	132.7	36.3
12:00	B4	21.7	30	46.9	23.5
12:00	T3	42	14.7	110.3	27.0
12:00	K1	36.3	39.4	45.2	29.7
12:00	T2	20.2	23.1	122.3	47.1
13:00	T11	45.8	11.2	107.2	20.0
13:00	B3	13.9	34	46.6	26.4
13:00	J2	16	40.2	84.1	56.3
13:00	J8	49	19.5	68.2	22.2
15:00	B1	21.8	30	46.9	23.5
15:00	B2	12.4	34.8	46.6	27.0
16:00	T1	21.2	22.7	122	46.2
16:00	A3	45	13	148.4	32.2
16:00	T5	44.6	13.7	107.1	24.5
17:00	T6	42	14.6	110.3	26.8
17:00	J1	36.2	27.5	75.7	34.7
19:00	K2	15	58.5	45.6	44.5
19:00	J3	38.9	25.9	74	31.9
19:00	K5	36.1	39.5	45.2	29.8
20:00	J6	44.6	22.3	44.6	16.6
20:00	T7	24	21.6	121	43.6
22:00	A1	34.2	17	148.4	42.0
23:00	J5	39.5	25.4	73.5	31.1

Table D.13: Timely distribution and calculated charging data of vehicles in Case 14

Time (hour)	Vehicle	SoC (%)	Estimated Recharge Time (mins)	Average Charge Power (kW)	Estimated Energy Consumption (kWh)
02:00	B2	13.5	34.2	46.6	26.6
03:00	J7	26.7	33.5	80.3	44.8
06:00	T8	47.6	10.7	104	18.5
07:00	T9	35.8	14.5	124.7	30.1
07:00	K5	30.6	44.5	45.4	33.7
09:00	J1	45.9	21.4	69.8	24.9
09:00	T1	11	26.6	124.3	55.1
09:00	T7	25.1	21.2	120.7	42.6
10:00	B4	16.4	32.7	46.7	25.5
11:00	A3	43.1	13.7	148.4	33.9
11:00	T4	28.4	19.9	119.4	39.6
11:00	J8	41.5	24.2	72.2	29.1
12:00	B1	42	19.6	47.5	15.5
12:00	A1	45.1	13	148.9	32.3
12:00	K3	28.1	46.7	45.4	35.3
13:00	J5	18.8	38.5	83.2	53.4
13:00	J6	29.2	32	79.4	42.3
14:00	B3	39.5	20.9	47.5	16.5
14:00	T11	35.9	14.5	124.7	30.1
14:00	K1	31.2	43.9	45.4	33.2
15:00	A5	14.2	24.4	147.1	59.8
16:00	T5	26.4	20.7	120.3	41.5
16:00	J3	46.6	21	69.2	24.2
16:00	J4	34.5	28.6	76.3	36.4
17:00	T2	36.8	16.7	114.4	31.8
17:00	T3	30.2	18.2	118.5	35.9
17:00	A4	44.3	13.3	148.4	32.9
18:00	T10	30.3	16.3	132.7	36.1
18:00	K4	45.2	31.3	44.6	23.3
19:00	A2	14.3	24.4	147.1	59.8
19:00	T6	32.5	18.3	116.9	35.7
20:00	K2	13.7	59.7	45.5	45.3
21:00	K6	31.2	43.9	45.4	33.2
22:00	J2	42.3	23.7	72.2	28.5

Table D.14: Timely distribution and calculated charging data of vehicles in Case 16

Time (hour)	Vehicle	SoC (%)	Estimated Recharge Time (mins)	Average Charge Power (kW)	Estimated Energy Consumption (kWh)
00:00	T6	38.4	16.1	113.7	30.5
05:00	K6	22	52.2	45.6	39.7
06:00	T8	37.8	13.9	121.5	28.1
07:00	B3	19.5	31.3	46.8	24.4
08:00	J7	49	19.5	68.2	22.2
09:00	B4	12.8	34.6	46.6	26.9
10:00	K4	29	45.9	45.8	35.0
10:00	J1	38.2	26.3	74.6	32.7
10:00	J4	39.7	25.4	73.5	31.1
10:00	T10	10.9	22.7	147.6	55.8
11:00	T5	23.8	21.7	121	43.8
11:00	A1	14.3	24.4	147.1	59.8
12:00	T7	23.1	22	121.4	44.5
12:00	K1	15.4	58.1	45.6	44.2
12:00	T1	33.6	17.9	116.3	34.7
12:00	T11	22.7	18.8	139.7	43.8
13:00	T2	22.1	22.3	121.7	45.2
13:00	T9	24.4	18.3	138.8	42.3
14:00	J5	26	33.9	80.7	45.6
14:00	A2	14.5	24.3	147.2	59.6
15:00	J6	27.6	33	79.9	43.9
15:00	A3	12.7	25	146.8	61.2
16:00	B1	30.4	25.5	47.1	20.0
16:00	A5	11.5	25.5	146.8	62.4
16:00	K3	39	36.9	45	27.7
17:00	T4	41.9	14.7	110.3	27.0
17:00	B2	15.2	33.4	46.6	25.9
18:00	K5	26.6	48.1	45.5	36.5
18:00	K2	17	56.7	45.6	43.1
20:00	J3	47.1	20.7	69.2	23.9
20:00	A4	29.1	18.9	148.2	46.7
20:00	J2	29.5	31.8	78.9	41.8
21:00	T3	27	20.5	119.9	41.0
21:00	J8	28.3	32.5	79.9	43.3

Table D.15: Timely distribution and calculated charging data of vehicles in Case 17

Time (hour)	Vehicle	SoC (%)	Estimated Recharge Time (mins)	Average Charge Power (kW)	Estimated Energy Consumption (kWh)
01:00	A5	25.3	20.3	148.1	50.1
05:00	B1	46.5	17.2	47.7	13.7
06:00	T10	31.5	16	130.3	34.7
06:00	A3	38	15.6	148.4	38.6
07:00	K3	35.3	40.2	45.2	30.3
10:00	T2	16.7	24.4	123.1	50.1
10:00	J3	15.5	40.6	84.1	56.9
10:00	J4	28.2	32.5	79.9	43.3
10:00	T6	42.7	14.4	109.3	26.2
11:00	T4	49	12	102	20.4
11:00	J7	25.6	34.2	80.7	46.0
11:00	J1	13.7	41.7	84.6	58.8
12:00	T7	37.8	16.3	113.7	30.9
13:00	K5	46.8	29.9	44.4	22.1
13:00	B3	23.8	28.9	46.9	22.6
13:00	T8	25.2	18	137.9	41.4
14:00	A1	44.7	13.1	148.4	32.4
14:00	J5	40.1	25.1	73.5	30.7
14:00	K1	30	45	45.4	34.1
14:00	A4	46.6	12.4	148.4	30.7
15:00	B4	30.7	25.4	47.1	19.9
15:00	B2	15.7	33.1	46.7	25.8
16:00	J6	17	39.6	83.8	55.3
16:00	T11	28.7	16.9	133.9	37.7
16:00	K6	30.5	44.6	45.4	33.7
17:00	J8	17.8	39.1	83.5	54.4
17:00	T5	28.7	19.8	119	39.3
18:00	J2	40.2	25	73.5	30.6
18:00	A2	39.2	15.2	148.4	37.6
19:00	K4	30.3	44.8	45.4	33.9
19:00	T1	29.3	19.6	119	38.9
20:00	T9	36.6	14.3	123.1	29.3
23:00	T3	17	24.3	123.1	49.9
23:00	K2	43	33.3	44.7	24.8

Table D.16: Timely distribution and calculated charging data of vehicles in Case 18

Time (hour)	Vehicle	SoC (%)	Estimated Recharge Time (mins)	Average Charge Power (kW)	Estimated Energy Consumption (kWh)
00:00	J7	46.9	20.8	69.2	24.0
03:00	T9	35.9	14.5	124.7	30.1
07:00	T1	40.3	15.3	112.1	28.6
08:00	A1	24.9	20.5	148.1	50.6
08:00	J2	46.6	21	69.2	24.2
09:00	T5	18	23.9	122.9	49.0
09:00	T3	25.6	21	120.3	42.1
10:00	K6	32.3	42.9	45.3	32.4
10:00	B3	14.8	33.5	46.6	26.0
10:00	T7	11.5	26.4	124.1	54.6
11:00	T10	25.2	18	137.9	41.4
11:00	J6	33.1	29.5	77.4	38.1
12:00	B4	19.4	31.2	46.8	24.3
12:00	A5	43.5	13.6	148.4	33.6
12:00	K2	47.3	29.4	44.4	21.8
13:00	B2	43.5	18.8	47.6	14.9
13:00	A4	44.8	13.1	148.4	32.4
13:00	B1	24.9	28.3	46.9	22.1
14:00	J1	17.4	39.4	83.8	55.0
14:00	K1	31	44.1	45.4	33.4
15:00	J5	27.8	32.8	79.9	43.7
15:00	T11	23.5	18.6	138.8	43.0
16:00	T8	19.9	19.8	142.1	46.9
16:00	K4	40.9	35.2	44.9	26.3
16:00	J4	42.5	23.6	71.6	28.2
17:00	T2	20.5	22.9	122	46.6
17:00	K3	17.9	55.9	45.6	42.5
18:00	K5	11.1	62.1	45.5	47.1
18:00	T4	14.9	25.1	123.6	51.7
19:00	A3	30.8	18.3	148.3	45.2
19:00	J8	34.6	28.5	76.3	36.2
20:00	J3	45.3	21.8	70.4	25.6
21:00	T6	14.2	25.4	123.8	52.4
23:00	A2	33.7	17.2	148.4	42.5

Table D.17: Timely distribution and calculated charging data of vehicles in Case 19

Time (hour)	Vehicle	SoC (%)	Estimated Recharge Time (mins)	Average Charge Power (kW)	Estimated Energy Consumption (kWh)
02:00	A5	17.4	23.3	147.4	57.2
05:00	K1	32.3	43	45.3	32.5
06:00	T10	23.8	18.5	138.8	42.8
07:00	J1	36.3	27.5	75.7	34.7
08:00	K3	45.6	30.9	44.5	22.9
09:00	A4	31.3	18.1	148.3	44.7
10:00	T2	30.8	19	118	37.4
10:00	J6	42.9	23.4	71.6	27.9
10:00	K6	32	43.2	45.3	32.6
10:00	T11	14.1	21.6	146	52.6
11:00	T5	21.3	22.7	122	46.2
11:00	J7	24.7	34.8	81.1	47.0
12:00	K5	11.6	61.5	45.5	46.6
12:00	T8	49.8	9.9	100.7	16.6
13:00	T6	28.7	19.8	119	39.3
13:00	A1	14.2	24.4	147.1	59.8
13:00	K4	48.4	28.4	44.2	20.9
13:00	T4	13.6	25.6	123.8	52.8
14:00	J8	11.1	43.3	85.3	61.6
14:00	B3	26.7	27.4	47	21.5
15:00	T9	18.3	20.3	143.5	48.6
16:00	B1	42.1	19.5	47.5	15.4
16:00	A2	36.9	16	148.4	39.6
17:00	J2	44.7	22.2	70.4	26.0
17:00	T7	33.2	18.1	116.9	35.3
17:00	K2	13.1	60.2	45.5	45.7
17:00	A3	31.7	17.9	148.3	44.2
18:00	T3	27	20.5	119.9	41.0
19:00	T1	48.9	12	102	20.4
19:00	J3	44	22.7	71	26.9
19:00	B4	15.4	33.2	46.6	25.8
20:00	B2	49.2	15.8	47.8	12.6
22:00	J4	25.2	34.5	81.1	46.6
22:00	J5	20.6	37.4	82.6	51.5

Table D.18: Timely distribution and calculated charging data of vehicles in Case 20

Time (hour)	Vehicle	SoC (%)	Estimated Recharge Time (mins)	Average Charge Power (kW)	Estimated Energy Consumption (kWh)
00:00	T6	36.5	16.8	114.4	32.0
05:00	T5	35.6	17.1	115.1	32.8
06:00	T7	40.7	15.2	111.2	28.2
06:00	J8	49.1	19.4	68.2	22.1
08:00	B1	29.3	26.1	47.1	20.5
09:00	A1	23	21.2	147.9	52.3
09:00	T1	35.9	17	115.1	32.6
09:00	A4	24.3	20.7	148	51.1
10:00	K3	39.7	36.3	44.9	27.2
10:00	J3	13.1	42.1	84.8	59.5
10:00	J1	29.5	31.8	78.9	41.8
10:00	B3	33.6	23.9	47.2	18.8
12:00	J4	34.6	28.5	76.3	36.2
12:00	K4	13.9	59.5	45.5	45.1
12:00	T4	17.9	24	122.9	49.2
13:00	T11	35	14.8	126.2	31.1
13:00	B2	49.3	15.8	47.8	12.6
13:00	J6	42.6	23.5	72.2	28.3
13:00	K1	39.9	36.1	44.9	27.0
14:00	A5	43.7	13.5	148.4	33.4
15:00	T3	29.7	19.4	118.5	38.3
15:00	T8	12.7	22.1	146.6	54.0
15:00	K2	32.3	43	45.3	32.5
16:00	K5	27.1	47.6	45.5	36.1
17:00	A2	16.8	23.5	147.4	57.7
17:00	T2	44.9	13.5	107.1	24.1
17:00	T9	47.3	10.7	105.6	18.8
18:00	J7	13	42.1	84.8	59.5
18:00	K6	36.9	38.8	45.1	29.2
19:00	T10	23.6	18.5	138.8	42.8
19:00	J5	15.8	40.4	84.1	56.6
20:00	A3	28.5	19.1	148.2	47.2
21:00	J2	30.4	31.2	78.9	41.0
22:00	B4	48.7	16.1	47.8	12.8

References

[1] Intergovernmental Panel on Climate Change (IPCC), "AR5 Climate Change 2014: Mitigation of climate change," New York, 2014.

[2] H. Ritchie, "Sector by sector: Where do global greenhouse gas emissions come from?" *Our World in Data*, 2020. [Online]. Available at: https://ourworldindata.org/ghg-emissions-by-sector. [Accessed: 08-Jun-2021].

[3] Committee on Climate Change, "Net Zero: The UK's contribution to stopping global warming," London, 2019.

[4] International Energy Agency, "CO_2 emissions in 2022," Mar. 2023.

[5] Z. Hausfather, "Factcheck: How electric vehicles help to tackle climate change," *Carbon Brief*, May. 2019. [Online]. Available at: https://www.carbonbrief.org/factcheck-how-electric-vehicles-help-to-tackle-climate-change. [Accessed: 08-Jun-2021].

[6] A. Penistone, "2018 UK provisional greenhouse gas emissions," *Department for Business, Energy & Industrial Strategy*, 2015 [Updated Mar. 2021].

[7] R. Philipsen, T. Schmidt, J. V. Heek, and M. Ziefle, "Fast-charging station here, please! User criteria for electric vehicle fast-charging locations," *Transportation Research Part F: Traffic Psychology and Behaviour*, vol. 40, 2016.

[8] Department for Business, Energy, and Industrial Strategy (DBEIS), "2016 UK Greenhouse gas emissions, final figures," *Statistical Release: National Statistics*, London, 2018.

[9] L. Eyers and E. Page, "Transport statistics Great Britain 2020," *Department for Transport*, 2020.

[10] International Energy Agency, "Global CO_2 emissions in transport by mode in the Sustainable Development Scenario, 2000-2070," Paris, 2022.

[11] Department for Transport, "Transport and environment statistics 2022," 2022.

[12] Office for Low Emission Vehicles, "Energising our electric vehicle transition," *EV Energy Task Force*, London, 2020.

[13] M. Contestabile, M. Alajaji, and B. Almubarak, "Will current electric vehicle policy lead to cost-effective electrification of passenger car transport?" *Energy Policy*, vol. 110, 2017.

[14] Committee on Climate Change, "Net Zero: Technical report," London, 2019.

[15] A. Grundi, "Electrification of transport could cut its emissions by 60%, says BNEF," *Current±*, 2020. [Online]. Available at: https://www.current-news.co.uk/news/electrification-of-transport-buildings-industrial-sectors-could-cut-emissions-by-60. [Accessed: 17-Apr-2020].

[16] BloomBerg, "New energy outlook 2020: Executive summary," 2020.

[17] R. Harrabin, "Electric car emissions myth 'busted'," *BBC News*, 2020. [Online]. Available at: https://www.bbc.co.uk/news/science-environment-51977625. [Accessed: 10-Jun-2021].

[18] D. Hall and N. Lutsey, "Effects of battery manufacturing on electric vehicle life-cycle greenhouse gas emissions," International Council on Clean Transportation, 2018.

[19] International Renewable Energy Agency (IRENA), "Reviews of cutting-edge technology and country data on low-carbon industry and transport," [Online]. Available at: https://www.irena.org/industrytransport. [Accessed: 08-Jun-2021].

[20] H. M. Langbroek, J. P. Franklin, and Y. O. Susilo, "The effect of policy incentives on electric vehicle adoption," *Energy Policy*, vol. 94, 2016.

[21] G. Cecere, N. Corrocher, and M. Guerzoni, "Price of performance? A probabilistic choice analysis of the intention to buy electric vehicles in European countries," *Energy Policy*, vol. 118, , 2018.

[22] HD. Newbery and G. Strbac, "What is needed for battery electric vehicles to become socially cost competitive?" *Economics of Transportation*, vol. 5, 2016.

[23] D. Efthymiou, K. Chrysostomou, M. Morfoulaki, and G. Aifantopoulou, "Electric vehicles charging infrastructure location: a genetic algorithm approach," *European Transport Research Review*, vol. 9, 2017.

[24] M. Ehsani, Y. Gao, S. Longo, and K. Ebrahimi, "Modern electric, hybrid electric, and fuel cell vehicles," 3rd edition Boca Raton: CRC Press, 2018.

[25] EVgo, "Battery Electric Vehicles, BEVs, EVs, HEVs, BHEV's," [Online]. Available at: https://www.evgo.com/ev-drivers/types-of-evs. [Accessed: 13-Jul-2020].

[26] Z. Shahan, "Top 12 fully electric vehicles in UK (Oct 2019 — Sept 2020)," Clean Technica. [Online]. Available at: https://cleantechnica.com/2020/12/26/tesla-model-3-31-of-uk-electric-vehicle-sales. [Accessed: 20-Jul-2020].

[27] H. S. Das, C. W. Tan, and A. H. M. Yatim, "Fuel cell hybrid electric vehicles: A review on power conditioning units and topologies," *Renewable and Sustainable Energy Reviews*, vol. 76, 2017.

[28] Dragonfly Energy, "Why does energy density matter in batteries?" 2022. [Online]. Available at: https://dragonflyenergy.com/why-does-energy-density-matter-in-batteries. [Accessed: 24-Feb-2023].

[29] V. Henze, "Battery pack prices fall to an average of $132/kWh, but rising commodity prices start to bite," *Bloomberg*, 2021. [Online]. Available at: https://about.bnef.com/blog/battery-pack-prices-fall-to-an-average-of-132-kwh-but-rising-commodity-prices-start-to-bite. [Accessed: 24-Feb-2023].

[30] K. Mongird, et. al., "Energy storage technology and cost characterisation report," *HydroWires Department of Energy*, 2019.

[31] V. N. Serneri, "Range anxiety: What it is and how to defeat it," *Chargetrip*, 2020. [Online]. Available at: https://medium.com/chargetrip/range-anxiety-what-it-is-and-how-to-defeat-it-3e7aa61cd7a5. [Accessed: 23-Jan-2022].

[32] V. M. Iyer, S. Gulur, G. Gohil, and S. Bhattacharya, "Extreme fast charging station architecture for electric vehicles with partial power processing," *2018 IEEE Applied Power Electronics Conference and Exposition (APEC)*, 2018.

[33] S. A. Adderly, D. Manukian, T. D. Sullivan, and M. Son, "Electric vehicles and natural disaster policy implications," *Energy Policy*, vol. 112, 2018.

[34] D. Ronanki, A. Kelkar, and S. S. Williamson, "Extreme fast charging technology — prospects to enhance sustainable electric transportation," *Energies*, vol. 12, 2019.

[35] J. S. Choksey, "Electric vehicle range testing: Understanding NEDC vs. WLTP vs. EPA," J. D. Power, 2020. [Online]. Available at: https://www.jdpower.com/cars/shopping-guides/electric-vehicle-range-testing-understanding-nedc-vs-wltp-vs-epa. [Accessed: 22-Jan-2022].

[36] EVSpecifications. [Online]. Available at: https:// https://www.evspecifications.com. [Accessed: 22-Jan-2022].

[37] N. Deb, R. Singh, R. R. Brooks, and K. Bal, "A review of extremely fast charging stations for electric vehicles," *Energies*, vol. 14, 2021.

[38] T. S. Bryden, G. Hilton, A. Cruden, and T. Holton, "Electric vehicle fast charging station usage and power requirements," *Energy*, vol. 152, 2018.

[39] X. H. Sun, T. Yamamoto, and T. Morikawa, "Fast-charging station choice behaviour among battery electric vehicle users," *Transportation Research Part D: Transport and Environment*, vol. 46, 2016.

[40] D. Meyer and J. Wang, "Integrating ultra-fast charging stations within the power grids of smart cities: A review," *IET Smart Grid*, vol. 1, 2018.

[41] M. ElMenshawy and A. Massoud, "Modular isolated DC-DC converters for ultra-fast EV chargers: a generalised modelling and control approach," vol. 13, 2020

[42] Team ChargePoint, "When and how to use DC fast charging." [Online]. Available at: https://www.chargepoint.com/blog/when-and-how-use-dc-fast-charging. [Accessed: 22-Jan-2022].

[43] R. O. Oliyide, "Load management of electric vehicles and heat pumps in emerging electricity system," PhD Thesis, Cardiff University: School of Engineering, 2019.

[44] C. Foote, P. Djapic, G. Ault, J. Mutale, G. Burt, and G. Strbac, "United Kingdom generic distribution system: Summary of EHV networks," *DTI Centre for Distributed Generation and Sustainable Electrical Energy*, 2006.

[45] Manitoba Hydro International Ltd., "Three-phase battery system — A generic example," 2018. [Online]. Available at: https://www.pscad.com/knowledge-base/article/462. [Accessed: 31-Jan-2022].

[46] O. Tremblay, L. A. Dessaint, and A. I. Dekkiche, "A generic battery model for the dynamic simulation of hybrid electric vehicles," *Vehicle Power and Propulsion Conference (VPCC)*, 2007.

[47] Western Power Distribution, "Changing load profiles," *Distribution System Operability Framework*, 2018.

[48] R. Summers, "Standard technique: SD8B/4 (Part 1) relating to LV underground cable ratings," *Western Power Distribution*, 2016.

[49] Department for Transport, "Electric chargepoint analysis 2017: Local authority rapids (revised)," 2018.

[50] T. O'Neill, "Distribution of charge time starts at rapid devices, Q4 2020," *Zap-Map*, 2021.

[51] B. Lane and T. O'Neill, "Zap-map EV charging survey: Insights report 2020 — extracts," *Zap-Map*, 2020.

[52] SkyRC Technology Co., Ltd., "MC3000 Universal battery charger and analyser," 2022. [Online]. Available at: https://www.skyrc.com/MC3000_Charger. [Accessed: 11-May-2022].

[53] M. B. Arias, M. Kim, and S. Bae, "Prediction of electric vehicle charging-power demand in realistic urban traffic networks," *Applied Energy*, vol. 195, 2017.

[54] Capital Enterprise, "IDEALondon future mobility — road to zero emissions," 2020. [Online]. Available at: https://www.youtube.com/watch?v=rZ5asgkVOPI. [Accessed: 11-Jun-2021].

[55] "The road to electrification — from the internal combustion engine to the battery electric vehicle," *The Faraday Institution*, 2019.

[56] Department for Transport, "Decarbonising transport: Setting the challenge," London, 2020.

[57] M. A. H. Rafi and J. Bauman, "A comprehensive review of DC fast-charging stations with energy storage: Architectures, power converters, and analysis," *IEEE Transactions on Transportation Electrification*, vol. 7, 2021.

[58] International Energy Agency, "Global EV outlook 2021," Paris, 2021.

[59] K. Adler, "IHS market forecasts global EV sales to rise by 70% in 2021," IHS Markit, 2021. [Online]. Available at: https://ihsmarkit.com/research-analysis/ihs-markit-forecasts-global-ev-sales-to-rise-by-70-percent.html. [Accessed: 08-Jun-2021].

[60] International Energy Agency (IEA), "Global EV outlook 2022: Securing supplies for an electric future," Paris, 2017.

[61] P. Nieuwenhuis, C. Liana, and H. B. Sonder, "The electric vehicle revolution." In. Letcher, Trevor ed. Future Energy 3rd Edition: *Improved, Sustainable and Clean Options for Our Planet, Elsevier*, 2020.

[62] D. Hirst, N. Dempsey, P. Bolton, and S. Hinson, "Electric vehicles and infrastructure," *Briefing paper CBP07480*, House of Commons Library, 2020.

[63] Deloitte LLP, "The opportunities around electric vehicle charge points in the UK," Rzeszov, 2019.

[64] NewMotion, "EV driver survey report 2020," Amsterdam, 2020.

[65] L. Wang, Z. Win, T. Slangen, P. Bauer, and T. V. Wijk, "Grid impact of electric vehicle fast charging stations: Trends, standards, issues and mitigation measures — an overview," *IEEE Journal of Power Electronics*, vol. 2, 2021.

[66] M. Kane, "China is developing new GB/T fast charging standard at 900 kW," *InsideEVs*, 2018. [Online]. Available at: https://insideevs.com/news/338620/china-is-developing-new-gb-t-fast-charging-standard-at-900-kw. [Accessed: 09-Apr-2020].

[67] International Energy Agency, "Global EV outlook 2020," Paris, 2020.

[68] V. Joel and M. Frankie, "High granularity projections for low-carbon technology uptake — electric vehicle, heat pumps and solar PV," Exeter: Regen, 2020.

[69] Department for Transport, "New 'league table' reveals electric car charging availability across UK as transport secretary calls on local authorities to do more," 2019. [Online]. Available at: https://www.gov.uk/government/news/new-league-table-reveals-electric-car-charging-availability-across-uk-as-transport-secretary-calls-on-local-authorities-to-do-more. [Accessed: 08-Jun-2021].

[70] Office for Low Emission Vehicles, "Overview of the electric vehicle homecharge scheme: guidance for customers," 2021. [Online]. Available at: https://www.gov.uk/government/publications/customer-guidance-electric-vehicle-homecharge-scheme/electric-vehicle-homecharge-scheme-guidance-for-customers. [Accessed: 08-Jun-2021].

[71] Autocar, "How to charge your electric car at home," May. 2021. [Online]. Available at: https://www.autocar.co.uk/car-news/advice-electric-cars/how-charge-your-electric-car-home. [Accessed 09-Jun-2021].

[72] Department for Transport, "Public electric vehicle charging infrastructure: Deliberative and quantitative research with drivers without access to off-street parking," *Britain Thinks*, 2022.

[73] Electric Brighton, "How do people with no driveway charge their electric cars?" 2021. [Online]. Available at: https://electricbrighton.com/faqs/how-do-people-with-no-driveway-charge-their-electric-cars. [Accessed: 08-Jun-2021].

[74] C. Lilly, "Charging at work," Zap-Map, May. 2022. [Online]. Available at: https://www.zap-map.com/charge-points/charging-work. [Accessed: 02-Jul-2022].

[75] Office for Low Emission Vehicles, "Workplace charging scheme: guidance for applicants, chargepoint installers and manufacturers," 2020. [Online]. Available at: https://www.gov.uk/government/publications/workplace-charging-scheme-guidance-for-applicants-installers-and-manufacturers/workplace-charging-scheme-guidance-for-applicants-chargepoint-installers-and-manufacturers. [Accessed: 08-Jun-2021].

[76] O. Halevi, "The critical components of an EV fleet charging management solution," *Driivz*, 2020. [Online]. Available at: https://driivz.com/blog/ev-fleet-charging-management. [Accessed: 08-Jun-2021].

[77] Tesla, "Destination charging locations," 2021. [Online]. Available at: https://www.tesla.com/destination-charging. [Accessed: 08-Jun-2021].

[78] C. Appleby, "Ecotricity and GRIDSERVE announce new partnership to power up the Electric Highway," 2021. [Online]. Available at: https://www.ecotricity.co.uk/our-news/2021/ecotricity-and-gridserve-to-power-the-electric-highway. [Accessed: 08-Jun-2021].

[79] GRIDSERVE, "GRIDSERVE opens UK's first electric forecourt," 2020. [Online]. Available at: https://www.gridserve.com/2020/12/06/gridserve-opens-uks-first-electric-forecourt.
[Accessed: 08-Jun-2021].

[80] National Grid ESO, "Future energy scenarios data workbook," 2019.

[81] T. K. Miao, V. K. Ramachandaramurthy, and J. Y. Yong, "Integration of electric vehicles in smart grid: A review on vehicle to grid technologies and optimisation techniques," *Renewable and Sustainable Energy Reviews*, vol. 53, 2016.

[82] V2GHub, "V2G around the world," 2021. [Online]. Available at: https://www.v2g-hub.com. [Accessed: 09-Jun-21].

[83] M. Yilmaz and P. T. Krein, "Review of the impact of vehicle-to-grid technologies on distribution systems and utility interfaces," *IEEE Transactions on Power Electronics*, vol. 28, 2013.

[84] S. Habib, M. Kamran, and U. Rashin, "Impact analysis of vehicle-to-grid technology and charging strategies of electric vehicles on distribution networks — A review," *Journal of Power Sources*, vol. 277, 2015.

[85] Electric Nation, "Nissan EV drivers invited to take part in vehicle-to-grid trial," 2021. [Online]. Available at: https://electricnation.org.uk. [Accessed: 09-Jun-21].

[86] Element Energy, "V2GB Vehicle-to-grid Britain," 2019. [Online]. Available at: http://www.element-energy.co.uk/wordpress/wp-content/uploads/2019/06/V2GB-Public-Report.pdf. [Accessed: 09-Jun-21].

[87] M. Dubarry, A. Devie, and K. McKenzie, "Durability and reliability of electric vehicle batteries under electric utility grid operations: bidirectional charging impact analysis," *Journal of Power Sources*, vol. 358, 2017.

[88] K. M. Tan, V. K. Ramachandaramurthy, J. Y. Yong, S. Padmanaban, L. Mihet-Popa, and F. Blaabjerg, "Minimisation of load variance in power grids — investigation on optimal vehicle-to-grid scheduling," *Energies*, vol. 10, 2017.

[89] Ideal Energy Solar Inc., "Peak shaving with solar & storage," 2020. [Online]. Available at: https://www.idealenergysolar.com/peak-shaving-solar-storage. [Accessed: 12-Jul-2021].

[90] R. Stompf, "Innovative battery solutions and electric vehicles are solar energy's strongest allies," *Energy Storage News*, 2021. [Online]. Available at: https://www.energy-storage.news/innovative-battery-solutions-and-electric-vehicles-are-solar-energys-strongest-allies. [Accessed: 22-Jan-2022].

[91] GRIDSERVE, "GRIDSERVE launches the 'GRIDSERVE Electric Highway' to revolutionise EV charging across the UK, and eliminate charging anxiety," 2021. [Online]. Available at: https://www.gridserve.com/2021/06/30/gridserve-launches-the-gridserve-electric-highway. [Accessed: 12-Jul-2021].

[92] A. Stauch, "Does solar power add value to electric vehicles? An investigation of car-buyer's willingness to buy product-bundles in Germany," *Energy Research & Social Science*, vol. 75, 2021.

[93] M. A. Delmas, M. E. Kahn, and S. L. Locke, "The private and social consequences of purchasing an electric vehicle and solar panels: Evidence from California," *Research in Economics*, vol. 71, 2017.

[94] Tesla, "Exclusive green mountain power solar and powerwall offer," 2020. [Online]. Available at: https://www.tesla.com/solarpanels. [Accessed: 22-Jan-2022].

[95] EE-News, "Einstieg in die Elektromobilität: Sonnen stellt Abo-Modell für Elektroautos und Photovoltaik-Anlagen mit Batteriespeichern vor," 2019. [Online]. Available at: https://www.ee-news.ch/de/article/42417/einstieg-in-die-elektromobilitat-sonnen-stellt-abo-modell-fur-elektroautos-und-photovoltaik-anlagen-mit-batteriespeichern-vor. [Accessed: 23-Jan-2022].

[96] Sonnen, "Sonnen produkte," 2020. [Online]. Available at: https://sonnen.de/produkte. [Accessed: 22-Jan-2022].

[97] A. Priessner and N. Hampl, "Can product bundling increase the joing adoption of electric vehicles, solar panels, and battery storage? Explorative evidence from a choice-based conjoint study in Austria," *Ecological Economics*, vol. 167, 2020.

[98] Zemo Partnership, "UK to introduce mandatory installation of EV chargepoints for all new homes," London, 2019. [Online]. Available at: https://www.zemo.org.uk/news-events/news,uk-to-introduce-mandatory-installation-of-ev-chargepoints-for-all-new-homes_3983.htm. [Accessed: 09-Jun-2021].

[99] European Commission, "Benchmarking in smart metering deployment in the EU-28," *Tractebel Impact*, 2019.

[100] Department for Transport, "Electric vehicle smart charging," London, 2019.

[101] Western Power Distribution, "Flexibility map", 2020. [Online]. Available at: https://www.westernpower.co.uk/network-flexibility-map-application. [Accessed: 11-Jun-21].

[102] M. Lempriere, "New National Grid ancillary services platform goes live as modernisation programme shifts gear," *Current± News*, 2019. [Online]. Available at: https://www.current-news.co.uk/news/national-grid-launched-a-new-platform-for-ancillary-services.
[Accessed: 12-Jul-21].

[103] Energy UK, "Ancillary services report 2017," 2017. [Online]. Available at: https://www.energy-uk.org.uk/publication.html?task=file.download&id=6138.
[Accessed: 11-Jun-21].

[104] T.-H. Jin, H. Park, M. Chung, K.-Y. Shin, A. Foley, and L. Cipcigan, "Review of virtual power plant applications for power system management and vehicle-to-grid market development," *The Transactions of the Korean Institute of Electrical Engineers*, vol. 142, 2017.

[105] P. Papadopoulos, O. Akizu, L. Cipcigan, N. Jenkins, and E. Zabala, "Electricity demand with electric cars in 2030: Comparing Great Britain and Spain," *Proceedings of the Institution of Mechanical Engineers. Part A Journal Power Energy*, vol. 225, 2011.

[106] V. Slednev, P. Jochem, and W. Fichtner, "Impacts of electric vehicles on the European high and extra high voltage power grid," *Journal of Industrial Ecology*, vol. 26, 2022.

[107] N. Uthathip, P. Bhasaputra, and W. Pattaraprakorn, "Stochastic modelling to analyse the impact of electric vehicle penetration in Thailand," *Energies*, vol. 14, 2021.

[108] H. Lin, et. al., "Characteristics of electric vehicle charging demand at multiple types of location — Application of an agent-based trip chain model," *Energy*, vol. 188, 2019.

[109] M. Marinelli, "The ACES project — Large-scale integration of electric vehicles into the electric power system," *Proceeding Creating Technology for Sustainable Society*, Lyngby, Denmark: Technical University of Denmark, 2018.

[110] L. Calearo, A. Thingvad, K. Suzuki, and M. Marinelli, "Grid loading due to EV charging profiles based on pseudo-real driving pattern and user behaviour," *IEEE Transactions on Transportation Electrification*, vol. 5, 2019.

[111] F. M. Aboshady, I. Pisica, and C. J. Axon, "A stochastic model for estimating electric vehicle arrival at multi-charger forecourts," *Energy Reports*, vol. 8, 2022.

[112] A. Ul-Haq, C. Cecati, and E. El-Saadany, "Probabilistic modelling of electric vehicle charging pattern in a residential distribution network," *Electric Power Systems Research*, vol. 157, 2018.

[113] D. Wu, D. Aliprantis, and K. Gkritza, "Electric energy and power consumption by light-duty plug-in electric vehicles," *IEEE Transactions on Power Systems*, vol. 26, 2011.

[114] M. Kintner-Meyer, K. Schneider, and R. Pratt, "Impacts assessment of plug-in hybrid vehicles on electric utilities and regional US power grids Part 1: Technical analysis," Pacific Northwest National Laboratory, 2007.

[115] J. C. Gomez and M. M. Morcos, "Impact of EV battery chargers on the power quality of distribution systems," *IEEE Transactions on Power Delivery*, vol. 18, 2003.

[116] S. W. Hadley and A. A. Tsvetkova, "Potential impacts of plug-in hybrid electric vehicles on regional power generation," *The Electricity Journal*, vol. 22, 2009.

[117] C. Clement-Nyns, E. Haesen, and J. Driesen, "The impact of charging plug-in hybrid electric vehicles on a residential distribution grid," *IEEE Transactions on Power Systems*, vol. 25, 2010.

[118] D. Steen, L. A. Tuan, O. Carlson, and L. Bertling, "Assessment of electric vehicle charging scenarios based on demographical data," *IEEE Transactions on Smart Grid*, vol. 3, 2012.

[119] N. Daina, A. Sivakumar, and J. W. Polak, "Modelling electric vehicles use: A survey on the methods," *Renewable and Sustainable Energy Reviews*, vol. 68, 2017.

[120] J. Su, T. T. Lie, and R. Zamora, "Modelling of large-scale electric vehicles charging demand: A New Zealand case study," *Electric Power Systems Research*," vol. 167, 2019.

[121] C. G. Hoehne and M. V. Chester, "Optimising plug-in electric vehicle and vehicle-to-grid charge scheduling to minimise carbon emissions," *Energy*, vol. 115, 2016.

[122] C. Crozier, T. Morstyn, and M. McCulloch, "A stochastic model for uncontrolled charging of electric vehicles using cluster analysis," vol. 14, 2015.

[123] R. C. Leou, C. L. Su, and C. N. Lu, "Stochastic analyses of electric vehicle charging impacts on distribution network," *IEEE Transactions on Power Systems*, vol. 29, 2014.

[124] L. K. Panwar, K. S. Reddy, R. Kumar, B. K. Panigrahi, and S. Vyas, "Strategic energy management (SEM) in a micro grid with modern grid interactive electric vehicle," *Energy Conversion and Management*, vol. 106, 2015.

[125] G. Angrisani, M. Canelli, C. Roselli, and M. Sasso, "Integration between electric vehicle charging and micro-cogeneration system," *Energy Conversion and Management*, vol. 98, 2015.

[126] L. Drude, L. C. Pereira, and R. Ruther, "Photovoltaics (PV) and electric vehicle-to-grid (V2G) strategies for peak demand reduction in urban regions in Brazil in a smart grid environment," *Renewable Energy*, vol. 68, 2014.

[127] C. Will, P. Jochem, S. Pfahl, and W. Fichtner, "Economic and sustainability-potential of carbon-neutral charging services for electric vehicle customers," *Proceedings of the 30th International Electric Vehicle Symposium & Exhibition*, EVS30, Stuttgart, Germany, 9–11 Oct. 2017.

[128] A. Ensslen, C. Will, and P. Jochem, "Simulating electric vehicle diffusion and charging activities in France and Germany," *World Electric Vehicle Journal*, vol. 10, 2019.

[129] C. Wu, F. Wen, Y. Lou, and F. Xin, "Probabilistic load flow analysis of photovoltaic generation system with plug-in electric vehicles," *Electrical Power and Energy Systems*, vol. 64, 2015.

[130] Y. Ko, K. Jang, and J. D. Radke, "Toward a solar city: trade-offs between on-site solar energy potential and vehicle energy consumption in San Francisco, California," *International Journal on Sustainable Transportation*, vol. 11, 2017.

[131] A. G. Anastasiadis, E. Voreadi, and N. D. Hatziargyriou, "Probabilistic load flow methods with high integration of renewable energy sources and electric vehicles — case study of Greece," *2011 IEEE Trondheim PowerTech*, Trondheim, Norway, 2011.

[132] X. Ni and K. L. Lo, "A methodology to model daily charging load in the EV charging stations based on Monte Carlo simulation," *2020 8th International Conference of Smart Grid and Clean Energy Technologies*, 2020.

[133] Q. Yan, C. Qian, B. Zhang, and M. Kezunovic, "Statistical analysis and modelling of plug-in electric vehicle charging demand in distribution systems," *2017 19th International Conference on Intelligent System Application to Power Systems (ISAP)*, 2017.

[134] Y. Nie, C. Y. Chung, and N. Z. Xu, "System state estimation considering EV penetration with unknown behaviour using quasi-newton method," *IEEE Transactions on Power Systems*, vol. 31, 2016.

[135] L. Yu, T. Zhao, Q. Chen, and J. Zhang, "Centralised bi-level spatial temporal coordination charging strategy for area electric vehicles," *CSEE Journal of Power and Energy System*, vol. 1, 2015.

[136] B. Sun, Z. Huang, X. Tan, and D. H. K. Tsang, "Optimal scheduling for electric vehicle charging with discrete charging levels in distribution grid," *IEEE Transactions on Smart Grid*, vol. 9, 2018.

[137] O. Beaude, S. Lasaulce, M. Hennebel, and I. Mohand-Kaci, "Reducing the impact of EV charging operations on the distribution network," *IEEE Transactions on Smart Grid*, vol. 7, 2016.

[138] T. Liting, S. Shuanglong, and J. Zhuo, "A statistical model for charging power demand of electric vehicles," *Journal of Power System Technology*, vol. 34, 2010.

[139] A. Ashtari A, E. Bibeau, Shahidinejad S, and T. Molinski, "PEV charging profile prediction and analysis based on vehicle usage data," *IEEE Transactions on Smart Grid*, vol. 3, 2012,

[140] S. W. Hadley and A. Tsvetkova, "Potential impacts of plug-in hybrid electric vehicles on Regional Power Generation," Oak Ridge National Laboratory, Oak Ridge, 2008.

[141] S. Letendre and R. A.Watts, "Effects of plug-in hybrid electric vehicles on the Vermont electric transmission system," *Proceeding Transportation Research Board 88th Annual Meeting*, Washington, DC, 2009.

[142] M. D. Nigris, I. Gianinoni, S. Grillo, S. Massucco, and F. Silvestro, "Impact evaluation of plug-in electric vehicle (PEV) on electric distribution networks," *Proceedings of the 14th International Conference on Harmonics* and Quality of Power *(ICHPQ 2010)*, Bergamo, Italy, 26–29 Sep. 2010.

[143] C. Lei and L. Siyu, "Research on the influence of electric vehicle charging on distribution network of residential district," *Southern Energy Construction*, 2018.

[144] W. Yi, W. Feihong, and H. Xingzhe, "Random access control strategy of charging for household electric vehicle in residential area," *Automation of Electric Power Systems*, 2018

[145] C. Guo, D. Liu, and W. Geng, "Modelling and analysis of electric vehicle charging load in residential area," *2019 4th International Conference on Power and Renewable Energy*, 2019.

[146] G. Yi, H. Zechun, and Z. Hongcai, "A statistical method to evaluate the capability of residential distribution network for accommodating electric vehicle charging load," *Journal of Power System Technology*," vol. 9, 2015.

[147] Y. Bing, W. Lifang, and L. Chenglin, "Charging load calculation method of large-scale electric vehicles with coupling characteristics*," Automation of Electric Power Systems*, vol. 22, 2015.

[148] E. Pashajavid and M. A. Golkar, "Charging of plug-in electric vehicles: Stochastic modelling of load demand within domestic grids" *20th Iranian Conference on Electrical Engineering (ICEE2012)*, Tehran, Iran, 15–17 May. 2012.

[149] E. Pashajavid and M. A. Golkar, "Copula-based multivariate stochastic modelling of load demand due to plug-in electric vehicles in order to be integrated distribution system planning," *22nd International Conference on Electricity Distribution (CIRED 22)*, Stockholm, Sweden, 10–13 Jun. 2013.

[150] Y. Wang and D. Infield, "Markov chain Monte Carlo simulation of electric vehicle use for network integration studies," *International Journal of Electrical Power & Energy Systems*, vol. 99, 2018.

[151] M. K. Gray and W. G. Morsi, "Power quality assessment in distribution systems embedded with plug-in hybrid and battery electric vehicles," *IEEE Transactions on Power Systems*, vol. 30, 2015.

[152] J. García-Villalobos, I. Zamora, K. Knezovic, and M. Marinelli "Multi-objective optimisation control of plug-in electric vehicles in low voltage distribution networks," *Applied Energy*, vol. 180, 2016.

[153] J. Jiandong, H. Wenwen, and Y. Zijun, "The modelling of electric vehicle charging load in residential areas," *Journal of Zhengzhou University (Natural Science Edition)*, vol. 51, 2019.

[154] M. S. Islam and N. Mithulananthan, "Impacts of EV charging on business grid: A case study for the university of Queensland," *2016 Australas University Power Engineering Conference*, Brisbane, Australia, 25–28 Sep. 2016.

[155] S. Sachan and N. Adnan, "Stochastic charging of electric vehicles in smart power distribution grids," *Sustainable Cities*, vol. 40, 2018.

[156] G. Li and X. P. Zhang, "Modelling of plug-in hybrid electric vehicle charging demand in probabilistic power flow calculations," *IEEE Transactions on Smart Grid*, vol. 3, 2012.

[157] S. G. Mitrakoudis and M. C. Alexiadis, "Modelling electric vehicle charge demand: Implementation for the Greek power system," *World Electric Vehicle Journal*, vol. 13, 2022.

[158] J. Axsen, et. al., "Electrifying vehicles: Insights from the Canadian plug-in electric vehicle study," Simon Fraser University, Canada, 2015.

The Appendices

[159] S. Wang, C. Li, Z. Pan, and J. Wang, "Probabilistic method for distribution network electric vehicle hosting capacity assessment based on combined cumulants and gram-charlier expansion," *10th International Conference on Applied Energy (ICAE2018)*, China, 2018.

[160] E. Ivarsoy, B. N. Torsæter, and M. Korpâs, "Stochastic load modelling of high-power electric vehicle charging — A Norwegian case study," *2020 International Conference on Smart Energy Systems and Technologies (SEST)*, 2020.

[161] F. Bizzarri, et. al., "Electric vehicles state of charge and spatial distribution forecasting: A high-resolution model," *Proceedings of the IECON 2016 — 42nd Annual Conference of the IEEE Industrial Electronics Society*, Italy, 2016.

[162] S. Bae S and A. Kwasinski, "Spatial and temporal model of electric vehicle charging demand," *IEEE Transactions on Smart Grid*, 2012

[163] L. Yorick, H. Vrubel, and G. Hubert, "Local energy storage and stochastic modelling for ultrafast charging stations," *Energies*, vol. 12, 2019.

[164] Y. Zhang, et. al., "Modelling of fast charging station equipped with energy storage," *Global Energy Interconnection,* vol. 1, 2018.

[165] F. H. Malik and M. Lehtonen, "Analysis of power network loading due to fast charging of Electric Vehicles on highways," *2016 Electric Power Quality and Supply Reliability*, Tallinn, 2016.

[166] Z. Darabi Z and M. Ferdowsi, "Plug-in hybrid electric vehicles: Charging load profile extraction based on transportation data," P*ower and Energy Society General Meeting Conference*, 2011.

[167] S. Shahidinejad, S. Filizadeh S, and E. Bibeau, "Profile of charging load on the grid due to plug-in vehicles," *IEEE Transactions on Smart Grid*, vol. 3, 2012.

[168] J. Singh and R. Tiwari, "Probabilistic modelling and analysis of aggregated electric vehicle charging station load on distribution system," *2017 14th IEEE India Council International Conference (INDICON)*, 2017.

[169] Z. Ren, W. Li, R. Billinton, and W. Yan, "Probabilistic power flow analysis based on the stochastic response surface method," *IEEE Transactions on Power Systems*, vol. 31, 2016.

[170] R.-C. Leou, J.-H. Teng, and C.-L. Su, "Modelling and veryfing the load behaviour of electric vehicle charging stations based on field measurements," *IET Generation, Transmission & Distribution*, vol. 9, 2015.

[171] K. Qian, C. Zhou, and M. Allan, "Modelling of load demand due to EV battery charging in distribution systems," *IEEE Transactions on Power Systems*, vol. 26, 2011.

[172] J. Quiros-Tortos, A. Navarro-Espinosa, L. F. Ochoa, and T. Butler, "Statistical representation of EV charging: Real data analysis and applications," *Proceedings of the Power Systems Computation Conference (PSCC)*, Dublin, Ireland, 11–15 Jun. 2018.

[173] X.-H. Sun, T. Yamamoto, and T. Morlkawa, "Charge timing choice behaviour of battery electric vehicle uses," *Transportation Research Part D Transport and Environment*, vol. 37, 2015.

[174] A. Gerossier, R. Girard, and G. Kariniotakis, "Modelling and forecasting electric vehicle consumption profiles," *Energies*, 2018.

[175] Y. Zheng, Z. Shao, Y. Zhang, and L. Jian, "A systematic methodology for mid-and-long term electric vehicle charging load forecastic: The case study of Shenzhen, China," *Sustainable Cities and Society*, vol. 56, 2020.

[176] C. Crozier, T. Morstyn, and M. McCulloch, "The opportunity to mitigate the impact of electric vehicles on transmission and distribution systems," *Applied Energy*, vol. 268, 2020.

[177] National Operational Guidance, "High voltage networks (national grid)." [Online]. Available at: https://www.ukfrs.com/promos/17142. [Accessed: 25-Feb-2023].

[178] J. H. Moon, H. N. Gwon, G. R. Jo, W. Y. Choi, and K. S. Kook, "Stochastic modelling method of plug-in electric vehicle charging demand for Korean transmission system planning," *Energies*, vol. 13, 2020.

[179] N. Hartmann and E. Özdemir, "Impact of different utilisation scenarios of electric vehicles on the German grid in 2030," *Journal of Power Sources*, vol. 196, 2011.

[180] H. Heinrichs and P. Jochem, "Long-term impacts of battery electric vehicles on the German electricity system," *The European Physical Journal Special Topics*, vol. 225, 2016.

[181] P. Staudt, M. Schmidt, J. Gärttner, and C. Weinhardt, "A decentralised approach towards resolving transmission grid congestion in Germany using vehicle-to-grid technology," *Applied Energy*, vol. 230, 2018.

[182] P. Grahn, K. Alvehag, and L. Soder, "PHEV utilisation model considering type-of-trip and recharging flexibility," *IEEE Transactions on Smart Grid,* vol. 5, 2014.

[183] S. I. Vagropoulos, G. A. Balaskas, and A. G. Bakirtzis "An investigation of plug-in electric vehicle charging impact on power systems scheduling and energy costs," *IEEE Transactions on Power Systems*, vol. 32, 2017.

[184] L. Jia, Z. Hu, W. Liang, W. Lang, and Y. Song, "A novel approach for urban electric vehicle charging facility planning considering combination of slow and fast charging," *2014 International Conference on Power System Technology*, 2014.

[185] British Standard Institute, "Voltage characteristics of electricity supplied by public electricity networks," 2015.

[186] A. T. Procopiou J. Quirós-Tortós, and L. F. Ochoa, "HPC-based probabilistic analysis of LV networks with EVs: Impacts and control," *IEEE Transactions on Smart Grid*, 2017

[187] G. Gruosso, "Analysis of impact of electrical vehicle charging on low voltage power grid," *Proceedings of the 2016 International Conference on Electrical Systems for Aircraft, Railway, Ship Propulsion and Road Vehicles & International Transportation Electrification Conference (ESARS-ITEC)*, Toulouse, France, 2–4 Nov. 2016.

[188] E. Sortomme, M. M. Hindi, S. D. J. MacPherson, S. S. Venkata, "Coordinated charging of plug-in hybrid electric vehicles to minimize distribution system losses," *IEEE Transactions on Smart Grid*, vol. 2, 2011.

[189] M. Muratori, "Impact of uncoordinated plug-in electric vehicle charging on residential power demand," *Nature*, 2018.

[190] T. Pothinun and S. Premrudeepreechacharn, "Power quality impact of charging station on MV distribution networks: A case study in PEA electrical power system," *2018 53rd International Universities Power Engineering Conference (UPEC)*, 2018.

[191] B. Pea-Da and S. Dechanupaprittha, "Impact of fast charging station to voltage profile in distribution system," *2014 International Electrical Engineering Congress (IEECON 2014)*, 2014.

[192] S. M. Alshareef and W. G. Morsi, "Impact of fast charging stations on the voltage flicker in the electric power distribution systems," *2017 IEEE Electric Power and Energy Conference (EPEC)*, 2017.

[193] M. Geske, P. Komarnicki, M. Stötzer, and Z. A. Styczynski, "Modelling and simulation of electric car penetration in the distribution power system — Case study," *Proceedings of the International Symposium on Modern Electric Power Systems*, Wroclaw, Poland, 2011.

[194] P. Juanuwattanakul and M. A. Masoum, "Identification of the weakest buses in unbalanced multiphase smart grids with plug-in electric vehicle charging stations," *Proceedings of the Innovative Smart Grid Technologies*, Perth, Australia, 13–16 Nov. 2011.

[195] C. Zhang, C. Chen, J. Sun, P. Zheng, X. Lin, and Z. Bo, "Impacts of electric vehicles on the transient voltage stability of distribution network and the study of improvement measures," *Proceedings of the IEEE Asia Pacific Power and Energy Engineering Conference (APPEEC)*, Hong Kong, China, 7–10 Dec. 2014.

[196] M. Nour, H. Ramadan, A. Ali, and C. Farkas, "Impacts of plug-in electric vehicles charging on low voltage distribution network," *2018 International Conference on Innovative Trends in Computer Engineering (ITCE 2018)*, 2018.

[197] M. Oliinyk, J. Džmmra, and D. Pál, "The impact of an electric vehicle charging on the distribution system," *2020 21st International Scientific Conference on Electric Power Engineering (EPE)*, 2020.

[198] S. Deilami, "Online coordination of plug-in electric vehicles considering grid congestion and smart grid power quality," *Energies*, vol. 11, 2018.

[199] A. Bosovic, M. Mustafa, and S. Salih, "Analysis of the impacts of plug-in electric vehicle charging on the part of a real low voltage distribution network," *2015 IEEE Eindhoven PowerTech*, 2015.

[200] I. Karakitsios, E. Karfopoulos, and N. Hatziargyyriou, "Impact of dynamic and static fast inductive charging of electric vehicles on the distribution network," *Electric Power Systems Research*, vol. 140, 2016.

[201] X. Jiang, E. Corr, B. Stephen, and B. G. Stewart, "Impact of increased penetration of low-carbon technologies on cable lifetime estimations," *Electricity*, vol. 3, 2022.

[202] S. Johansson, J. Persson, S. Lazarou, and A. Theocharis, "Investigation of the impact of large-scale integration of electric vehicles for a Swedish distribution network," *Energies*, vol. 12, 2019.

[203] K. Qian, C. Zhou, and Y. Yuan, "Impacts of high penetration level of fully electric vehicles charging loads on the thermal ageing of power transformers," *Electrical Power and Energy Systems*, 2015.

[204] Q. Gong, S. Midlam-Mohler, V. Marano, and G. Rizzoni, "Study of PEV charging on residential distribution transformer life," *IEEE Transactions on Smart Grid*, vol. 3, 2012.

[205] S. Qian, X. Zhang, C. Chen, H. Wang, J. Guo, and Y. Xu, "Ageing evaluation of the distribution transformer under varying load due to electric vehicle charging," *2021 International Conference on Electrical Materials and Power Equipment (ICEMPE)*, 2021.

[206] S. Shokrzadeh, H. Ribberink, I. Rishmawi, and E. Entchev, "A simplified control algorithm for utilities to utilise plug-in electric vehicles to reduce distribution transformer overloading," *Energy*, vol. 133, 2017.

[207] U. Datta, A. Kalam, and J. Shi, "Smart control of BESS in PV integrated EV charging station for reducing transformer overloading and providing battery-to-grid service," *Journal of Energy Storage*, vol. 28, 2020.

[208] A. Trivedi, B. Menon, D. Srinivasan, A. Sharma, W. Fong, and D. Nicholas, "Multi-objective siting and sizing of E-charging stations in the distribution system," *2015 IEEE Innovative Smart Grid Technologies — Asia (ISGT ASIA)*, 2015.

[209] B. Liao, et. al., "A planning model for charging facilities of electric vehicles considering spatial and temporal characteristics of charging demands," *2016 IEEE 2nd Annual Southern Power Electronics Conference (SPEC)*, 2016.

[210] F. de Paula Garcia-Lopez, M. Barragan-Villarejo, and J. M. Maza-Ortega, "Grid-friendly integration of electric vehicle fast charging station based on multiterminal DC link," *International Journal of Electrical Power and Energy Systems*, 2019.

[211] R. S. Rao, K. Ravindra, K. Satish, and S. Narasimham, "Power loss minimisation in distribution system using network reconfiguration in the presence of distributed generation," *IEEE Transactions on Power Systems*, vol. 28, 2013.

[212] A. Arief and M. B. Nappu, "DG placement and size with continuation power flow method," *5th International Conference on Electrical Engineering and Informatics 2015*, 2015.

[213] H.-T. Kim, J. Lee, M. Yoon, M.-J. Lee, N. Cho, and S. Choi, "Continuation power flow based distributed energy resource hosting capacity estimation considering renewable energy uncertainty and stability in distribution systems," *Energies*, vol. 13, 2020.

[214] H. Saadat, "Power system analysis," Publisher: K. Kane, 1999.

The Appendices

[215] U. P. Anand and P. Dharmeshkumar, "Voltage stability assessment using continuation power flow," *International Journal of Advanced Research in Electrical, Electronics and Instrumentation Engineering*, vol. 2, 2013.

[216] S. Velamuri, S. H. C. Cherukuri, S. K. Sudabattula, N. Prabaharan, and E. Hossain, "Combined approach for power loss minimisation in distribution networks in the presence of gridable electric vehicles and dispersed generation," *IEEE Systems Journal*, 2021.

[217] S. K. Injeti and V. K. Thunuguntla, "Optimal integration of DGs into radial distribution network in the presence of plug-in electric vehicles to minimize daily active power losses and to improve the voltage profile of the system using bioinspired optimization algorithms," *Protection and Control of Modern Power Systems*, vol. 5, 2020.

[218] R. Sanjay, T. Jayabarathi, T. Raghunathan, V. Ramesh, and N. Mithulananthan, "Optimal allocation of distributed generation using hybrid grey wolfoptimiser," *IEEE Access*, vol. 5, 2017.

[219] K. H. Truong, P. Nallagownden, I. Elamvazuthi, and D. N. Vo, "A quasi oppositional-chaotic symbiotic organisms search algorithm for optimal allocation of DG in radial distribution networks," *Applied Soft Computing*, vol. 88, 2020.

[220] S. Saha and V. Mukherjee, "A novel multi-objective chaotic symbiotic organisms search algorithm to solve optimal DG allocation problem in radial distribution system," *International Transactions on Electrical Energy Systems.*, vol. 29, 2019.

[221] A. Selim, S. Kamel, and F. Jurado, "Efficient optimisation technique for multiple DG allocation in distribution networks," *Applied Soft Computing*, vol. 86, 2020.

[222] I. A. Quadri, S. Bhowmick, and D. Joshi, "A hybrid teaching-learning based optimisation technique for optimal DG sizing and placement in radial distribution systems," *Soft Computing*, vol. 23, 2019.

[223] A. G. Expósito, et. al., "City-friendly smart network technologies and infrastructures: The Spanish experience," *Proceedings of the IEEE*, vol. 106, 2018.

[224] J. Irla, M. Heleno, and G. Cardoso, "Optimal sizing and placement of energy storage systems and on-load tap changer transformers in distribution networks," *Applied Energy*, vol. 250, 2019.

[225] M. Armendáriz, K. Paridari, E. Wallin, and L. Nordström, "Comparative study of optimal controller placement considering uncertainty in PV growth and distribution grid expansion," Electric Power Systems Research, vol. 155, 2018.

[226] M. Armendáriz, M. Heleno, G. Cardoso, S. Mashayekh, M. Stadler, and L. Nordström, "Coordinated microgrid investment and planning process considering the system operator," *Applied Energy*, vol. 200, 2017.

[227] H. Hosseinpour and B. Bastaee, "Optimal placement of on-load tap changers in distribution networks using SA-TLBO method," *International Journal of Electrical Power and Energy Systems*, vol. 64, 2015.

[228] L. Cheng, Y. Chang, and R. Huang, "Mitigating voltage problem in distribution system with distributed solar generation using electric vehicles," *IEEE Transactions on Sustainable Energy*, vol. 6, 2015.

[229] D. Sbordone, I. Bertini, B. D. Pietra, M. C. Falvo, A. Genovese, and L. Martirano, "EV fast charging stations and energy storage technologies: A real implementation in the smart micro grid paradigm," *Electric Power Systems Research*, vol. 120, 2014.

[230] H. Mehrjerdi and R. Hemmati, "Electric vehicle charging station with multilevel charging infrastructure and hybrid solar-battery-diesel generation incorporating comfort of drivers," *Journal of Energy Storage*, 2019.

[231] A. Hussain, V. H. Bui, J. W. Baek, and H. M. Kim, "Stationary energy storage system for fast EV charging stations: Simultaneous sizing of battery and converter," *Energies*, vol. 12, 2019.

[232] X. Ding, W. Zhang, S. Wei, and Z. Wang, "Optimisation of an energy storage system for electric bus fast-charging station," *Energies*, vol. 14, 2021.

[233] D. McPhail, "Evaluation of ground energy storage assisted electric vehicle DC fast charger for demand charge reduction and providing demand response," *Renewable Energy*, vol. 67, 2014.

[234] J. Deng, J. Shi, Y. Liu, and Y. Tang, "Application of a hybrid energy storage system in the fast-charging station of electric vehicles," *IET Generation, Transmission and Distribution*, vol. 10, 2016.

[235] K. Mahmud, M. J. Hossain, and G. E. Town, "Peak-load reduction by coordinated response of photovoltaics, battery storage, and electric vehicles," *IEEE Access*, vol. 6, 2018.

[236] K. Mahmud, M. J. Hossain, and J. Ravishankar, "Peak-load management in commercial systems with electric vehicles," *IEEE Systems Journal*, vol. 13, 2019.

[237] T. R. Ayodele, A. S. O. Ogunjuyigbe, and N. O. Oyelowo, "Hybridisation of battery/flywheel energy storage system to improve ageing of lead-acid batteries in PV-powered applications," *International Journal of Sustainable Engineering*, vol. 13, 2020.

[238] L. Barelli, et. al., "Flywheel hybridisation to improve battery life in energy storage systems coupled to RES plants," *Energy*, vol. 173, 2019.

[239] W. Wei, L. Wu, J. Wang, and S. Mei, "Expansion planning of urban electrified transportation networks: A mixed-integer convex programming approach," *IEEE Transactions on Transportation Electrification*, vol. 3, 2017.

[240] Z. Liu, F. Wen, and G. Ledwich, "Optimal planning of electric vehicle charging stations in distribution systems," *IEEE Transactions on Power Delivery*, vol. 28, 2013.

[241] C. H. Dharmakeerthi, N. Mithulananthan and T. K. Saha, "Impact of electric vehicle fast charging on power system voltage stability," *International Journal of Electrical Power and Energy Systems*, vol. 57, 2014.

[242] Luc, "What determines the charge speed?" Fastned, 2021. [Online]. Available at: https://fastnedcharging.com. [Accessed: 31-Jan-2022].

[243] M. Al Essa and L. Cipcigan, "Reallocating charging loads of electric vehicles in distribution networks," *Applied Sciences*, vol. 6, 2016

[244] S. Ingram, S. Probert, and K. Jackson, "The impact of small-scale embedded generation on the operating parameters of distribution networks," PB Power, Department of Trade and Industry (DTI): London, UK, 2003.

[245] Regen, "Electric vehicles and electricity system rapid charging hubs webinar," 2020. [Online]. Available at: https://www.youtube.com/watch?v=O7jIo9pG3gA. [Accessed: 29-Jan-2022].

[246] I. A. Adejumobi and O. I. Adebisi, "Power loss reduction on primary distribution networks using tap-changing technique," *International Journal of Recent Research and Applied Studies*, vol. 10, 2012.

[247] L. Cipcigan, "Distributed generation, system design and regulations: Voltage control," Cardiff University.

[248] Western Power Distribution, "Project network equilibrium: Voltage limits assessment discussion paper," 2016.

[249] Superchargers, 2023. [Online]. Available at: https://supercharge.info/charts. [Accessed: 25-Feb-2023].

[250] Tesla, "Supercharger locations," 2023. [Online]. Available at: https://www.tesla.com/en_gb/supercharger. [Accessed: 25-Feb-2023].

[251] "Kent active system management distribution network losses and strategies for reducing losses," *Bigwood Systems*, Inc. in Collaboration with UK Power Networks, 2017.

[252] B. Wang, Y. Sun, F. Lu, X. Wu, Z. Liu, and W. Dong, "The calculation and analysis of distribution network loss with photovoltaic power generation connected," *International Conference on Advances in Energy and Environmental Science (ICAEES 2015)*, 2015.

[253] UK Parliament, "Losses and leakages." *Energy and Climate Change*, 2014. [Online]. Available at: https://publications.parliament.uk/pa/cm201415/cmselect/cmenergy/386/38607.html. [Accessed: 25-Feb-2023].

[254] "UK Solar & PV Market Report 2019." *UK Business Energy*, 2018.

[255] K. Kahle, F. R. Blanquez, and C. M. Genton, "The design and performance of static var compensators for particle accelerators," *EPE*, 2015.

[256] N. A. Daw and A. H. Salih, "Choosing the best place of static var compensator in IEEE 14 bus system to improve voltage using Neplan software," *2019 19th International Conference on Sciences and Techniques of Automatic Control & Computer Engineering (STA)*, Sousse, Tunisia, 24–26 Mar. 2019.

[257] D. E. G. Carson, C. Brozio, and R. Bryans, "Calculation of system fault levels," *SP Power Systems Ltd.*, 2017.

[258] Made-in-China: connecting buyers with Chinese suppliers, "11 kV 200-kVAr static var compensator," 2022. [Online]. Available at: https://cnfarady.en.made-in-china.com/product/vdYfFrnwrPkX/China-11kv-200kvar-Static-Var-Compensator.html. [Accessed: 11-May-2022].

[259] NewMotion, "AC charging vs DC charging." [Online]. Available at: https://newmotion.com/en-gb/support/faq/ac-charging-vs-dc-charging. [Accessed: 29-Jan-2022].

[260] R. Shi, X. P. Zhang, D. C. Kong, N. Deng, and P. Y. Wang, "Dynamic impacts of fast-charging stations for electric vehicles on active distribution networks," *IEEE PES Innovative Smart Grid Technologies (ISGT)*, 2012.

[261] T. Kalitjuka, "Control of voltage source converters for power system applications," M.Sc Thesis, Norwegian University of Science and Technology Department of Electric Power Engineering, 2011

[262] P. Wang, "A multi-terminal modular multilevel converter based HVDC system with an offshore wind farm," PhD Thesis, The University of Birmingham, 2016.

[263] M. I. Tor, S. G. Sverre, and U. Tore, "Multilevel converters for a 10 MW, 100 kV transformer-less offshore wind generator system," *2013 15th European Conference on Power Electronics and Applications (EPE)*, 2013.

[264] J. Ögren, "PLL design for inverter grid connection: Simulations for ideal and non-ideal grid conditions," 2011.

[265] S. Golestan, J. M. Guerrero, and J. C. Vasquez, "Three-phase PLLs: A review of recent advances," *IEEE Transactions on Power Electronics*, vol. 32, 2017.

[266] Microsemi, "Park, inverse park, and Clarke, inverse Clarke transformations: MSS software implementation user guide," 2013.

[267] H. Chen and H. Zhao, "Review on pulse-width modulation strategies for common-mode voltage reduction in three-phase voltage-source inverters," *IET Power Electronics*, vol. 9, 2016.

[268] M. N. Raju, J. Sreedevi, R. P. Mandi, and K. S. Meera, "Modular multilevel converters technology: A comprehensive study on its topologies, modelling, control and applications," *IET Power Electronics*, vol. 12, 2019.

[269] P. S. V. Kishore, P. S. Kumar, and K. Ramesh, "Comparison of multi-carrier PWM techniques applied to five-level CHB inverter," *International Journal of Pure and Applied Mathematics*, vol. 114, 2017.

[270] A. Ul-Haq, C. Carlo, and E. A. Al-Ammar, "Modeling of a photovoltaic-powered electric vehicle charging station with vehicle-to-grid implementation," *Energies,* vol. 10, 2016.

[271] A. Arancibia and K. Strunz, "Modelling of an electric vehicle charging station for fast DC charging," *2012 IEEE International Electric Vehicle Conference*, 2012.

[272] Manitoba Hydro International Ltd., "Three-phase battery energy storage system," 2019.

[273] R. Fuller, "Panasonic NCR 18650 PF what are the advantages for lithium cells from country battery services," 2019. [Online]. Available at: https://www.countybattery.co.uk/the-battery-experts/panasonic-ncr-18650-pf-what-are-the-advantages-for-lithium-cells. [Accessed: 13-Jun-2022].

[274] T. Boyer, "Tesla 18650, 2170 and 4680 battery cell comparison basics," *Torque News*, 2021. [Online]. Available at: https://www.torquenews.com/14093/tesla-18650-2170-and-4680-battery-cell-comparison-basics. [Accessed: 13-Jun-2022].

[275] Greenway Battery, "Tesla 18650 battery specs — Introduction, quantity and dimensions." [Online]. Available at: https://m.greenway-battery.com/news/Tesla-18650-Battery-Specs---Introduction,-Quantity-and-Dimensions-1444.html. [Accessed: 12-May-2022].

[276] S. Thomas, "Understanding the role of BMS in electric vehicles," *eInfochips*, 2021. [Online]. Available at: https://www.einfochips.com/blog/understanding-the-role-of-bms-in-electric-vehicles. [Accessed: 12-Jan-2023].

[277] C. Gavin, "Special feature — seasonal variations in electricity demand," 2014.

[278] J. Armas and A. Ivanov, "Determination of the total cost of active power losses and methods to reduce power losses in low-voltage distribution networks," *2019 IEEE 60th International Scientific Conference on Power and Electrical Engineering of Riga Technical University (RTUCON)*, 2019.

[279] OFGEM, "Check if the energy price cap affects you," 2022. [Online]. Available at: https://www.ofgem.gov.uk/information-consumers/energy-advice-households/check-if-energy-price-cap-affects-you. [Accessed: 12-May-2022].

[280] Electronics Notes, "Electrical resistivity table for common materials." [Online]. Available at: https://www.electronics-notes.com/articles/basic_concepts/resistance/electrical-resistivity-table-materials.php. [Accessed: 31-Jan-2022].

[281] T. Pakenham, "V2G: Democratising the energy system," *OVO Energy*, 2021.

[282] Department for Transport, "Electric vehicle charging device statistics: January 2021," 2021.

[283] Department for Transport, "National travel survey 2021: Household car availability and trends in car trips," 2022.

[284] Office for National Statistics, "Over half of younger drivers likely to switch to electric in next decade," *Census 2021*, 2021.

[285] "JavaScript array splice: Delete, insert, and replace," JavaScript Tutorial, 2021. [Online]. Available at: https://www.javascripttutorial.net/javascript-array-splice. [Accessed: 31-Jan-2022].

[286] C. Lilly, "Electric car market statistics," Next Green Car Ltd, 2021. [Online]. Available at: https://www.nextgreencar.com/electric-cars/statistics. [Accessed: 31-Jan-2022].

[287] "Electric vehicle database," [Online]. Available at https://ev-database.uk. [Accessed: 08-Jun-2021].

[288] "How long does it take to charge an electric car?" *Pod Point*, 2021. [Online]. Available at: https://pod-point.com/guides/driver/how-long-to-charge-an-electric-car.
[Accessed: 31-Jan-2022].

[289] R. Guillemot, "How to roll a dice in JavaScript?" 2019. [Online]. Available at: https://medium.com/@rocambille/how-to-roll-a-dice-in-javascript-ec543f8ffda1.
[Accessed: 31-Jan-2022].

[290] "JavaScript demo: Math.random()," *MDN Web Docs*, 2022. [Online]. Available at: https://developer.mozilla.org/enUS/docs/Web/JavaScript/Reference/Global_Objects/Math/random. [Accessed: 31-Jan-2022].

[291] B. Nyland, "Model 3 vs e-tron charging on Ionity 350 kW charger," 2019. [Online]. Available at: https://www.youtube.com/watch?v=PPrVZtzAqX4. [Accessed: 12-May-2022].

[292] LG chem, "Product specification: Rechargeable lithium-ion battery model: INR18650HG2 3000mAh," 2015.

[293] DNK Power, "Cylindrical batteries more suitable for electric vehicles?" 2020. [Online]. Available at: https://www.dnkpower.com/cylindrical-batteries-suitable-electric-vehicles. [Accessed: 20-Feb-2023].

[294] M. Murnane and A. Ghazel, "A closer look at State of Charge (SoC) and State of Health (SoH) estimation techniques for batteries," *Analog Devices*, 2017.

[295] W.-Y. Chang, M. Brünig and E. D. Nardo, "The state of charge estimating methods for battery: A review," vol. 2013, 2013.

[296] K. Thoubboron, "Depth of discharge (DoD): What does it mean for your battery, and why is it important?" *Energysage*, 2022. [Online]. Available at: https://news.energysage.com/depth-discharge-dod-mean-battery-important. [Accessed: 02-Jul-2022].

[297] J. C. Das, "Power system harmonics and passive filter designs," Hoboken, New Jersey: IEEE Press/Wiley, 2015.

[298] Manitoba Hydro International Ltd., "Type-4 wind turbine model," 2018.

[299] S. Heier, "Grid integration of wind energy conversion systems," John Wiley & Sons Ltd, 1998.

[300] J. Sedo, and F. Slavomir, "Design of output LCL filter and control of single-phase inverter for grid-connected system," *Electrical Engineering*, vol. 99, 2017.

[301] "Design of LCL filter for three-phase grid connected inverter," Tech Simulator, 2020. [Online]. Available at: https://www.youtube.com/watch?v=VmR1NYy9F0M. [Accessed: 31-Jan-2022].

[302] "Low voltage and medium voltage polymeric insulated cables manufactures in accordance with British Standard BS7870 for use by distribution and generation utilities," *Eland Cables*, 2022. [Online]. Available at: https://www.elandcables.com/electrical-cable-and-accessories/cables-by-standard/bs-7870. [Accessed: 31-Jan-2022].